TRANSACTIONS

Series A

Journal of ENGINEERING FOR POWER

January 1959

Divisions: POWER • GAS TURBINE POWER • NUCLEAR ENGINEERING • FUELS OIL AND GAS POWER • **Research Committees:** FURNACE PERFORMANCE FACTORS CORROSION AND DEPOSITS FROM COMBUSTION GASES • BOILER FEEDWATER STUDIES • HIGH TEMPERATURE STEAM GENERATION • CONDENSER TUBES PROPERTIES OF STEAM • **Committees on:** AIR POLLUTION CONTROLS • SOLAR ENERGY APPLICATION • **And:** POWER TEST CODES COMMITTEES

THE AMERICAN SOCIETY OF MECHANICAL ENGINEERS

TRANSACTIONS
OF THE ASME
Series A

EDITORIAL DEPARTMENT

Editor, J. A. JAKLITSCH, JR.
Editor Emeritus, GEORGE A. STETSON
Consulting Editor, LEO BLODGETT
Production, JEAN NORTH
Art Editor, HENRY BALFOUR

OFFICERS OF THE ASME

President, G. B. WARREN
Secretary, O. B. SCHIER, II
Treasurer, E. J. KATES
Assistant Treasurer, H. J. BAUER

PUBLICATIONS COMMITTEE

Chairman, JOHN de S. COUTINHO
R. A. A. BROTZKI
HENDLEY H. BLACKMON
R. D. HINDLIN
MARTIN GOLAND
Junior Representatives
A. T. WUSKA
A. S. GOLDSTEIN

REGIONAL ADVISORY BOARD

Region I, ROY L. PARSELL
Region II, GLENN R. FRYLING
Region III, F. J. HEINZE
Region IV, FRANCIS C. SMITH
Region V, H. M. CATHER
Region VI, C. R. EARLE
Region VII, M. POPOVICH
Region VIII, LINN HELANDER

Published quarterly by The American Society of Mechanical Engineers. Publication office at 20th and Northampton Streets, Easton, Pa. The editorial department is located at the headquarters of the Society, 29 West Thirty-Ninth Street, New York 18, N. Y. Cable address, "Mechaneer," New York. Price $5.00 a copy, $10.00 annually; to members, $1.50 a copy, $6.00 annually. Add 50 cents for postage to all countries outside the United States, Canada, and Pan American Union. Changes of address must be received at Society headquarters seven weeks before they are to be effective on the mailing list. Please send old as well as new address.... By-Law: The Society shall not be responsible for statements or opinions advanced in papers or ... printed in its publications (B13, Par. 4).... Entered as second-class matter March 2, 1928, at the Post Office at Easton, Pa., under the Act of August 24, 1912.... © Copyrighted, 1958, by The American Society of Mechanical Engineers. Reprints from this publication may be made on condition that full credit be given the Transactions of the ASME, Series A—Journal of Engineering for Power, and the author, and that date of publication be stated.

TRANSACTIONS OF THE ASME
is indexed by the Engineering Index, Inc.

Journal of
ENGINEERING FOR POWER
VOLUME 81 • SERIES A • NUMBER 1
January 1959

CONTENTS

1 **Studies of Air Pollution Control by Southern California Edison Company**
A. J. Haagen-Smit

7 **Characteristics of Airborne Particles**
T. A. Rich

13 **Stage Performance and Radial Matching of Axial Compressor Blade Rows**
Jeffrey Watkins

24 **The Measured and Visualized Behavior of Rotating Stall in an Axial-Flow Compressor and in a Two Dimensional Cascade**
Gino Sovran

35 **Availability Balance of Steam Power Plants**
C. A. Meyer, G. J. Silvestri, and J. A. Martin

43 **Pulverized-Coal Transport Through Pipes**
R. C. Patterson

55 **Operating Results of an Experimental Supercritical Steam Generator**
E. Daman, H. Phillips, J. Vail, and S. Ling

66 **Some Notes on the Strength of the Enrico Fermi Reactor Vessel Structure**
F. R. Beyer

73 **Some Thoughts About the Development of Automotive-Gas-Turbine Units**
A. T. Bowden and W. Hryniszak

97 **Electrostatic Shaft Voltage on Steam-Turbine Rotors**
J. M. Gruber and E. F. Hansen

Studies of Air Pollution Control by Southern California Edison Company

A. J. HAAGEN-SMIT

Professor of Biochemistry, California Institute of Technology, Pasadena, Calif.

The relative contribution of various pollutants found in the Los Angeles area is discussed. Processes designed to curtail the emission of oxides of sulfur and nitrogen are described, as well as some results of experiments at the Southern California Edison Company's El Segundo Steam Station.

In recent years the unpleasant discovery was made that the air over our densely populated areas is not unlimited, and stringent regulations have been made after several serious accidents had occurred. The best known are those of London, Donora, and Poza Rico, Mexico. No such accidents have been reported from smog-plagued Los Angeles, and extensive studies by epidemiologists have not been able to produce evidence that permanent damage to the health occurs in this area. Nevertheless, the frequent visitation by the eye-irritating smog cloud has resulted in the adoption of a number of relief measures, some based on extensive research and others on experience gained in other areas.

Research has shown that the major cause of Los Angeles smog difficulties lies in the release of large quantities of organic material, mostly from automobiles [1].[1] These compounds are photochemically oxidized in the air by simultaneously emitted oxides of nitrogen, and these reactions give rise to eye-irritating and plant-damaging substances. Aerosols are formed which are believed to be mainly responsible for the dense haze which accompanies the eye-irritating cloud. An interesting side reaction during this oxidation produces relatively high concentrations of ozone which attacks rubber tires and is largely responsible for the so-called oxidant effect of Los Angeles smog, currently used as an objective measurement of smog severity [2, 3]. The oxidant, being the result of a photochemical phenomenon, rises in the daytime and is low in the evening and during the night. These findings have resulted in extensive recovery measures in the oil industry, and in research on better combustion in the automobile. A practical solution of this problem, and also the control of oxides of nitrogen, is still far away.

Based on experience gained in other areas, a great deal of stress has been laid on the control of directly visible pollution, dust, and fume-producing sources. As a result, dustfall has been reduced to half its former value; open dumps, foundries, steel mills, and many sources of readily detectable, objectionable fumes have been corrected.

Careful investigations were made of industrial and municipal fuel-burning installations which were known to contribute considerably to air pollution in other areas. The problem in Los Angeles is, however, completely different, and a comparison with Eastern cities and their approach to clean air is rather useless, for no coal is burned in this area at all. Nearly all the power generated in this area is derived from petroleum products—fuel oil, gas, and gasoline.

The power plant engineer is an expert in obtaining the maximum efficiency from his fuel. Routine industrial Orsat analyses are not able to detect any carbon monoxide; infrared spectrophotometric methods revealed the presence of only a few ppm of carbon monoxide. The concentration of hydrocarbons, aldehydes, and organic acids do not exceed, as a rule, 20 ppm. We may therefore conclude that the combustion is, for all practical purposes, 100 per cent complete. A constant check on this is part of the regular routine in the station. Moreover, smoke density is continuously measured in the stack, and this information is recorded in the control room. Also, the correct burning of the fuel is checked by means of a television set looking into the furnace. Under these ideal conditions, it would be expected that the stack gas would be wholly composed of carbon dioxide and water, the unused oxygen, and all the nitrogen and other normal components of air. Unfortunately, this view is rather optimistic, for we are not dealing with pure hydrocarbons in fuel, but with a product which contains, because of its origin, organic sulfur and nitrogen compounds. The inorganic materials, also present in the oil, give rise to a dust consisting, for the most part, of oxides of iron, nickel, and vanadium.

During the combustion, organically bound sulfur is oxidized completely to oxides of sulfur, mostly sulfur dioxide, with a small amount of the trioxide. Depending on the nature of the nitrogen compounds, small amounts of oxides of nitrogen may be formed in addition to those produced in the fixation of atmospheric nitrogen at the high temperatures reached in the flame. A typical analysis of stack gas from a fuel-oil burning plant (Southern California Edison Company, El Segundo Steam Station) is shown in Table 1. The Los Angeles County Air Pollution Control District has made estimates of the total quantities of all the various pollutants from the various sources in the Los Angeles Basin. Table 2 lists the relative contribution of different fuels to the emissions from combustion sources alone. These estimates have been rounded off, because it is rare when greater accuracy than 20 to 30 per cent is obtained.

Table 1 Analysis of stack gas

Gas velocity, ft/sec	22
Gas temperature, deg F	688
Insoluble solids, gr/SCF	0.055
lb/hr	0.52
Soluble solids, gr/SCF	0.119
lb/hr	1.13
Water, per cent	9.4
Sulfur trioxide, SO_3, ppm	21.3
Sulfur dioxide, SO_2, ppm	945
Oxides of nitrogen, NO_2, ppm	670
Orsat analysis	
CO_2, per cent	14.6
O_2, per cent	3.0
CO, per cent	0.0
N_2, per cent	82.4

[1] Numbers in brackets designate References at end of paper.

Contributed by the Power Division and presented at the Semi-Annual Meeting, San Francisco, Calif., June 9–13, 1957, of The American Society of Mechanical Engineers.

Note: Statements and opinions advanced in papers are to be understood as individual expressions of their authors and not those of the Society. Manuscript received at ASME Headquarters, April 2, 1957. Paper No. 57—SA-59.

Table 2 Pollutants (tons/day) emitted to the atmosphere in Los Angeles County from combustion processes

Fuel	Organics	Oxides of Nitrogen (as NO_2)	Oxides of Sulfur (as SO_2)	Aerosols, Dust
Gas	20	100	50	10
Oil	10	200	300	30
Gasoline	1,000	400	40	30
Refuse	100	20	20	100
Total combustion	1,000	700	400	200
Total emissions	2,000	700	500	200

Where methods of control are available, their application will be quite expensive in initial cost as well as maintenance, and it is therefore necessary to discuss first the question why emissions of power plant stacks should be controlled. In attempting to answer this question, it is well to distinguish here between local and widespread effects.

While there is no debate about the necessity of controlling nuisance effects, there is considerable difference of opinion in the need for control when no physiological effects are noticed on plants or animals. This is the case in the Los Angeles area, where complete lack of plant damage shows that the SO_2 content is less than 0.2 or 0.3 ppm. Chemical methods confirm these low values. There is no indication that there is any free sulfuric acid in the Los Angeles atmosphere, and any sulfate found was in bound form, either as calcium sulfate or ammonium sulfate, both harmless substances.

The investigations of Gerhard and Johnstone [4] have shown that the oxidation of SO_2 to SO_3 is quite slow, and that during a 24-hour period only $^1/_2$ per cent of the SO_2 is converted to sulfuric acid. The authors came to the conclusion that the gas phase oxidation of sulfur dioxide of naturally polluted atmospheres in natural sunlight would not be significant in effectively reducing the visibility, since it would require approximately 100 hours of noon sunlight to reduce the visibility to one mile.

There is a distinct possibility that more rapid oxidation may take place in liquid phase reactions in fog droplets, or in a combustion of gas phase and liquid phase reactions at high humidity, whereby the presence of metal oxides may exercise a catalytic effect. In speculations of this kind, we should also take into account that the concentrations of SO_2 and NO at the exit of the stack are several thousand times higher than at some distance away. Some conversion does take place at these higher concentrations, a fact which is familiar to anyone who has made attempts to determine accurately the concentration of SO_2 and SO_3 in exhaust gases.

It is well known that the appearance of the plume varies greatly with atmospheric conditions, especially with high humidity and low temperature. Plume formation due to the presence of SO_3 is noticeable at concentrations of SO_3 above 20 ppm. The concentration of SO_3 measured in the flue gas of the El Segundo Station under ordinary conditions represents a borderline case. At times of high humidity or low temperature the plume is more pronounced than on dry and hot days, and on those hot, dry days the visible plume is probably caused, for the most part, by inorganic dust. These considerations are, of course, of interest to anyone who installs corrective equipment. If the plume is caused by a conversion of SO_2 into SO_3, the removal of the sulfur trioxide is indicated. On the other hand, if dust is the major cause, electrostatic precipitation would be the method of choice. At present, the opinions are divided on this subject, and while this question remains undecided, both controls will have to be considered.

To study the removal of dust and sulfur trioxide, a Western Precipitation pilot installation has been in operation at the Redondo Steam Station, and more recently, a more refined unit of the same type was built at the El Segundo Station of the Edison Company to obtain data on the efficiency of collections at higher flow rates. An APRA precipitation unit, operating at a temperature of 700 F, is being tested at El Segundo.

Studies on the control of the emissions of oxides of sulfur and nitrogen by the electrostatic precipitator units show that dust and aerosol particles are collected, and gases such as the oxides of sulfur and nitrogen are not removed. There is some removal of sulfur trioxide, or sulfuric acid, and its concentration is reduced to 10–20 ppm, or about half of its original value. There is reason to believe that, after installation of full-scale units of this type, the plume will have largely disappeared.

It is not expected that the removal of dust and sulfur trioxides from power plant emissions will have a noticeable effect on the smog conditions in general in the Los Angeles basin. Attempts are therefore made to combine the installation of dust removal equipment with means of reducing the sulfur oxides, and especially, the oxides of nitrogen which are known to be essential components in smog formation.

Control of Emission of Oxides of Sulfur

Processes have been developed in the past which reduce sulfur oxides occurring in stack gases at concentrations of several thousand ppm to about one thousand ppm. In the burning of oil with low sulfur content, sulfur dioxide concentration in the stack gas is already down to the thousand ppm level, or lower. There is, at present, no satisfactory process which could handle economically the large quantity of gas of the order of half a million cfm and reduce the sulfur dioxide concentration appreciably. The same is true for the removal of oxides of nitrogen. Processes are known for the control of these gases in nitric acid plants, but, here again, the concentrations are many times higher than we find in flue gases of Los Angeles power plants.

There are several approaches to the problem of reducing the sulfur dioxide content of stack effluents:

(1) Use of gas or fuel with lower sulfur content.
(2) Scrubbing of exhaust gases with (*a*) liquids and (*b*) solids.
(3) Adsorption processes.
(4) Chemical conversions and coupling with processes 2 or 3.

The Edison Company uses the maximum quantity of gas available, but the use of gas is unfortunately limited through its supply, and unless heroic measures are taken to increase importation of additional supplies, this shortage will be even more severe in coming years when more power is needed. The removal of sulfur from fuel is expensive, and would run into an increase in the fuel bill of several million dollars/year. The sulfur is present in complex ring systems and cannot be removed simply by washing with alkali.

The oil industry has been trying for years to break the heavy fuel oil to more valuable volatile products, but has not yet succeeded in doing this in an economically feasible manner. It is conceivable that a hydrogenation and special kinds of cracking processes could furnish more volatile fuel from which the sulfur has been removed as hydrogen sulfide. Any one of these processes will increase the cost of power considerably.

Scrubbing methods have been applied on large power plants in England along the Thames River. In the Battersea effluent process, SO_2 is removed by scrubbing with very large quantities of slightly alkaline river water. In the Howden I.C.I. noneffluent process the gas is scrubbed with a water slurry of lime or chalk. The resultant calcium sulfate is removed by sedimentation and filtration and is discarded. One of the objections to any scrubbing process is the cooling of the gases. Even though the gases are discharged from tall stacks they fall to the ground from time to time near the power station. This results in a nuisance, according to reports from England, where two stations are equipped with scrubbing devices. In order to prevent local

Table 3

Process	Capital Cost	Annual Operating Cost (Dollars/Ton of Coal)	
		No Credit	Credit
Limestone	$1,431,450	$1.23	$1.23
Ammonia	2,855,500	3.00	1.40
Sodium Sulfite	2,176,650	1.99	1.79

complaints, it is necessary to remove almost completely both the obnoxious gases, SO_2 as well as NO, or reheat the flue gases before they leave the stack.

Other scrubbing processes use ammonia in ammonium sulfite with the intention of producing some usable product in the form of ammonium sulfate or sulfur dioxide or sulfuric acid. Aqueous ammonia solutions are being used by the Olin Matheson Chemical Corporation for the removal of sulfur dioxide, and it is claimed that one-stage scrubbing will reduce the concentration of SO_2 in flue gas to 800 ppm; a second scrubbing brings the concentration down to 300 ppm.

In the Fulham-Simon-Carves Ammonia Process, gases are scrubbed with a concentrated solution of ammonium salts (gas liquor), ammonia being added at a rate corresponding to that of the absorption of oxides of sulfur. Oxidation of sulfur dioxide to the trioxide was encouraged through the addition of iron hydroxide and air. Even with low incoming gas concentrations of 500 ppm, reduction in concentration to 30 ppm was accomplished.

Wet scrubbing with organic solvents, such as xylidine, has been considered and is similar to the Gerbitol process whereby H_2S is removed from refinery wastes with diethanolamine and similar basic solvents. In principle, the method can be applied to the removal of SO_2. The low concentration of the SO_2 and losses in solvents through the large volume of inert gas to be treated are not encouraging.

In general, the wet scrubbing processes do not seem too promising after the experience in London. The cost seems rather prohibitive when operating with low SO_2 concentrations. A cost estimate has been made by the U. S. Bureau of Mines [5] for the coal industry, and Table 3 gives the costs of three different processes, based on an assumed capacity of 20 million SCF/hr, equivalent to 475,000 tons of coal/year. Annual operating costs are estimated for cases with and without the formation of salable by-products.

Dry scrubbing is generally not regarded as economical because of poor penetration of the gases into the chemical agent or adsorbent. On the other hand, a selective removal of SO_2 and NO by a solid has the advantage that cooling of the gases as in a wet scrubber may be prevented. The combination with alkaline chemicals is probably limited to the use of lime. In this respect, a combination of the waste products of cement plants and power plants deserves consideration, when the location of the plants is favorable and means of disposing of the combined waste products are available. This solution is, of course, only feasible in a few selected areas and other means have to be found which are more generally applicable.

A modification of the dry scrubbing method consists in the introduction of potential alkaline reagents, such as chalk, dolomite, or lime in the fuel bed at different locations [6]. Some experiments along these lines are being conducted at the Southern California Edison Company El Segundo Station, mainly for the purpose of reducing the amount of sulfur trioxide. These methods are not expected to reduce materially the SO_2 or NO_x concentration. One disadvantage of the method is the addition of several tons of dust, which adds to the required size of the precipitators. However, this disadvantage is readily offset by the decrease in corrosiveness of the gases. Also important is a considerable lowering of the dewpoint allowing a more efficient use of the hot stack gases in preheaters and economizers.

Several of the experimentally tested methods of SO_2 control have been described in Mallette's "Problems and Control of Air Pollution" [7].

Adsorption Methods

Adsorption on nonreactive media such as charcoal, silica, and exchange resins opens the possibility of regenerating the adsorbed gases in more concentrated form by a simple process such as heating, treatment with steam, or elution with aqueous ammonia solutions. Bench experiments at the Southern California Edison Company El Segundo Station have shown that activated charcoal adsorbs considerable quantities of sulfur, as well as nitrogen oxides, even at temperatures of 150 F. The quantities adsorbed on different kinds of charcoal are listed in Table 4. Recovery was accomplished by heating to 500–700 F, whereby the SO_2 is removed in concentrated form. After the adsorption and desorption the charcoal can be used again.

It has been observed that the oxides of nitrogen are adsorbed ahead of the sulfur dioxide, and that they are gradually desorbed when the well-defined SO_2 adsorption boundary moves forward to the end of the column. Both oxides are concentrated in this process and existing methods of recovery could be applied without difficulty.

One of the best grades of charcoal adsorbs all sulfur dioxide from 2 ft^3 of flue gas, which means that at a rate of half a million ft^3/min of flue gas, one needs every minute $2^1/_2$ tons of charcoal. The possibility exists of accomplishing the adsorption in a flowing bed, as is being done for the separation of hydrocarbons by the petroleum industry. The conditions for sulfur dioxide adsorption are more favorable than for hydrocarbons because of the large quantities of SO_2 adsorbed. Some of the charcoals used adsorb as high as 30 per cent of their weight of sulfur dioxide at room temperature and 10 per cent at 150 F, notwithstanding the high water and CO_2 concentrations. A process of this type is expensive, as shown in Table 5, since a large sized bed is needed to effect good absorption and prevent pressure drop. In addition, losses in carbon occur in repeated adsorption and desorption. Although the adsorption power remains high, the loss in weight amounted to 20 per cent in fifty adsorption cycles. Nevertheless, there may be application for this type of control on smaller

Table 4 Adsorption of sulfur dioxide on charcoal

Charcoal*	Adsorption Temperature (°F.)	Flow Rate Ft.³/min.	Mgs. SO_2/g. Charcoal
A	77	0.1	153
	300	0.1	19
B	77	0.1	285
	150	0.1	127
	300	0.1	29
C	77	0.1	54
	300	0.1	30
D	77	0.1	244
	150	0.1	82
	220	0.1	62
E	77	0.1	143
F	77	0.1	253
G	77	0.1	225

* "A", "B", "C", etc., are code letters for the different charcoals tested.

Table 5 Cost comparison of recovery processes (single unit, 175,000 kw)

Process	Initial Cost	Annual Operating Cost (1)	Cost per Barrel
Catalytic SO_2 Oxidation Process with MnO_2 + O_3	$ 25,000,000.	> $ 3,000,000.	$ 1.40
Cyclic Lime Process (98% Removal)	3,000,000.	> 1,000,000.	0.50
Ammoniacal Liquor Process (90% Removal with Precipitator)	6,000,000.	2,000,000.	1.00
Ammoniacal Liquor Process (90% Removal without Precipitator)	5,000,000.	2,000,000.	1.00
Sodium Sulfite Process	4,000,000.	1,500,000.	0.75
Vanadium SO_2 Oxidation	12,000,000.	> 3,000,000.	1.40
Charcoal Adsorption	15,000,000.	> 5,000,000.	2.50
Desulfurization of Oil	?	2,000,000. (?)	1.00 (?)

(1) Includes chemicals, labor, maintenance, taxes, insurance, depreciation, and overhead.

Reference: Ira C. Bechtold
Report to Southern California Edison Co.
February, 1958

units when it is essential to obtain quantitative removal of sulfur dioxide and other gases.

Chemical Conversions

Many attempts have been made to convert sulfur dioxide into forms which would be easier to remove from the gas stream. Reduction to hydrogen sulfide and sulfur, as well as oxidation to sulfuric acid have been carried out. Because of the low concentration of sulfur dioxide in flue gas, coupled with the presence of excess air, reduction methods seem not very promising. Oxidation to sulfuric acid, on the other hand, is carried out in the wet scrubbing Fulham-Simon-Carves process, whereby the oxidation is catalyzed by manganese and iron salts.

Recently, a process was developed whereby the catalytic action of manganese salts is assisted through the presence of ozone. In our laboratories a 90 per cent oxidation of the sulfur dioxide in flue gas was accomplished with a commercial vanadium pentoxide catalyst. The resulting sulfuric acid was collected in a precipitator operating at a temperature of 280 F, yielding directly concentrated sulfuric acid of 80 per cent strength. Although in the pilot plant no interference from dust was observed, a large-scale process of this kind would probably require dust removal before the catalyst bed, increasing still further the cost of this process. Engineering estimates on both processes are given in Table 5. The operating conditions are as follows:

Vanadium Catalyst

1105 grams Monsanto Va Catalyst (T-748)
Bed: $15^1/_2 \times 3$ in.
Temp: 800–900 F
Rate: 3.5–4.0 cfm
Precipitation @ 300 F Acid: 75–85 per cent

The Control of Oxides of Nitrogen

In general, the oxides of nitrogen are more difficult to remove than the SO_2. Scrubbing with alkaline reagent removes only a part of the oxides of nitrogen, even though strong bases are used. The major portion of the oxides of nitrogen originate in the fixation of atmospheric nitrogen at the high temperatures of combustion. The rapid cooling of the gases is an important factor in the relatively high nitrogen oxide content of the stack effluent, since rapid cooling presents a shift of the equilibrium to the lower NO concentrations normally found at lower temperatures. It follows that a change in cooling rate or combustion temperature through changes in burner design or in the furnaces themselves might effect a considerable reduction in the nitrogen oxides formed. It was found that an important reduction in NO could be obtained when burning oil by operating with a deficiency of air through the burner auxiliary openings.

Recent developments indicate that by modifications in burners and furnaces, such as use of auxiliary sources of combustion air, elimination of approach cone plates, changes in burner throats, and relocation of burners, it will probably be possible to reduce the NO emission of existing front-fired furnaces by as much as 40 per cent, and of future front-fired boilers by 50 per cent. Arrangements are being made to test these possibilities on an operating unit at El Segundo.

Parallel with these investigations, attempts were made to develop a catalytic decomposition of the oxides of nitrogen into nitrogen and oxygen, as well as an oxidation to nitric acid. About forty catalysts were tested without noticeable success. Adsorption processes were also tried. Both charcoal and molecular sieve materials selectively adsorbed oxides of nitrogen, which could be partially recovered afterwards. In both cases, however, the cost seems prohibitive for application to a power plant. While thus far we have found no satisfactory catalyst, theoretical considerations predict that such a catalyst probably exists, and work is being continued.

In the course of studies on the reduction of stack effluents an urgent need was felt for an improvement in existing analytical methods for the determination of oxides of sulfur and oxides of nitrogen, as well as dust load. A thorough study of these methods led to modifications and standardizations which have been essential in the evaluation of the experimental work.

It is clear from the foregoing that no matter which process will ultimately be developed, the cost will be high. The return on valuable by-products will be small, and even doubtful when all fuel burners begin to recover sulfur and nitrogen oxides. There is also no doubt that there will be a demand for ever-increasing completeness of the control since the end of the population increase is nowhere in sight.

Such situations demand extraordinary methods, and one of these is the decision of all power generating agencies to work together to exchange information on anything that may lead to a solution to the problem of stack gas control. This decision is comparable to one taken several years ago in Pittsburgh when a council was formed by a group of people who had only one goal in mind—to clean up Pittsburgh. Forgetting private interests, these representatives of different industries prepared and carried out a campaign in air-pollution control, which resulted in a marked improvement in the Pittsburgh atmosphere.

In Los Angeles, the Joint Research Council on Power Plant Air Pollution Control has been operating quietly since March of 1956. Its members include representatives from all the power companies in this area, together with delegates from the Los Angeles and Orange County Air Pollution Control Districts. These men meet regularly to exchange information on the research program now under way and this in itself is a big step in the right direction.

Addendum

Since the presentation of this paper, the program on air-pollution control at the Southern California Edison Company has arrived at a point where research is being translated into engineering. Through a study of the economic feasibility of several control processes, the necessity for large and densely populated areas to use gas in power production has been clearly established. Steps have been taken to secure additional quantities of gas, and the necessary alterations for gas burning have been made at all Edison Company steam stations. At the same time, the pro-

gram has resulted in the development of several means of burning fuel oil within the legal limits of plume density.

A full-scale Western Electrostatic Precipitator is being constructed at a cost of close to one million dollars. This marks the first attempt on the part of industry to control the effluent from an oil-fired burner. On this unit, experiments will continue on the addition of alkaline reagents. It is anticipated that the removal of dust, plus some of the sulfur oxides, will eliminate any trace of visible plume except on rare days of cool temperature coupled with high humidity.

Studies on plume formation and on the feasibility of a reduction of stack temperature have shown distinct possibilities for a heat recovery process which may, to some degree, offset the cost of air-pollution control equipment and its maintenance.

Finally, ways have been found to obtain a drastic reduction in the formation of nitrogen oxides, an accessory in the formation of typical Los Angeles smog. During this time the accuracy and the reliability of the analytical procedures have been greatly improved. Instrumental analyses have been developed which are seen as a decisive factor in the reduction and control of oxides of nitrogen.

These accomplishments were made possible by the concerted efforts of many agencies who participated in the research program of the Southern California Edison Company. Among them were the Bechtel Corporation, the APRA Corporation, Truesdail Laboratories, and the Western Precipitation Company. In addition, helpful support was given by the California Research Corporation and members of the Joint Research Council, which include the Air Pollution Control Districts of the Los Angeles basin, as well as the other power companies.

References

1 A. J. Haagen-Smit, "Chemistry and Physiology of Los Angeles Smog," *Industrial and Engineering Chemistry*, vol. 44, no. 6, 1952, pp. 1342–1346.

2 A. J. Haagen-Smit and M. M. Fox, "Ozone Formation in the Photochemical Oxidation of Organic Substances," *Industrial and Engineering Chemistry*, vol. 48, no. 9, 1956, pp. 1484–1487.

3 A. J. Haagen-Smit and M. M. Fox, "Photochemical Ozone Formation With Hydrocarbons and Automobile Exhaust," *Air Repair*, vol. 4, no. 3, 1954, pp. 105–108.

4 E. R. Gerhard and H. F. Johnstone, "Photochemical Oxidation of Sulfur Dioxide in Air," *Industrial and Engineering Chemistry*, vol. 47, no. 5, 1956, pp. 972–976.

5 J. H. Field, L. M. Brunn, W. P. Haynes, and H. E. Benson, "Cost Estimates of Liquid-Scrubbing Processes for Removing of Sulfur Dioxide from Flue Gases." *Journal of the Air Pollution Control Association*, vol. 7, 1957, pp. 109–115.

6 E. C. Huge and E. C. Piotter, "The Use of Additives for the Prevention of Low-Temperature Corrosion in Oil-Fired Steam-Generating Units," TRANS. ASME, vol. 77, 1955, pp. 267–276.

7 F. S. Mallette, "Problems and Control of Air Pollution," Reinhold Publishing Corporation, New York, N. Y., first edition, 1955.

DISCUSSION

FREDERICK S. MALLETTE[2]

At the time of writing, the author was reporting on research by the Southern California Edison Company which had been under way for less than a year. Therefore, his paper is essentially a progress report indicating promising advance. It is unfortunate that the paper by Hotchkiss, et al., mentioned by the author is not being presented. Presumably it would have supplemented the discussion of the chemical aspects of the research with those more directly relating to mechanical engineering. For example, the Hotchkiss paper might have shed further light (or possibly Dr. Haagen-Smit himself may oblige) on the statement that ". . . . .after installation of full-scale units of this type, the plume will have largely disappeared." Experience indicates that, even when collection efficiencies are quite high, the resulting reduction in stack plumes is not entirely complete. Before complete disappearance of plumes which are composed of fine particles, collection efficiencies must approach 100 per cent.

Although the stated objective of the described research is praiseworthy—namely, to focus on the control of particulate matter and of the oxides of nitrogen as being most directly related to reduction of the over-all Los Angeles smog—it is not so certain that the results when obtained will result in the satisfaction of residents near the power plants. These persons, not so fully acquainted with the fine points of smog chemistry, believe that a visible plume—however reduced in magnitude—is a definite sign of pollution. It is to be hoped that the author's optimism is fruitful.

The principal hopes for reduction of sulfur-stack gases are the substitution of low-sulfur gas or oil for present fuels, the possible use (as a heroic measure) of wet-scrubbing, dry-scrubbing by alkaline dusts, or by adsorption methods.

The author has adequately presented the fact on the first two methods. I can only add that my own experience supports his findings regarding the influence of alkaline dusts commonly used to modify boiler slags. I have found no influence on sulfur dioxide, and while these dusts do combine with sulfur trioxide, the resulting product is more voluminous, difficult, or impossible to collect, and scarcely less corrosive.

Although it is too early to judge their exact place in the field of control, the possibilities of adsorption methods are intriguing. However, judging from experience in controlling odors, there is little doubt that they will be very expensive. Furthermore, the enormous gas volumes involved will require huge adsorption vessels, aside from the necessary gas-cleaning equipment.

Power plant effluents—even from a relatively high sulfur fuel—are still too lean for economical conversion to sulfuric acid. The day may come when native sulfur supplies are exhausted so that power plants can afford to recover that element, but at present it appears too far off to be of comfort.

If, then, available methods for the reduction or removal of sulfur are unattractive, the picture for oxides of nitrogen is even more so. However, it is more heartening to learn of the strenuous efforts on stack effluents by the Southern California Edison Company, especially as work on the problem on a large scale in this country has not been pursued energetically. So far, the British have spent more time and money on the problem of stack effluents, particularly on the sulfur gases, but now the problem must be faced by the large consumers of fuel here. The author's sponsors are to be complimented for their pioneering efforts. Further reports will be awaited with interest.

A minor correction: The reduction of smoke in the Pittsburgh atmosphere was brought about almost entirely by voluntary and involuntary changes in the domestic fuel pattern and not, as is commonly believed, by control of industrial effluents. Except in a few cases, such as the railroads where diesels replaced steam locomotives, industry in the Pittsburgh area has been, and still is, in violation of the local ordinance. Recent reports indicate that official pressure is being brought to bear on some of the large industrial offenders.

R. A. VANMETER[3]

It is always a pleasure to hear or read a paper by this author, who has so successfully brought his penetrating insight and productive talents to bear on diverse problems of air pollution.

[2] Executive Secretary, Committee on Air Pollution Controls, The American Society of Mechanical Engineers, New York, N. Y.

[3] Technical Assistant to the Chief, Division of Bituminous Coal, Bureau of Mines, United States Department of the Interior, Washington, D. C.

Through knowledge of the role of hydrocarbon vapors in Los Angeles air pollution gained from his own research he has led others, by stages, from initial skepticism of that role, through growing recognition, to the present widespread efforts by many competent scientists and technologists to reduce that role substantially. Characteristically, the author is again conducting pioneering research studies in another great class of combustion processes which he believes is a significant factor in urban air pollution. I feel confident that others will follow his lead, and that real progress will result from these efforts to control air polluting emissions from combustion in furnaces, at or near atmospheric pressure. Ultimately and hopefully, technology may be developed so that small commercial furnace units, and even household space heating units, may come under a measure of effective control of their stack emissions to the extent that atmosphere purity considerations dictate a need.

It is appropriate that the author has selected for his basic study in this field an industry that consumes prodigious quantities of fuel by burning it in a highly efficient manner. The electric utility is to be congratulated for its vision in instituting and so generously supporting this work, which I understand goes well beyond efforts for mere compliance with maximum legal emission levels.

This paper appears to be a sound interim appraisal of the stack-emission problem from a viewpoint of a particular power plant. Although many of the aspects apply to power plants in general, the character of the fuel, and the up-to-date design of the furnace and boiler are not typical of power plant installations across the country. It would be helpful on a national scale to have similarly conceived and executed studies for a major plant burning pulverized coal, another burning coal fed by spreader stoker, and yet another for a comparable gas-burning installation. Ultimately, it appears that similar studies should be made on typical smaller scale combustion installations, diversely fueled and fired.

This discusser is in complete agreement with the author that no simple and inexpensive panaceas are in sight to cure the remaining ills of noxious stack effluents. The skills and efforts of many competent scientists and engineers will be required to cope with the stack-effluent-control phase of maintaining urban air quality at satisfactory levels.

I should like to see developed more significant data for the content of such substances as CO and perhaps total organics in the El Segundo Station stack effluent. Since the Orsat-analysis value for carbon monoxide is reported to the nearest tenth of a per cent, it means to me only that CO, if present, was there to an extent less than 500 ppm. The manner of reporting the absence of aldehydes and organic acids leaves no insight into what might be maximum concentration values for these classes of compounds. It is believed that there are available techniques for concentration and ultimate quantitative determination of the types of compounds mentioned. In this day of recognition of the profound air-pollution-reaction effects of certain compounds when they are present in minute concentrations, we must be cautious in dismissing as insignificant in amount any possible products of combustion.

In closing, it has been a privilege to discuss this valuable interim report and survey paper.

AUTHOR'S CLOSURE

The Los Angeles Air Pollution Control District has determined the organic constituents at the Southern California Edison Company El Segundo Steam Station. The results are as follows:

Organic acids	7 ppm
Aldehydes	26 ppm
Hydrocarbons	13 ppm
Carbon monoxide	<1 ppm

From these data we calculate that, in burning 3000 tons of oil and producing 350,000 kw, the total organic material emitted to the air amounts to only 4 tons per day. It is interesting to compare this figure with that of the emission of the automobile in the Los Angeles area. The two and a half million automobiles, consuming 12,000 tons of gasoline per day, emit during that time about 1000 tons of organics. These figures show clearly the efficient combustion in a power plant as compared to the relatively poor performance of the automobile engine.

As a part of our research program pilot plants have been installed which are of such dimensions that a reasonable extrapolation can be made to a full-scale unit. In these units, designed for 5000 and 20,000 cu ft per minute, the plume disappears when the precipitator is operating at 90 to 95 per cent efficiency. We feel confident that under normal operating and weather conditions this will also be the case with a full-scale unit. It is almost certain that in cold and damp weather a plume will be formed when the dewpoint of the flue gas is reached. At that time, however, the plume is not due to dust but to sulfuric acid droplets. The precipitator does remove some sulfuric acid as metal sulfates. The intended addition of alkaline reagents has been shown to remove further quantities of sulfuric acid. Under these conditions the flue gas dewpoint is quite low, and weather conditions will therefore have less influence.

T. A. RICH

Consulting Engineer, Instrumentation, Engineering Physics and Analysis Laboratory, General Electric Company, Schenectady, N. Y.

Characteristics of Airborne Particles

Airborne particulates are primarily responsible for the visible effects of air pollution and contribute appreciably to the total mass of pollutants. A substantial fraction of the particulates is submicroscopic so optical methods are not suitable for following their life history. Techniques for measuring number and average size of submicroscopic particles over wide ranges have been developed but are not widely known or used outside the laboratory. A review is given here of some of the more useful parameters of particles and methods by which these can be measured.

Introduction

THERE IS A considerable body of scientific literature on airborne particles in which will be found a number of contradictions in detail and some fairly large discrepancies in the values of various constants. In general, the relations which have been derived in the literature apply to uniform aerosols. Under field conditions there is always a wide variety of sizes and usually a time variation in population which forces the use of approximations and averages. The approach here is to make simplifying approximations in the mechanisms involved so that the derivations are simplified. It is possible to make such assumptions because others have gone through a more rigorous solution which makes it possible to evaluate the assumption. The results given here are approximations and should be so regarded. In this field, one must not expect the precision of measurement associated with more established technologies.

The most important mechanism for the production of an aerosol is the condensation of a supersaturated vapor. A spark between silver contacts (on a relay, for example) vaporizes a minute amount of silver and, as this vapor cools, the silver condenses into numerous tiny particles. Opening a 10-amp, 110-volt, noninductive circuit may produce 10^{12} particles. Heating a liquid, such as oil, will produce a vapor above the surface that will form particles if the vapor is cooled. In a flame, many materials will be vaporized and subsequent cooling will produce supersaturation and the formation of particles.

The size of the particles will depend upon a number of factors, but mainly on how many centers of combinations exist in the first cooling and the length of time before dilution occurs. Once small particles are formed they tend to coagulate; that is, when two collide by random thermal motion they stick together.

The total number of particles in any one locality varies over very wide limits. An industrialized area may run around 50,000 particles per cc, while a busy airport may exceed 100,000, and in busy metropolitan traffic the count may exceed 500,000.

Junge [1][1] has suggested a "normal" distribution of natural aerosols that can be expressed as the number greater than a given size

$$C_{>r} \doteq \frac{K}{r^3} \tag{1}$$

where $C_{>r}$ is concentration of particles per cc with a radius greater than r; K = constant depending on total number in range of radii between 5×10^{-6} cm and 2×10^{-3} cm.

This can be plotted as in Fig. 1. The chances of finding such a distribution are most likely when the aerosol being measured is a mixture from many different sources.

The size distribution in any one situation can vary over wide limits, and Junge's relation gives us a standard of comparison rather than a "law" of size distribution.

The weight of material in a geometric interval is constant in the restricted range of sizes covered by the foregoing relation.

The size of particles in Dublin air is given as 2 to 4×10^{-6} cm radius by Prof. J. J. Nolan [2]. Particles formed from the

Contributed by the Power Division and presented at a joint session of the Power Division and the Committee on Air Pollution Controls at the Semi-Annual Meeting, San Francisco, Calif., June 9–13, 1957, of THE AMERICAN SOCIETY OF MECHANICAL ENGINEERS.

NOTE: Statements and opinions advanced in papers are to be understood as individual expressions of their authors and not those of the Society. Manuscript received at ASME Headquarters, April 1, 1957. Paper No. 57—SA-56.

[1] Numbers in brackets designate References at end of paper.

Nomenclature

C = particle concentration, number/cc
C_0 = initial concentration
K = proportionality constant
r = radius of particle, cm
w = weight, grams
ρ = density, grams/cc
H_E = relative humidity for water drop equilibrium
l = length of tube, cm
x = distance, cm
t = time, sec
D = diffusion constant, cm²/sec
n = number of particles
A = area, sq cm
U_h = velocity at h, cm/sec
h = radial distance from wall, cm
Q = flow, cm³/sec
R = radius, cm
F_d = fractional loss from diffusion, flowing
F'_d = fractional loss from diffusion in place, static
U_g = limiting velocity due to gravity, cm/sec
TC = time constant, coagulation loss, sec
i = small ion pair per cc
α = recombination coefficient of small ions (1.6×10^{-6})
λ = coagulation coefficient of particles
e = electronic charge, statcoulombs
k = Boltzmann constant (1.38×10^{-16}ergs/T)
T = degrees Kelvin
W = mobility $\left(\frac{\text{cm}}{\text{sec}} \text{ per } \frac{\text{stratvolt}}{\text{cm}}\right)$
C_c = concentration of charged particles of either sign, number/cc
C_u = concentration of uncharged particles, number/cc
$F\pm$ = fraction of particles charged with either sign
q = ion pairs per sec

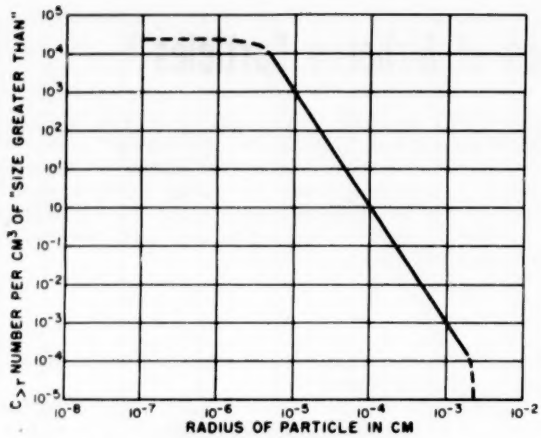

Fig. 1 "Normal" distribution of natural aerosols

photolysis of SO_2 or by sparking silver contacts in an air blast are numerically abundant with radii between 10^{-7} and 10^{-6}.

Measurement of Number of Particles

The easiest method of measuring the number of particles in an aerosol is to copy Nature by producing a fog and then to measure the fog density [3–8]. Water vapor will not condense on itself; it requires a particle to start with, and the smaller the particle the higher the relative humidity required. Condensation can take place on a flat water surface at 100 per cent relative humidity; in fact it is this property that defines relative humidity. The relative humidity for equilibrium is

$$H_E \doteq 100 + \frac{1.1 \times 10^{-5}}{r} \qquad (2)$$

when $r > 10^{-6}$. If the humidity is higher than this equilibrium value, the drop will grow.

When a sudden expansion produces a relative humidity high enough to start condensation on the particles, the water drops form rapidly. In several types of counters, the expansion chamber is lined with a wet blotter. The expansion cools the air (maybe 20 C), the excess water vapor condenses and heats the air (some 15 C). The blotter stays substantially at room temperature and water evaporates from it into the colder air, and it, in turn, condenses on the drops to heat the air further, so that in a few seconds both drops and air are substantially back to room temperature.

The growth of water drops is fast—a typical value of time to use up the water vapor available in a matter of milliseconds. The smaller particles grow faster than the large particles so that the final drops are all nearly the same size. It has been calculated [9] that two particles having radii in a 100 to 1 ratio produce water drops differing by only 1 per cent.

Attempts to determine the size of particles by Equation (2) have been disappointing. When the particle is anything but a water drop, correction factors must be applied that will be unknown in a natural aerosol, or even in most cases of artificially produced aerosols. The "condensation radius" can be defined as the radius of a water drop that would start to grow at the same supersaturation required by the unknown aerosol. This parameter can be useful in predicting the behavior of the aerosol under fog-forming conditions but it is not a reliable measure of physical size.

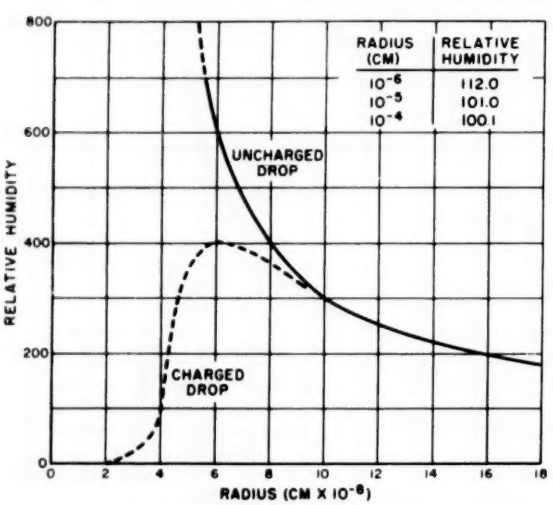

Fig. 2 Equilibrium humidities of water

Light Transmission

The scattering of light by small particles is a complex affair that has been treated at length in the literature [10, 11]. A dangerously oversimplified behavior is shown in Fig. 3 which presents the effective area per gram of water when subdivided in drops of the radius shown. In the larger sizes, the scattering is proportional to the total cross section of the drops as would be expected. In the very small sizes, the scattering follows Rayleigh's law. In the intermediate sizes, where the radius of the particle is in the neighborhood of the wavelength of the light by which the particle is being observed, the Mie theory applies. The variations in this region are more complex than is shown.

It would be convenient if one could use visual inspection to estimate the amount of material coming out of a chimney, for example, but a visual inspection will reflect only the presence of those particles in a comparatively narrow range of sizes. Undesirable gases may be present which contribute far more in mass than that which is observed. Small particles may grow to visible size owing to their hygroscopic properties under some conditions immediately on meeting the air, while under other conditions their growth might be retarded until dispersion left no visible plume. The emphasis on visual appearance by the public is understandable but it puts a premium on avoiding the appearance of an evil without necessarily making any improvement.

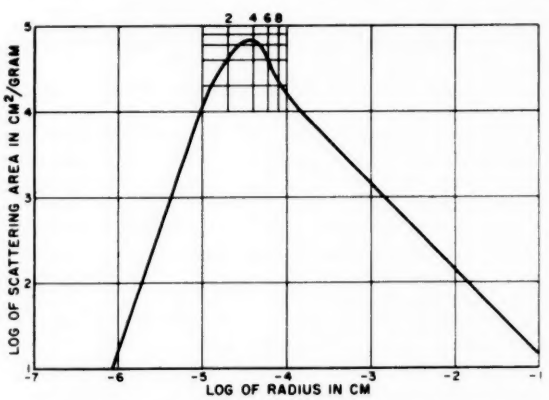

Fig. 3 Approximate light scattering effect of water drops

The cure of air pollution is difficult enough as it is without having energies diverted into possibly useless channels.

Diffusion

One of the useful parameters of a particle is its diffusion constant. Diffusion is commonly a property associated with a gas, and the particles of an aerosol can be treated like a gas of high molecular weight and very low pressure. The exception is that, unlike a gas, the particles stick together if they collide with one another and stick to the walls of a container if they hit it.

The particles are being bombarded continuously by air molecules, and have on the average the same energy as the gas molecules. Their path in still air is a series of jumps in a perfectly random fashion. The most probable distance (x) that such a particle would move in time (t) is

$$x^2 = 2Dt \tag{3}$$

where D is the diffusion constant. A more useful form gives the particles (n) per second crossing a plane in terms of the concentration gradient normal to the plane.

$$\frac{dn}{dt} = AD\frac{dC}{dx} \tag{4}$$

where A is the area of the plane and C is the concentration in particles per cc. An approximate expression for the value of D in air at normal temperatures is

$$D = \frac{12 \times 10^{-12}}{r}\left(1 + \frac{9 \times 10^{-6}}{r}\right) \tag{5}$$

where, as before, r is the radius of the particle in cm.

When an aerosol is passed through a tube, there will be a diffusion of particles to the walls of the tube so that there will be fractional loss in passage. This fractional loss is a function of size and can be calculated for a single-sized aerosol. The calculations are most unwieldy but an approximation can be obtained by the following assumptions: The air flowing through the tube has a laminar flow and the velocity at the walls is zero. The air at the entrance of the tube has a uniform concentration of particles. At all points on the wall surface the concentration is zero—on the quite valid assumption that particles that hit the wall will stick there and become part of the wall. An average path of particles might, such as sketched in Fig. 4(b). The particles are carried axially by the air flow and move radially owing to the difference in concentration between the core and the walls. We assume, for purposes of calculation, that the particles in a differential cylinder move axially only with the air flow to a point where the diffusion forces would produce an equal flow of particles in a radial direction, and that all those reach the walls. The concentration gradient is assumed to be uniform from this break-point to the walls. The velocity near the tube walls

$$U_h = \frac{4Qh}{\pi R^3}$$

The number of particles per second that enter the differential annular area is

$$2\pi(R - h)C_0U_h dh$$

This same number leaves the annulus over the length dx due to a concentration gradient $\frac{C_0}{h}$ governed by Equation (4). If h is small compared with R

$$2\pi RC_0U_h dh = 2\pi RD\frac{C_0}{h}dx$$

$$h = R\left(\frac{3\pi Dx}{4Q}\right)^{1/3} \tag{6}$$

The fractional loss due to diffusion F_d is equal to the particles lost to the wall per second divided by the number entering per second

$$F_d = \frac{\int_0^l 2\pi RD\frac{C_0}{h}}{Q\,C_0}dx = 5.2\left(\frac{\pi Dl}{2Q}\right)^{2/3} \tag{7}$$

If at time $t = 0$ the concentration is uniform throughout the tube, at a later time t it is assumed that the concentration increases from zero at the wall in a linear fashion to the original concentration at a distance h from the walls. The loss in number during the time t is half the original population in the annulus of which the gradient exists. The loss per second can be calculated by Equation (4). From these relations there results for the loss in the tube under static conditions

$$F_d' = \frac{2(Dt)^{1/2}}{R} \tag{8}$$

In spite of the approximations made, this value checks within 25 per cent of the results obtained by a rigorous treatment [12].

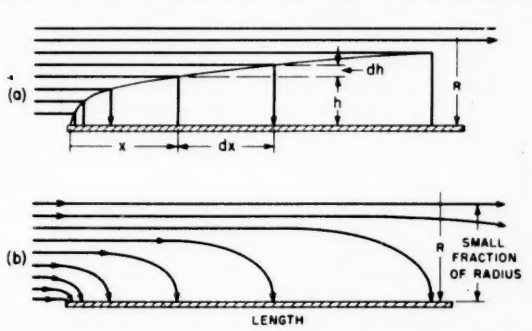

Fig. 4 Average diffusion (b) of particles and mathematical assumption (a)

Rate of Fall

The determination of size by the settling velocity under the influence of gravity depends directly on the density of the particles and this is rarely known. The limiting velocity in cm per sec at normal pressures and temperatures is given by (for unit density)

$$U_g = 1.2r^2 \times 10^6\left(1 + \frac{9 \times 10^{-6}}{r}\right) \tag{9}$$

Table 1 Limiting velocities

Radius of particle r in cm $\rho = 1.0$	Limiting velocity
10^{-3} cm	1.2 cm/sec ≡ 2.4 ft/min
10^{-4} cm	0.012 cm/sec ≡ 1.4 ft/hr
10^{-5} cm	1.2×10^{-4} cm/sec ≡ 1 ft/3 days
10^{-6} cm	1 ft/month

Equation (9) will apply to free air aerosols, of course. In Fig. 5 are shown the trajectories of particles of various sizes and Table 1 gives some limiting velocities. It can be appreciated from these figures why aerosols of any appreciable age have few particles greater than 2×10^3 cm as shown by Junge's normal distribution.

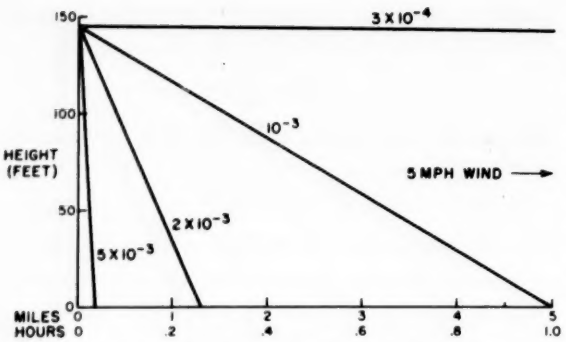

Fig. 5 Trajectory of particles of various sizes in air

Coagulation

In a monodisperse aerosol, when two particles approach within a center-to-center distance of $2r$, they stick together and two particles become one. It has been shown that

$$\left.\begin{aligned} \frac{dC}{dt} &= 8\pi DrC^2 \\ \text{or at NPT} \quad \frac{dC}{dt} &= 3 \times 10^{-10} C^2 \left(1 + \frac{9 \times 10^{-6}}{r}\right) \end{aligned}\right\} \tag{10}$$

A useful concept of doubtful ancestry is the "time constant" of an aerosol; that is, the time to decay to zero if the instantaneous decay rate were maintained

$$\mathrm{TC} = \frac{C}{\frac{dC}{dt}} = \frac{1}{3 \times 10^{10} \left(1 + \frac{9 \times 10^{-6}}{r}\right) C} \tag{11}$$

Table 2 shows the variation in time constant with radius and concentration. Equation (11) can be used for size determination whenever coagulation is the major source of decay.

Table 2 Time constant of aerosols

C	Radius in cm				
No./cm³	5×10^{-8}	10^{-7}	10^{-6}	10^{-5}	
10^8	0.15	0.33	3	15	Secs
10^7	1.5	3.3	30	150	Secs
10^6	15	33	300	1500	Secs
10^5	0.042	0.092	0.83	4.2	Hours
10^4	0.42	0.92	8.3	42	Hours
10^3	4.2	9.2	83	420	Hours

Electrical Aspects

Some of the particles in the air carry an electrical charge and the electrical forces between charged particles can have a substantial effect on coagulation rates. The older literature in particular reports some rather confusing evidence on the existence of charged particles. The most important source of particles in the sizes smaller than 10^{-6} cm is the condensation of a vapor. Probably most of these are born uncharged. If there is a luminous flame near their birthplace, they are likely to be charged by the ions in the flame or, if not then, a certain fraction will be charged in time by the ions produced by natural radiation.

Natural radiation varies from place to place. There is a component due to cosmic rays which is substantially the same over both land and sea, and a component due to radioactive material in the earth, probably radon. This radiation knocks an electron loose from an air molecule, leaving a positively charged molecule. The free electron is soon captured by another air molecule making a negatively charged molecule. Each of these charged molecules picks up a cluster of other uncharged molecules—probably water—resulting in a positive and negatively charged cluster of molecules known as a small-ion pair. Such small ions of the same sign of charge will not usually collide with one another because the electrical forces created on their mutual approach are greater than those due to thermal motion. Small ions of opposite sign collide more frequently than would be expected from their size and thermal motion. When there are i small ion pair per cm³, and no other particles

$$\frac{di}{dt} = \alpha i^2 \tag{12}$$

where α is the recombination coefficient (analogous to λ) for small ions. Its value is given as 1.6×10^{-6}. Equation (11) is the death rate of small ions in clean air. The birth rate may vary from place to place. Over land the value is often taken as 10 ion pair per cm³ per sec $\alpha i^2 = 10$ or $i = 2500$ in clean air.

These small ions have the same average kinetic energy as the air molecules $^3/_2\ KT$ or 6×10^{-14} ergs at normal temperature. If a particle is already charged, the work required to bring another charge to its surface would be e^2/r where e is the electronic charge 4.77×10^{-10} statcoulombs. When $r = 3.8 \times 10^{-6}$, the two quantities are equal, and so all particles this size or smaller should carry no more than one charge. An approximation of the fraction of particles charged with either sign as derived from Junge's theory is

$$F\pm \cong \frac{2}{3 + \frac{5.2 \times 10^{-6}}{r}} \tag{13}$$

This indicates that when $r = 5.2 \times 10^{-6}$ that $F = {}^1/_2$ or ${}^1/_2$ the particles are charged in equilibrium—for an aerosol of uniform size and which is singly charged.

The fraction of charged particles is an easily determined parameter of an aerosol and is an indication of size of particles. The number of particles can be measured in their original state and then passed through a strong electrical field to remove the charged particles and measured again. There are several derivations of the relation between size and the charged fraction and there are substantial differences between them. By varying the strength of field to remove successively particles of lower and lower mobilities, a distribution of mobilities can be obtained. Even if the exact function of size and mobility is somewhat dubious, a parameter is obtained which can be useful in comparing two aerosols.

Natural aerosol or new-born aerosols are sometimes not in equilibrium. An exposure to gamma radiation will bring about equilibrium quickly and is necessary in laboratory created aerosols in order to get consistent results.

Under the same assumptions as Equation (13), the number of small ions at equilibrium can be obtained approximately by

$$q \cong \alpha i^2 + (C_u r) i \tag{14}$$

Conclusion

Practical methods are available to measure the number of particles in an aerosol in free air. Indexes of size can be obtained from the properties of coagulation, diffusion, mobility, and limiting rate of fall. The sizes so obtained are strictly true for a nondisperse aerosol only; for a mixture of sizes an apparent radius is obtained which may differ from the average geometric radius.

Problems of sampling and measuring aerosols under high temperature conditions have not been completely resolved. A wider use of the techniques already available for size and numbers of an aerosol would not only throw light on some of the problems of air pollution but would certainly lead to further improvements in our knowledge of aerosols.

References

1 C. Junge, "The Size of Distribution and Aging of Natural Aerosols as Determined From Electrical and Optical Data on the Atmosphere," *Journal of Meteorology*, vol. 12, 1955, pp. 13–25.

2 J. J. Nolan and V. H. Guerrini, "The Diffusion Coefficients and Velocities of Fall in the Air of Atmospheric Condensation Nuclei," *Proceedings, Royal Irish Academy*, vol. 43, section A, 1935, pp. 5–24.

3 Scholz, "Ein neuer Apparat zur Bestimmung der Zahl der geladenen und ungeladenen Kerne," *Zeitschrift für Instrumentenkunde*, vol. 51, 1931, pp. 505–522.

4 J. Aitken, "On a Simple Pocket Dust-Counter," *Trans. Royal Society, Edinburgh*, vol. 18, 1890/91. Collected Scientific Papers, No. 18.

5 B. Vonnegut, "A Continuous Recording Condensation Nuclei Meter," Proceedings, First National Air Pollution Symposium, Stanford Research Institute, 1951, pp. 36–44.

6 T. A. Rich, "A Photo-Electric Nucleus Counter With Size Discrimination," *Geofisica Pura e Applicata*, vol. 31, 1955-II, pp. 60–65.

7 W. Holl and R. Muhleisen, "A New Condensation Nuclei Counter With Continuous Oversaturation," *Geofisica Pura e Applicata*, vol. 31, 1955-II, pp. 21–25.

8 L. W. Pollak, "A Condensation Nuclei Counter With Photographic Recording," *Geofisica Pura e Applicata*, vol. 22, Jan.-March 1952, pp. 22.

9 Private communication, S. B. Dunham.

10 J. A. Stratton, "Electromagnetic Theory," McGraw-Hill Book Co., Inc., New York, N. Y., 1941, pp. 563–573.

11 D. Sinclair, "Optical Properties of Aerosols," Handbook on Aerosols, U. S. Atomic Energy Commission, Washington, 1950, Chapter 7, pp. 81–96.

12 R. Furth, "On the Theory of Diffusion and Sedimentation of Condensation Nuclei in Cylindrical Containers," *Geofisica Pura e Applicata*, vol. 31, 1955, pp. 80–89.

DISCUSSION

EDWARD G. FOCHTMAN[2]

This paper has served to emphasize a factor in visual evaluation of stack effluents that is commonly overlooked. That is the presence of high concentrations of particles which are too small to scatter appreciable amounts of light but are sufficient in size to serve as condensation points for nucleation of liquid droplets. The effect of these nuclei upon the general air pollution situation may be considerable. As these materials diffuse throughout an urban area and are subjected to changes in temperature and humidity, they can serve to collect water and soluble gases which may react to produce a very stable and noxious particle.

It is my understanding that one of the objectives of this session was to evaluate the significance of stack plumes as an index of air pollution. Although the author has touched on this subject, a more thorough treatment would serve to emphasize the utility of visual measurements of stack plumes.

The visual evaluation of stack plumes for grayness or opacity can be done by most people after a few hours of instructions. To the best of my knowledge no one has related this Ringelmann number to any other measure of air pollution. This is probably due to the fact that visual measurements are not necessarily related to total weight of material in the plume. The factors affecting the Ringelmann measurement are many: Particle size, physical properties of the particles, angle of illumination, level of illumination, angle of viewing, contrast of plume with the background, diameter of the stack, and velocity of discharge, all have an influence on the relationship between the Ringelmann number and the amount of particulate matter discharged.

If there were a hypothetical area which was polluted with but one stack discharging a material of constant physical properties at a given velocity, and this were the only source of pollution, it seems likely that some relationship of general pollution level and Ringelmann number could be obtained. Since such a case is not likely to be encountered in practice we must resort to a system of averages of visual measurements and relate this to other means of pollution measurement.

As a test of the relationship between the level of air pollution as measured by dustfall gages and the amount of visual discharge, the 1953 smoke observation reports for the City of Chicago were examined.[3] These results are shown in Fig. 6. It may be noted that there appears to be a general trend in that when the smoke

[2] Supervisor, Chemical Engineering Research, Armour Research Foundation of Illinois Institute of Technology, Chicago, Ill.

[3] These results are a portion of a study sponsored by Midwest Air Pollution Prevention Association and reported at their Annual Meeting, November 9, 1954.

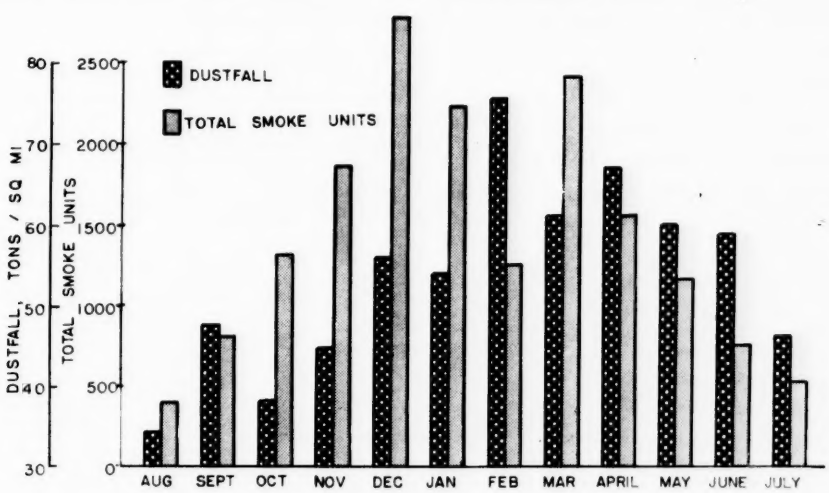

Fig. 6 Dustfall and smoke units by month

increases the dustfall increases and vice versa. These data are representative of the 10,000 smoke reports in the files of the Chicago Department of Air Pollution Control for the year 1953. This is presented as a possible trend only since many factors appear to influence both dustfall and Ringelmann readings.

In conclusion it should be noted that visual methods of assessing individual stacks as sources of air pollution are convenient, inexpensive, and probably worthy of continued use. They are not a basic scientific measure with absolute units and should be placed in their proper position in the array of air-pollution measurement instruments.

A. J. HAAGEN-SMIT[4]

For those living in the coastal area of Los Angeles it is a common sight to see pollution clouds blown out to sea during the night. These clouds extend quite far as has been measured by State and Federal agencies, and high oxidant values characteristic of Los Angeles smog can be found as far as Catalina and San Clemente Islands 20 and 50 miles off the coast. Early in the morning this cloud comes back as a sea fog, usually crossing the coastline somewhere near Venice and Playa del Rey. During that time, one can measure high oxidant values and oxides of nitrogen and sulfur while the wind is coming from the direction of the sea.

Using the author's nuclei counter we found a remarkable change in the number of condensation nuclei as soon as the polluted sea fog came rolling in. Early morning and night counts were usually high but as soon as the visibility started to decrease the counts dropped from as high as 100,000 to 10,000 per cc. I suppose that the condensation had removed a large amount of the nuclei.

I thought this was a good illustration of the fact that visibility has only an indirect connection with the nuclei count. There seems to be some misunderstanding about this and some people seem to think that the counters can be used as an objective measurement of haze. Would you clarify this point for us?

Plume formation from stack gases as well as formation of smog clouds due to chemical reactions start on a nucleus. The study of the initiation of the condensation reaction is therefore of great importance, especially to those interested in air-pollution problems. I hope that the author will clarify some points of practical interest. Is it feasible to reduce, for example, a plume from a boiler stack by reducing the number of nuclei or are there also so many that such a procedure would be hopeless? The reverse of this procedure would be to add so many nuclei that the condensed water droplets become so small that there is no scattering of the light. In other words, would addition of large numbers of nuclei make the plume disappear?

VINCENT J. SCHAEFER[5]

A proper understanding of the appearance and behavior of stack plumes is primarily dependent on the formation of nuclei from condensed gases, liquids, and solids, their growth within the stack, and the behavior beyond its top. The visible appearance of the stack plume is dependent on many complicated factors—some physical, some chemical, and interactions between them. The meteorological environment through which the plume moves determines some of these characteristics. The degree of stability in the air, its moisture content, and the number of condensation nuclei it contains are also of considerable importance. The position of the sun, the presence of high cloudiness, the degree of contrast between the plume, its surroundings, and the size and color of the individual smoke particles are all features which determine the appearance of stack plumes.

This paper is of much significance since it is concerned with the establishment of a better understanding of the fundamental nature of particles and their growth in an effluent, from its vapor state to the more or less stable liquid and solid aerosol particles, which emerge from the stack to form a plume. Until much more work of a similar nature is carried out, we will be confronted with ambiguous terms, poorly understood interrelationships and perplexing, confusing phenomena.

It is obvious that, until we have a better knowledge of the role played by individual particles and their growth while moving along a hot air stream both within and without a stack, much frustration is likely to result in our effort to understand what we see and try to measure. Basic studies of the sort touched upon by Rich's paper, presented in simple and intelligible language, is one of the most important needs in air pollution studies. It is to be hoped that much more work along this line will be undertaken.

AUTHOR'S CLOSURE

Neither the visibility of a plume nor the particulate count is a reliable index of the mass of material in it. Dr. Haagen-Smit's report on fogs brings out this point. Mr. Fochtman suggests that a more thorough treatment would emphasize the utility of visual measurement of stack plumes. The visual method is justified to pick up cases of inefficient combustion and gross pollution, but the value of visual methods alone in cases of efficient combustion is decidedly dubious. The visibility of light colored plume which is mainly water has little or no relation to the pollution contribution.

The Ringelmann number is the result of a complex of effects as is the level of pollution. If enough observations are averaged it may be possible to express one in terms of the other as suggested, but it does not follow that any single visual observation can be interpreted in terms of such an average.

Dr. Haagen-Smit's question on the practicality of removing nuclei or overseeding with nuclei is appropriate. The answer is probably both yes and no; with efficient combustion there are some stack conditions where the visibility of the plume might be reduced by nuclei control, but it would not be universally applicable. The visibility of the plume might be changed, but it would not reduce the total discharge.

[4] Professor of Biochemistry, California Institute of Technology, Pasadena, Calif.

[5] Director of Research, The Munitalp Foundation, Inc., Schenectady, N. Y.

Stage Performance and Radial Matching of Axial Compressor Blade Rows

JEFFREY WATKINS

Chief Analytical Engineer, Solar Aircraft Company, San Diego, Calif. Mem. ASME

To obtain the ultimate in performance from an axial compressor stage it is necessary that the operation of the blade rows comprising the stage be thoroughly understood. Appreciable advances have been accomplished in recent years, but much still remains to be done. This paper aims to present practical hypotheses concerning the nature of the flow between the blades and deals with design techniques in relation to this flow.

In addition, some elements of two-dimensional cascade data and a discourse on practical secondary flows are presented.

IN THE EARLY DAYS of the employment of axial compressors in gas turbines, average stage pressure ratios no greater than 1.150 were utilized. For aircraft applications it was of prime importance, however, to reduce the weight and size of the engine, and so it was necessary to raise the attainable stage pressure ratios and, at the same time, obtain higher through flows per unit of frontal area. This was made possible by not only an improved understanding of the axial matching of the compressor stages, but also by more effective radial matching of the stationary and rotating blade rows comprising the stage.

The advent of the transonic compressor at least proved that rotors could be designed to operate quite efficiently at these Mach numbers, providing careful attention was paid to the details of the design. Possibly the greatest virtue of this type of compressor is that it enables the middle and rear stages of a multistage machine to be designed to produce much higher pressure ratios without overloading, and without the necessity of increasing the diameter. Such compressors are operating today quite efficiently [85 per cent isentropic efficiency (η) or thereabouts at design point] with mean stage pressure ratios of 1.250 and flows per unit of frontal area of 30 lb/sec/sq ft or more. Single stage transonic units producing pressure ratios up to 1.800 are also being used today for small shaft engine applications, requiring relatively low flows per unit of frontal area.

These advances have been made possible by an improved understanding of the mechanics of compressor stage operation, but much still remains to be accomplished in this field.

Contributed by the Gas Turbine Power Division and presented at the Semi-Annual Meeting, Detroit, Mich., June 15–19, 1958, of THE AMERICAN SOCIETY OF MECHANICAL ENGINEERS.

NOTE: Statements and opinions advanced in papers are to be understood as individual expressions of their authors and not those of the Society. Manuscript received at ASME Headquarters, February 25, 1958. Paper No. 58—SA-21.

Two-Dimensional Cascade Performance

In the past, considerable effort has been spent in an endeavor to evolve forms of camber line and airfoil base profiles to satisfy flow conditions encountered by existing machines, or those deemed to be desirable in the general development of axial compressors. It was logical to believe that changing the position of maximum thickness of the base profile, and the position of maximum camber with respect to chord, in addition to changing the base ordinates of the airfoil profile, would alter the performance of the cascade with respect to Mach number and aerodynamic loading.

However, in this country it has been the practice to utilize the NACA 65 base profile almost exclusively, this having essentially a modified circular arc camber line with the position of maximum

Nomenclature

p = static pressure, lb/sq in. abs
ρ = air density, slugs/cu ft
T = total tdmperature, deg R
P = total pressure, lb/sq in. abs
g = acceleration given to unit mass by unit force
C_p = specific zeat at constant pressure, Btu/lb/deg F
γ = ratio of specific heats,
J = mechanical equivalent of heat, ft-lb/Btu

$\frac{\Delta H}{u^2}$ = work coefficient = $\frac{gJC_p\Delta T}{u^2}$

V = absolute air velocity, ft/sec
M = Mach number
u = blade peripheral velocity, ft/sec
i = incidence = air inlet angle relative to axial direction minus blade inlet angle, deg
δ = deviation = air outlet angle relative to axial direction minsu blade outlet angle, deg
ϵ = air turning angle, deg
α = air angle relative to axial direction, deg
C_L = lift coefficient
C_D = drag coefficient
H = blade span
C = blade chord
C = blade pitch
Δ = difference
O = blade throat width
ζ = blade stagger angle, deg
y = boundary layer radial displacement

ψ = pressure function = $\frac{gJC_p\Delta T'}{u^2}$

ϕ = flow coefficient = $\frac{V_A}{u}$

W = air weight flow, lb/sec

$\eta = \frac{T_1\left[(P_0/P_1)^{\frac{\gamma-1}{\gamma}} - 1\right]}{T_0 - T_1}$

Subscripts:

1 = rotor blade inlet conditions
2 = rotor blade outlet conditions
3 = stator blade inlet conditions
0 = stator blade outlet conditions
A = axial direction
θ = tangential direction
i = induced conditions
c = critical condition
fs = free stream
st = stalling

Superscripts:

$'$ = isentropic conditions
$*$ = nominal conditions

thickness at 40 per cent of the chord. In Britain the procedure has been to use a base profile derived from the old RAF section with the position of maximum thickness varying between 30 and 40 per cent of the chord and having a true circular arc camber line. Cascade tests have shown appreciable performance changes with variation in base profile and camber line geometry, but these changes have been somewhat obscured when incorporated in a compressor. With the advent of transonic and supersonic compressors, base profile and camber line geometry become more important. Some successful transonic compressors have been built using basic double circular arc type base profiles on a circular arc camber line.

Fig. 1 shows the two-dimensional performance of a cascade of airfoils operating at varying incidence and Mach number. The maximum lift/drag ratio occurs at an incidence dependent, at any Mach number, on the aerodynamic loading and the combination of camber and solidity necessary to achieve this loading. As the Mach number is increased, the incidence for maximum lift/drag ratio changes, being dependent on the cascade base profile, the shape of the mean camber line, and the nose radius.

Thick nose airfoils having circular arc mean camber lines demonstrate a tendency for the incidence at which maximum lift/drag ratio is obtained to increase with Mach number when the camber and solidity are high, e.g., in rotor blade hub sections. At low cambers and solidities, the maximum lift/drag incidence reduces slightly with increasing Mach number. The incidence giving maximum lift/drag for thin nose airfoil tends to increase for all cambers and solidities. The useful range of the airfoil is governed by the ratio of surface velocity to inlet flow velocity, which in turn defines the surface pressure gradients and hence the stall and choke characteristics of the airfoil. At high Mach numbers the effective range of the airfoil will be reduced. As the Mach number is increased, at a fixed incidence, the static pressure rise across a cascade, expressed as

$$\Delta p \Big/ \frac{1}{2} \rho V_1^2 \tag{1}$$

where

ρ = inlet density

and V_1 = inlet absolute velocity

either remains constant or increases slightly until a critical value M_c is reached after which $\Delta p \Big/ \frac{1}{2} \rho V_1^2$ falls until a maximum flow is reached. As the incidence is increased (mass flow reduced), at a constant Mach number, the ratio of blade throat area to inlet flow area increases, which reduces the velocity at the throat of the cascade, and so lowers the drag.

It is preferable to base critical Mach number on drag coefficient rather than on a static pressure rise basis. Sometimes with the higher values of ratio of throat area to inlet flow area $\Delta p \Big/ \frac{1}{2} \rho V_1^2$ tends to remain constant with increasing Mach number apparently suggesting a high value of critical Mach number. This may not necessarily be the case as $\Delta p \Big/ \frac{1}{2} \rho V_1^2$ would conceivably increase if there were not attendant critical effects over that region. The critical Mach number is taken for convenience to be the inlet Mach number at which, for any incidence, the drag coefficient has increased to twice the minimum value. Fig. 2 illustrates a typical polar diagram derived from two-dimensional cascade results to show the envelope of Mach number and air inlet angle bounding the region of efficient operation. At low incidences and Mach number, negative stall, i.e., flow breakaway from the pressure surface of the airfoil, will precede the true choking condition.

Some work has been completed and reported by Carter [1][1] on the effect on cascade performance of changing the position of maximum camber of the airfoil. Tests were carried out on a series of aerodynamically equivalent cascades of parabolic arc mean camber lines, varying between maximum camber at 30 per cent chord to 60 per cent chord. In addition, these blades were compared with an equivalent circular arc camber line. The following conclusions were reached:

a Moving the position of maximum camber forward gives a wider working range and a higher choking mass flow.

b Moving the position of maximum camber back gives a higher work capacity and a higher drag critical Mach number.

c There is little doubt that for use in conventional compressors, blades having their position of maximum camber at 50 per cent of the chord from the leading edge give the best all around combination of working range and good high-speed performance, provided adequate throat area can be maintained. It is possible

[1] Numbers in brackets designate References at end of paper.

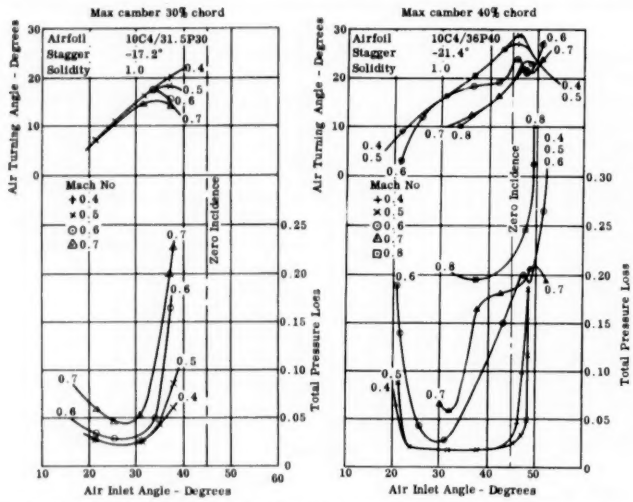

Fig. 1 Cascade characteristics—effect of changing position of maximum camber

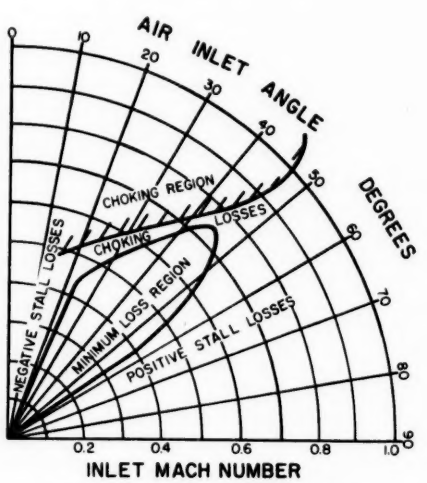

Fig. 2 Polar diagram of cascade losses

that blades having their position of maximum camber at greater than 50 per cent of the chord would be advantageous for high Mach number operation.

Fig. 3 summarizes the performance differences resulting from this change in maximum camber. An important feature is the reduction in optimum incidence as the position of maximum camber is brought forward, which factor coincides with a reduction in work capacity, and increase in choking mass flow. It is debatable whether an improvement in part load operation could be obtained by using blades of this type in the rear stages of an axial compressor. The lower work capacity of the section would necessitate the use of more stages, and the wide working range is not so pronounced at high Mach numbers due to shock stall.

At high speeds the main criteria of performance are the drag critical Mach number and the maximum Mach number. Fig. 3 shows that the former decreases steadily as the position of maximum camber is brought forward, due to the attainment of higher suction surface velocities at a fixed inlet velocity. It is desirable on this account to have the position of maximum camber as far back as possible.

Effect of Airfoil Nose Radius

Airfoil nose radius has an appreciable effect on cascade performance. It was previously mentioned that thick nose airfoils having high camber and solidity operate more efficiently at higher incidence as inlet Mach number is increased. Higher suction surface velocities occur for a given camber and solidity when the nose radius is large, and the increased incidence necessitates reduced stagger, which increases the throat area of the cascade and so lowers the acceleration in the passage. For the case of typical thick nose sections having low camber and solidity in conjunction with high stagger, such as at the rotor tip, the tendency is for highest efficiency to occur at slightly lower incidences as the Mach number is increased. In this case the higher suction surface velocity nullifies the increase in throat area at reduced stagger, necessitating some increase in blade inlet angle to minimize this surface velocity.

The acceleration around the leading edge of thin nose airfoils is less than for corresponding thick nose sections, and the tendency is for higher lift/drag ratios to be obtained at increased incidences at high Mach numbers. Similarly, it is feasible to expect that the high-camber high-solidity cascades would function in a like manner. This type of cascade, normally used for rotor hub sections, is seldom required to operate at high inlet Mach numbers, and the main concern of the designer is to obtain a section having sufficient throat area to pass the design flow efficiently. In this respect a relatively high incidence can be employed without fear of positive stall due to the large useful operating range at low Mach numbers. For conventionally loaded blades there should be no great concern regarding inferior part load operation with hub sections operated at high design incidence, due to the inherent range increase with blades of high solidity and low stagger.

At Mach numbers lower than critical it appears that the range of incidence from choke to stall is greater with the thick nose airfoil, due to the suction surface peak velocity occurring nearer to the leading edge. This reduces the suction surface pressure gradient and permits more stable operation at higher incidences.

Nominal Conditions

It is convenient for the designer to be able to utilize curves of turning angle and incidence plotted for a range of cascade geometries. Because of the difficulty of selecting the incidence and turning angle to give maximum lift/drag ratio, it is useful to utilize nominal conditions which correspond to the turning angle and associated incidence at 0.8 stalling turning angle, $\epsilon^* = 0.8\epsilon_{st}$. Reasonably accurate nominal rules for thick nose circular arc airfoil sections having a thickness/chord ratio of 10 per cent are:

$$i^* = \frac{293}{(\epsilon^*)^{0.7}} - 10.4 - 25.6\,S/C \qquad (2)$$

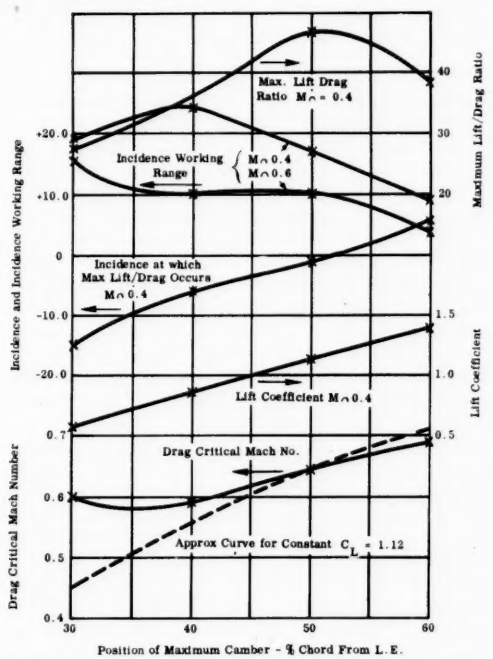
Max. Lift Drag Ratio M∞ = 0.4
Incidence Working Range
M∞ 0.4
M∞ 0.6
Incidence at which Max Lift/Drag Occurs M∞ 0.4
Lift Coefficient M∞ 0.4
Drag Critical Mach No.
Approx Curve for Constant C_L = 1.12
Incidence and Incidence Working Range
Maximum Lift/Drag Ratio
Lift Coefficient
Drag Critical Mach Number
Position of Maximum Camber - % Chord From L.E.

Fig. 3 Cascade characteristics conditions at working point for various positions of maximum camber

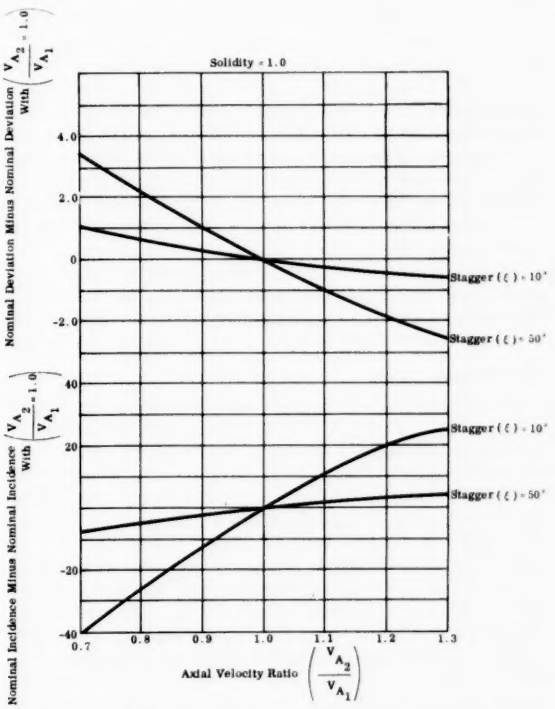
Solidity = 1.0
Nominal Deviation Minus Nominal Deviation With $\left(\frac{V_{A_2}}{V_{A_1}} = 1.0\right)$
Stagger (ξ) = 10°
Stagger (ξ) = 50°
Nominal Incidence Minus Nominal Incidence With $\left(\frac{V_{A_2}}{V_{A_1}} = 1.0\right)$
Axial Velocity Ratio $\left(\frac{V_{A_2}}{V_{A_1}}\right)$

Fig. 4 The effect on nominal incidence and nominal deviation of changing axial velocity across cascade

$$\delta^* = (0.42 + 0.004\,\alpha_2^*)\epsilon^* S/C \qquad (3)$$

where

i^* = nominal incidence
δ^* = nominal deviation
ϵ^* = nominal turning
α_2^* = nominal outlet air angle
S/C = pitch/chord ratio

It is of greater value to define the nominal conditions as those producing 80 per cent of the maximum static pressure rise at a constant axial velocity ratio across the blade row. If the outlet axial velocity falls relative to that at the cascade inlet, the nominal incidence will fall, and simultaneously there will be an increase in the deviation and therefore in air outlet angle. Reducing axial velocity across the cascade increases the airfoil aerodynamic loading and causes stall to occur at a lower incidence. The revised nominal conditions shown in Fig. 4 allow for this effect.

It is necessary for the designer to know also the variation in optimum incidence and turning with Mach number. He should be able to evaluate the critical Mach number for any cascade geometry, in order to choose the most desirable design conditions.

Cascades in Three Dimensions

A knowledge of two-dimensional flow over a cascade of airfoils is not sufficient to determine fully the performance of the airfoil when operating either in a static or a rotating blade row in an axial compressor. However, many designers rely on two-dimensional data to select the blade profile and blade setting angles of the rotors and stators with very good results. The tendency in axial compressors is for flow discrepancies to be rectified by the self compensating nature of the flow.

In a static or rotating blade row, the boundary layer on the end walls and on the blade surfaces themselves will modify the ideal two-dimensional flow, and, in addition, will induce radial flows with the formation of vortexes and attendant higher losses. To allow for these complex flows the designer has for convenience used empirical factors to modify (*a*) the work requirement from the stage or (*b*) the annulus area necessary for a certain mean velocity or (*c*) the radial efficiency distribution, and so on.

Compressors today have more stringent requirements concerning flow per unit of frontal area and work output per stage, in addition to the need for light weight. Considerable advances have been made in recent years by a more thorough knowledge of flow patterns in the machine.

To bring about appreciable reduction in the secondary losses would appear to be an impossible task, and the best one can do is endeavor to maintain the existing losses with the higher aerodynamic loadings necessary today.

Stator Secondary Flows

To analyze secondary flows even in nonrotary blade rows is not an easy task. However, some conclusions can be obtained by considering the adjacent blades to be the bounding walls of a curved channel.

A pressure gradient will exist across the passage from the suction to the pressure surface which, in the main stream, will balance the centrifugal force exerted on particles of fluid describing the path. The pressure will be greatest on the outer wall (pressure surface) and least on the inner wall (suction surface). Owing to the boundary layer on the annulus walls, the fluid in their neighborhood will have less velocity, and so will require a smaller pressure gradient to sustain equilibrium. The pressure gradient, however, will not be changed by the existence of the boundary layer, and an out-of-balance condition will exist, resulting in a crossflow from the pressure surface of one airfoil to the suction surface of the adjacent airfoil. This crossflow will occur at both end walls in the case of shrouded stator blades. It is significant that from a correlation of limited available stator deviation data, the reduction in deviation which should result at the outer wall from the secondary flows described above was not apparent. In fact, the data indicated that appreciably increased deviation existed at the stator outer diameter, and some reduction at the inside diameter.

Because of the finite length of the blade, axisymmetric entropy variations and of nonuniform inlet flow conditions, vortexes will exist immediately downstream of the trailing edge. The vorticity will be concentrated chiefly near the ends of the blades, and being unstable will roll up into two trailing vortexes, and their presence will be indicated by cores of high loss in traverses taken downstream of the blade.

In the case of cantilever stators where relative motion exists between the blade and the inner end wall the scraping flow on the pressure surface replaces the tip clearance vortex by a less well defined roll-up near the pressure surface. The scraping minimizes the possibility of flow occuring from the pressure surface into the clearance region. Carter [1] suggests that the induced incidence at the blade mid-span resulting from the existence of the trailing vortexes can be evaluated approximately by

$$i_i = \frac{1}{4}\,\frac{C_L}{S/C}\left(1 - \frac{h'}{H}\right) \qquad (4)$$

where

h' = distance between the vortexes (cores of loss)

and

h = span of blade

In like manner the induced drag can be represented by

$$C_{Di} = \frac{1}{4}\,\frac{C_L^2}{S/C}\left(1 - \frac{h'}{h}\right)\frac{h'}{h} \qquad (5)$$

The distance h' may be measured experimentally as the distance between the peaks of high loss.

Rotor Secondary Flows

Although measurements behind rotating cascades have shown incidences and deviations at design to agree closely with those predicted from two-dimensional cascade tests, it is expected that the secondary flows existing within the rotor blades would be appreciably different from those in the stator. These differences are due to the centrifuging action of low energy regions in the hub casing boundary layer and on the blades themselves. It is likely that the induced secondary flows near the rotor hubs with cantilever stators (moving inner wall) would not be the same as with shrouded stators where the hub casing boundary layer is constantly interrupted.

Pressure readings behind moving blade rows, measured by rotating rakes, have indicated the nature of rotor secondary flows at low speeds. At high speeds the hot wire anemometer has been a useful tool to indicate low flow regions.

At the hub of the rotor at low speeds, high loss regions exist near the suction surface of the blades, and as the angle of incidence is increased the region extends to engulf the wake of the blade. This crossflow is similar to that exhibited by stationary blades, and is caused by the hub casing boundary layers. The retarded region is not greatly discernible at blade sections other than the hub.

The blade mean section measured loss profile is not much different from that of the equivalent two-dimensional cascade, except at high angles of attack when the wake widens appreciably on the suction surface possibly due to centrifuging of the separated inboard blade section boundary layer, along the low

pressure surface. This phenomenon has been observed by Ruden [3] and Weske [4].

Near the blade tip, loss regions exist from the viscous interaction effect of the blade and the casing boundary layer. These loss regions are manifest, in addition to the blade wake, near the pressure surface. This is in contradistinction to conditions existing at the hub, where the high loss region moves toward the suction surface by the action of the cross blade pressure gradient. At the tip the pressure gradient is apparently overcome by viscous effect. As the incidence angle is increased, the blade wake widens and spreads toward the center of the passage.

In the case of shrouded stators where alternate rotating and stationary shrouds exist, at the blade root, the hub casing boundary layer is constantly parted, which implies that a greater force is needed to turn the boundary layer than in the case of cantilever stators. The controversy of shrouded versus cantilever stators has existed for some time without any definite conclusion as to the relative merits of one over the other. British practice has been to utilize cantilever stators in all stages except the first three or four. It is of interest that a compressor originally containing cantilever stators throughout except for stages 1 to 4 when modified to include shrouded vanes in stages 5, 6, and 7 in addition, showed a marked decrease in surge pressure ratio in the middle and low speed range, characterized by a distinct region of discontinuity.

Fig. 5 shows the over-all pressure loss compared with the equivalent two-dimensional cascade loss at different radii for an intermediate and for a high incidence angle. It will be observed that at the lower incidence angle the hub wake has been partially centrifuged, while at the higher incidence it has been centrifuged to such an extent as to raise the loss over that of the cascade at all radii.

At high speeds, hot wire anemometers have indicated a somewhat different three-dimensional picture. The conventional blade wakes have been observed at radial positions near the midspan of the blade. At sections close to the tip, however, a region of high loss has been shown to exist in addition to that contributed by the wake, and considerably larger in magnitude than

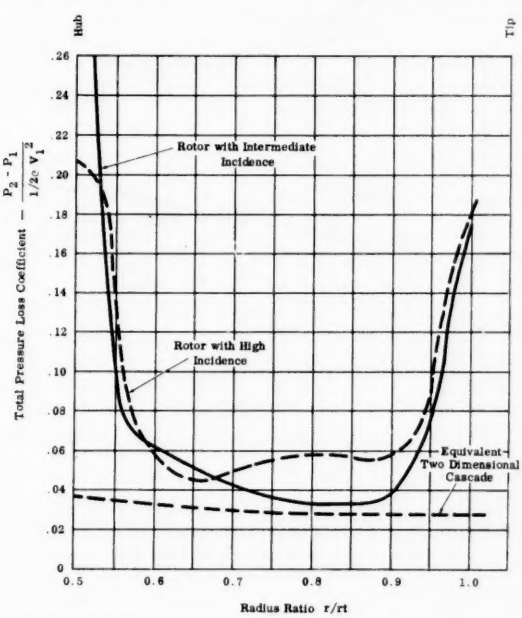

Fig. 5 Losses behind compressor rotor, measured with rotating rake, for two angles of attack

the scraping loss observed at low speeds. At operating conditions near choke, the region of loss lies close to the suction surface of the blade, but as the incidence angle is increased toward stall the loss region increases in magnitude and extends into the space between the blade rows, and, close to stall, exhibits pronounced instability. No indication of the high loss region near the pressure surface was apparent as in the rota ting pressure rake tests at low speeds. The reason for this high loss has not been satisfactorily resolved. Whether it is the result of interaction between the centrifuged blade boundary layer and the tip clearance vortex, or a combined Mach number aerodynamic loading effect, is uncertain. It is fairly clear, however, that the magnitude of the loss is reduced as the loading and Mach number are lowered, and this, to the designer, is all important.

Radial Matching of Blade Elements

It is of prime importance to the designer of axial compressors to know how much he can rely on simple two-dimensional cascade performance, and the modifications, if any, he has to introduce to arrive at a satisfactory blade solution in three dimensions. Some knowledge of secondary flows is an advantage, but basically he only needs to know (*a*) how these affect the two-dimensional performance and (*b*) when they commence to become the major contribution to the over-all losses.

It is likely that as the aerodynamic loading of the blade is increased, the secondary losses become a greater percentage of the whole. In other words, once a certain limit of two-dimensional loading has been reached, further loading will increase the secondary losses at a greater rate than the profile loss. This is borne out by the work on transonic compressors, when stage loading has been raised simultaneously with inlet Mach number. The increase in secondary loss described previously, at the rotor tip, appears to grow out of proportion to the blade wake loss.

There is little doubt, however, that the profile and the secondary losses will advance together, the latter being chiefly the result of interaction of the boundary layer on the annulus walls and blades, and the static pressure gradient between two adjacent blades.

It is imperative that the designer should know when to expect the two-dimensional and three-dimensional losses to increase disproportionately, but it is equally important that he should know how to match the stages both axially and radially to achieve satisfactory performance over the whole speed range. It is true that, if he designs his blade rows to be too heavily loaded, or if he lays out inadequate sections for the Mach number at which they are to operate, he will obtain a low level of efficiency at high speeds. If, on the other hand, he correctly loads his blade rows but matches them incorrectly, he may obtain a low level of efficiency at all speeds.

Radial Variation of Tangential Velocity

Successful compressors have been designed over a wide range of vortex types, from free-vortex to constant reaction. Early compressor designs tended toward the free-vortex principle; however, because of the then existing limitation on entry Mach number of 0.8 to 0.85, which was no doubt necessary with the thick-nosed sections employed at the time, the trend swung toward the reaction type. This was desirable to obtain higher stage pressure rise, in addition to increasing the flow per unit of frontal area. At this period the first stage rotor hub was the limiting section, and, with the tip Mach number fixed at the aforementioned value, a stage pressure rise was chosen so that the hub operated at just below its critical Mach number. Figs. 6 through 9 show the radial variation of rotor inlet Mach number and air turning angle for blades of different vortex type, satisfying the principle of simple radial equilibrium. It is seen that the major differences in angle occur on the stator and at the hub of

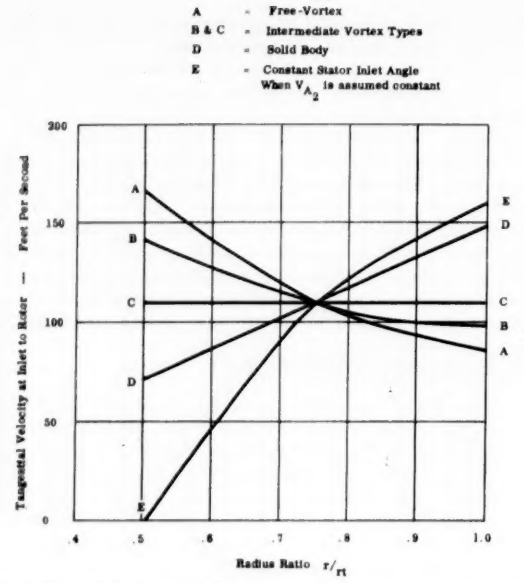
A = Free-Vortex
B & C = Intermediate Vortex Types
D = Solid Body
E = Constant Stator Inlet Angle
When V_{A_2} is assumed constant
Tangential Velocity at Inlet to Rotor — Feet Per Second
Radius Ratio r/r_t

Fig. 6 Tangential velocity distributions corresponding to air angles and Mach numbers of Figs. 7, 8, and 9

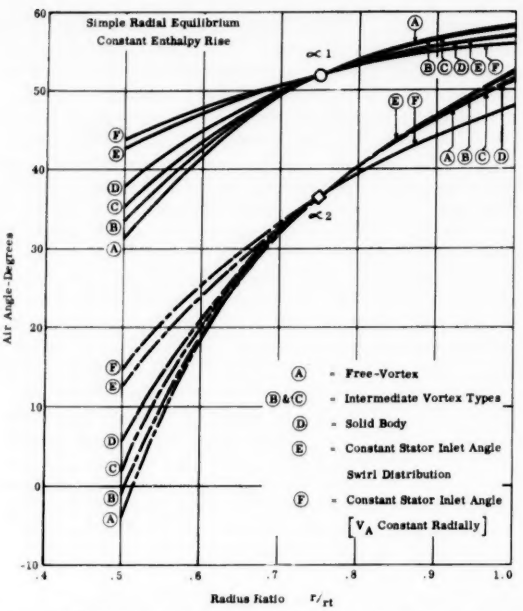

Fig. 7 Air angles at inlet and outlet of rotor blades, with different tangential velocity distributions

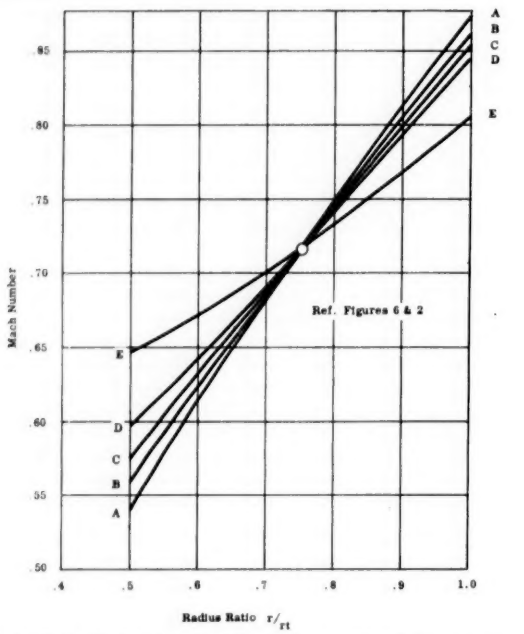

Fig. 8 Rotor blade relative Mach numbers with different tangential velocity distributions

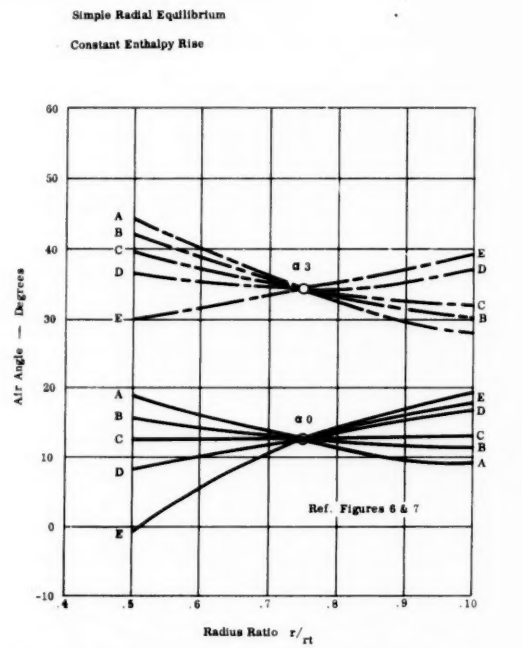

Fig. 9 Air angle at inlet and outlet of stator blades with different tangential velocity distributions

the rotor. It is obvious that, when radial equilibrium is considered, vortex type in itself is not a major design criterion, and should be subordinated to the achievement of satisfactory aerodynamic blade sections with representative flow conditions at the design point. Even a combination vortex type will perform satisfactorily if loading criteria, operating incidence, Mach number limitations, and other design factors are carefully observed.

Most early designs were based on the concept of radially constant axial velocity and enthalpy rise, although the condition of radial equilibrium suggested that considerable gradients of axial velocity should exist. Detailed flow traverses confirmed that velocity gradients did in fact exist, and that they approximated the simple radial equilibrium rule when an allowance was made for stream tube curvature. Fig. 10 shows the radial velocity variation based upon flow measurements at exit of a typical compressor first stage rotor which had been designed on reaction

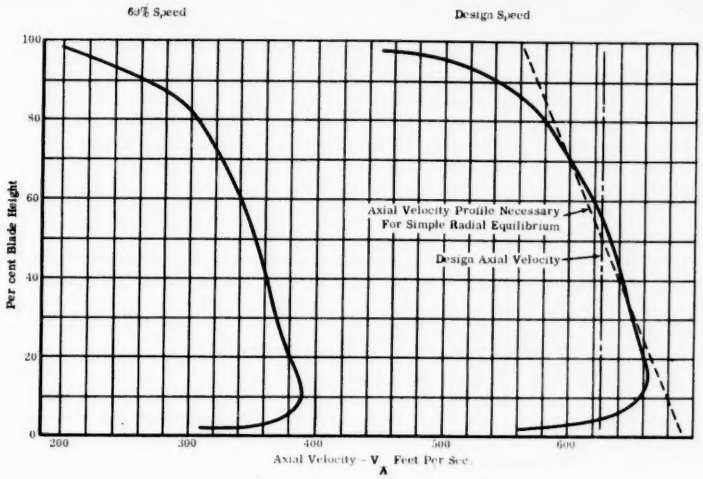

Fig. 10 Measured axial velocity at exit of a first stage rotor

principles but with the assumption of radially constant axial velocity.

It is evident that such a rotor blade would operate with higher than design flow incidence at its tip section, and lower incidence at the hub. This would result in the establishment of a radial gradient of enthalpy rise—a higher value occurring at the tip, which would operate nearer to stall at design, and the converse at the hub. The enthalpy gradient would have the effect of straightening the velocity profile from that necessary for radial equilibrium with design enthalpy rise. However, the following stator blade would still experience a higher than design incidence at its outside diameter, and vice versa at the inside diameter. This process would be repeated in the succeeding stages until the flow finally settled to a steady condition where constant enthalpy rise would be obtained at all radii. With blades of low hub-tip radius ratio, impaired stage operating range would, no doubt, result.

Recently, high performance machines have been designed to satisfy the condition of simple radial equilibrium with some empirical correction allowing for stream curvature. Also a number of very successful transonic compressors have been designed which incorporate the principle of free-vortex flow. In this case the rotor tip entry Mach number was raised into the transonic regime and the blade tip loading was minimized by employing free-vortex tangential velocity distributions. Higher blade peripheral speeds were employed, which partially offset the original free-vortex requirement of higher rotor hub turning angles for a given temperature rise. In addition the higher blade tip speeds enable more work to be obtained from the intermediate and rear stages where the design point Mach number is not so critical. In the case of the first rotor a transonic Mach number can be employed without the rotor mean effective Mach number becoming excessive. It has been established that transonic compressors can be very efficient, but most designs exhibit the tendency to lose efficiency very rapidly once the tip inlet Mach number has exceeded unity. This is not always the case, however, as some machines have produced high efficiencies which show no sign of deterioration until speeds in excess of design are reached.

Total pressure ratios of around 1.800 can be obtained with over-all isentropic efficiencies of the order of 83 per cent in relatively high hub to tip radius ratio single stages, with rotor inlet relative Mach numbers of 1.35 or thereabouts. To achieve this performance the aerodynamic loading of the rotor blades must be limited by a satisfactory selection of area ratio across the blade row, combined with the necessity to restrict the stator entry Mach number to a maximum of 0.8.

Stage Performance

The performance of a compressor stage may be represented as shown in reference [4] by the pressure function

$$\psi = \frac{gJC_p\Delta T'}{U^2} = \frac{gJC_pT_1}{U^2}\left[P_0/P_1^{\frac{\gamma-1}{\gamma}} - 1\right] \qquad (6)$$

where

T_1 = total temperature at stage inlet
$JC_p\Delta T'$ = isentropic total enthalpy rise
P_0/P_1 = stage total pressure ratio
γ = ratio of specific heats

and

$$\phi = V_A/U \text{ or flow coefficient} \qquad (7)$$

where

V_A = axial velocity at rotor entry
U = blade peripheral speed

Much use has been made in the past of this method of presenting the stage performance, and a great deal of successful development has been based on the method, which necessitates knowing only the stage static pressures at the various running conditions

There is little doubt that the appearance of the stage characteristics is greatly influenced by the blade geometry at all radii, and is not merely a function of that at the mean section. Design section characteristics based on cascade results for a typical moderately loaded, fairly high hub-to-tip ratio compressor stage at the tip, mean, and hub are shown in Fig. 11. It is seen that the tip section possesses a somewhat more peaked characteristic, compared to that at the hub which is relatively flat. This is due to the nature of the velocity triangles. At the tip, where the blade speed is high and tangential velocity difference small, changes in axial velocity result in marked differences in the ratio of $\Delta V\theta/U$ (work coefficient) whereas, at the hub, little change in this factor results from varying the axial velocity. For highly loaded hub sections where the relative leaving angle from the rotor is in the direction of rotation, the work coefficient will diminish as the axial velocity is lowered. The range of the characteristic, from the peak pressure stalling value to choke, is dependent on section aerodynamic loading and operating Mach number rela-

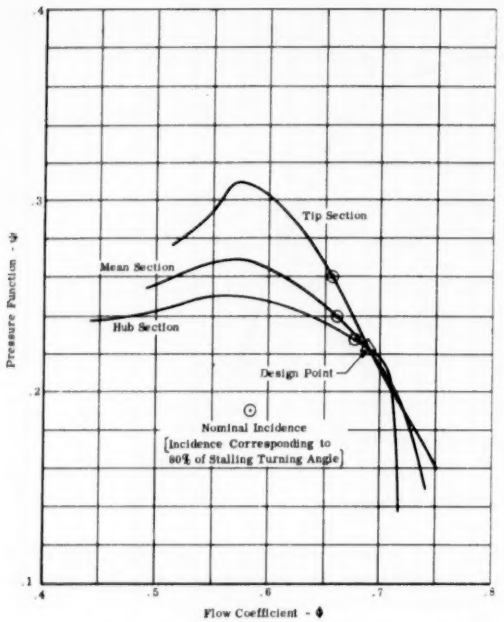

Fig. 11 Stage section characteristics computed from two-dimensional cascade tests

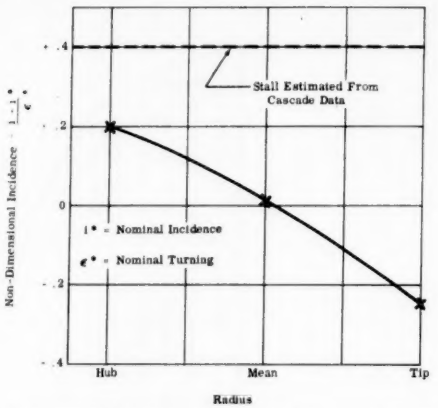

Fig. 12 Incidence of first stage rotor designed to prevent premature tip stall

tive to the section critical value. Hence at high stage pressure ratio, the range of the tip section on a velocity basis will be reduced relative to that at the hub when reaction blading is employed instead of free-vortex.

The matching of the radial blade elements is of prime importance in the appearance of the stage characteristic and, under ideal flow conditions, this is no great problem. In an actual machine, however, the flow is far from ideal; wake fluctuations, boundary layers, and the attendant three-dimensional flows make the problem more complex.

The reduction in velocity due to casing boundary layer is quite critical at the blade tips and in many instances effective stalling exists even at the design condition. Large pressure losses occur, but the blade section enthalpy rise increases, raising the temperature and stabilizing the flow.

To allow for the loss in pressure, compressor designers use either a workdone factor in the Euler equation or an empirical flow factor in the computation of annulus area. Both methods have produced extremely successful designs.

Some attempts have been made to design compressor stages for velocity profiles based on computations or measurement. Redesigning blades based on measured profiles has resulted in little success. The difficulty is largely due to the influence of the energy gradient in stabilizing the flow, and unless the redesigned blade can be made to produce the original radial energy variation, the velocity profile will change and bear no resemblance to the one originally measured and used as a basis of redesign. In this case the matching could feasibly be impaired.

Some work has been done in an effort to compute the velocity profile by the substitution of an entropy term in the radial equilibrium equation. This effectively produces the expected velocity profile, if the pressure losses are known.

A philosophy of considerable merit is to design the controversial end sections to give the same enthalpy rise as the rest of the blade with the velocity gradient necessary for corrected simple radial equilibrium, but with incidences appreciably smaller than optimum for the section. The reduction of incidence would be determined by the velocity profile to be expected in the boundary regions. It has been established that the simple turbulent pipe flow law of von Karman satisfactorily defines the velocity gradient in the annulus boundary layer of an axial compressor at the condition of steady state.

$$V = V_{ts}\left(\frac{y}{y_{ts}}\right)^{1/7} \tag{8}$$

where

V = velocity in the boundary layer
V_{ts} = velocity at maximum displacement of boundary layer
y = boundary layer radial displacement
y_{ts} = boundary layer maximum radial displacement

In the early stages the boundary layer is not fully developed, and this simple law cannot define it with any accuracy. The adequacy of the constant enthalpy pipe flow formula after stabilization apparently derives from the inherent tendency of the blades to produce enthalpy gradients which counterbalance the natural velocity reduction associated with blade end pressure losses.

Designing the blade ends in this manner allows the sections to operate at lower incidence even with the reduced velocity, and still produce the necessary enthalpy rise for stable flow. Fig. 12 shows the relative matching of the hub, mean, and tip of the rotor blade to achieve this effect.

It is emphasized that for highly loaded blades the range of the tip section becomes relatively small and peaked, and large changes in design incidence would be needed to counteract the boundary layer velocity gradient. This may necessitate a considerable increase in camber and/or stagger at the tip, with an attendant reduction in flow area between the blades. In this case radial inflow may occur, particularly in the stators, where the camber at the outside diameter is already high, and a further increase may result in a relatively large reduction in throat width tending to offset the improved effect of incidence.

This method of matching has been used with considerable success, and has resulted in the production of smooth-stalling single-value stage characteristics.

The Stage Characteristic as a Function of the Rotor Radial Elements

As the mean flow coefficient is increased, radial enthalpy gradients are set up inducing outward radial flows which tend to delay the onset of tip stall beyond that indicated by two-dimensional cascade data for the same local incidence. The outflow effectively reduces the angle of incidence and changes the flow path across the tip section, both factors reducing the tip aerodynamic loading.

The stalling mechanism has been covered by numerous authorities, and the blockage theory of Marble [5] appears to describe the phenomenon adequately. Reduction of the mean flow coefficient will induce the formation of stall zones at the radial location which possesses the highest local stalling flow coefficient. Stall zones have been seen to appear first at both hub and tip. In most conventional correctly loaded, well matched stages, however, they occur first at the tip, even when the stage has been designed on the reduced incidence principle described previously. Additional stall zones will appear as the mean flow coefficient is further reduced until the air flow can no longer negotiate the circumferential obstruction, and will flow radially inward on entering the blade passage, causing an increased flow across the midspan of the blade. This results in the mean section operating effectively at a locally increased flow coefficient, and hence a reduced pressure rise will occur. The reduced flow through the tip section will further increase the local incidence, adding to the lowering of the pressure ratio. The net result is a tendency for the stage pressure rise to lessen abruptly at some mean flow coefficient, when the tip stall has sufficiently progressed.

Abrupt stall will also occur if the rotor hub section stalls first. In this case stall will be effective at a higher mean flow coefficient and will cause premature surge in a multistage machine. It is likely that the use of shrouded stators induces premature hub stall and causes more inferior intermediate and low speed surge lines than those of equivalent cantilever stators.

Rotor blades of low hub-to-tip radius ratio will possess a wide variation in operating range between the hub and tip sections, due to the large difference in stagger angle and hence ratio of throat to pitch widths. It is believed that this type of blade will stall progressively with a minimum pressure discontinuity if the tip is matched at design point to have negative incidence relative to that for optimum lift-to-drag ratio. This is, of course, difficult to accomplish in transonic compressors where it is necessary for the high Mach number tip section to operate at design with relatively high incidence, if design point efficiency is to be obtained. This is one of the penalties the designer incurs when he reduces the section operating range by running with high inlet Mach number. As mentioned previously, however, the thin nose sections employed in transonic designs tend to stall at higher incidences as Mach number is increased, and it is quite possible that little difference in stalling incidence exists at low speeds compared to equivalent blunt nose sections.

Rotor blades of relatively high hub-to-tip radius ratio will always tend to stall abruptly due to the smaller difference in peripheral velocities and to less pronounced radial influence of Mach number.

Fig. 13 shows performance stage characteristics for a typical highly loaded rotor tip section and Fig. 14 shows the same characteristic in relation to those at the hub and mean sections. Considerable differences exist between the curves obtained from test measurements in the rotating blade row and those expected from simple cascade tests with similar inlet-to-exit axial velocity ratio.

The performance of the hub section agrees quite closely at all flow coefficients with that expected from equivalent two-dimensional cascade data; and, except for choking occurring at lower flow coefficients, little change results as Mach number is increased.

At the tip and mean sections some scatter in pressure function variation with Mach number exists and, in addition, the values of pressure function at flow coefficients less than design are lower than those expected from equivalent two-dimensional cascade data. The change in pressure function with speed appears to be logical if one considers the effect of Mach number on lift coefficient. This is shown on Fig. 15 and indicates that lift coefficient increases with Mach number to a point, after which it remains sensibly constant and then reduces again as drag increases. It appears that the Mach number was sufficiently low at 60 per cent design speed to cause a marked reduction in pressure function and, with increased speed, recovery to 115 per cent occurred as the lift

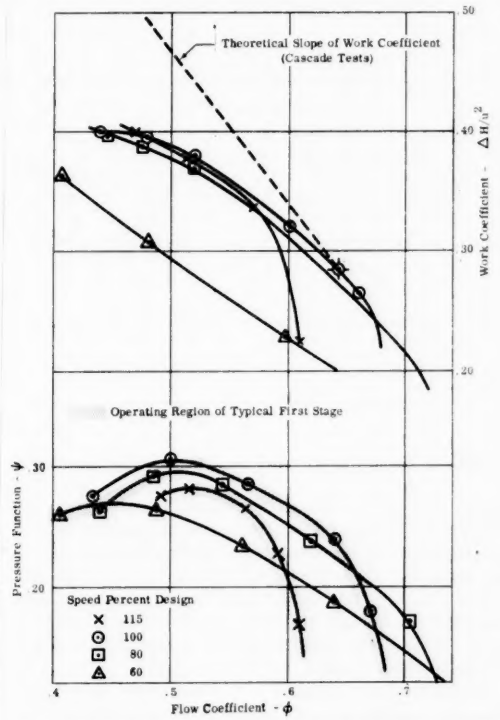

Fig. 13 Pressure function and work coefficient versus flow coefficient at tip section of low hub-tip ratio motor

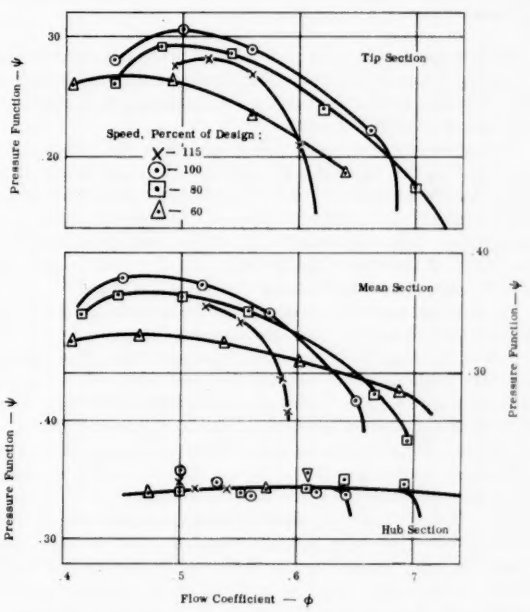

Fig. 14 Typical performance characteristics at hub, mean, and tip sections of compressor rotor

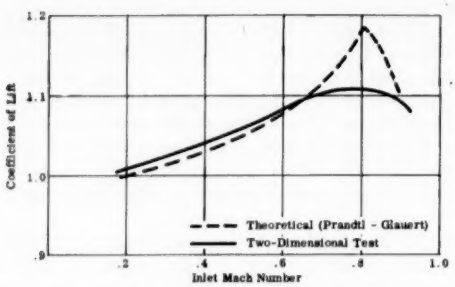

Fig. 15 Effect of Mach number on lift coefficient

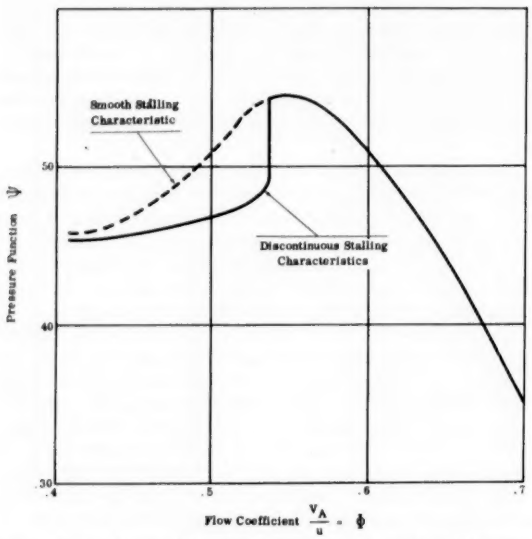

Fig. 16 Stage characteristics showing double and single value stalling pressure function

coefficient increased. The peak value of pressure coefficient was a maximum and reduced at higher speeds as the drag increased. The variation in stalling incidence and choking flow coefficient with speed is clearly indicated.

Operation of a compressor first stage covers the shaded region indicated on Fig. 13. This is, basically, the shape of the stage characteristic which would be obtained from measurements of wall static pressure in an actual compressor. It is seen that the lower peak value of pressure function at 60 per cent speed influences the shape of the stage characteristic, and that stall occurs over a wide range of flow coefficient as the speed is changed.

As the axial velocity is reduced, the static pressure rise at the tip will tend to increase at a rate in excess of that at the hub, by virtue of the shapes of the pressure characteristics. Thus a larger pressure gradient would exist at the rotor exit, not in keeping with that necessary for the condition of radial equilibrium. The correct static pressure gradient would be obtained if flow were displaced outward within the rotor. This would result in the axial velocities at exit of the rotor at the outer sections being increased, with corresponding reduction in work coefficient at these locations. Hence a less steep slope of work coefficient with flow coefficient based on inlet velocity would exist at sections other than the hub. In addition, a reduction in stalling flow coefficient would result. The rotor outlet static pressure gradient would not, of course, be identical to that at the design flow coefficient; the outward flow displacement necessitating a rather higher gradient due to stream curvature between the rotor and

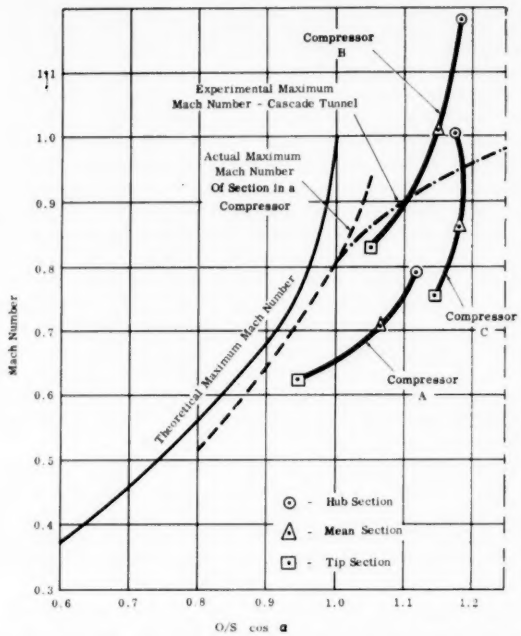

Fig. 17 Throat area—Mach number relations for typical axial compressor first stage rotor blades

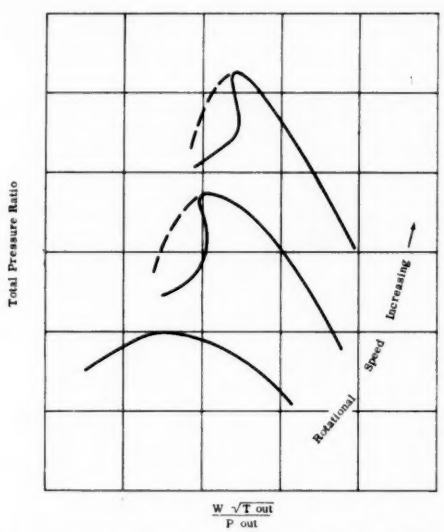

Fig. 18 Stage characteristics based on outlet flow conditions

stator. The rate of change of efficiency with flow coefficient at any speed considered also determines the amount of outward flow displacement, by virtue of its effect on the pressure function, and hence the static pressure. A lower than design efficiency usually exists at the tip section, due to the accumulation of secondary losses, and the interaction of the casing boundary layer. Similar flow conditions will occur whether a stage be designed on free-vortex or reaction principles.

A more complex physical flow pattern will exist in the rear stages of a compressor, due largely to the nonuniform conditions at entry resulting from passage of the flow through the early stages. However, a continuous radial static pressure gradient

will again occur, and the section pressure functions will satisfy the requirements. Due to the necessarily higher hub-to-tip ratios of these stages the theoretical slopes of the pressure function or flow coefficient curves will be more nearly equal, but additional effects will exist by virtue of the nonuniform entry conditions.

It is believed that improvement in part-load performance of the early stages would occur if the slope of the hub section characteristic could be increased to agree more closely with that of the tip section. This is, of course, impossible to achieve, the slope being a function of only the design tangential velocity change and blade peripheral velocities as shown in the following equation:

$$\frac{d\Delta T}{\Delta T'} = \frac{dV_A}{V_A'}\left[1 - \frac{u}{\Delta V\theta}\right] \tag{9}$$

where

ΔT = stage temperature rise
V_A = axial velocity
$\Delta V\theta$ = absolute tangential velocity change across rotor
u = blade peripheral velocity
$'$ = design condition

However, similar effects would occur if the hub sections were designed to produce larger enthalpy rises than the outer sections (reducing enthalpy rise with radius with the tip section still designed on its aerodynamic loading limit). This would enable the tip section to produce higher pressure ratios at lower than design flow coefficients, due to smaller flow displacement within the rotor passages toward the outer radii. The slope of the tip performance characteristic would now more nearly approach that shown to be possible from two-dimensional cascade tests. The higher work designed into the hub section augmented by the higher possible tip work would then result in the attainment of greater stage pressure ratios at lower than design flow coefficients.

Fig. 16 shows a typical stage characteristic constructed from wall static pressures, indicating a marked pressure reduction at stall. The dotted portion shows the pattern of the stage characteristic if smooth stall could be produced.

The over-all operating range of the stage can be increased by extending the range of the rotor tip section. In conventional subsonic designs, the hub section of the rotor blade is likely to choke first. This causes radial outflow to occur which helps to relieve the hub until a considerable portion of the blade row chokes and no further increase in mass flow will be possible. In transonic blade rows where the ratio of throat area to critical area is almost constant over the blade height, the rotor would choke without any three-dimensional relief. Fig. 17 shows the position of the hub, mean, and tip sections of a number of compressor first stage rotors at design point relative to the blade row choking line. Cases A and B passed the required mass flow exactly whereas case C passed 8 per cent higher than required flow.

If the stage characteristic be replotted dimensionally with outlet nondimensional mass flow as the abscissa and stage pressure ratio as the ordinate, it is possible that the characteristic would possess a positive slope in the region of the two legs of the curve. Fig. 18 indicates this effect.

The lowest speed at which the unstable region exists will be a function of the magnitude of both the nondimensional pressure function and the flow coefficient. If this critical speed occurs at 60, 70, or 80 per cent design speed on the characteristic of the first stage, it is likely that a surge line knee will exist.

It is highly unlikely that meticulous radial matching alone of the elements of axial compressor rotor and stator blades will enable operation of high pressure ratio compressors to be carried out over the entire running range without the aid of variable stators and/or bleed, etc.—the axial matching of the stages is of major importance in this respect—it will, however, enable improvements to be made in part-load performance, and, what is possibly more important, will enable higher efficiencies to be obtained with higher average blade loading and flow throughputs. This is of considerable importance in small compressors where the attendant friction effects and clearance losses assume large proportions.

References

1 A. D. S. Carter, "Some Tests on Compressor Cascades of Related Airfoils Having Different Positions of Maximum Camber," A.R.C. Tech. Report R & M No. 2694, 1953.

2 A. D. S. Carter, "Three-Dimensional Flow Theories for Axial Compressors and Turbines," *Proceedings of the Institution of Mechanical Engineers*, vol. 159, 1948.

3 P. Ruden, "Investigation of Single Stage Axial Fans," NACA TM No. 1062, April, 1944.

4 John R. Weske, "An Investigation of the Aerodynamic Characteristics of a Rotating Axial-Flow Blade Grid," NACA TN No. 1128, February, 1947.

5 Frank E. Marble, "Propagation of Stall in a Compressor Blade Row," *Journal of the Aeronautical Sciences*, vol. 22, 1955, pp. 541–554.

6 Aubrey Stone, "Effects of Stage Characteristics and Matching an Axial-Flow Compressor Performance," ASME Paper No. 57—A-139, December, 1957.

The Measured and Visualized Behavior of Rotating Stall in an Axial-Flow Compressor and in a Two-Dimensional Cascade

GINO SOVRAN

Research Staff, General Motors Corporation, Detroit, Mich.

The technique of smoke-flow visualization has been used to show clearly the action of the flow field upstream of a single rotor during rotating stall. The flow processes on the blades and in the blade passages of a stationary compressor cascade also have been observed using the same technique. An audio method of detecting rotating-stall patterns has been developed and has indicated that some compressor operating conditions at which no periodic flow disturbance was previously thought to occur actually contained rotating-stall patterns whose number of stalled regions changed very quickly from one value to another. The absolute speed of rotation of a stall zone was reduced to zero and its over-all shape clearly outlined by means of smoke visualization. The qualitative results of all these investigations have given a good physical picture of the rotating-stall phenomenon. Severe reverse flows were found to exist during rotating stall and these caused the formation of reversed flow regions extending upstream of a blade row. Furthermore, the distortions of the flow field in the vicinity of a blade row were found to be of such large magnitude that it does not seem likely that they can be described adequately by any linearized theory. Quantitative investigations were made into the effects of guide-vane turning and axial position on the rotating-stall characteristics of an axial-flow-compressor rotor. The absolute direction of the fluid entering such a configuration was found to affect nearly all facets of rotating-stall behavior.

Introduction

THE PROBLEM of rotating stall in the compressor element of gas-turbine systems is one that has received much attention in the past few years. In connection with the Allison Division of the Corporation and the Air Force, the General Motors Research Staff has been taking part in this activity and has been conducting studies of a fundamental nature with compressors of the axial-flow type. Some of the results to date have yielded considerable insight into the basic physical flow processes involved in this extremely interesting and perplexing phenomenon, and these results are now being made generally available.

One of the major difficulties in making analytical attacks on the problem of rotating stall is the proposition of a physical flow model that is sufficiently simple to be amenable to theoretical investigations and yet one that accurately describes the mechanism of the actual flow processes involved. The physical concept of rotating stall currently existing is rather sketchy as far as detailed mechanism is concerned. The only reported investigations into the detailed nature of the flow field have been the schlieren and interferometer studies made at Massachusetts Institute of Technology [1][1] and some rudimentary smoke-visualization studies made in France [2]. In the investigations reported here, the technique of smoke-flow visualization has been used with considerable effect to make direct observations of the flow processes involved in the rotating-stall phenomenon.

Smoke-Flow Visualization Studies of Rotating Stall

The work to be reported in this paper involves investigations of both a qualitative and a quantitative nature. The qualitative results will be considered first. These investigations have been carried out in two different test facilities. The first facility used contains a low speed, axial-flow compressor. This compressor is a 2-stage, variable-geometry unit that is commercially available. Each blade in both rotors and stators is individually adjustable to any desired setting angle and any combination of the two stages can be used. This unit has been incorporated into the facility in such a way that the methods of flow visualization can

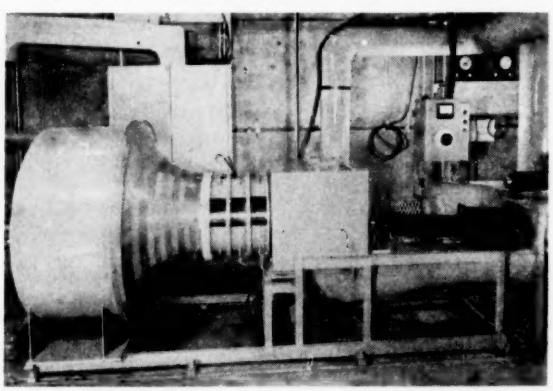

Fig. 1 Axial-compressor flow-visualization facility

[1] Numbers in brackets designate References at end of paper.

Contributed by the Gas Turbine Power Division and presented at the Semi-Annual Meeting, Detroit, Mich., June 15–19, 1958, of THE AMERICAN SOCIETY OF MECHANICAL ENGINEERS.

NOTE: Statements and opinions advanced in papers are to be understood as individual expressions of their authors and not those of the Society. Manuscript received at ASME Headquarters, March 16, 1958. Paper No. 58—SA-20.

be used for observing the air-flow conditions. The complete installation is shown in Fig. 1.

Air passes through the unit from left to right. The inlet section contains flow straighteners, screens, and a contraction nozzle, all of which reduce the turbulence level of the air entering the compressor to a value compatible with good flow visualization. The compressor is located in the center, and in this case has three windows cut in its side to permit visual observation of the flow. In the tests that have been conducted to date, only a single rotor-blade row has been investigated and it is located at the beginning of the right-hand window. The compressor discharges into a plenum chamber which has a glass end wall. Air can be pulled through the unit independently of the compressor speed by means of exhaust blowers connected to this chamber. Lighting for visualization is provided either by two slide projectors located downstream of the glass end wall of the plenum or by a battery of flashlights located inside the plenum at the point where the compressor annulus discharges into it. In each case, small-diameter, concentrated beams of light pass up through the rotating blade row to light its upstream flow field. The smoke used for visualization consists of a fog of very small droplets of kerosene produced in a special generator [3]. This smoke is introduced into the air stream through small tubes extending from the trailing edge of an airfoil-shaped reservoir that is located on the left side of the window area.

Successful visualization of the flow processes involved during rotating stall has been achieved in this facility, and motion pictures have been taken at rates up to 64 frames per sec. These movies show very clearly the severe flow distortions that are caused in the flow field upstream of the blade row by the propagation of the stall regions.

Fig. 2 Smoke visualization of flow field upstream of a rotor during rotating stall

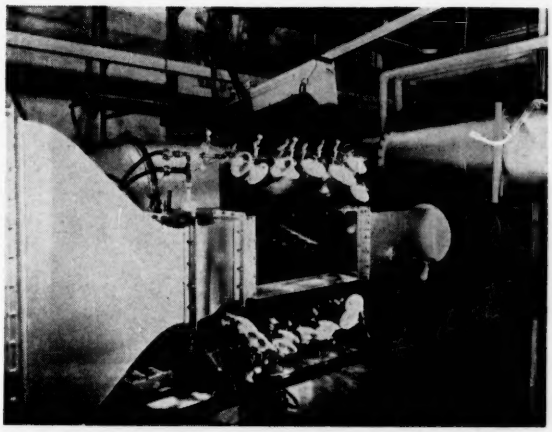

Fig. 3 Two-dimensional cascade used for flow visualization of propagating stall

In these particular tests, disturbances in the upstream flow field were found to extend several feet in front of the blade row under some conditions. As stall regions propagate around the compressor annulus, the through-flow of the compressor is forced to divert around them, causing periodic tangential oscillations of the incoming streamlines. This action can be seen in Fig. 2, but is much more pronounced and startling when seen in motion pictures. At certain compressor operating conditions the number of regions in a pattern changes very quickly from one value to another. Using smoke visualization this is observed as a change in the frequency and amplitude of the upstream tangential streamline oscillations. Visual observation also indicates that severe reverse flows can exist in the upstream region, and this is verified by results obtained in a stationary cascade.

Investigations in the axial compressor have yielded a clear picture of the flow conditions existing upstream of a rotor during rotating stall. However, they do not permit observation of what is going on inside the passages of the blade row itself. To circumvent this, a two-dimensional, stationary compressor cascade has been built and is shown in Fig. 3. Air is moved through the unit both by an inlet blower at the left and a discharge suction fan at the right. As with the smoke compressor, rather elaborate steps are taken to reduce the turbulence level by using inlet straighteners, screens, and a nozzle. The test section is 12 in. high, 6 in. from front to back, and has plexiglas walls on three sides. Lighting is by automotive-type spot lamps located above and below the section. The blades of the cascade are made of plastic and are mounted on a rotatable steel plate, forming the back wall of the test section, so that the cascade inlet angle can be varied. Each blade is individually adjustable and all interior surfaces of the unit are painted a glossy black. Using the same kerosene smoke that was used in the axial compressor, good flow visualization during propagating stall has been achieved successfully. Again motion pictures at 64 frames per sec have been taken as well as some at higher camera speeds.

Contrary to generally accepted beliefs, these studies indicate that it is possible for a compressor cascade to experience a condition of uniform blade stall. This occurs before the breakdown into propagating stall and visualization indicates that each blade of the cascade has badly separated flow on its suction surface. This is indicated in Fig. 4.

By careful adjustment of the inlet-air angle and the blade-

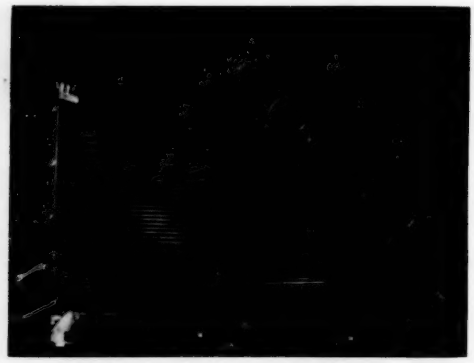

Fig. 4 Uniform blade stall in a two-dimensional compressor cascade

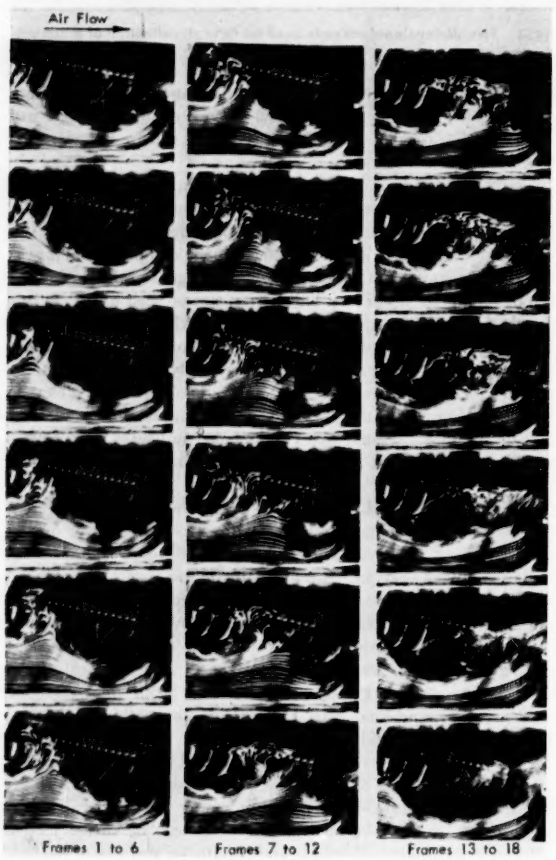

Fig. 5 Propagating stall in a two-dimensional compressor cascade

setting angles, it was possible to produce a large amplitude propagating stall on the cascade, Fig. 5. The flow distortions resulting from this propagation were periodic and the smoke made it possible to observe much of the detail of the flow patterns as the stall regions propagated along the row. By introducing smoke only downstream of the blade row it was possible to see that the void region indicated upstream of the row was actually filled with air that had flowed back upstream through the row. This reverse-flow region extended a fairly large distance upstream of the row and was essentially symmetrical about a line perpendicular to the

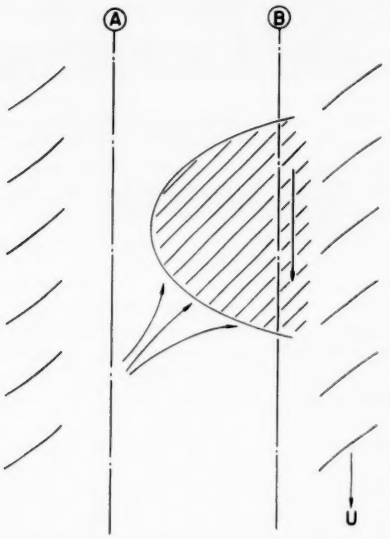

Fig. 6 Model of rotating-stall region upstream of rotating blade row

plane of the cascade. Reverse flows of such magnitude are not considered in any of the theoretical treatments of rotating stall.

Because of the absolute motion of the stall regions, even the stationary-cascade visualization did not give a clear enough outline of the over-all stall-zone shape or its internal-flow characteristics. By returning to the single-rotor axial compressor, more definite information on these points was obtained. By locating hot wires at various distances upstream of the rotor, the tangential extent of the stall zones as a function of axial distance was determined. The edges of the stall regions cannot be defined very accurately by this method, but the general results obtained are shown in Fig. 6. The cross-hatched region indicates the reverse-flow region upstream of the rotor row and this region will hereafter be referred to as the stall region. When these measurements were made, a set of inlet vanes located 9 in. upstream of the rotor was used to impart inlet prerotation to the air entering the rotor. Even though the air did not enter the rotor axially, the stall regions still seemed to be symmetrical about an axial line.

Confirmation of this over-all shape of a stall region and information on its internal-flow conditions were obtained by reducing the absolute speed of stall-pattern rotation to zero. This was done by using inlet prerotation vanes and resulted in stall zones remaining at fixed positions in the compressor annulus for prolonged periods of time.

The average inlet-velocity diagram of a rotor when it is operating in rotating stall without any inlet vanes is shown in Fig. 7. Relative to the blades, rotating stall propagates from their pressure to their suction surfaces with a speed that is here indicated as S_R. It will be noted that S_R is in a direction opposite to that of rotor rotation and is of smaller magnitude than the wheel speed. In an absolute sense, therefore, the stall propagates in the same direction as that in which the rotor is moving but at a lower speed S_A. Since the absolute propagation speed S_A is equal to $U - S_R$, the relative stall speed S_R and the wheel speed U must be made equal if S_A is to be reduced to zero.

The relative stall speed S_R is primarily a function of the relative inlet-air angle β_1 and the relative inlet velocity W_1 to a blade row. It will be assumed for the moment that it is a function only of these two variables. As a result, if a given β_1 and W_1 can be maintained while the wheel speed U is reduced, then S_R will remain constant but the absolute stall speed S_A will decrease by an

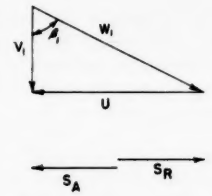

Fig. 7 Average inlet-velocity diagram during rotating stall

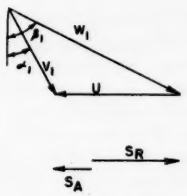

Fig. 8 Average inlet-velocity diagram during rotating stall with negative prerotation

amount equal to the reduction in U. This can be accomplished by using inlet vanes to impart negative prerotation to the incoming air. In Fig. 8, the air has been turned in a direction opposite to that in which the rotor is moving by an amount α_1. The relative inlet angle and velocity have been maintained at the same values as in Fig. 7 and the relative stall speed S_R is therefore presumed to be unchanged. The wheel speed has been reduced, however, so that the absolute stall speed S_A has been reduced correspondingly. It is apparent, if this line of reasoning is correct, that there must be some negative prerotation angle that will reduce S_A to zero. Furthermore, if greater values of negative prerotation are used it should be possible to make S_A negative; i.e., cause the stall zones to rotate, in an absolute sense, in a direction opposite to that in which the rotor is moving.

Both of these conditions have been achieved in the axial compressor. Although the foregoing suppositions on stall behavior are not exactly correct, they are qualitatively valid and do indicate the proper trends. The proper amount of negative prerotation cannot be calculated accurately, however, but eventually must be obtained experimentally after an approximate value has been determined by the method indicated in the previous paragraph. The turning angle finally required was about −65 deg. The inlet vanes used to produce this inlet prerotation were located as far upstream of the rotor as possible in the test facility. This was done so that they would merely serve to turn the air and would have a minimum of influence on the flow distortions upstream of the rotor and on the stall behavior of that blade row. This axial spacing turned out to be quite important, and a value of 9 in. was used. When the spacing was 4 in. or less, interaction effects between the inlet vanes and the rotor were so pronounced that no amount of negative inlet prerotation would bring the stall regions to rest. As the speed of a given pattern was reduced to a low value under these conditions, the pattern invariably changed to one containing more regions and moving at a higher rotative speed before the original pattern could be brought to rest.

In nearly all cases the final reduction from a very low rotative speed to one of zero required taking advantage of the rotating-stall hysteresis effect. This can best be explained by using Fig. 9. This shows the speed of stall rotation as a per cent of rotor speed plotted against rotor relative-inlet angle. As the inlet angle was increased by reducing the air flow at constant rotor speed, rotating stall eventually was initiated. In this case a pattern containing two stall regions was formed rotating at a very low absolute speed. As the compressor air flow was decreased further, the speed of stall rotation increased until the pattern suddenly changed to a single stall at a lower rotative speed. If the air flow was decreased further from this point, the speed of rotation of the single stall pattern increased in the same manner as that previously found with the two-stall pattern. If the air flow was carefully increased, however, the single-stall region could be maintained to flows greater than that at which the pattern had formed, and its absolute speed reduced to zero. This fact could be observed visually, by means of smoke, and also by the indications of hot wires in the compressor annulus. This stationary-stall region was

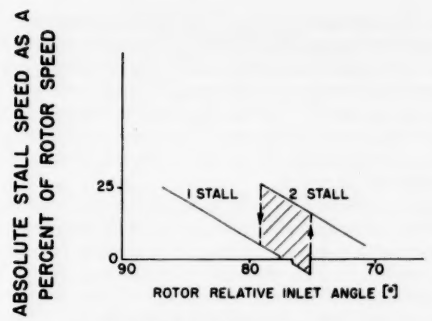

Fig. 9 Method for stopping stall

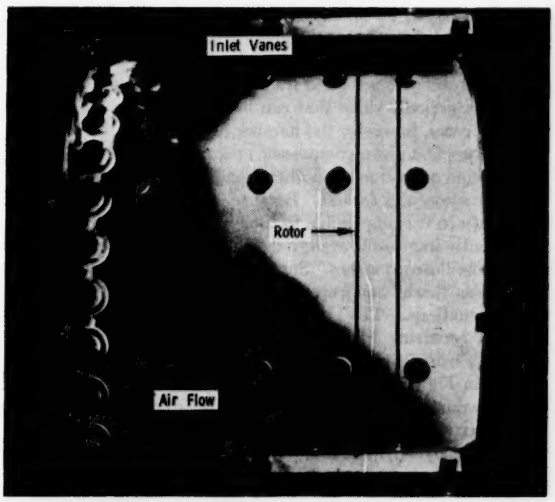

Fig. 10 Flow visualization of a stationary-stall region

very stable and remained fixed for long periods of time, occupying about half the annulus. As indicated in Fig. 9, a continuation of the process often resulted in the stall region rotating in a direction opposite to that of the rotor before the pattern eventually changed to one containing two regions rotating in the normal direction.

The stationary-stall region was visualized by employing a smoke technique different from that formerly used. When a stall region was brought to rest, a smoke bomb was placed in the downstream plenum chamber of the compressor. Previous results have indicated that a stall region is characterized by a large region of reverse flow extending upstream of a blade row. As a result, the downstream smoke from the bomb was carried forward through the rotor into this region and clearly visualized it. Movies were taken and typical results are shown in Fig. 10. This clearly shows the symmetrically shaped stall region extending in front of the rotor and containing reverse-flow air. The internal-flow characteristics, on the other hand, are quite difficult to determine. Although comparatively stable, the axial and tangential extent of the stall region varies continually in a random manner even when the region is stationary. In addition, blades are continually passing through the region so that local conditions are time dependent. These two factors make detailed observations of internal-flow patterns very difficult to make.

The existence of a large upstream reverse-flow region requires that quantitative experimental measurements of pressure, velocity, and air angle upstream of a rotor be very carefully inter-

preted. The type of variations measured by any stationary probe in the upstream region will depend on whether the probe is close enough to the stalled blade row to have the reversed-flow regions pass over it, or whether it is far enough away to see only the air coming from upstream. This is illustrated by sections A and B in Fig. 6. In the two cases the measured pressure variations will be different and cognizance of this fact must be taken before valid conclusions can be drawn.

Another interesting facet of rotating-stall behavior has been revealed by using an audio technique of stall observation. The usual method of detecting rotating stall involves the use of hot-wire anemometers. These heated wires are sensitive to air velocity and are placed in the flow annulus at various circumferential and radial positions. As stall regions rotate past a stationary probe, the flow distortions associated with these regions cause a decrease in the output signal from the hot wire. This signal is usually displayed on an oscilloscope. In a well-established stall pattern the stall regions are equally spaced and the pattern rotates at a uniform speed. As a result, stall regions pass a given hot-wire probe with a regular frequency and the hot-wire output signal is a periodic wave that can be tuned on the oscilloscope. In many cases, however, the number of regions in the stall pattern existing at a given compressor operating point changes very rapidly from one value to another, remaining at a given value for only a fraction of a second. Because of the short duration of a given pattern it is impossible to tune it on an oscilloscope, and it is frequently impossible even to detect regularity from high-speed films of oscilloscope traces. Such conditions were previously referred to as "hash" and were thought to be irregular, nonperiodic flow fluctuations. The basic regularity of the rapidly changing patterns occurring at such conditions is, however, indicated clearly by using the audio method of stall observation that is indicated in Fig. 11. This technique was used with a facility in which various stages of the compressor from an Allison T-56 turboprop engine were being investigated. A fluctuating air velocity is shown diagrammatically at the upper left. As it passes over the hot-wire probe the signal produced is, after amplification, displayed on a scope. However, the signal is also fed through an audio amplifier and into a speaker. Since the regions in the patterns pass a fixed probe with a regular frequency, the signal can be heard from the speaker as a clear and audible tone. The sounds heard over the speaker are not the actual noise produced in the compressor but in some cases, when the stall intensity is high, the same tones can be heard coming directly from a concrete-walled test cell. By the use of this technique, as many as five different stall patterns have been detected at a given compressor operating point. Tape recordings of stall tones obtained in this manner have been made.

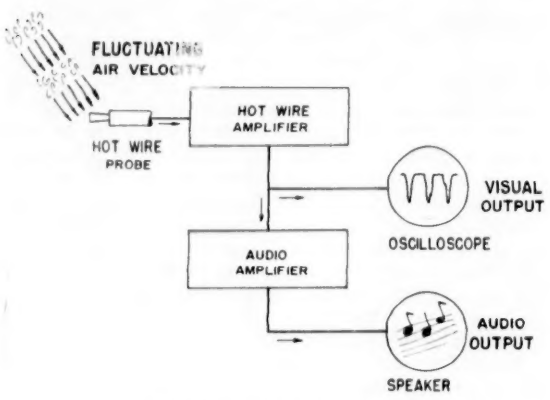

Fig. 11 Audio hot-wire circuit

The major result from the use of this technique is the revelation of the rather amazing propensity that rotating stall has for basic uniformity and regularity. Regardless of the shortness of the time duration during which a given stall pattern exists, the regions of the pattern are essentially evenly spaced and the pattern rotates at a uniform speed.

The flow visualization and audio techniques just described have revealed some of the basic characteristics of the rotating-stall phenomenon. These may be summarized briefly as follows:

1 The stall regions in a given pattern are usually symmetrically spaced, and the pattern as a whole rotates at a regular speed.

2 The stall zones can involve severe reverse flows, resulting in the formation of regions extending upstream of the stalled blade row that contain fluid originating from downstream of the row.

3 The effects of rotating stall extend a considerable distance upstream of a stalled blade row.

4 The absolute speed of stall-pattern rotation can be reduced to zero by means of negative inlet prerotation.

Some Effects of Guide-Vane Turning and Axial Position on the Rotating-Stall Characteristics of an Axial-Flow Compressor Rotor

In addition to the qualitative results just discussed, many quantitative observations of rotating stall also have been made. The low-speed, axial-flow compressor in which flow-visualization studies were conducted has been used to investigate the effects of guide-vane turning and axial position on the rotating-stall characteristics of an axial-flow rotor. This rotor was of 18 in. diam and had a constant hub-tip ratio of 0.69. The blades had an RAF No. 6 propeller section with a thickness-to-chord ratio of 12 per cent and a twist of 4 deg from root to tip. A setting angle at the mean line of the blades of 30 deg was used. The blades used as guide vanes were the stator blades designed for the compressor. These were made of sheet metal, had a moderate camber, and were twisted 8 deg from root to tip. When used to provide positive prerotation of the incoming air, these vanes had to be installed backwards. Although the radial gradient of leaving angle was reversed from that obtained when the vanes were in their proper orientation, this effect was neglected in the following analysis. The turning angle at the pitch line of the vanes was the one used to characterize any given test configuration. Since the vanes were not designed for the high turning angles at which they were sometimes used, they were often very badly stalled. In view of the large flow distance between the vanes and the rotor, however, this stalled condition is not thought to have affected the reported results in any major way.

Because of the low air velocities, high hub-tip ratio, small blade twists, and cylindrical annulus used in this investigation, the flow in the machine was considered to be two-dimensional in so far as its effects on rotating-stall behavior were concerned. This assumption was validated by the fact that all the stall patterns observed indicated essentially no variation in flow conditions across the annulus.

During these tests the inlet vanes were located at various axial positions in front of the rotor. These were dictated by reasons of physical convenience and the cambered inlet vanes were placed $1^1/_2$, 4, $6^1/_2$, and 9 in. upstream of the rotor. Some radial, uncambered inlet vanes also were used in the investigation and these were most conveniently located $^1/_2$ and 5 in. upstream of the rotor. The various amounts of guide-vane turning used at these positions and the different configurations tested are given in Table 1.

The Reynolds numbers based on blade chord that were achieved in rotating stall during these tests varied from 26,000 to 130,000. This represented rotor speeds from about 250 to 1680

Table 1

Guide-vane type	Axial distance upstream of rotor, in.	Guide-vane turning angle α, deg
Cambered	9	Range of positive and negative prerotations
Cambered	$6^1/_2$	−62
Cambered	4	Range of positive and negative prerotations
Cambered	$1^1/_2$	−62
Uncambered	5	0
Uncambered	$^1/_2$	0
None	...	...

rpm. Initially the stall data obtained for each constant-speed run were plotted separately, but little difference was found between the various speeds. This indicates that no significant Reynolds-number effect was present and is probably due to the fact that the inlet vanes induced enough turbulence in the flow to make the effective Reynolds numbers much higher than the values mentioned previously. As a result, all the data for a given configuration were correlated by a single curve.

The independent variables considered in the investigation were the following: (1) The axial spacing between the inlet vanes and rotor; (2) the amount of guide-vane turning, α; and (3) the physical presence or absence of stationary vanes. Their effect on the following dependent variables was investigated: (*a*) Absolute stall speed, (*b*) number of stall regions in the patterns, (*c*) angle of attack at which rotating stall was initiated, (*d*) slope of stall characteristic, (*e*) manner in which the number of stall regions in the patterns changed with decreasing air flow, and (*f*) relative stall speed. These dependent variables will be considered one at a time and in the order indicated.

Absolute Stall Speed. As was indicated previously when the problem of reducing the absolute speed of stall rotation to zero was considered, the absolute direction of the inlet air entering a rotor has an effect on absolute stall speed. This was proved in that particular case by the fact that a stall pattern could be brought to rest in an absolute sense. In general, the experimental effects of inlet prerotation are those shown in Figs. 12(*a*) and 12(*b*). With the absolute stall speed as a per cent of rotor speed of a particular pattern plotted against the relative inlet angle to the rotor, it is seen that for a given inlet angle the stall speed decreases as the amount of prerotation decreases. Prerotations greater than 24 deg are not shown because 1 and 2 stall patterns could not be obtained at these conditions. Tests were conducted with prerotations up to 65 deg, however, and the trend of absolute stall speed with amount of inlet prerotation for a given pattern was found to extend up to that point. At absolute inlet angles greater than 65 deg, however, spot checks indicated that the absolute stall speed of a given pattern was lower than that obtained at 65 deg. This angle therefore represents the condition for the maximum value of this effect of absolute inlet angle on absolute stall speed with this particular facility.

It will be noted that the results of Fig. 12 were obtained with the guide-vanes located 4 in. upstream of the rotor. Tests also were made with the vanes 9 in. in front of the rotor and the same effect on absolute stall speed was found.

One of the peculiar facets of this ability to vary the absolute speed of stall rotation is the comparative ease with which it is possible to obtain zero speed. The possibility of having a fine enough adjustment on operating conditions to be able to obtain any given preselected stall speed exactly would seem to be rather remote. In the case of zero speed, however, this can be done without too much difficulty. As the absolute stall speed approaches zero the pattern actually seems to seek that value and remain at it for a small range of flow conditions, rather than existing only at one distinct operating point, Fig. 9. In addition, as the magnitude of the absolute stall speed approaches zero it becomes more

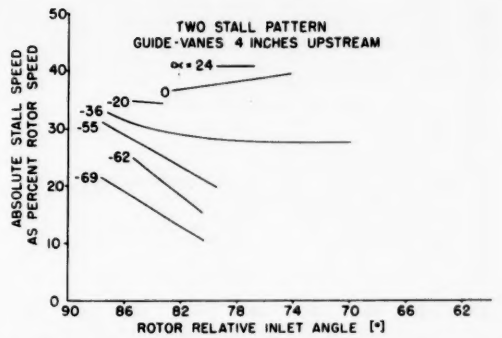

Fig. 12(a) Effect of guide-vane turning angle on absolute stall speed and slope of stall characteristic; two-stall pattern

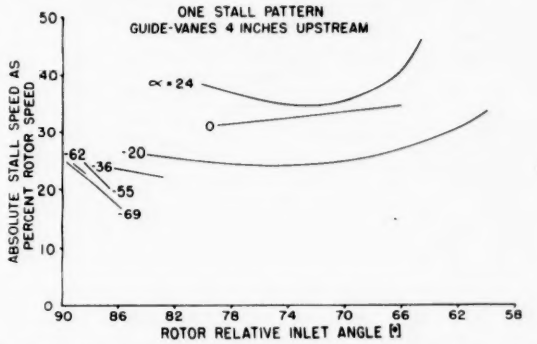

Fig. 12(b) Effect of guide-vane turning angle on absolute stall speed and slope of stall characteristic; one-stall pattern

and more unsteady. Since the rotor speed is being held constant this means that the relative stall-propagation rate on the rotor is varying. In the range of absolute speeds from +10 to −10 per cent of rotor speed the effect is noticeable enough that only average values of absolute speed can be determined. At zero per cent speed, however, the stall speed is absolutely steady and the relative propagation rate is therefore also steady. The fact that zero absolute speed can be maintained over a small range of operating conditions rather than just at a single point, and that relative stall speeds become unsteady when absolute stall speeds approach zero indicates that stall behavior is not entirely determined by the flow conditions relative to the rotor; it is also apparently dependent on flow conditions in the absolute frame of reference. This point will be considered in more detail in the following sections.

The speed of stall-pattern rotation is affected by blade-row interaction effects as well as by the amount and direction of guide-vane turning. This factor was investigated by varying the axial spacing between the guide vanes and the rotor while the setting angles of both blade rows were held fixed. The inlet vanes were placed 9, $6^1/_2$, 4, and $1^1/_2$ in. in front of the rotor while providing a negative prerotation of 62 deg. The results are shown in Fig. 13. The absolute speed of stall rotation of a given pattern at a given relative inlet-air angle is seen to decrease as the spacing between blade rows decreases. No data are recorded for the $1^1/_2$-in. spacing because the stall patterns were so unstable with this configuration that stall numbers and stall speeds were difficult to measure accurately. The data had considerable scatter and an adequate stall-speed curve could not be drawn.

The guide vanes used in these tests constituted accelerating blade passages and therefore had a drop in static pressure across

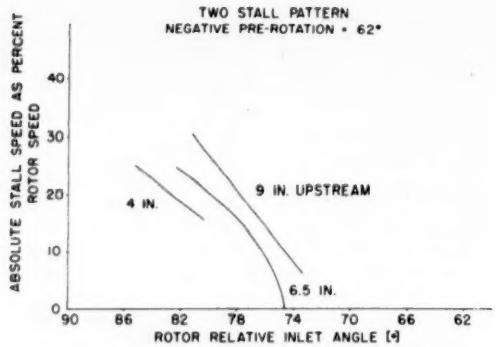

Fig. 13 Effect of guide-vane position on absolute stall speed

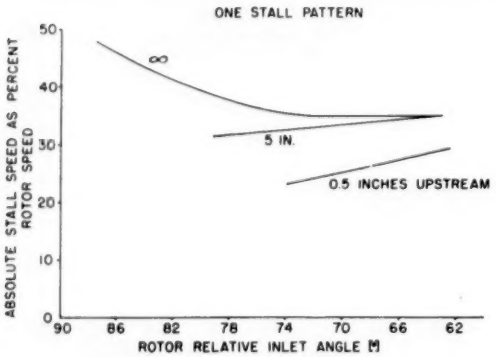

Fig. 14 Effect of position of radial vanes on absolute stall speed

them. Since rotating stall is not normally associated with this type of blade row, the possibility exists that the presence of such a row in the neighborhood of a diffusing blade row would have a stabilizing influence on the stall behavior of that row. This stabilizing effect would be dependent on the spacing between the rows and could have been a factor in the measured variation of absolute stall speed with guide-vane axial position mentioned in the previous paragraph. Since the stall regions rotate in an absolute sense in the annulus, however, it also would seem that the physical presence of any stationary element in the neighborhood of a stalled blade row would have an effect on absolute stall speed since the stalled regions and their effects would then have to pass over these elements.

To investigate this factor separately from that of the stabilizing influence, a set of uncambered radial inlet vanes was constructed. This consisted of sheet-metal blades 1 in. in chord and 35 in number and was aerodynamically neutral, so to speak; i.e., having neither accelerating nor diffusing passages. Because of the manner in which it was held in the unit, this set of vanes could be placed at only two different axial positions, each of which was different from any used with the cambered vanes. Tests were made with the radial vanes $^1/_2$ and 5 in. upstream of the rotor, and with no inlet vanes at all. The results of the tests with no inlet vanes were considered to be equivalent to those that would be obtained with the radial vanes an infinite distance upstream of the rotor. The results of these tests are shown in Fig. 14. The curves are for a single-stall pattern and it can be seen that, as with the cambered vanes, the absolute stall speed at a given rotor-inlet angle decreased as the spacing between the blade rows decreased.

On the basis of these results for the effect of axial spacing and on tests made in another facility but not reported here, the generalization can be made that the addition of a stationary blade

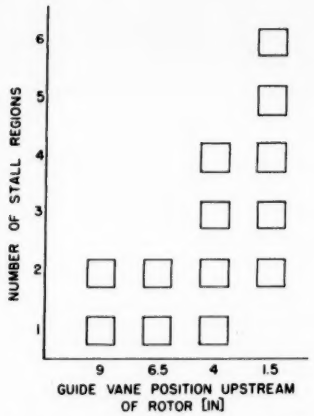

Fig. 15 Effect of guide-vane position on number of stall regions. Negative prerotation = 62 deg.

row either in front of or behind any compressor build-up always results in a decrease in absolute stall speed.

Number of Stall Regions in Patterns. The number of stall regions that may exist in a given stall pattern can vary over rather wide limits. Two factors which have been found to affect this number are the axial spacing between the inlet guide vanes and a rotor, and the amount and direction of inlet prerotation.

The effect of variations in axial spacing with a fixed amount of inlet prerotation is shown in Fig. 15, where stall patterns with different numbers of regions are plotted against guide-vane axial position. As the spacing between the blade rows decreased, there was an increase in both the number of regions in the patterns and the number of different patterns that formed. As has been indicated previously, rotating stall on a blade row affects the flow field in front of the row as well as that in and behind it. The larger the size of a stall region, the further upstream its effects extend. When inlet vanes are used, the upstream flow field affected by rotating stall is principally restricted to that between the vanes and the rotor. As this field is reduced, therefore, the effects of rotating stall cannot extend as far upstream and this is accommodated by the formation of patterns containing smaller stall regions of greater number. Greater numbers of regions in the patterns almost invariably lead to a greater variety of patterns found with a given configuration. This is probably due to the fact that the greater the number of stall regions in a pattern, the smaller the difference in air-flow conditions between that pattern and ones with slightly more or slightly fewer regions. It should be remembered that in this test the setting angles of the two-blade rows were kept fixed and only the relative positions of the rows changed. The results therefore indicate that the stall behavior of a given combination of blades can be rather drastically affected by their relative spacing.

The effect of the amount and direction of inlet prerotation on the number of regions in the stall patterns is not as clear-cut as that of the axial spacing, but a trend does exist. With the vanes located 4 in. upstream of the rotor, the general tendency is for both the number of regions in a pattern and the number of patterns found on a given rotor to increase when either large amounts of negative or positive prerotation are employed. This indicates the possible effect of the increased static pressure drop across the guide vanes at these extreme positions. This would make their stabilizing tendency more pronounced and could cause the formation of the smaller regions of larger number whose effects on the flow field would not extend as far upstream of the rotor.

Angle of Attack at Which Stall Is Initiated. The angle of attack at which rotating stall begins on a blade row is normally thought

to depend only on conditions relative to the blade row. These investigations, however, have shown that it is also dependent on both the axial spacing between the inlet vanes and the rotor, and on the amount and direction of inlet prerotation. The effect of guide-vane position is shown in Fig. 16. For a constant amount of prerotation, the initiation of rotating stall is retarded to larger values of angle of attack as the spacing between the blade rows is reduced. The effect is rather small, a reduction of 7.5 in. in the spacing increasing the stalling angle by only 3 deg, but it is definitely there. Being a nozzle row with accelerating flow, the inlet vanes exert a stabilizing influence on air-flow disturbances and make it more difficult for the diffusing passages of the rotor to exhibit rotating stall. As shown in Fig. 16, this effect increases as the guide vanes are placed closer and closer to the rotor and represents an interaction effect between the two blade rows.

When the axial spacing between the uncambered radial vanes and the rotor was varied, no effect on the initiation of rotating stall was observed. This would tend to confirm the conclusions of the previous paragraph since in this case there would be essentially no pressure drop across the radial vanes.

A much larger influence on the initiation of rotating stall is exerted by the amount and direction of guide-vane turning. This effect is shown in Fig. 17 where the results obtained with vanes $8^1/_2$ in. upstream of the rotor are shown. Although the data for positive prerotations are not very conclusive, the results in the range of negative prerotations indicate that larger and larger angles of attack are required to initiate rotating stall on the rotor when the guide-vane turning is reduced.

The inception of rotating stall was determined by means of hot-wire anemometers located in the compressor annulus upstream of the rotor. The exact definition of the stall-initiation point, however, was difficult to establish. Periodicity in the hot-wire signals could not be used as a criterion since the stall pattern at the point of stall initiation often can be so unstable and change so quickly that periodicity cannot be established without an audio system. An audio system, however, could not be used in this compressor because of the low frequency with which stall regions passed a fixed point. As a result, the initiation of rotating stall was taken arbitrarily to be that point at which the amplitude of the hot-wire signal reached a particular predetermined magnitude. Since the inlet-vane setting angle was continuously variable, it was possible to conduct this particular test in a short length of time and conformity in the definition of stall initiation was thereby maintained at the various inlet angles.

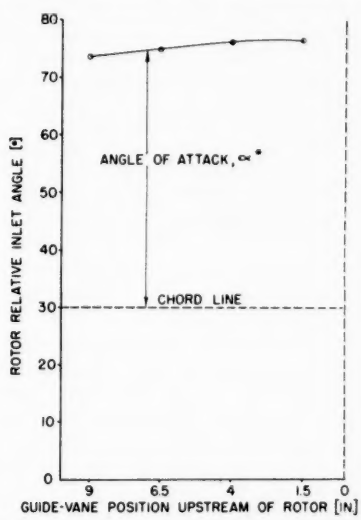

Fig. 16 Effect of guide-vane position on initiation of rotating stall. Negative prerotation = 62 deg.

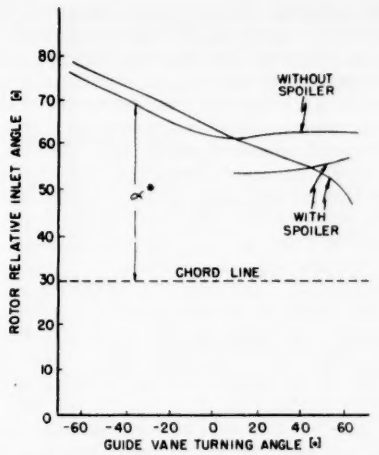

Fig. 17 Effect of guide-vane turning angle on initiation of rotating stall. Guide vanes $8^1/_2$ in. upstream of rotor.

In the range of negative prerotation the amplitude of the hot-wire signal increased rather abruptly when rotating stall began. The data were checked at three different rotor speeds and there was very little change in the results. Furthermore, the results were the same as those obtained when the inlet vanes were located only 4 in. in front of the rotor. On the other hand, little confidence is placed in the data obtained with positive prerotation. In this region the hot-wire signals grew gradually and continuously as the rotor angle of attack was increased and this made it impossible to get any degree of reproducibility in the definition of the stall. This was aggravated by the fact that the calculation of rotor relative inlet-air angle is much more susceptible to errors in air-flow measurement when positive values of inlet prerotation are used. In these tests the air flow at stall was small and could not be measured with great precision so this was an important factor in the scatter of the data obtained with positive prerotation.

Even though only the negative-prerotation part of the curve in Fig. 17 be used, it still indicates a variation of some 15 deg in the stall-initiation angle as the absolute inlet-air angle was varied from 0 to −65 deg. The important conclusion of the tests is therefore that, within the limits of experimental accuracy, the stall-initiation angle of a single rotor is dependent on the absolute entering flow direction.

The effect on rotating-stall initiation of a pressure-loss device such as a spoiler located downstream of a blade row was investigated. The spoiler consisted of an annular plate extending inward from the outer case of the compressor and blocking half the flow-passage area. It was placed 3 in. downstream of the rotor, just at the point of discharge into the downstream plenum chamber. The relative rotor-inlet angle at which rotating stall was initiated was measured over the complete range of inlet prerotation angles and the results are shown in Fig. 17. For negative prerotations the data were consistent and reproducible. It indicates that the effect of the spoiler was to retard the onset of rotating stall by about 2.5 deg over this complete range. When positive prerotation was used the data were inconsistent and not reproducible. Curves obtained in this region on two different days are shown and indicate the difficulty of getting good data. For the same reasons that already have been indicated for the tests with no spoilers, the data for positive prerotations should be disregarded and those in the range of negative prerotations considered to be indicative of the effect of a downstream spoiler on

rotating-stall behavior. The fact that a downstream pressure-loss device such as a spoiler has an effect on rotating-stall initiation is further indication that stall establishment is not exclusively determined by the relative angle of attack of a blade row.

The initiation of rotating stall is not determined by the attainment of some critical angle of attack on a compressor cascade. It seems reasonable to assume that the angle of attack must exceed some lower limit before rotating stall is possible, but these results show that the attainment of such a limiting angle is not a sufficient condition for the existence of rotating stall. Furthermore, considerable care must be exercised in using the word "stall." In the case of an isolated airfoil or a cascade of blades, stall is associated with operation just beyond the condition of maximum lift. Physically, it represents a flow condition in which the fluid stream is no longer attached to the suction surface of the airfoil or blades. In rotating stall, however, flow separation from the blade suction surfaces, i.e., blade stall, is a necessary but not a sufficient condition for existence. As has been observed visually in the two-dimensional cascade, Fig. 4, it is possible to have a condition where the flow on each blade of a compressor cascade is separated without having any propagating phenomenon. The word stall, therefore, has a different connotation in the terms "blade stall" and "rotating stall."

Slope of Stall Characteristic. Investigations into the effect of guide-vane turning on the slope of the rotating-stall characteristic have revealed some pertinent information on the factors affecting (1) the rotative speed of a given stall pattern and (2) the manner in which the number of stall regions in a pattern varies with operating conditions. The stall characteristic referred to here results from a plotting of absolute stall speed as a per cent of rotor speed against relative inlet angle to the rotor, with increasing values of the inlet angle being plotted toward the left. The scale of the relative angle has been reversed so that, as in the case of a conventional compressor map, increased blade loading is indicated by movement to the left on the figure. In some configurations the slope of the characteristic was found to be negative whereas in others it was positive. Accompanying this change in slope was a difference in the manner in which the number of stall regions in the patterns varied as the angle of attack on the rotor row was increased. As will be discussed presently, the type of variation obtained is apparently influenced by the slope of the stall characteristic.

The effect of guide-vane setting angle on the slope of the stall characteristic was shown previously in Figs. 12(a) and 12(b), the results being for a two-stall pattern and a one-stall pattern, respectively. In each case the vanes were located 4 inches upstream of the rotor. Although the curves are not all straight lines, in each case they show that as the inlet prerotation increased from large negative values to positive ones, the slope of the stall characteristic changed from large negative values to essentially positive ones. There are some minor inconsistencies in the trend but the over-all effect is readily apparent.

The fact that the slope of the stall characteristic can vary in this manner is not generally known. Most experimental investigations reported in the literature [1, 6, 7] have indicated positive slopes. On the other hand, [2, 4, 5] indicated that the stall-propagation rate was independent of the angle of attack. All of these tests were run either without inlet guide vanes or with guide vanes providing only positive prerotation, and so fit into the pattern indicated in Fig. 12. Only when negative prerotation was used was it possible to get negative slopes in these tests. The magnitudes of the negative slopes are of as much interest as the slopes themselves. With the large values found, the rate of stall propagation changed very markedly with changes in relative inlet angle.

The theory of reference [7] predicts that stall regions of large circumferential extent will propagate more slowly in an absolute sense than those of smaller extent. Furthermore, experimental evidence indicates that the stall regions in a given stall pattern grow in circumferential extent as the angle of attack on a blade row increases. These two statements are compatible when the stall characteristic has a positive slope but are incompatible when the slope is negative. As a result, it would appear that the dependence of absolute stall-propagation rate on stall-region size derived in reference [7] is not generally valid.

Change in Number of Stall Regions With Increasing Angle of Attack. No rotating-stall theory has ever been proposed that will satisfactorily predict (1) the number of regions that will exist in a stall pattern, (2) why the number of regions in a stall pattern changes, or (3) in what direction it will change. Some, in fact, do not even consider that different numbers of regions can exist. In most of the rotating-stall data available in the literature, the number of regions in the pattern has increased as the blade loading was increased. Coupled with the observation that the circumferential width of the regions in a given pattern also has increased under these conditions, this has led to a more or less intuitive feeling that a stall region breaks up into smaller regions of greater number when its size tends to become excessive. This would presume that the number of regions always would increase with increased blade loading. Furthermore, since all the regions in a given pattern are presumably identical, each should behave in the same manner and the number of regions therefore should increase by factors of 2. In some compressors, however, the number of regions decreases as the blade-row angle of attack increases. Furthermore, in the investigations reported here both types of behavior were found. With certain amounts of inlet prerotation the number of regions was found to increase with increasing angle of attack while with others the number of regions decreased.

A satisfactory explanation of the mechanism by which the number of regions in a pattern is determined would go a long way toward revealing the basic nature of the rotating-stall phenomenon. In the following, a possible correlation involving the manner in which the number of regions changes with flow conditions is discussed. Although admittedly empirical in nature it does have the virtue of satisfying a large amount of experimental data.

As has already been indicated, these investigations have shown that the stall characteristic can have a positive or a negative slope, depending on the inlet prerotation that is used. This is shown schematically in Fig. 18. Now, all available experimental data indicate that when the stall pattern of a compressor changes at a given operating point, the pattern with the greater number of regions always has the greater absolute rotative speed. Consider the case where the stall characteristics have a positive slope and the angle of attack of the blade row is being increased continuously. When the stall pattern changes, the absolute speed of the new pattern formed is greater than that of the one previously existing. On the basis of the previously mentioned experimental information this requires that the new pattern contain a greater number of regions than the old one. The number of stall regions therefore increases as the angle of attack increases. The opposite effect is present when the characteristics have negative slope. The number of regions then decreases with increasing angle of attack.

The preceding correlation is admittedly rather qualitative in nature and perhaps somewhat simplified. In some cases the data cannot be characterized by a single value of slope and in others, when the slope is nearly zero, it is somewhat difficult to establish the trend. The gross effects, however, are there. It seems likely that the slope of the stall characteristic is merely a reflection of some other variable that actually is responsible for the difference in the manner in which the number of stall regions varies. What this other variable is remains to be determined, but it is probable

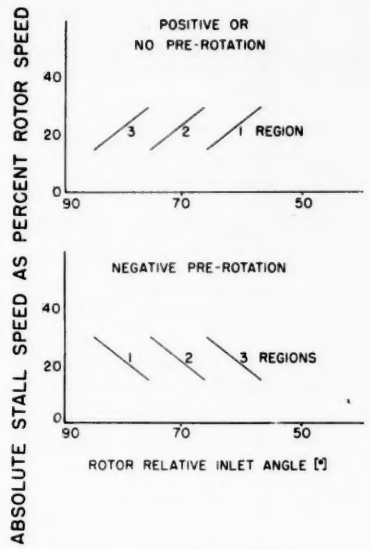

Fig. 18 Slope of stall characteristic

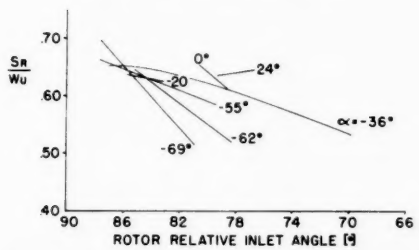

Fig. 19 Dependence of relative stall speed on absolute inlet prerotation and relative inlet angle. Two-stall pattern.

that a knowledge of it would aid our understanding of the rotating stall phenomenon materially.

Relative Stall Speed. All rotating-stall theories are developed on the basis of flow conditions relative to a blade row, and the primary variable affecting the stall-propagation rate relative to the row is considered to be the angle of attack of the incoming fluid stream. If the blade row on which the stall is propagating happens to be moving, no consideration is given to the absolute frame of reference in which the stall regions actually propagate and in which additional inertia and viscous effects may be present. The absolute speed of stall propagation is considered to be only a resultant effect that is obtained in a purely algebraic manner from the relative stall speed and the rotor speed by using the relationship $S_A = U - S_R$.

The results of these investigations indicate that although the flow conditions relative to a stalled blade row are the primary variables determining stall-propagation rates, these rates are modified by conditions in the absolute frame of reference. This is shown in Fig. 19 where the relative stall speed has been nondimensionalized by dividing by the tangential component of the relative inlet velocity W_u and plotted against the relative inlet angle β. Values of inlet prerotation are used as the parameter and the curves pertain to a given stall pattern. Although somewhat erratic because of the small number of experimental points at a few of the inlet prerotations, the curves do indicate that the relative stall speed S_R is dependent on the absolute inlet prerotation. No existing stall theory predicts this and it therefore appears that all of them are lacking some fundamental ingredient. This dependence on the flow conditions in the absolute frame of reference is one of the most important conclusions to be drawn from the experimental work reported in this paper.

Cascade of Circular Cylinders

In concluding this presentation of the qualitative and quantitative experimental results of these rotating-stall investigations, mention will be made of one last set of interesting and thought-provoking observations that have been made. The visualization of propagating stall in the two-dimensional cascade indicated a rather remarkable similarity between the flow conditions that were observed and those found in a Karman vortex street. In order to investigate the possibility that a fundamental relationship between the two might exist, the blades of the cascade were replaced by an array of circular cylinders. These cylinders were $^7/_8$ in. diam and they turned the air in the same manner that the airfoil-shaped blades had done previously. By careful adjustment of the cascade angle and of the flow conditions in the tunnel, it was possible to establish a periodic flow fluctuation on this cascade that bore a remarkable resemblance to that observed during propagating stall on the cascade of conventional blades.

To test this further, the blades in the low-speed axial compressor also were replaced by these cylinders. Air was pulled through the compressor by the downstream exhaust blower and the wheel rotated. Again flow conditions that were remarkably similar to those found during rotating stall could be obtained. With conventional blading, rotating stall is initiated and its intensity increased either by increasing the wheel speed at a given air flow, or by decreasing the air flow at a given wheel speed. When either of these two things was done with the cylinders installed in the unit, the following phenomena occurred: A flow disturbance was created near the tips of the cylinders and could be observed both visually, by using smoke, and by means of hot-wire traces. This disturbance grew in size and extended further upstream while occupying a larger and larger portion of the blade height. Reverse flows could be observed, particularly in the tip region, and the incoming-air streamlines oscillated back and forth. This sequence of phenomena was almost identical to that which had been observed previously in compressors during rotating stall and was practically indistinguishable from it.

On the basis of these results some interesting questions can be raised. How can a circular cylinder stall and unstall in the same sense that an airfoil does? Is the term rotating stall a proper one for the problem under investigation? The indications appear to be that the phenomenon may not be directly concerned with the detailed structure of a cascade or the detailed mechanism of the flow processes around its blades. Rotating stall is found in compressors of such varying types and sizes, that it may be concerned only with the gross, over-all characteristics of a system rather than with its detailed nature.

Conclusions

The use of smoke-flow visualization and an audio technique has revealed some of the basic characteristics of the large-amplitude type of rotating stall found in axial-flow compressors. These techniques have shown the basic symmetry and uniformity of the phenomenon and have indicated the large magnitude of the flow distortions involved. Severe reverse flows can exist and the effects of stall propagation extend a considerable distance upstream of a stalled blade row.

The investigations of a single-rotor row have indicated that the absolute direction of the fluid entering such a configuration has an effect on nearly all facets of rotating-stall behavior. This dependence on the absolute frame of reference tends to show that

the phenomenon of rotating stall is concerned with the gross, over-all characteristics of a compressor system rather than with the details of its structure or flow processes. The occurrence of rotating stall on a cascade of circular cylinders adds additional emphasis to this point of view.

The results of these investigations have provided a much clearer physical picture of this unusual phenomenon. They have shown behavior characteristics that are not accounted for in any existing theoretical treatment and it is hoped that they will serve as a stimulant for new and creative thinking on the problem.

Acknowledgments

The author would like to express his appreciation to Dr. Warren E. Snyder, formerly of the Research Staff, for the large part he played in the direction of these investigations and for his contributions to the development of the techniques involved. He would also like to thank E. D. Klomp and R. C. Mellin of the Research Staff for their efforts in obtaining the experimental results that are reported.

References

1 A. R. Kreibel, "Stall Propagation in a Cascade of Airfoils," Report No. 36, Gas Turbine Laboratory, Massachusetts Institute of Technology, Cambridge, Mass.

2 J. Valensi, "Experimental Investigation of the Rotating Stall in a Single-Stage Axial Compressor," Preprint No. 700, Institute of Aeronautical Sciences Annual Meeting, January, 1957.

3 D. Hazen and R. F. Lehnert, "Smoke Studies Conducted at Princeton University," Research Bulletin, Report No. 290, The James Forrestal Research Center.

4 S. Goldstein and A. L. Jaumotte, "Le Décrochage Tournant des Machines Axiales Génératrices Monoétages. Lois de Similitude," *Zeitschrift für Angewandte Mathematik und Physik*, vol. 8, 1957, pp. 235–251.

5 J. Fabri and R. Siestrunck, "Rotating Stall in Axial Flow Compressors," Preprint No. 692, Institute of Aeronautical Sciences Annual Meeting, January, 1957.

6 E. L. Costilow and M. C. Huppert, "Some Effects of Guide-Vane Turning and Stators on the Rotating Stall Characteristics of a High Hub-Tip Ratio Single Stage Compressor," NACA TN 3711, April, 1956.

7 A. H. Stenning, A. R. Kriebel, and S. R. Montgomery, "Stall Propagation in Axial-Flow Compressor," NACA TN 3580, June, 1956.

Availability Balance of Steam Power Plants

C. A. MEYER
Advisory Engineer, Mem. ASME

G. J. SILVESTRI
Development Engineer, Assoc. Mem. ASME

J. A. MARTIN
Design Engineer, Assoc. Mem. ASME

Steam Division, Westinghouse Electric Corporation, Philadelphia, Pa.

The well-known expression for availability, $b = h - T_0 s$, is developed in a simple yet general manner. The changes in availability throughout several typical single and double reheat steam plants having different steam conditions have been calculated. Balances of availability are presented for each of the several plants. These balances show the net plant output as the difference between the availability added in the boiler and the various losses in availability throughout the plant.

The maximum plant thermal efficiency (or minimum heat rate) is easily obtained from the ratio of the increase in availability to the heat added in the boiler.

The availability balances present in fine detail the loss distribution throughout the plant. Some very interesting results are obtained. For example, an assumed average plant will have a calculated maximum thermal efficiency of about 75 per cent based on the ratio of the availability and the heat in the high temperature combustion gases. Due to the heat transfer through a temperature difference, this value is reduced to 50 per cent when based on the ratio of the availability and the heat added to the steam in the boiler. This average plant will lose an additional 10 points in thermal efficiency, due to internal losses in availability, resulting in a 40 per cent thermal efficiency (excluding boiler and auxiliary losses). These latter 10 points due to internal losses are roughly divided as follows:

Pressure drop	0.9
Turbine blading	5.0
Turbine leakage	0.6
Turbine leaving and hood	1.0
Mechanical and generator	0.7
Feed and heating system and Feed pump and motor inefficiency	1.3 / 0.5
	10.0

An availability balance enables one to make an accurate assessment of the losses in any power plant and therefore serves as a very accurate guide in directing development effort toward reducing the more significant losses.

Introduction

THE CONVERSION of heat into work has attracted the attention of many great minds since the time when Carnot first proposed (1824) his rules for efficiently converting heat into work. Since that time a number of excellent thermodynamics books, for example, [1, 2, 3][1] and articles [5, 6] have contained statements of the rules governing heat engines, each in its own individual way. In the interest of completeness we will restate (in our individual way) the laws governing heat engines.

"A reversible engine has the greatest thermal efficiency of any engine when operating between given temperature limits."

The thermal efficiency is defined, as usual, as the ratio of work output to heat added to the heat engine. The proof of this statement is elementary and is based on the fact that if any given engine had a thermal efficiency greater than a reversible engine it could drive the reversible engine in a reversed direction and therefore cause the reversible engine to deliver more heat to a hot body than the given engine needs to draw from the same hot body. In this way the two engines acting together could cause heat to flow from a cold body to a hot body without the expenditure of mechanical effort. This would be in opposition to the second law of thermodynamics.

A second statement which easily follows from the first is this: "All reversible engines have the same efficiency when operating between the same temperature limits."

This statement is proved in a similar manner to the first statement by having alternately one and then the other of two reversible engines drive the other in a reversed direction and requiring that the heat delivered to the hot body by the driven engine be equal to or less than the heat drawn from the hot body by the driving engine.

The thermal efficiency of all reversible engines can be obtained by calculating the thermal efficiency of any one reversible engine. As is usually the case we select the Carnot engine (although any reversible engine would serve as well) and arrive at the well-known Carnot efficiency which shows the efficiency to be dependent on the temperature of the hot source and the cold sink.

$$\eta_e = \frac{T_H - T_C}{T_H} \tag{1}$$

where T_H and T_C represent the absolute temperature of the hot source and the cold sink, respectively. Equation (1) then

[1] Numbers in brackets designate References at end of paper.

Contributed by the Power Division and presented at a joint session of the Power and Fuels Divisions at the Semi-Annual Meeting, Detroit, Mich., June 15–19, 1958, of THE AMERICAN SOCIETY OF MECHANICAL ENGINEERS.

NOTE: Statements and opinions advanced in papers are to be understood as individual expressions of their authors and not those of the Society. Manuscript received at ASME Headquarters, February 27, 1958 Paper No. 58—SA-16.

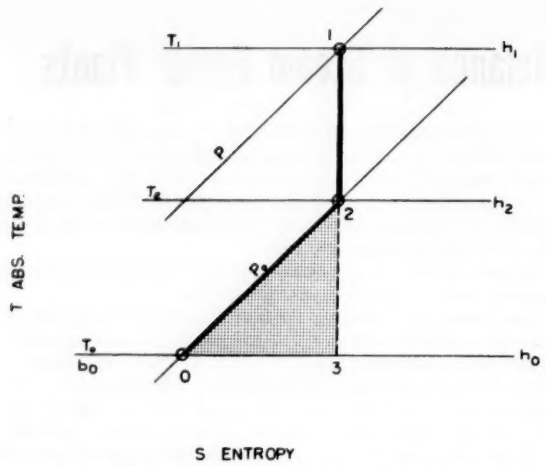

Fig. 1 The availability of any substance at point 1 is $(h_1 - T_0 s_1) - (h_0 - T_0 s_0) = b_1 - b_0$

gives us the upper limit of thermal efficiency of any heat engine. Of course we know that most of our modern power generation engines do not operate between an infinite heat reservoir and an infinite heat sink, but rather operate through the combustion of fuel which results in a finite quantity of hot gases. As heat is removed from the combustion gases the temperature must fall. In fact, if one assumes a reversible engine operating by means of combustion of fuel, he will find it has a thermal efficiency which is less than that given by Equation (1) due to the fact that the finite source delivers heat over a range of temperatures as the gas is cooled. Further, Equation (1) does not give us information on the amount of energy that can be converted to work if we have, for instance, a compressed gas which is at atmospheric temperature.

Availability

What is the amount of energy (the availability) which we can convert to work from a quantity of substance (any substance, to be general) which is at a temperature (T) and a pressure (P) which is different from those of our surroundings (T_0 and P_0)? (See Fig. 1.)

First, the substance could be expanded isentropically from 1 to 2 giving directly work (per unit weight) equal to the difference in the enthalpies.

$$ {}_1W_2 = (h_1 - h_2) \tag{2} $$

Secondly, the substance now at pressure P_0 (atmospheric) and temperature T_2 (which is higher than atmospheric) could be used to supply heat to an engine working on the cycle 0230 and thus deliver work equal to the shaded area, Fig. 1.

$$ {}_2W_0 = {}_0Q_2 - {}_0Q_3 \tag{3} $$

where Q represents heat added or rejected. Since process 2-0 is a constant pressure process, ${}_0Q_2 = h_2 - h_0$.

Also from the definition of entropy (s)

$$ {}_0Q_3 = T_0(s_3 - s_0) = T_0(s_1 - s_0) $$

so that Equation (3) becomes

$$ {}_2W_0 = h_2 - h_0 - T_0(s_1 - s_0) \tag{3a} $$

Adding the works ${}_1W_2$ and ${}_2W_0$, from Equations (2) and (3a) we obtain the total work W (per unit weight)

$$ W = {}_1W_2 + {}_2W_0 = (h_1 - T_0 s_1) - (h_0 - T_0 s_0) $$
$$ = b_1 - b_0 \tag{4} $$

where

$$ b = h - T_0 s \tag{5} $$

is the availability.[2]

Notice that since h and s are state functions so also is b, once T_0 is given.

The maximum work obtainable per unit mass of any substance in continuous flow[3] is then the difference between the value of b and the value b_0 of the substance in stable equilibrium with the surroundings. It is interesting to note that saturated steam at atmospheric temperature, $t_0 = 70$ F, has negligible availability (-0.04) with respect to the surroundings although its enthalpy is very different (1054.3 Btu's) from water at atmospheric conditions. The zero point for availability should be taken at atmospheric pressure even for condensing steam plants.

Losses of Availability

There is no law of conservation of availability. In fact, the difference between the availability entering and leaving a region is the loss of availability in that region.

$$ \Delta b = \Sigma b_i - \Sigma b_e \tag{6} $$

where b_i and b_e are inlet and exit availabilities, respectively.

Turbine Losses

The loss in availability (Δb_t) in a turbine is the amount by which the decrease in availability in the working fluid exceeds the work output W_t (which is taken as completely available)

$$ \Delta b_t = b_i - b_e - W_t $$

since

i = inlet

e = exhaust

t = turbine

$$ W_t = h_i - h_e $$

$$ \Delta b_t = T_0(s_e - s_i) \tag{7} $$

In words, the loss in availability is equal to the absolute temperature of the surroundings times the increase in entropy.

Also for a turbine efficiency defined as:

$$ \eta_i = \frac{dh}{dh_s} \approx \frac{dh}{vdp} $$

$$ dq_f = (1 - \eta_i) v dP = T ds $$

$$ db_t = T_0 ds = (1 - \eta_i) \frac{(dP)}{(P)} RT_0 = \frac{dq_f T_0}{T} \tag{8} $$

where subscript "s" refers to isentropic

v = specific volume

dq_f = friction heat

[2] The symbols B (total), b (specific) rather than A, a are used for available energy to avoid conflict with the Helmholtz free energy function $A = U - TS$ or with A for area. The origin of the definition for available energy is attributed to Darrieus [4]. The word "availability" is used rather than "available energy" since the latter is frequently used when referring to the turbine isentropic enthalpy drop.

[3] The much less used "nonflow" (internal) available energy (Ua) is obtained from Equation (5) by subtracting the available displacement work $(P - P_0)\, v$ from b.

Equation (8) indicates that since η_t and R are nearly constant the availability loss in a given turbine is nearly independent of the temperature for a given pressure ratio.

Since

$$dh \approx \eta_t v dp \approx \eta_t RT \frac{dP}{P}$$

we have from (8)

$$\frac{db_t}{dh} = \frac{(1 - \eta_t)}{\eta_t} \frac{T_0}{T} \tag{9}$$

The loss in availability per unit output varies inversely as the absolute temperature at which the friction heat is generated.

In words this means that when a quantity of energy (Q) originally in kinetic form (100 per cent available) is dissipated as friction into heat, the heat is available for conversion to work at the Carnot efficiency corresponding to the temperature. Thus the net loss is less than Q by the amount of Carnot efficiency.

$$\text{Net loss} = Q(1 - \eta_c) = \frac{T_0 Q}{T} \tag{10}$$

For best effect our friction losses should occur at high temperatures. In fact, Equation (9) shows that a 90 per cent efficient turbine at 100 F will have the same loss in availability per unit output ($\Delta b_t \Delta/h$) as an 81.8 per cent efficient turbine at 660 F (twice the absolute temperature). A rough rule would be that 10 per cent losses ($\eta_t = 0.9$) at low temperature are equivalent to twice these losses (18.2 per cent) at twice the absolute temperature. The use of a reheat factor is another way of accounting for the availability rebate due to friction losses.

Pump or Compressor Losses

The loss in availability in a pump or compressor is the amount by which the gain in availability of the pumped fluid falls short of matching the driving energy (which was 100 per cent available). In the case of an intercooled compressor the loss in availability is the amount by which the change in availability of the working fluid and the cooling fluid fall short of matching the work input,

$$\Delta b_p = W_p - (b_e - b_i)$$

since

$$W_p = h_e - h_i$$

$$\Delta b_p = T_0(s_e - s_i) \tag{11}$$

where s_e and s_i are the exit and inlet entropies.

The amount of pump work required in a cycle, although it influences plant capability, is only important to heat rate when carried out inefficiently. This occurs when the work expended (100 per cent availability) is not converted to an equal increase in availability in the pumped fluid.

Since pump inefficiency cannot be avoided, we should try to dissipate the friction heat at as high a temperature as possible consistent with the fact that the pump work and therefore the losses increase with liquid volume or temperature.

Heat-Transfer or Feed Mixing Losses

The loss of availability due to heat transfer or mixing is again the difference between the availabilities at inlet to the heat exchanger (or mixer) and the availabilities at exit from the exchanger.

$$\Delta b_{ex} = \Sigma b_i - \Sigma b_e \tag{12}$$

Satisfying the energy equation we obtain

$$\Delta b_{ex} = T_0 \Delta s \tag{13}$$

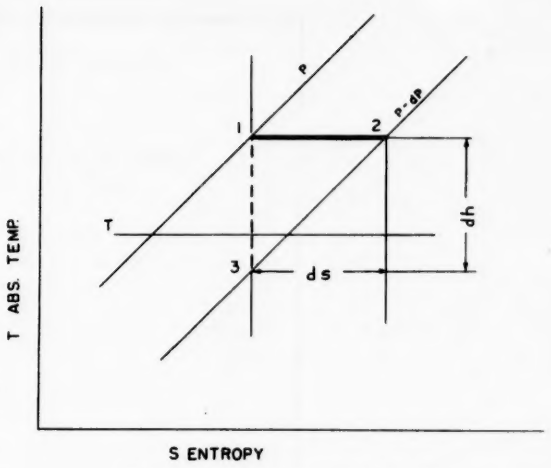

Fig. 2 The loss in availability due to throttling

where Δs is the net change in entropy within the exchanger or mixer.

Equation (13) is perfectly general and allows for pressure losses together with the fact that the transferred heat has a lower Carnot efficiency after transfer to the lower temperature than it originally possessed at the higher temperature.

Pressure or Throttling Losses

The loss of availability due to throttling or pipe pressure losses is again the difference between the availability before and after the pressure drop. For small pressure drops it is convenient to develop an approximate formula rather than pick entropies from the steam chart. Referring to Fig. 2 we have

$$\Delta b_{1-2} = T_0 \Delta S_{2-1} \approx T_0 \Delta q_{2-2}/T \approx T_0 \Delta h_{1-3}/T \approx T_0 v \Delta P_{1-2}/TJ$$

$$\Delta b_{1-2} \approx T_0 \frac{R}{J} \frac{\Delta P_{1-2}}{P} \tag{14}$$

Fig. 3 gives the value of R/J for steam so that given the fractional pressure drop, $\Delta P/P$, the entropy increase $R\Delta P/(JP)$ and the availability loss can easily be computed using Equation (14). Fig. 3 also shows the relative importance of a given fractional pressure loss for the superheated steam and for the liquid.

Cycle Analysis

The heat supplied to the steam in a steam plant causes an increase in the availability ($h - T_0 s$) of the steam. If this availability were completely converted to work in the cycle (without losses in availability), the thermal efficiency of the cycle would be:

$$\eta_A = \frac{\Delta b_A}{Q_A} = \frac{\Delta b_A}{\Delta h_A} \tag{15}$$

where

η_A = the thermal efficiency of the heat added, (maximum possible thermal efficiency)
Δb_A = increase in availability of steam due to heat added
Δh_A = enthalpy added to steam (assumed at constant pressure)
Q_A = heat added

This thermal efficiency is the maximum possible thermal efficiency obtainable assuming no further losses in availability within the cycle. The thermal efficiencies of the heat added in

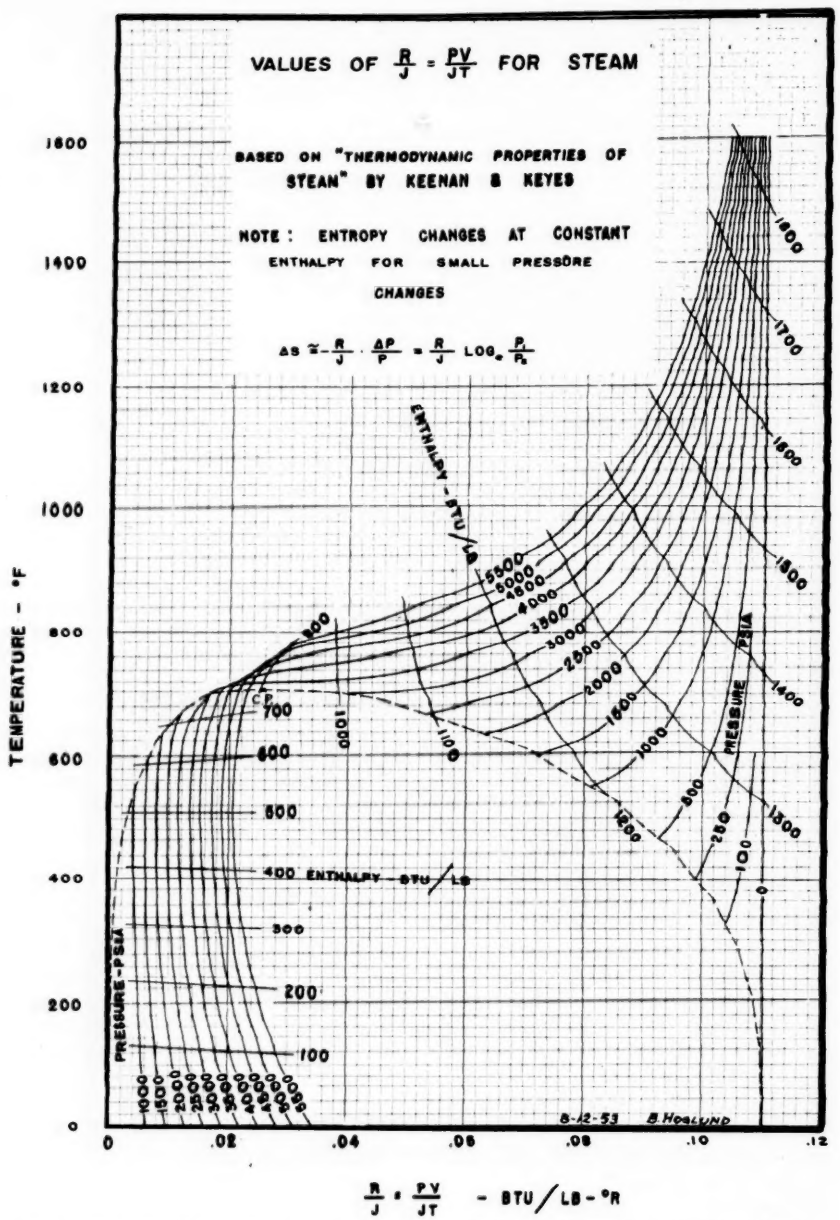
VALUES OF $\frac{R}{J} = \frac{PV}{JT}$ FOR STEAM
BASED ON "THERMODYNANIC PROPERTIES OF STEAN" BY KEENAN & KEYES
NOTE: ENTROPY CHANGES AT CONSTANT ENTHALPY FOR SMALL PRESSORE CHANGES
$\Delta S \cong -\frac{R}{J} \cdot \frac{\Delta P}{P} = \frac{R}{J} \log_e \frac{P}{P_2}$
TEMPERATURE - °F
ENTHALPY - BTU/LB
PRESSURE - PSIA
400 ENTHALPY - BTU/LB
8-12-53 B. HOGLUND
$\frac{R}{J} = \frac{PV}{JT}$ - BTU/LB - °R

Fig. 3 The value R/J for steam which is useful in calculating the throttling or pipe pressure drop losses

the boiler or reheaters can be handled separately or in combination as desired.

It is interesting to notice that Equation (15) gives the ideal efficiency for any cycle including the well-known Rankine cycle

$$\eta_R = \frac{b_t - b_f}{h_t - h_f}$$

$$= \frac{(h_t - T_c s_t) - (h_f - T_c s_f)}{h_t - h_f} = \frac{h_t - h_2 - P}{h_t - h_c - P} \quad (16)$$

since

$$T_c(s_2 - s_c) = h_2 - h_c$$

$$s_2 = s_t$$

$$s_c = s_f \quad \text{and} \quad P = h_f - h_c$$

where

P = pump work
h_t, s_t = enthalpy and entropy at turbine inlet
h_c, s_c = enthalpy and entropy of condensate
h_f, s_f = enthalpy and entropy of feedwater
h_2, s_2 = enthalpy and entropy at turbine exhaust

Equation (15) can be applied to any cycle, i.e., to single reheat, double reheat, feed heating, gas turbine cycles, etc.

In general, a power plant can be treated as shown in Fig. 4

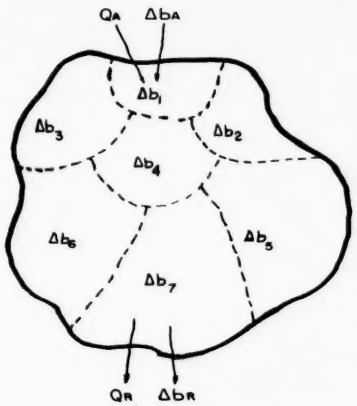

Fig. 4 Sketch of a power plant broken down into components showing the loss in availability of each component

where the various parts of the plant such as turbines, feed system, pump, etc., are examined for losses in availability.

The thermal efficiency of the complete plant is the thermal efficiency of the heat added less the summation of the losses in availability in the various parts of the plant and less any availability rejected by the plant all divided by the heat added.

$$\eta th = \frac{\Sigma \Delta b_A}{\Sigma Q_A} = \frac{\Delta b_1}{Q_A} - \frac{\Delta b_2}{Q_A} \ldots - \frac{\Delta b_n}{Q_A} - \frac{\Delta b_R}{Q_A} \quad (17)$$

$$\eta th = \eta_A - \Delta\eta_1 - \Delta\eta_2 \ldots - \Delta\eta_n - \Delta\eta_R \quad (18)$$

An alternate method of treatment is to use loss correction factors thusly:

$$\eta th = \eta_A[1 - (C_t + C_f + C_l + C_n \ldots C_r)] \quad (19)$$

where C_t, C_f, C_l, C_r are loss correction factors for turbine, feed system, leakage, etc. The loss correction factor for the turbine would be

$$C_t = \frac{\Delta b_t}{\Delta b_A} \quad (20)$$

where

Δb_t = loss in availability in the turbine
Δb_A = availability added to the cycle

In using this method to define "ideal cycles" we should recall that the definition of ideal cycle is quite arbitrary. One could define the ideal cycle as one in which all components are ideal including the turbine as is done in the case of the Rankine cycle [Equation (16)]. The method just described does not require the assumption of a perfect turbine in calculating the heat added thermal efficiency. For example, the heat added in the reheater and its thermal efficiency can be calculated starting with the actual conditions before the reheater rather than those corresponding to an isentropic turbine state line.

The ratio of the work output to the availability supplied to the plant is possibly a better criterion for gaging plant "effectiveness." This criterion is different from the Rankine cycle ratio in that it compares the performance with the actual availability supplied rather than the availability which would be supplied if all the plant components were ideal. Any irreversibilitie due to such items as having a finite number of feed heaters or using superheated steam to heat the feedwater should be considered as part of the cycle internal losses. The heat added thermal efficiency η_A is only a function of the availability and the heat supplied and is independent of the internal cycle details.

Availability Balance

As an indication of the method several availability balances have been carried out, the results of which are summarized in Table 1.

Some very interesting facts are immediately evident upon examination of this table. For instance (calculation No. 15), the thermal efficiency of reheating (64.49 and 63.28) (excluding pressure losses) is higher than the thermal efficiency of the boiler (57.68). However, the heat added in each reheater is unfortunately only about one seventh of the total heat added to the plant. The net improvement in thermal efficiency is thus only about one seventh of the difference of these values.

A further disturbing fact is that when allowance is made for pressure losses in the reheaters, the thermal efficiency of the heat added in the reheaters is often less than for the boiler. This shows up in cycles which we would normally not suspect (cycles Nos. 5, 17, 19, and 20, for instance). In these cycles the pressure losses overcome the thermodynamic gain due to reheating, in some of the reheaters. However, the over-all cycle performance is generally improved not by reheating itself but by the reduction in turbine moisture loss and due to the turbine losses occurring after the reheat at a higher absolute temperature [refer to Equation (9)].

Another interesting fact (although not shown in Table 1) is this: If we calculate the ratio of the reduction of availability in the combustion gases in the boiler to their reduction in enthalpy, we will find the maximum thermal efficiency based on the boiler gases is approximately 75 per cent. The loss in efficiency in transferring heat from the hot gases to the steam causes the reduction from 75 per cent to approximately 50 per cent as given in Table 1. The total losses, in the cycles calculated, amount to between 15 and 20 per cent of the availability supplied in the steam. Expressed differently, this means the various cycles convert from 80 to 85 per cent of the availability in the steam into useful output.

We notice from Table 1 that the pressure losses account for 0.04 of a point efficiency loss for each per cent pressure drop. A per cent pressure drop is worth about 0.04 point (about 0.1 per cent) efficiency or about 7 Btu/kwhr in heat rate. Fifteen per cent pressure drop could account for about 105 Btu in heat rate. The internal turbine blading losses, Table 1, account for about 5 points, on the average, in thermal efficiency or about 850 Btu/kwhr in heat rate. These blading losses are between 40 and 50 per cent of the total cycle losses (excluding boiler and auxiliary losses).

Turbine leaving and exhaust hood losses average about one point in thermal efficiency or about one fifth of the turbine blading losses (170 Btu/kwhr in heat rate).

External leakage losses average about 0.6 point or about one eighth of the internal turbine losses (about 100 Btu/kwhr). These losses, of course, depend greatly on the pressure level and turbine arrangement and must be weighed against the cycle gain due to increased steam pressure. For instance, cycles Nos. 16 and 15, Table 1, show the external leakage loss to be approximately proportional to the throttle pressure (0.46 compared to 1.18) in going from 2000 to 5000 psi throttle pressure. The gain in heat added efficiency in the boiler jumps from 53.07 to 57.68 per cent (approximately 1.3 points of this increase is due to the increased feed temperature). The losses due to inefficiency in the boiler feed pump and its driving motor also increase as the throttle pressure (and the pump work) increases, partially offsetting the thermodynamic gain in going to a higher throttle pressure. On an average the pump and motor inefficiency account for 0.5 point in thermal efficiency or about one tenth the internal turbine blading loss (about 85 Btu/kwhr).

The mechanical and generator loss averages about 0.7 point

Table 1 Availability balances of several steam plants

SINGLE REHEAT

CALCULATION NO.				①		②		③		④		⑤		⑥		⑦		⑧		⑨		⑩	
CYCLE	THROT	TEMP	PRESS	1000	1250	1200	2000	1200	5000	1100	2365	1100	2365	1000	1815	1000	1815	1000	1815	1050	2015	1000	1465
	REHTR	"	"	1000	312.5	1200	500	1200	1250	1050	477	925	455.2	1000	394	1000	396	1000	405	1000	394	1000	372
	REHTR	"	"	—	—	—	—	—	—	—	—	—	—	—	—	—	—	—	—	—	—	—	—
	EXHT	°R	IN HG	539	1"	539	1"	539	1"	552	1.5"	552	1.5"	552	1.5"	552	1.5"	552	1.5"	569	2.5"	552	1.5"
	FEED	TEMP	NTPS	416	7	462	8	565.9	11	513.1	8	510.8	8	488.6	7	488.8	7	459.2	6	495.9	8	440.5	5
				Δh	Δb	η	Δh	Δb	η	Δh	Δb	η	Δh	Δb	η	Δh	Δb	η	Δh	Δb	η	Δh	Δb	η	Δh	Δb	η	Δh	Δb	η
BOILER				1103.79	545.90	49.46	1152.05	612.66	53.18	968.30	559.24	57.76	1024.1	537.86	52.52	1026.50	538.50	52.46	1006.10	507.68	50.46	1005.5	506.67	50.39	1044.86	523.27	50.08	1022.78	509.41	49.81	1070.20	523.65	48.93
REHEAT				171.93	33.76	58.02	192.46	121.29	63.02	219.34	137.26	62.58	156.5	91.35	58.37	105.16	59.26	56.35	165.29	93.24	56.43	165.42	93.43	56.48	163.94	93.22	56.86	156.36	86.89	55.57	149.19	85.71	57.45
RENEAT																															
ADDED				1275.76	645.65	50.61	1344.49	733.94	54.59	1187.64	696.52	58.65	1180.6	629.21	53.30	1131.66	597.76	52.82	1171.83	600.32	51.30	1170.92	600.10	51.25	1208.80	616.49	51.00	1179.06	596.30	50.57	1209.35	609.36	49.97
					Δb %	Δ ηPT.		Δb %	Δ ηPT.		Δb %	Δ ηPT.		Δb %	Δ ηPT.		Δb %	Δ ηPT.		Δb %	Δ ηPT.		Δb %	Δ ηPT.		Δb %	Δ ηPT.		Δb %	Δ ηPT.		Δb %	Δ ηPT.
THROTTLE Δ P LOSS				(ΔP 4%)	0.36	0.18	(ΔP 4%)	0.29	0.16	(ΔP 4%)	0.29	0.17	(ΔP 4%)	0.32	0.17	(ΔP 4%)	0.32	0.17	(ΔP 4%)	0.37	0.19	(ΔP 4%)	0.37	0.19	(ΔP 4%)	0.35	0.18	(ΔP 4%)	0.38	0.19	(ΔP 4%)	0.38	0.19
Δ P 1ST REHTR.				(10%)	0.85	0.43	(10%)	0.75	0.11	(10%)	0.75	0.44	(12.5%)	1.01	0.54	(12.5%)	1.02	0.54	(12.5%)	1.05	0.54	(12.5%)	1.01	0.52	(12.5%)	1.06	0.54	(12.5%)	1.09	0.55	(12.5%)	1.20	0.60
Δ P 2ND REHTR.																															
Δ P TOTAL					1.21	0.61		1.04	0.57		1.04	0.61		1.33	0.71		1.34	0.71		1.42	0.73		1.38	0.71		1.41	0.72		1.47	0.74		1.58	0.79
INTER. TURBINE LOSS					8.05	4.08		7.95	4.43		9.53	5.59		7.13	3.80		7.69	4.06		7.54	3.87		7.38	3.78		7.94	4.05		6.70	3.39		7.40	3.70
LEAVING & HOOD LOSS					1.82	0.92		2.33	1.27		2.15	1.26		1.65	0.88		1.70	0.90		1.64	0.84		1.76	0.90		1.96	1.00		1.03	0.52		1.48	0.74
LOSS, LEAKAGE, EXT.					0.40	0.20		0.62	0.34		1.52	0.89		0.79	0.42		0.81	0.43		0.57	0.29		0.60	0.31		0.84	0.43		0.85	0.43		0.60	0.30
LOSS MECH. - GEN.					1.42	0.72		1.43	0.78		1.42	0.83		1.58	0.84		1.59	0.84		1.38	0.71		1.25	0.64		1.73	0.88		1.74	0.88		1.56	0.78
BLR. FEED PUMP INEFF.					0.26	0.13		0.35	0.19		1.18	0.70		0.53	0.28		0.53	0.28		0.41	0.21		0.37	0.19		0.24	0.12		0.44	0.22		0.66	0.33
PUMP MOTOR INEFF.					0.08	0.04		0.11	0.06		0.36	0.21		0.08	0.04		0.08	0.04															
BL MIX., PRESS DROP, FEED THROT.					2.63	1.33		2.53	1.38		2.66	1.66		2.51	1.34		2.67	1.41		3.10**	1.53		2.56	1.31		2.43	1.24		2.37	1.50		2.82	1.41
TOTAL LOSSES					15.87	8.03		16.36	8.93		19.87	11.65		15.60	8.31		16.41	8.67		16.06	8.24		15.30	7.84		16.55	8.44		15.20	7.68		16.10	8.05
THERMAL EFF.						42.58			45.46			47.00			44.99			44.15			43.06			43.41			42.56			42.89			41.92
TURBINE HEAT RATE						7940			7524			7261			7587			7731			7925			7862			8019			7957			8145

** WITH EVAPORATOR

SINGLE REHEAT / DOUBLE REHEAT

CALCULATION NO.				⑪		⑫ x		⑬ x		⑭ x		⑮		⑯		⑰		⑱		⑲		⑳	
CYCLE	THROT	TEMP	PRESS	1000	1465	1050	2015	1050	2015	1050	2015	1200	5000	1200	2000	1200	5000	1000	2000	1000	5000	1150	5000
	REHTR	"	"	1000	382.5	1050	459	1050	459	1050	456	1200	2000	1200	800	1100	1250	1000	800	1000	2000	1050	1056
	"	"	"									1200	465	1200	186	1050	290.6	1000	186	1000	468	1050	250
	EXHT	°R	IN HG	552	1.5"	552	1.5"	551	1.46"	552	1.5"	539	1"	539	1"	539	1"	539	1"	539	1"	552	1.5"
	FEED	TEMP	NTPS	448.7	5	468.3	7	463	7	464.1	7	565.9	11	461.8	8	535	9	461.8	8	565.9	11	545	9
				Δh	Δb	η	Δh	Δb	η	Δh	Δb	η	Δh	Δb	η	Δh	Δb	η	Δh	Δb	η	Δh	Δb	η	Δh	Δb	η	Δh	Δb	η	Δh	Δb	η
BOILER				1061.7	520.63	49.03	1052.7	536.88	51.00	1052.8	537.88	51.09	1058.4	539.25	50.95	1148.30	658.32	57.68	1152.03	611.25	53.07	1103.95	575.24	57.93	1030.49	533.25	51.76	808.30	455.67	56.30	854.62	534.77	56.02
REHEAT				135.7	78.54	57.89	171.6	99.84	58.18	171.5	99.95	58.28	174.7	101.53	58.15	167.85	108.25	64.49	140.58	81.42	65.03	108.98	68.88	63.50	134.92	79.81	59.37	185.07	109.34	59.08	171.36	99.92	58.31
RENEAT																175.85	111.28	63.28	147.08	106.03	63.45	146.08	87.73	60.10	149.33	86.30	57.96	163.71	94.26	57.58	144.36	84.84	58.77
ADDED				197.4	99.07	50.03	122.43	63.72	52.01	122.43	63.83	52.10	123.31	64.84	51.97	1312.0	778.05	59.31	1459.49	808.70	55.40	1258.01	731.91	58.18	1314.78	693.96	53.24	1157.08	658.67	56.93	1270.52	713.58	56.64
					Δb %	Δ ηPT.		Δb %	Δ ηPT.		Δb %	Δ ηPT.		Δb %	Δ ηPT.		Δb %	Δ ηPT.		Δb %	Δ ηPT.		Δb %	Δ ηPT.		Δb %	Δ ηPT.		Δb %	Δ ηPT.		Δb %	Δ ηPT.
THROTTLE Δ P LOSS				(ΔP 4%)	0.38	0.19	(ΔP 4%)	0.34	0.18	(ΔP 4%)	0.345	0.18	(ΔP 4%)	0.34	0.18	(ΔP 4%)	0.26	0.16	(ΔP 4%)	0.27	0.15	(ΔP 4%)	0.28	0.16	(ΔP 4%)	0.28	0.15	(ΔP 4%)	0.26	0.15	(ΔP 4%)	0.28	0.16
Δ P 1ST REHTR.				(12.5%)	1.10	0.55	(12.5%)	1.02	0.53	(12.5%)	1.02	0.53	(12.5%)	1.02	0.53	(8%)	0.56	0.33	(8%)	0.56	0.31	(8%)	0.57	0.33	(8%)	0.62	0.33	(8%)	0.56	0.32	(10%)	0.74	0.42
Δ P 2ND REHTR																(10%)	0.71	0.42	(10%)	0.69	0.38	(10%)	0.67	0.39	(10%)	0.81	0.43	(10%)	0.83	0.47	(12%)	0.79	0.45
Δ P TOTAL					1.48	0.74		1.36	0.71		1.36	0.71		1.36	0.71		1.64	0.91		1.52	0.84		1.52	0.88		1.71	0.91		1.65	0.94		1.81	1.03
INTER. TURBINE LOSS					9.90	4.95		7.33	3.81		7.49	3.90		7.56	3.93		8.30	4.92		7.76	4.30		8.85	5.15		7.85	4.18		9.22	5.25		6.66	3.77
LEAVING & HOOD LOSS					1.22	0.61		0.87	0.45		0.84	0.44		0.83	0.46		1.92	1.14		2.22	1.23		2.06	1.20		2.76	1.47		2.51	1.43		1.36	0.77
LOSS, LEAKAGE, EXT.					1.12	0.56		0.44	0.23		0.50	0.26		0.56	0.29		1.93	1.18		0.83	0.46		1.89	1.10		0.77	0.41		1.88	1.07		0.84	0.48
LOSS MECH. - GEN.					1.92	0.96		1.54	0.80		1.52	0.79		1.52	0.79		1.52	0.90		1.55	0.86		1.53	0.89		1.45	0.77		1.49	0.85		1.55	0.88
BLR. FEED PUMP INEFF.					0.32	0.16		0.40	0.21		0.44	0.23		0.40	0.21		1.05	0.62		0.32	0.18		1.10	0.64		0.38	0.20		1.25	0.71		1.20	0.68
PUMP MOTOR INEFF.																	0.34	0.20		0.11	0.06		0.34	0.20		0.11	0.06		0.95	0.20		0.35	0.20
BL MIX., PRESS DROP, FEED THROT.					2.76	1.38		2.98	1.55		2.94	1.53		2.91	1.51		2.86	1.70		2.32	1.28		2.66	1.55		2.69	1.43		2.73	1.55		2.60	1.47
TOTAL LOSSES					18.72	9.36		14.92	7.76		15.09	7.86		15.20	7.90		19.51	11.57		16.63	9.21		19.95	11.61		17.72	9.43		21.00	12.00		16.37	9.28
THERMAL EFF.						40.67			44.25			44.24			44.07			47.74			46.19			46.57			43.81			44.93			47.36
TURBINE HEAT RATE						8391			7712			7714			7744			7149			7383			7328			7790			7596			7206

X CROSS COMPOUND, L.P. TURBINE @ 1800 RPM.

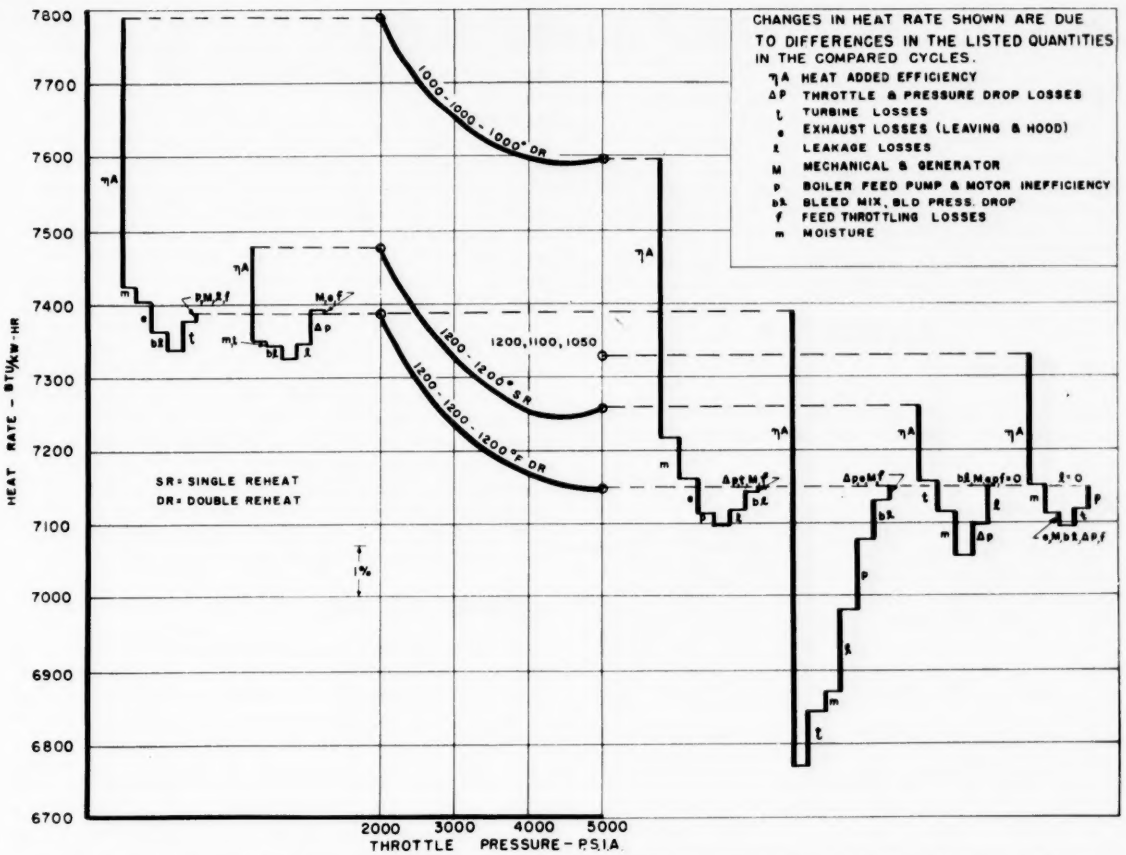

Fig. 5 Changes in availability losses due to changes in pressure, temperature, and a second reheat for a turbine of fixed capability

which is about one seventh the turbine blading losses (120 Btu/kwhr).

The feed heating system loses on the average 1.30 points in thermal efficiency, 0.1 point of which is due to feed throttling for boiler control purposes. The remainder is caused by heat transfer and mixing the bled steam with the colder feedwater. The feed loss averages about 220 Btu/kwhr or about one quarter of the turbine blading loss.

A more detailed insight into the effect of cycle pressure and temperature level on the loss distribution is shown in Fig. 5.

The changes in the heat added efficiency and the changes in the various internal losses are shown off to the side of the heat-rate curve. As an example in going from 1000, 1000, 1000 to 1200, 1200, 1200 F at 2000 psi there is first a gain in thermal cycle heat added efficiency (η_A) followed by small gains and losses due to changes in the other losses. The thermodynamic gain thus accounts for the principal gains.

The change from 2000 psi to 5000 psi at 1200, 1200, 1200 F, is quite different in that there is a considerable gain in heat added efficiency (η_A) a large portion of which is annulled by increase in the internal turbine, moisture external leakage, pump and bleed mixing losses. Thus only about 60 per cent of the theoretical gain is attained. Had the turbine capacity been increased proportionately to the pressure, the internal turbine and external leakage losses would not have increased and absorbed as much of the thermodynamic cycle gain.

Evidently the increase in the feed pump losses even for the same pump efficiency is a basic problem associated with the increase in cycle pressure. Due to the more difficult pump leakage control problems, the pump efficiency is also reduced with increasing cycle pressure.

Conclusion

The previously known concept of availability has been used to calculate balances of availability for several steam plants which operate at different steam conditions. These balances point out in fine detail the loss distribution throughout the plants. A new concept "the heat added thermal efficiency" η_A has been introduced which may be useful in analyzing power plants, particularly the more complicated ones such as the combined steam and gas turbine or the combined steam and nuclear power plants.

Others have in the past advocated power-plant analysis using "second law analysis" or "entropy balance" methods. These methods are evidently not widely used today. The present paper is another attempt with a different viewpoint and a different name, availability balance, to encourage use of these methods. It is possible that these more tedious types of analysis will be used more frequently in the future since they can be carried out quickly on electronic computers.

Acknowledgment

The authors wish to express their appreciation to C. B. Campbell for his advice and guidance during the writing of this paper.

References

1 G. A. Goodenough, "Principals of Thermodynamics," Henry Holt and Company, New York, N. Y., 1929.

2 J. H. Keenan, "Thermodynamics," John Wiley & Sons, New York, N. Y., 1941.

3 M. W. Zemansky, "Heat and Thermodynamics," McGraw-Hill Book Company, Inc., New York, N. Y., 1937.

4 G. Darrieus, "Definition for Thermodynamic Efficiency of Steam Turbines," *Engineering*, vol. 130, 1930, pp. 283–285.

5 A. Keller, "The Evaluation of Steam-Power-Plant Losses by Means of the Entropy-Balance Diagram," TRANS. ASME, vol. 72, 1950, p. 949.

6 E. A. Bruges, "Applications of Second Law Analysis," *The Engineer*, Oct. 8, 1954, pp. 483–484; also March 5, 1954, pp. 341–344.

DISCUSSION

J. H. KEENAN[4]

Analytical studies of power-plant cycles based on the second law of thermodynamics often shed light on the relative merits of the various details of cycles like reheat, regenerative feedwater heating, and so forth. The authors' Table 1 is evidence to this effect.

The terminology of this subject, however, has not completely crystallized. Since some responsibility may rest with the writer for the terminology used in this paper, this opportunity is seized upon to call attention to a paper[5] in which he attempted to bring some order into the subject. In that paper the suggestion is made that the term availability be reserved for what Gibbs, the originator of this subject, called "the available energy of the body and medium."[6] The availability so defined can never be less than zero.

The quantity called availability by the authors is the maximum shaft work in passing in steady flow from the state in question to the most stable state of equilibrium with the environment. This quantity may be greater than, equal to, or less than zero.

It appears that, since this paper is restricted to consideration of processes of steady flow, it is concerned primarily with a comparison of shaft work realized and maximum shaft work.

The symbolism employed is in one instance somewhat confusing. Although b is defined as the property $(h - T_0 s)$, Δb is not, in general, $\Delta(h - T_0 s)$.

The purpose of this discussion is to call attention to the more recent literature which, in the opinion of the writer, makes this subject more orderly and relates the present considerations to more general ones.

G. J. VAN WYLEN[7]

It is encouraging to know that engineers are more and more utilizing the concept of availability. This paper represents a very worth-while contribution in this direction and the authors are to be commended for an excellent job.

Three suggestions are made which may be helpful for those continuing along the general lines of this paper. First of all, the term Δb, which is called loss in availability, is rather misleading because it is necessary to make a distinction between a decrease in availability and a loss in availability. For this reason it would be better to introduce the term "irreversibility" which is defined in exactly the same way as the authors have defined loss in availability. This would avoid the possibility of confusion and the term "irreversibility" is also a very descriptive term.

The second point is a rather minor one but it is advantageous to consider R to be a constant for a given substance and to introduce the compressibility factor into an equation. In this scheme we write $Pv = ZRT$ where R is the ideal gas constant for the particular substance and Z is the compressibility factor which indicates the deviation from the ideal gas equation and state.

The third suggestion is to avoid the term "friction heat" and instead simply use a term such as dh_f, which would represent the increase in enthalpy as a result of the irreversibility associated with friction as compared to the reversible adiabatic case. The reason for this suggestion is that in thermodynamics it is desirable to reserve the term "heat" for energy crossing the boundary due to a temperature difference and also because, whenever possible, it is advantageous to talk in terms of change of a thermodynamic property associated with a given change of state.

It is believed that the introduction of these changes would be desirable in future work on this subject.

AUTHORS' CLOSURE

The use of proper terminology for this subject has always been a problem to the authors. In fact, the last revision of the manuscript prior to presentation was to replace the words "available energy" by the single word "availability" as suggested by several of the reviewers. This was done in order to conform with previous works on the subject and also to avoid a conflict with the usage established by power-plant designers who often use the words available energy when referring to turbine enthalpy drop. Unfortunately, the symbols on Table 1 were not changed.

The use of b as a symbol for availability and Δb as the symbol for losses in available energy is unfortunate. Professor Van Wylen's suggestion of using "irreversibility" is a good one. Possibly an I could be used as a symbol in an available energy equation.

$$\Sigma b_i + \Sigma \mathrm{KE}_i + \Sigma W_i = I + \Sigma b_o + \Sigma \mathrm{KE}_o + \Sigma W_o$$

where b = availability
I = irreversibility
KE = kinetic energy
W = work
i = inlet
o = outlet

Professor Van Wylen's suggestion to use dh_f in place of dq_f for friction heat, we feel is good but with the restriction to adiabatic constant pressure processes. A well-known expression for work may be written as

$$W = -dh + dq = vdp - dq_f$$

Evidently only when $dq + vdp = 0$ is $dq_f = dh$.

Of course, both Professor Van Wylen's and our developments assume adiabatic constant pressure processes. The question is, can we generally avoid reference to friction heat by using dh_f?

The comments of both Prof. J. H. Keenan and Prof. G. J. Van Wylen are greatly appreciated and we hope will serve to improve the terminology used for this subject.

---

[4] Professor and Head, Department of Mechanical Engineering, Massachusetts Institute of Technology, Cambridge, Mass. Fellow ASME.

[5] J. H. Keenan, "Availability and Irreversibility in Thermodynamics," *British Journal of Applied Physics*, vol. 2, 1951, pp. 183–192.

[6] "The Collected Works of J. Willard Gibbs," Longman, Green, Inc., London, England, 1931, p. 53.

[7] Chairman, Department of Mechanical Engineering, University of Michigan, Ann Arbor, Mich. Mem. ASME.

Pulverized-Coal Transport Through Pipes

R. C. PATTERSON

Director, Kreisinger Development Laboratory, Combustion Engineering, Inc., Chattanooga, Tenn.

Some typical problems related to pulverized-coal transport for steam generators have been investigated in a long-term test program.

The investigation has provided information relative to the performance of a commercial-type exhauster handling air-coal mixtures, friction factors for 8 and 12-in-diam pipe handling air-coal mixtures, general information as to the flow characteristics of air-coal mixtures in various piping systems, and methods and means for control of coal drifting in horizontal pipe.

Friction factors in the range of 0.017 to 0.035 for 8 and 12-in. pipe are indicated for the usual operating range.

FIRING of pulverized coal in progressively larger steam generators has posed several problems to the designer of pulverized-coal-handling systems. Methods of firing have changed, and simple extrapolation of the transport techniques for relatively small units of 25 years ago either is not feasible or is uneconomical for the large units and new firing methods used today.

For more than ten years the author's company has been investigating the problems of pulverized-coal transport. Much of the information developed has served as a guide in selection of equipment and designation of standards for piping design. Many of the more recent problems investigated were not clearly defined and recognized at the time the program was started, but became obvious as the work progressed.

Typical of the problems encountered in pulverized-coal transport are: (*a*) Capacity selection of exhausters; (*b*) line balancing when two or more transport pipes are used in parallel; (*c*) optimum transport velocities to permit line balancing while at the same time minimizing erosion of the pipes; (*d*) control of uniformity of splitting of primary air and pulverized fuel streams when one transport pipe is divided into two or four or more separate pipes; (*e*) and actual measurement, in commercial installations, of air velocities and pulverized-coal weight rates for the mixture flowing through individual pipes of a parallel arrangement.

With the general objective of obtaining practical answers to the foregoing problems, a test program was proposed and undertaken to obtain usable engineering information as follows:

1 Performance of a commercial exhauster handling air only, and performance of the same exhauster handling a commercial range of mixtures of pulverized coal and air.

2 Determination of piping friction losses in the transport of mixtures of pulverized coal and air.

3 Development of methods or devices for prevention of erosion of transport pipes, particularly at bends or restrictions.

4 Development of methods or devices for preventing "drifting" in transport pipes as an aid to reduction of system-pressure losses and maintenance of balanced flow in parallel-piping systems.

Item 4 was not in the original agenda, but preliminary results for the third piping system indicated the desirability of investigating the phenomenon of "settling out" or drifting.

Discussion of attempts to develop portable methods or devices for measuring coal and air flow individually in a pipe containing flowing mixtures has been omitted from the published version of this paper in the interest of brevity. Such work was done, however, and was successful in the measurement of air flow.

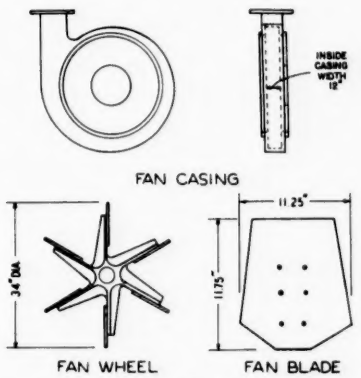

Fig. 1 Details of test exhauster

All of the test work was to be undertaken on full-size commercial equipment in order to insure that the results would be directly applicable to existing and proposed systems. The program initially was undertaken at the company's Raymond Division in Chicago. The equipment later was moved to the company's new Kreisinger Development Laboratory in Chattanooga, Tenn.

Description of Apparatus

In the course of the work, four variations of the basic exhauster design and seven full-scale piping arrangements were tested. The exhauster tests primarily were intended to evaluate the effect of wheel diameter and blade shape on the static pressure and capacity developed by the basic exhauster design. Modifications to minimize blade erosion also were studied. The exhauster used throughout the tests was a production-model Raymond exhauster designated as type C0L. The wheel diameters were 34 to 36 in. and fan speed normally was 1750 rpm or slightly less. This is a fan of rugged design used almost exclusively as a mill exhauster on the smallest of our commercial pulverizers. Features of the basic exhauster arrangement are shown in Fig. 1.

Tests of exhauster performance handling air only, or handling mixtures of pulverized coal and air, were made with the arrangement shown in Fig. 2. This arrangement had considerable versatility in that standard clean-air fan tests could be conducted

Contributed by the Power Division and presented at the Semi-Annual Meeting, Detroit, Mich., June 15–19, 1958, of THE AMERICAN SOCIETY OF MECHANICAL ENGINEERS.

NOTE: Statements and opinions advanced in papers are to be understood as individual expressions of their authors and not those of the Society. Manuscript received at ASME Headquarters, March 11, 1958. Paper No. 58—SA-24.

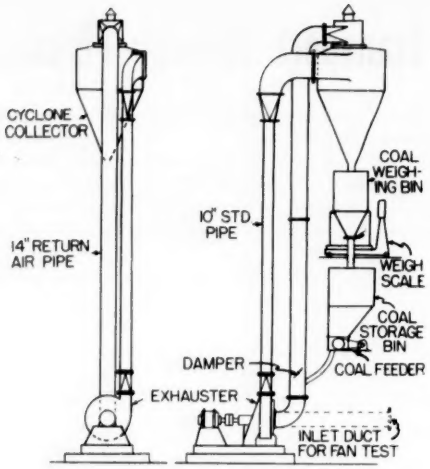

Fig. 2 First arrangement for exhauster evaluation

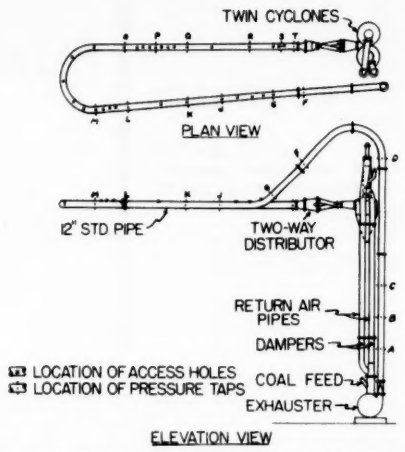

Fig. 3 Third arrangement, large loop of vertical and horizontal pipe for pipe friction losses (12-in. pipe)

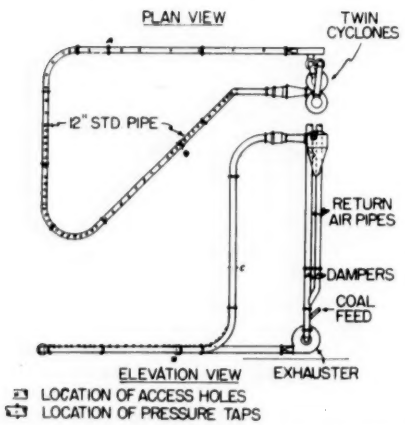

Fig. 4 Fourth arrangement, vertical and horizontal 12-in. pipe

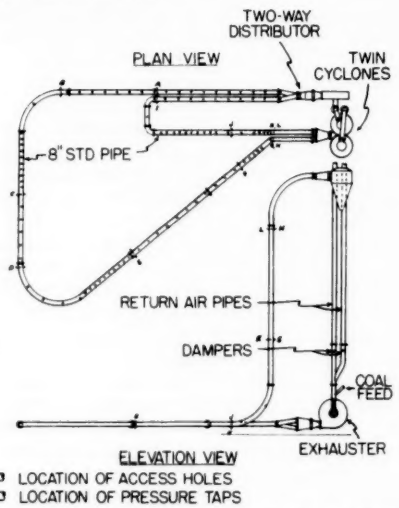

Fig. 5 Fifth arrangement, double loop of vertical and horizontal 8-in. pipe

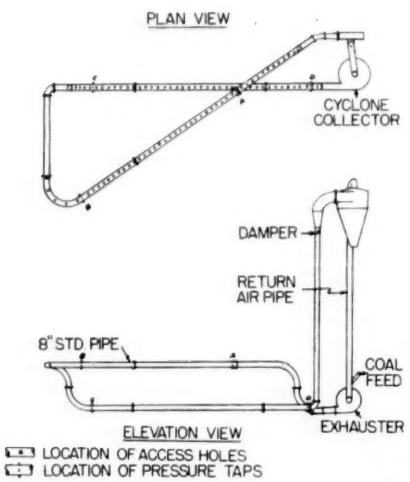

Fig. 6 Sixth arrangement, horizontal 8-in. pipe with vertical 90 deg bends

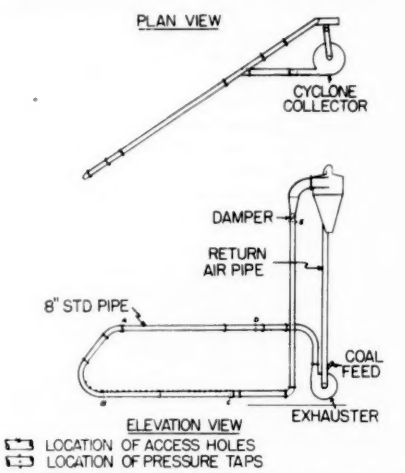

Fig. 7 Seventh arrangement, horizontal 8-in. pipe with one vertical 128-deg bend

merely by disconnecting the fan-inlet elbow and mounting the short horizontal length of full-inlet-diameter pipe shown in dotted outline on the sketch. Fan performance in handling mixtures was determined with the arrangement shown in solid outline in Fig. 2. Essentially, this arrangement consisted of the fan operating in a loop of 10-in. mixture riser pipe and 14-in. clean-air return pipe with a 5-ft-diam cyclone collector installed on the top of the loop. A weighing bin and platform scale were mounted directly under the cyclone discharge spout to receive the coal discharge and determine weight rates of the pulverized coal separated from the air circulating in the loop. After weighing, the pulverized coal could be dumped from the 1800-lb-capacity weigh bin into a 3500-lb-capacity storage bin directly underneath.

Pulverized coal was fed into the system by a rotary-table feeder mounted on the bottom of the storage bin. Coal discharged from this feeder by gravity and was sucked into the fan-inlet elbow by negative pressure maintained at that location due to system operating characteristics. Air flow in the system was regulated by a butterfly damper in the 14-in. air-return pipe. Capacity of the feeder was approximately 160 lb-per-min of coal. Feed rates were adjustable downward from that rate to as low as 20 lb per min by means of a variable-speed adjustable pulley drive. The coal-feed capacity was more than doubled in some of the later tests by addition of a second feeder in parallel.

The cyclone collector, coal bins, weigh scale, and coal feeders all were mounted on a specially designed steel structure some 30 ft high by 8 ft sq with necessary work platforms and access ladders.

The central structure, cyclone (or cyclones in later tests), coal bins, weigh scale, fan, and feeders were retained virtually unchanged in the subsequent testing of several other piping layouts derived from earlier test information.

Only very limited friction-loss information for vertical pipes could be determined from the arrangement shown in Fig. 2 and a somewhat similar double-pipe arrangement not shown. Therefore the arrangement shown in Fig. 3 was set up. Later arrangements, Figs. 4, 5, 6, and 7, were intended to supply somewhat specialized information on friction losses and coal drifting in horizontal and vertical piping with various combinations of long and short-radius bends in both the horizontal and vertical planes.

Testing Procedures

A detailed description of testing procedures given in the oral presentation has been omitted in the interest of brevity. Standard "code" test methods were used in so far as possible. Several novel methods of measurement of flow and coal drifting were used where necessary.

Test Results

1 Exhauster Performance. Exhauster performance with clean air was as expected, since considerable data were available for a whole series of exhausters of this particular type. A typical set of characteristic curves for the exhauster shown in Fig. 1, handling clean air in the test loop, is shown in Fig. 8. These characteristics were selected with the exhauster operating in a loop, rather than in a free-blow test, in order to simplify comparisons with the exhauster handling mixtures in the loop. Only slight differences existed between free-blow and loop tests.

Typical effects of variations in coal feed on exhauster performance are shown in Figs. 9 and 10. From these curves it is apparent that for any given fan-air delivery, the developed static head and fan-power consumption are essentially straight-line functions of the weight-rate of coal flowing. Points for zero coal feed were taken from clean-air tests in the loop.

Study of the data, which are too voluminous for pertinent inclusion, indicates that the nearest approximation of horsepower output of a centrifugal fan handling a mixture of pulverized coal and air may be obtained from the following equation

$$\mathrm{HP} = \frac{W \times h}{33{,}000}$$

where W is the weight of the *mixture* being handled, in lb per min, and h is developed head, in ft, of the *carrier air only*. When mixtures were involved, calculation of horsepower output on any other basis gave obviously erroneous results.

An explanation of the reason for the diverging lines of static pressure with increased rate of coal feed, Fig. 9, requires that the

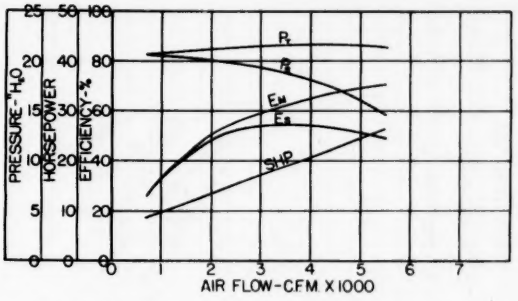

Fig. 8 Exhauster characteristic curve handling air only

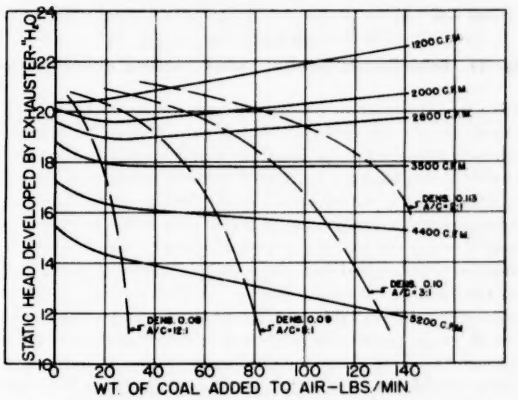

Fig. 9 Fan performance, relation of static head to weight of coal added

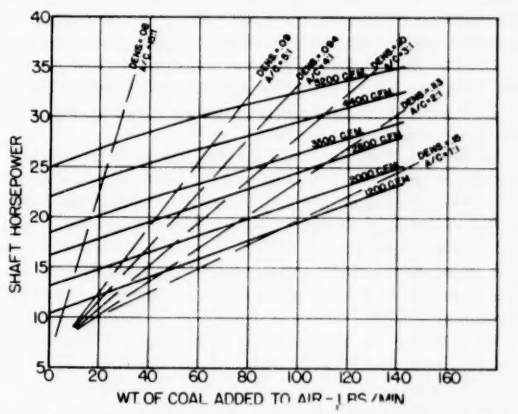

Fig. 10 Fan performance, relation of shaft horsepower to weight of coal added

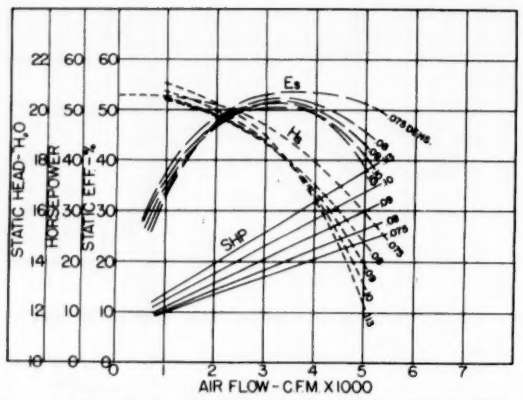

Fig. 11 Exhauster characteristic curves handling air-coal mixtures

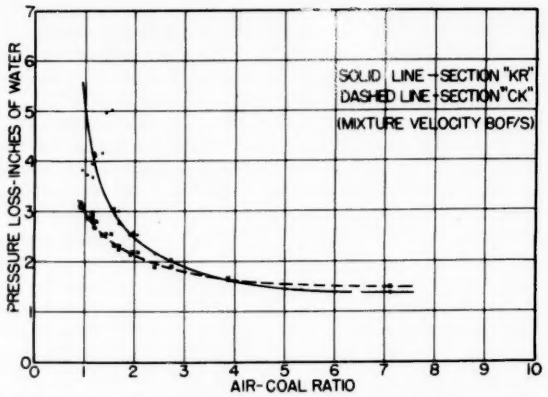

Fig. 12 Pressure loss versus air-coal ratio of sections *CK* and *KR* at mixture velocity of 80 fps (12 in. pipe, reference Fig. 3)

pulverized coal and air passing through the fan be considered as a nonhomogeneous mixture. At low rates of flow, when only air is handled by the fan, much of the kinetic energy in the air as it leaves the fan blades is converted to static pressure in the scroll by a reduction in air velocity. As the flow of air through the fan is increased, the conversion of velocity to static pressure is decreased while the velocity is proportionately higher. With the addition of pulverized coal, the energy or inertia of the coal leaving the fan blades becomes a factor. At high rates of air flow, the coal tends to act as a brake on the air in the scroll and a resultant loss in static pressure is sustained in maintaining coal velocity through the scroll to the fan discharge. At low rates of air flow, the inertia of the coal leaving the fan blades tends to have the opposite effect. The air acts as a brake on the coal and a resultant increase in static pressure of the air is obtained in reducing the coal velocity through the scroll. The trend of total pressures naturally follows the trend of static pressure, so is not shown.

The foregoing data, replotted as fan-characteristic curves for this exhauster handling various mixtures, are shown in Fig. 11 in order to give the reader a clearer concept of the effect of pulverized coal on over-all fan performance.

As mentioned earlier, several variations of this basic fan arrangement were tested to evaluate the effect of wheel diameter and blade protection on fan performance. Other than definite improvement in blade protection, no radical effects were noted on fan performance.

2 Piping Friction Losses—12-in. Pipe. Friction factors for piping are difficult to determine accurately even under relatively ideal conditions. To the problems usually encountered in such work must be added the complications of drifting in horizontal pipes and acceleration and deceleration effects of coal particles in the work reported here. Since little control could be exercised over these problems, it was necessary to determine friction losses and friction factors for relatively long lengths of piping, including bends. This strictly empirical approach resulted in voluminous pressure loss and drifting data, of which only material of general interest will be presented.

Considering first the 12-in-diam piping arrangement, Fig. 3, reproducible pressure losses and related data for sections *CK* and *KR* were determined. Typical pressure-loss data at a velocity of 80 fps for these 59 and 56-ft-developed-length sections are shown in Fig. 12. The difficulties encountered in obtaining reproducible pressure-loss data with heavy mixture densities are clearly apparent from these data, particularly for section *KR*. Although the two sections have approximately the same length, and almost identical pressure losses when handling air only, it can be seen from these curves that section *KR* has by far the higher pressure loss when a dense air-coal mixture is passed through the pipe. This was true at all velocities tested, 40 fps to 110 fps. One fact stands out clearly from these data—in a predominantly horizontal pipe such as *KR*, the pressure loss increases rapidly if the air-coal ratio drops below 1.5 to 2.0. Air-coal ratio is defined as the weight ratio lb-air/lb-coal flowing through the pipe in a unit time.

Friction factors were calculated for sections, *CF*, *KR*, and *CR* of Fig. 3. The friction factor used was taken from the equation

$$P = f \frac{L}{d} VP$$

where P is the pressure loss in inches, f is a dimensionless friction factor, L and d are the pipe length and diameter in feet, and VP is the theoretical mixture velocity pressure in inches *wg*.

No attempt was made to determine friction factors for individual bends, but some general conclusions on the resistance of vertical and horizontal pipes and bends will be made later.

Friction factors for section *CK* were affected very little by the air-coal ratio, but decreased gradually as the velocity increased from 40 to 100 fps. At 40 fps the air-friction factor for this section was about 0.02, but it decreased to about 0.014 at 100 fps. With an air-coal ratio of 1.0 (a very dense mixture in this work) the friction factor at 40 fps was only 0.025, and at 100 fps it was probably about 0.018 although the data do not include that high a velocity for an air-coal ratio of 1.0. The spread of the points was not great enough to warrant plotting friction-factor curves for section *CK*.

Friction factors for sections *KR* and *CR* are plotted in Figs. 13 and 14. Here the influence of drifting on apparent friction factors and line losses is quite pronounced. The effect of air-coal ratio is considerable, particularly at the lower velocities. At 40 fps and an air-coal ratio of 1.0 in section *KR*, the apparent friction factor is 0.091, or over four times that for air. Irregularity of the curves is due to drifting in the horizontal pipes. The location and extent of drifting are influenced by velocity, air-coal ratio, and piping arrangement as will be seen later. The general trend of these curves seems definite enough to be acceptable. The exception is the shape of the curves for air-coal ratios between 1.0 and 2.0 at velocities over 90 fps. There seems to be a tendency for friction factors to be on the increase in that region for no obvious reason, but it is difficult to say just how sharp an increase would be found if the curves could be extended. Indications are that the friction factor in section *KR* would be less than 0.035 at 100 fps if the air-coal ratio were kept above 1.5. Similarly, the friction factor in long section *CR* would be about 0.025 under the same conditions.

The friction-loss results for the arrangement of Fig. 3 were

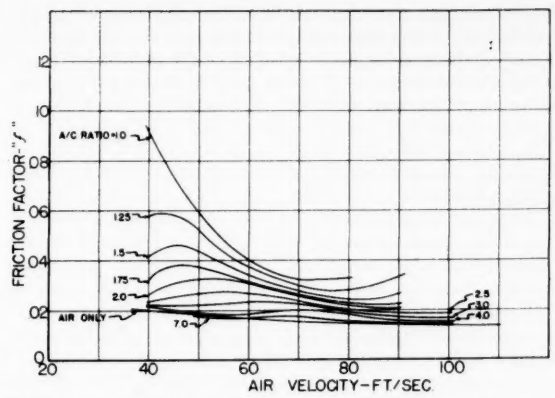

Fig. 13 *f* versus mixture velocity of section *KR* (12-in. pipe, reference Fig. 3)

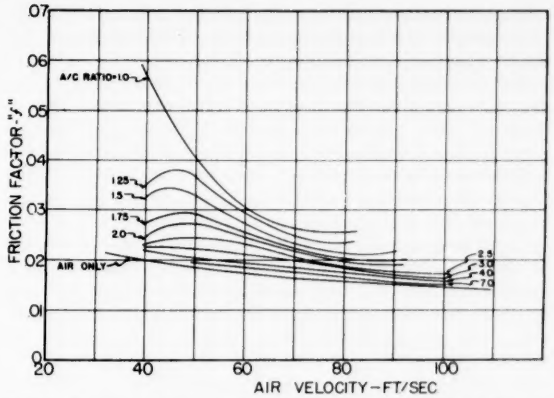

Fig. 14 *f* versus mixture velocity of section *CR* (12-in. pipe, reference Fig. 3)

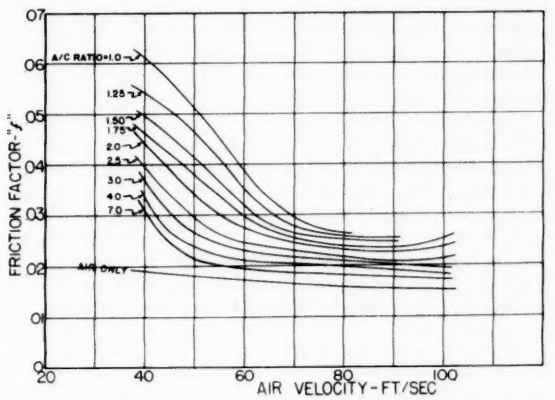

Fig. 15 *f* versus mixture velocity of section *AC* (12-in. pipe, reference Fig. 4)

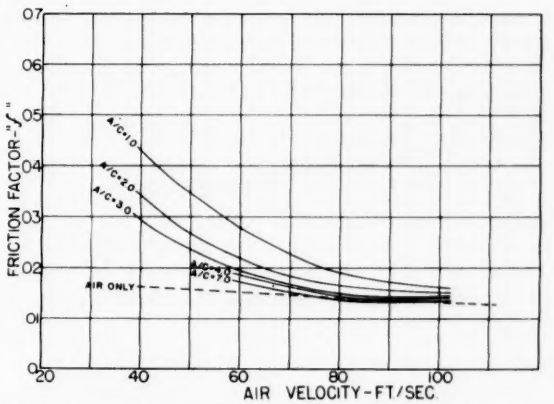

Fig. 16 *f* versus mixture velocity of section *AH* (8-in. pipe, reference Fig. 5)

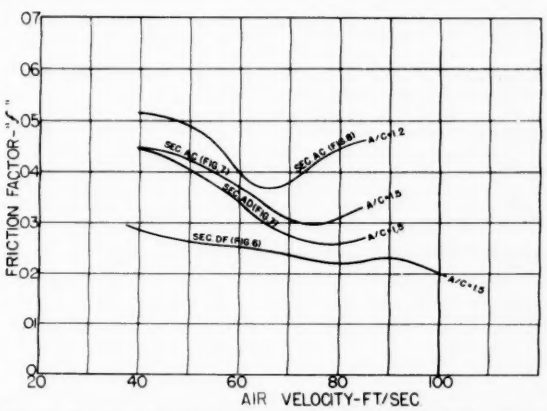

Fig. 17 *f* versus mixture velocity of sections *AC*, *AD*, *DF* of 8-in. pipe at an air-coal ratio of approximately 1.5

largely verified by the results for the arrangement in Fig. 4. Increases of coal-feeder and fan capacity made it possible for the test group to get more complete friction-loss data in the high-velocity, low-air-coal-ratio range than was possible in the earlier setup. Fig. 15 shows the friction factors for section *AC* of Fig. 4. Developed length of this section of pipe was 86 ft. These curves are very similar to those of Fig. 14 and can be considered identical for engineering purposes in the usual range of velocities and air-coal ratios. The differences encountered at the low velocity of 40 fps are only of academic interest since this is far below general operating velocities. Such differences are indicative of the somewhat different drifting characteristics encountered in the two arrangements. In summary, a friction factor of 0.024 to 0.026 for 12-in. pipe seems justified in the usual operating range.

Slightly lower air-friction factors were noted in the later series of runs. These were probably the result of the polishing action of the coal on the inside of the pipe.

3 Piping Friction Losses—8-in. Pipe. The arrangements shown in Figs. 5, 6, and 7 all were 8-in. pipe. Pressure losses and friction factors for the pipe in these arrangements showed the same general trends as previously found for 12-in. pipe. However, the results were surprising in that air-friction factors for 8-in. pipe tended to be significantly lower than would be expected from published data.[1] Mixture friction factors for 8-in. pipe also were generally lower than for 12-in. pipe.

Fig. 16 shows over-all friction factors for the large loop of the piping arrangement of Fig. 5. Similar over-all results were obtained for the arrangements of Figs. 6 and 7. Fig. 17 is a condensation of friction-factor results at about 1.5 air-coal ratio for relatively short sections of piping in Figs. 5, 6, and 7 each of which include horizontal and/or vertical bends. The relatively high

[1] L. F. Moody, "Friction Factors for Pipe Flow," TRANS. ASME, vol. 66, 1944, pp. 671–684.

R. J. S. Pigott, "Pressure Losses in Tubing, Pipe, and Fittings," TRANS. ASME, vol. 72, 1950, pp. 679–688.

resistance of downward-flow vertical bends and of horizontal pipe immediately following downward-flow vertical bends are apparent from comparison of these curves.

Vertical-pipe friction factors for upward flow are shown in Fig. 18. These curves are a composite of vertical-pipe results from the 8-in. and 12-in. piping arrangements. The low resistance of vertical pipes as compared to horizontal pipe is one of the significant results of this work and must be reckoned with by the designer. No results are available for downward flow in a vertical pipe since this is an arrangement seldom used in our modern designs. The expectation would be that downward flow would have an even lower friction factor than upward flow. Since the designer is usually concerned with over-all system resistance, major emphasis has been placed on interpretation of results for long

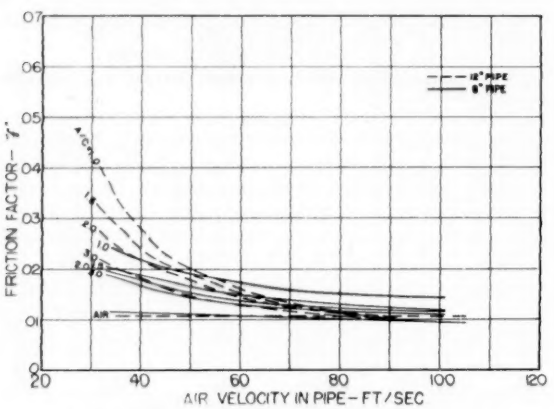

Fig. 18 Vertical-pipe friction factors (8-in. and 12-in. pipe)

lengths of piping in the various setups. This includes commonly used combinations of horizontal pipe, vertical pipe, and bends in various positions. On that basis, resistance of individual bends and relatively short lengths of pipe are primarily of academic interest, and design of piping systems based on average friction factors for long loops of these various piping arrangements is adequate. A friction factor of 0.017 to 0.018 for 8-in. pipe seems justified under these conditions in the usual operating range.

4 Drifting. Distinct similarities were noted in the drifting patterns obtained in 8-in. and 12-in. pipe. This proved to be a phenomenon which was directly related to velocity, air-coal ratio, and disturbances to flow in the pipe. However, it also appears from the data that 12-in-diam pipe in multiple parallel circuits would be subject to less unbalancing of circuits and danger of line plugging than would 8-in. pipe. As successive piping arrangements were tested, it became evident that virtually any conceivable disturbance to flow could produce drifting in a horizontal pipe downstream from the disturbance.

The effect of bends on drifting was of principal interest since bends would be the only disturbances encountered in horizontal portions of the piping arrangements generally used. These data were of particular interest since the pulverized coal used in the tests was extremely fine by commercial standards due to continual re-use and attrition of the coal "charge" in the system. For purposes of interpretation of the data, the coal fineness in all tests could be considered to be 99 per cent through 200 mesh and 90 per cent through 325 mesh (Tyler screens). It would be impossible to run tests in a loop such as this with commercial pulverized-coal sizing, due to continual attrition. A once-through system with 100 per cent make up of freshly pulverized coal would be necessary—a very expensive procedure for tests on this scale.

Several checks were made during the course of the tests to de-

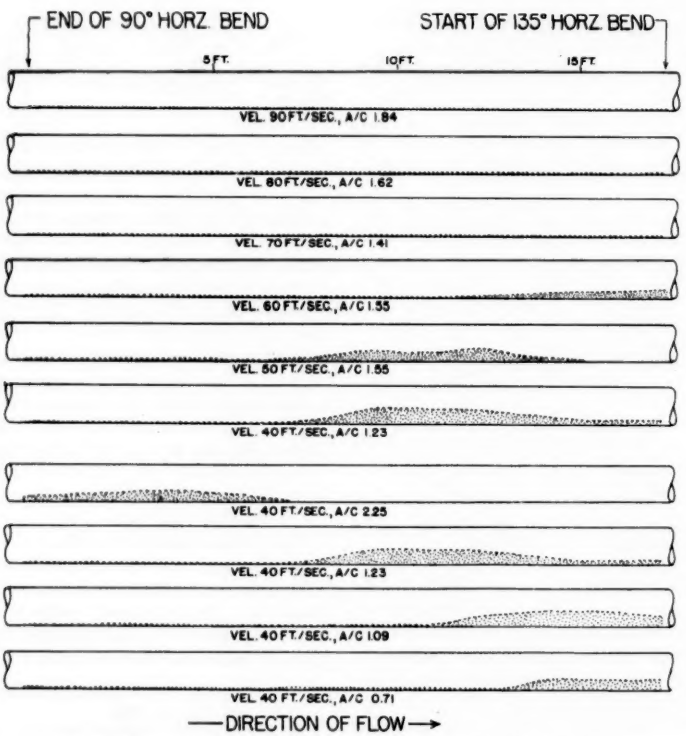
END OF 90° HORZ. BEND
START OF 135° HORZ. BEND
5 FT.
10 FT.
15 FT.
VEL. 90 FT/SEC., A/C 1.84
VEL. 80 FT/SEC., A/C 1.62
VEL. 70 FT/SEC., A/C 1.41
VEL. 60 FT/SEC., A/C 1.55
VEL. 50 FT/SEC., A/C 1.55
VEL. 40 FT/SEC., A/C 1.23
VEL. 40 FT/SEC., A/C 2.25
VEL. 40 FT/SEC., A/C 1.23
VEL. 40 FT/SEC., A/C 1.09
VEL. 40 FT/SEC., A/C 0.71
DIRECTION OF FLOW

Fig. 19 Representative longitudinal profiles of coal drifting in 12-in. pipe

termine the effect of addition of coarser coal in sizable amounts. This was carried to the point of making check runs immediately after the addition of 50 to 75 per cent raw slack coal to the bins. Except in the case of raw-slack additions, there was no appreciable effect of coarser coal on pressure losses and drifting characteristics. Immediately after the addition of raw slack, however, there was a noticeable increase in system-pressure losses and some increase in drifting following bends that tended to be the worst offenders. Such effects usually disappeared within 30 minutes to an hour, and could logically be attributed to the presence of considerable extremely coarse ($^1/_8$ to $^1/_4$-in.) coal before it was broken down to smaller sizes by attrition.

Table 1 shows the location, extent, and severity of drifting in horizontal pipes following the various types of bends used in the tests. The severity of drifting which occurred in many instances at the higher velocities was surprising, although it had been expected at the seldom-used lower velocities.

Typical sets of longitudinal drifting patterns for horizontal sections of 12 and 8-in. pipe following a 90-deg horizontal bend are shown in Figs. 19 and 20. These patterns are typical of scores of similar patterns developed for horizontal piping following all the bends tested. They show in pictorial form the patterns of drifting for only two of the many tests which have been broken down into numbers in Table 1. Complementing these longitudinal patterns are the cross-sectional profiles of drifting developed for a 135-deg 12-in. bend and for the 90-deg 8-in. bend of Fig. 20. These cross-sectional profiles are shown in Figs. 21 and 22.

These profiles, together with the data of Table 1, enable us to propose some rules regarding drifting in 8 and 12-in. pipe. It seems safe to assume that the same rules would apply to all pipe sizes in the range of 6 to at least 15 in.

For constant velocity and variable air/coal ratio: (*a*) Drifting moves closer to its "source" bend as *ACR* increases; (*b*) the maximum depth of drifting is relatively constant regardless of air/coal ratio; (*c*) following bends of 90 deg or less, the length or extent of drifting and total amount of drifted coal are fairly constant regardless of air/coal ratio; (*d*) following bends of greater turning radius than 90 deg, the length or extent of drifting, and total amount of drifted coal tend to decrease substantially as air/coal ratio increases.

For constant air/coal ratio and variable velocity: (*a*) Drifting moves closer to its source bend as velocity decreases; (*b*) maximum depth of drifting either remains constant or increases slightly as velocity decreases; (*c*) the extent and total amount of drifted coal either is constant or increases slightly as velocity decreases.

On a cross-sectional area basis, the tendency toward drifting is so much greater in 8-in. pipe than in 12-in. pipe that some of these general rules are difficult to visualize from Table 1.

The data are quite definite in showing that it is difficult, perhaps impossible, to accumulate drifted coal to a depth of more than $^1/_3$ the pipe diameter inside a 12-in. pipe. On the other hand, we had numerous cases in which coal drifted to a depth of more than $^1/_2$ the pipe diameter inside an 8-in. pipe. Thus it appears that, for multiple parallel circuits, the larger pipe diameters would be considerably safer from the danger of excessive drifting and plugging than would small-diameter pipe. We know very little of the flow patterns assumed by coal particles and air in this type of transport. Spiraling flow and undulating flow can be postulated following certain bend patterns. The effect of centrifugal forces in secondary flow through elbows is probably the principal contributor to drifting, but gravity effects can not be neglected in long horizontal runs. The distance to the "floor" of an 8-in. pipe is considerably less than in a 12-in. pipe. In cases of drifting to a depth of 4 in. inside a pipe, the ratio of maximum height through which a coal particle must move to be deposited in a drift is 2 to 1 in favor of 12-in. pipe as compared to 8-in. pipe. The height ratio for settling is always favorable to larger pipe diameters.

The progressive cross-sectional profiles invariably indicate a swirling flow pattern of the coal particles within the pipe. This is a complicating factor in drifting which we have made no attempt to evaluate. It is interesting to note the consistent differences in cross-sectional profiles for 8 and 12-in. pipe. Such profiles tend to be concave at the free surface in 8-in. pipe, whereas they tend to be convex at the free surface in 12-in. pipe. The reason for this is not obvious.

The observed differences in drifting may furnish a clue to the reason for lower apparent friction factors in 8-in. pipe than in 12-in. pipe. All the evidence seems to indicate that coal loading in an 8-in. pipe is much heavier in the bottom half of the pipe than in the top half. In fact, a majority of the coal particles may flow in the lower portion of the pipe in a fairly dense mixture at considera-

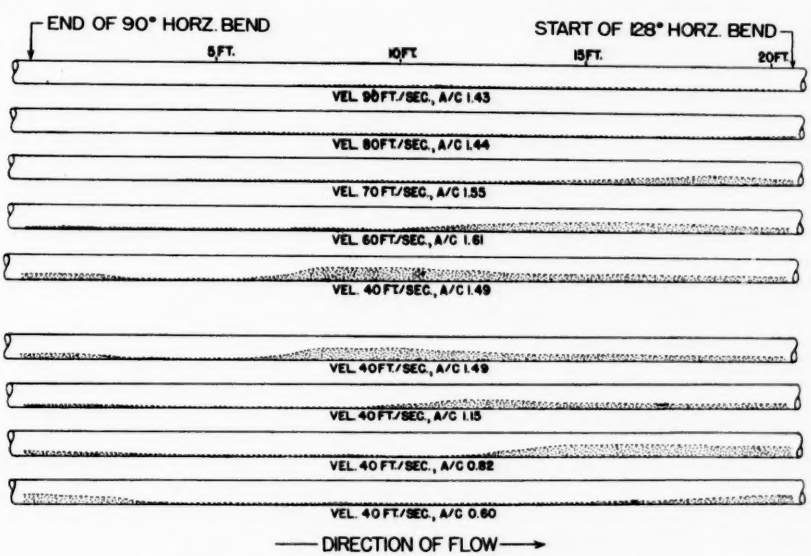

Fig. 20 Representative longitudinal profiles of coal drifting in 8-in. pipe

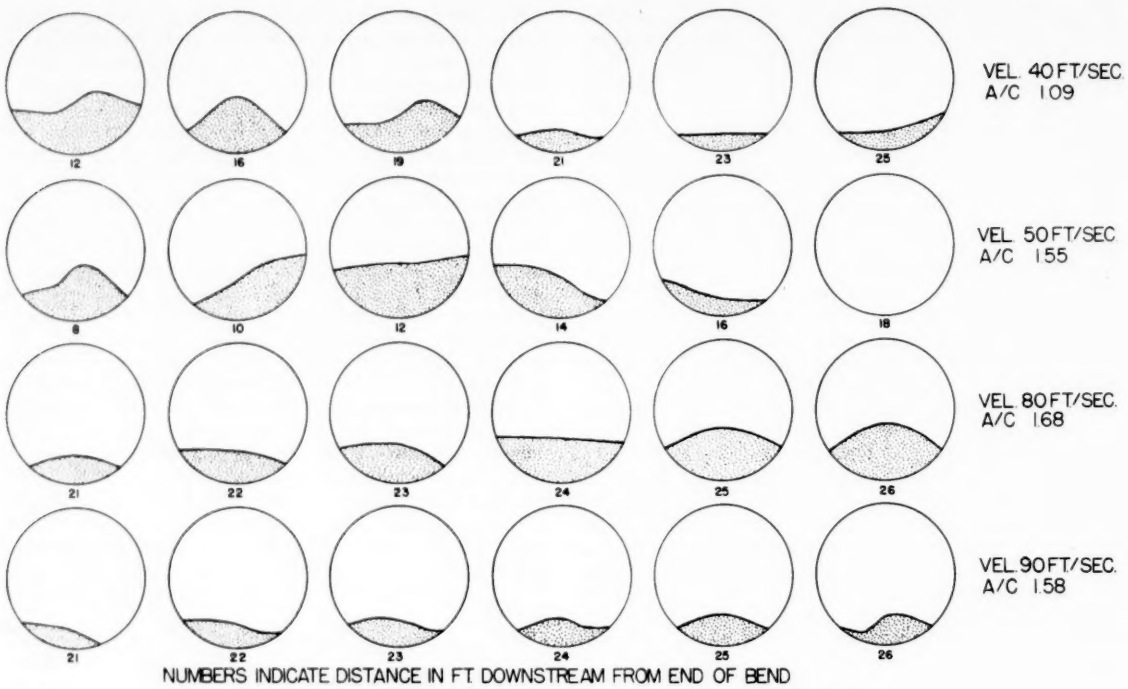

Fig. 21 Representative cross-sectional profiles of coal drifting in 12-in. pipe

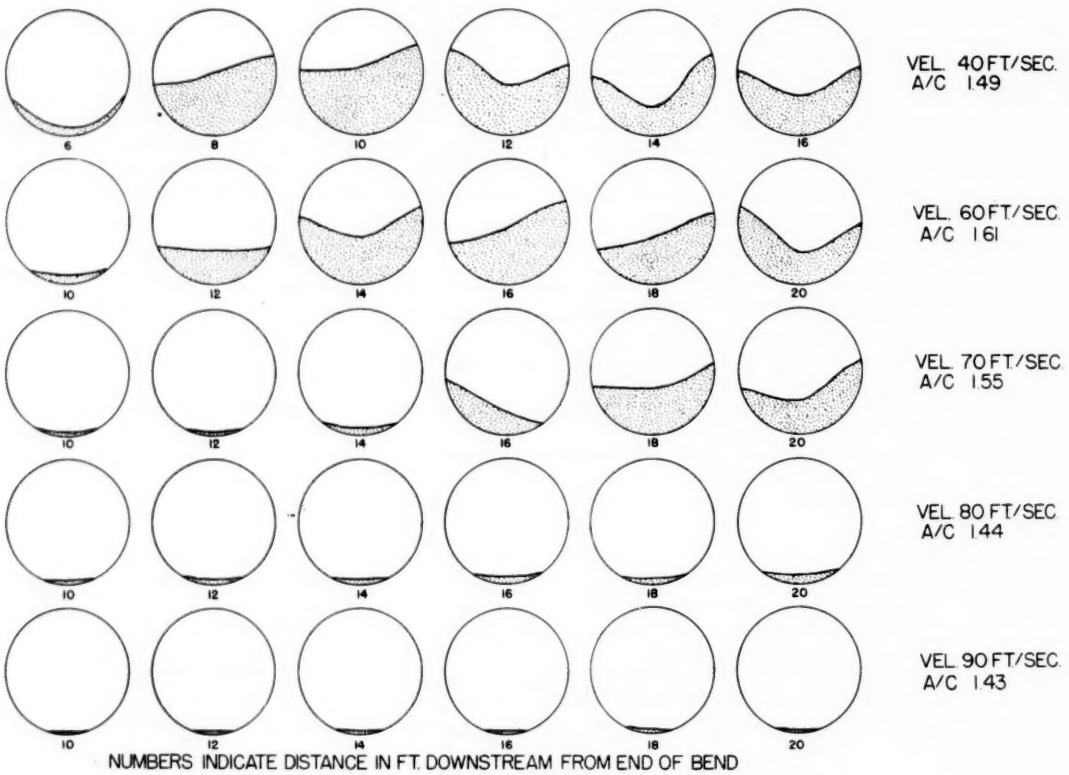

Fig. 22 Representative cross-sectional profiles of coal drifting in 8-in. pipe

Table 1 Table of drifting characteristics downstream from bends in 12-in. and 8-in. pipe

PIPE SIZE, INCHES	TYPE OF BEND	BEND RADIUS, INCHES	AIR-COAL RATIO, LBS/LBS	VELOCITY, FT/SEC	DISTANCE, FEET	LENGTH, FEET	DEPTH, INCHES
12	184° HORZ	60	1.04	80	10	>22	4 1/4
12	184° HORZ	60	1.35	80	10	15	4
12	184° HORZ	60	1.68	80	7	12	4 3/4
12	184° HORZ	60	2.08	80	5	10	2 3/4
12	184° HORZ	60	2.40	80	5	8	2 7/8
12	184° HORZ	60	1.68	90	0	30	4 3/8
12	184° HORZ	60	1.68	80	7	12	4 3/4
12	184° HORZ	60	1.74	70	0	15	4 1/2
12	184° HORZ	60	1.63	50		16	4 7/8
12	184° HORZ	60	1.82	40		22	4 1/4
12	135° HORZ	60	0.88	80	>25	—	3/4
12	135° HORZ	60	1.10	80	23	> 7	2 1/4
12	135° HORZ	60	1.25	80	19	> 8	3 1/2
12	135° HORZ	60	1.62	80	19	7	3 3/4
12	135° HORZ	60	2.03	80	14	5	3 1/4
12	135° HORZ	60	2.52	80	8	6	2 1/2
12	135° HORZ	60	1.60	90	18	>10	3
12	135° HORZ	60	1.41	70	19	> 9	4
12	135° HORZ	60	1.55	60	16	7	3
12	135° HORZ	60	1.55	50	6	9	4 1/2
12	90° HORZ	60	0.71	40	13	> 4	3 1/4
12	90° HORZ	60	1.09	40	11	> 6	5 1/2
12	90° HORZ	60	1.23	40	6	>11	5
12	90° HORZ	60	2.25	40	0	7	3
12	90° HORZ	60	1.84	90	—	—	—
12	90° HORZ	60	1.62	80	—	—	—
12	90° HORZ	60	1.64	70	—	—	—
12	90° HORZ	60	1.55	60	12	> 5	3
12	90° HORZ	60	1.55	50	7	8	3 3/4
8	128° HORZ	40	0.89	80	31	> 5	1
8	128° HORZ	40	1.09	80	19	16	2
8	128° HORZ	40	1.44	80	16	11	1 1/2
8	128° HORZ	40	1.63	80	9	10	1 1/4
8	128° HORZ	40	2.07	80	7	5	2
8	128° HORZ	40	2.73	80	6	5	2 1/2
8	128° HORZ	40	1.46	100	20	8	1 1/2
8	128° HORZ	40	1.43	90	22	8	2
8	128° HORZ	40	1.55	70	8	8	2 1/2
8	128° HORZ	40	1.61	60	7	12	3 1/4
8	128° HORZ	40	1.49	40	4	>37	4
8	90° HORZ	40	0.60	40	14	> 6	3
8	90° HORZ	40	0.82	40	12	> 8	4
8	90° HORZ	40	1.15	40	9	>12	3
8	90° HORZ	40	1.49	40	6	>14	4
8	90° HORZ	40	1.43	90	—	—	—
8	90° HORZ	40	1.44	80	18	> 2	1
8	90° HORZ	40	1.55	70	12	> 8	3
8	90° HORZ	40	1.61	60	10	>10	3 1/2
8	90° HORZ	8	0.84	80	—	—	—
8	90° HORZ	8	1.10	80	10	7	1 3/4
8	90° HORZ	8	1.70	80	—	—	—
8	90° HORZ	8	2.90	80	—	—	—
8	90° HORZ	8	1.50	100	—	—	—
8	90° HORZ	8	1.80	60	6	3	1 1/8
8	90° HORZ	8	1.50	40	0	>16	3 1/4
8	(DF) 128° VERT	40	1.17	84	13	>11	2 3/4
8	(DF) 128° VERT	40	1.21	63	7	8	3 1/2
8	(DF) 128° VERT	40	1.32	41	4	13	4 1/4
KICKER BLOCK INSTALLED 57" UPSTREAM FROM END OF BEND							
8	(DF) 128° VERT	40	1.20	80	16	8	1 3/4
KICKER BLOCKS INSTALLED 57" AND 26" UPSTREAM FROM END OF BEND							
8	(DF) 128° VERT	40	1.19	80	—	—	—
KICKER BLOCKS INSTALLED 57", 26" AND 0" UPSTREAM FROM END OF BEND							
8	(DF) 128° VERT	40	1.19	80	—	—	—
KICKER BLOCK INSTALLED 57" UPSTREAM FROM END OF BEND							
8	(DF) 128° VERT	40	1.23	40	6	14	4 3/4
KICKER BLOCKS INSTALLED 57" AND 26" UPSTREAM FROM END OF BEND							
8	(DF) 128° VERT	40	1.23	40	5	14	3 1/8
KICKER BLOCKS INSTALLED 57", 26" AND 0" UPSTREAM FROM END OF BEND							
8	(DF) 128° VERT	40	1.23	40	7	17	2 3/4
8	(DF) 90° VERT	40	1.19	82	23	11	3
8	(DF) 90° VERT	40	1.49	80	20	8	2
8	(DF) 90° VERT	40	1.98	80	13	6	2
8	(DF) 90° VERT	40	2.51	80	—	—	—
8	(DF) 90° VERT	40	2.98	80	—	—	—
8	(DF) 90° VERT	40	1.49	80	20	8	2
8	(DF) 90° VERT	40	1.50	60	12	8	2 1/2
8	(DF) 90° VERT	40	1.50	40	5	10	4 1/2
8	(UF) 90° VERT	40	1.19	82	—	—	—
8	(UF) 90° VERT	40	1.49	82	—	—	—
8	(UF) 90° VERT	40	1.98	82	—	—	—
8	(UF) 90° VERT	40	2.51	80	—	—	—
8	(UF) 90° VERT	40	1.25	40	—	—	<1
8	(UF) 90° VERT	40	1.50	40	—	—	<1
8	(UF) 90° VERT	40	2.00	40	—	—	<1
8	(UF) 90° VERT	40	2.40	40	—	—	<1

bly lower velocity than the main air stream. This flow may be in somewhat of a wave motion requiring relatively little energy from the air to keep it moving. Drifting and pressure-loss data for the two pipe sizes indicate that this is a distinct possibility. Although the data of Table 1 may seem to give cause for concern, it must be remembered that the loops that were tested were arranged to obtain the maximum information with the minimum number of setups and tests, and do not represent commercial installations in themselves.

The study of the data that has been made indicates many "outs." For instance, Table 1 shows that, in the usual degrees of turn, velocity, and air/coal ranges, downward-flow vertical bends immediately followed by horizontal pipe are by far the worst offenders in causing objectionable drifting. However, downward-flow vertical bends are seldom, if ever, used except immediately adjacent to burners. As a result there is insufficient length of horizontal pipe following such bends to permit significant drifting to occur in a commercial installation.

Upward-flow vertical bends in the range of 90 deg are commonly used, but there seems to be no tendency toward appreciable drifting following such bends regardless of the length of horizontal pipe following the bend.

Bends in the horizontal plane appear to require careful planning, since horizontal bends of various degrees of turn are commonly used, and such bends frequently are followed by long lengths of horizontal pipe. Fortunately, since the amount of drifting grows progressively greater as the degrees of turn increase, there seldom is need for more than a 90 deg turn in a horizontal bend. The amount of drifting following horizontal bends of 128 to 184 deg is virtually prohibitive of their use even in the 70 to 90 fps and 1.5 to 2.0 *ACR* range. At velocities below 70 fps use of such large degrees of turning in a horizontal bend could cause catastrophic line plugging in 8-in. pipe.

On the other hand, horizontal bends of 90 deg or less cause only tolerable drifting, if any, when velocities are maintained well above 70 fps and air-coal ratios are maintained in the range of 1.5 or higher. Interestingly enough, these limitations are applicable to bends of turning radius $R = 5d$. If the turning radius is reduced, the danger of drifting following the bend is significantly reduced. Horizontal bends or $R = d$ or $R = 1^1/_2 d$ show very little tendency to cause drifting downstream at normal velocities even with extremely dense mixtures (low air/coal ratios). Unfortunately, this benefit of very-short-radius bends is accomplished with considerable penalty in pressure loss as compared to more gradual bends, so their use must usually be restricted to special cases in order to conserve available head in the system.

In general, all bends may be safely used if the velocity, air/coal ratio, and amount of horizontal pipe following such bends conform to the obvious safe values which may be screened from Table 1. Although not an infallible rule, it was generally true that drifting initiated by a given bend would be dissipated by a second bend downstream, rather than continue into the second bend. This was illustrated in many series of tests in which a progressive movement of drifting downstream from a bend (as velocity or air/coal was varied) was eventually dissipated by movement into the following bend in the loop.

5 Erosion and Drifting Preventives. Erosion was never a problem in these tests, but under certain conditions in commercial installations, erosion can be a problem. Troublesome erosion is generally limited to bends and other devices in which a change of direction or velocity is encountered. As a general rule, excessive erosion of bends will not occur with the generally used pulverized coals of the United States unless line velocities in excess of 90 fps are used. Prevention of bend erosion is most easily accomplished by maintaining velocities below 90 fps. Where special coals or chars, or unusual velocities, make it necessary, bends can be adequately protected by use of cast wear-resistant-alloy elbows or by use of replaceable kicker blocks or steps. These blocks are bolted into the elbows at suitable locations to take the wear and also redistribute the coal somewhat in the air stream. Exact location of such kicker blocks in any given installation is dictated by the piping configuration before the bend to be protected. Brief tests of the benefit of kicker blocks in downward-flow vertical bends, showed that one or two properly located blocks would prevent or reduce drifting for a considerable distance downstream from the bend at no penalty or benefit to system-pressure loss. Pressure-loss advantage gained by elimination or partial elimination of drifting by the blocks was almost exactly offset by increased pressure loss in the bend and immediately after the bend

due to re-entrainment of coal in the air stream. These tests were made with blocks or steps of 2-in. rise in an 8-in. pipe.

The best drifting preventive is maintenance of adequate line velocity and air-coal ratio. At design capacities, velocities in the range of 70 to 90 fps and air/coal ratios in the range 1.3 to 2.0 permit considerable latitude in piping layouts.

Conclusions

The performance of various components of pulverized-coal-transport systems have been investigated and some flow characteristics of pulverized-coal and air mixtures have been developed. Many of the flow-characteristic data are empirical in nature since the work was aimed primarily at the solution of specific problems, and there is virtually no published information with which to compare these results.

Radial-blade fan performance, as influenced by passage of pulverized coal through the fan, has been described in detail. Horsepower output of the fan is a direct function of the dust loading imposed on the fan. Static head developed by the fan is a complex relationship dependent on both air output and dust loading.

Friction factors have been developed for representative arrangements of 8 and 12-in-diam pipe. Friction factors of 0.017 to 0.035 appear reasonable for representative piping systems, but the use of a specific factor must be tempered with a knowledge of the drifting characteristics which may be encountered in a given arrangement under design flow conditions.

Information as to the drifting characteristics of pulverized coal in transport pipes has been accumulated for several different piping arrangements. All bends or obstructions, which cause discontinuities in flow, will set up characteristic drifting patterns in horizontal, or nearly horizontal, pipe. Therefore, piping layouts, particularly those incorporating parallel circuits, must be carefully planned to circumvent drifting and danger of line plugging. This can be done using "rules of thumb" outlined in the body of the paper.

Acknowledgment

The author wishes to acknowledge the invaluable technical assistance and guidance contributed by the late Joe Crites and by Alexander Bogot during the major portion of the experimental work several years ago. He is especially indebted to W. A. Scheerer for able assistance during the test work and in preparation of the manuscript. The following individuals also took an active part in the conduct of the tests and collection of data: C. E. Blakeslee, E. Jesche, John Tucker, and W. P. Guhne.

DISCUSSION

M. WEINTRAUB[2]

This paper is a welcome addition to the literature on pneumatic transport of powders, because it provides specific information on pulverized-coal transport in concentrations usually present in transport between pulverizers and burner nozzles; i.e., air-to-coal ratios of 12 lb of air per lb of coal to 1 lb per lb. Such specific data are needed because no all-inclusive theory has yet been developed that is applicable to different materials in a range of pipe sizes. One limitation in wider application of this paper is indicated by the use of a single coal size that was appreciably finer than industrial usage because of recirculation and attrition, although the statement that only in extreme cases did the addition of coarser coal have an appreciable effect is encouraging. The high percentage of fines raises a question as to whether the cyclone was efficient enough to insure that the air to the metering orifice was sufficiently clean to provide accurate flow measurements.

The author provides an interesting and quite plausible description of the action of the solids in sometimes assisting and sometimes retarding the air flow from the exhauster. This, however, does not explain the relation shown in Fig. 11, wherein a small amount of coal injected into the 2000-cfm stream could cause a decrease in static head, while a larger amount causes an increase. A less complex relationship is shown by using feet of fluid flowing rather than inches of H_2O as a measure of static head. This value of head is also required in computing horsepower output and efficiency since the basic equation

$$\text{HP} = \frac{PV}{33{,}000} = \frac{\text{lb psf} \times \text{cfm}}{\text{ft-lb per min per HP}}$$

may be transformed by substituting

$P = h\rho$ and $V = W/\rho$ to yield the equation used by the author:

$$\text{HP} = \frac{Wh}{33{,}000}$$

In this transformation, W, h, and ρ must refer to the same fluid, the mixture of coal and air, in order that ρ shall not appear in the derived equation.

As shown in the accompanying Figs. 23 and 24, this introduction of the stream density eliminates the minima and the divergences exhibited in Fig. 11 and the disturbing "crossover" shown by the efficiency curves of Fig. 13. The crossovers shown in Fig. 23 are due to the use of the coal-flow rate, rather than a function of density, as the abscissa, as is demonstrated in Fig. 25, in which the head is plotted directly against the mixture density. The lower efficiencies, shown in Fig. 24, like the decrease in head with increasing density, shown in Fig. 25, reflect the fact that the fan cannot handle two phases with the same facility as a homogeneous stream.

The value of the friction-factor data for the various pipe configurations has been mentioned before. It may be instructive to compare this work with a recent report[3] in which the friction factor in $^1/_2$-in-diam straight pipes for air conveying 400-mesh glass beads was found to be about 0.015 for an air/solid ratio of 1.0. In connection with the writer's earlier comment on the effect of particle size, it may be noted that these investigators found that, when the particle size was increased by a factor of $2^1/_2$, the friction factor increased almost proportionately, and the entire mechani m of transport seemed to be altered. The writer would like to inquire whether consideration has been given in the calculations to the hydrostatic head of the suspensions in vertical runs. He estimates that this might exceed 0.5 in. H_2O in a 25-ft height.

The data on drifting are not only of highly practical value but suggest the probable mechanism of solids flow around bends. Centrifugal action throws the solids out of the fast-moving stream into the boundary layer on the outer radius. In upflow around a bend, the solids, after completion of the directional change, fall back into the main stream. In downflow, gravity helps to ma ntain the phase separation. A given gas velocity will impart the same centrifugal force to all particles; however, the heavier concentrations, after compacting against the outer radius, will offer less air and frictional resistance per unit mass of material than lighter concentrations, and hence will travel farther down the pipe. As the solids are slowed during this travel, local concentrations may increase to the point where choking occurs,

[2] Chemical Engineer, Combustion Section, Bureau of Mines, U. S. Department of the Interior, Pittsburgh, Pa.

[3] N. C. Mehta, J. M. Smith, and E. W. Comings, "Pressure Drop in Air-Solid Flow Systems," *Industrial and Engineering Chemistry*, vol. 49, 1957, pp. 986–992.

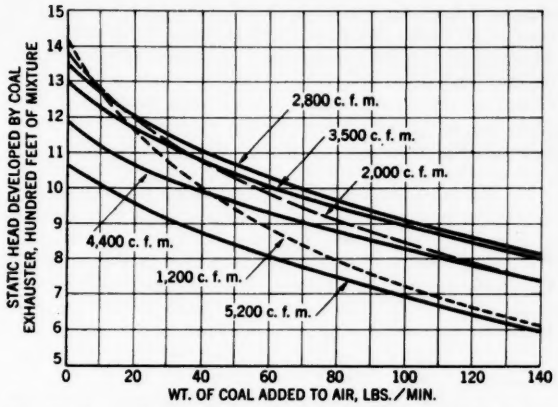
STATIC HEAD DEVELOPED BY COAL EXHAUSTER, HUNDRED FEET OF MIXTURE
WT. OF COAL ADDED TO AIR, LBS./MIN.
2,800 c. f. m.
3,500 c. f. m.
2,000 c. f. m.
4,400 c. f. m.
1,200 c. f. m.
5,200 c. f. m.

Fig. 23 Fan performance, relation of static head to weight of coal added

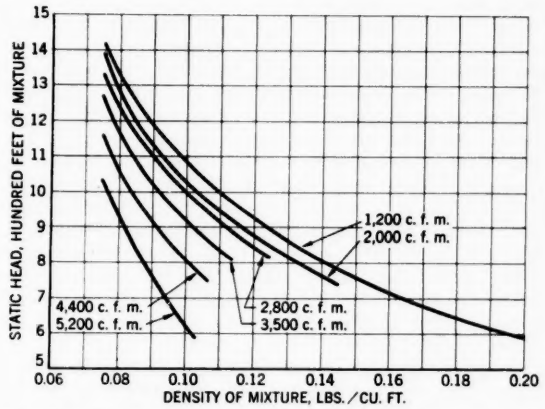

Fig. 25 Fan performance, relation of static head to mixture density

and at very high concentrations and low flows an additional drift may be created, such as is evidenced in the bottom diagrams of Fig. 22.

Many other effects exhibited in the author's Table 1 are similarly explainable by consideration of the amount of centrifugal force generated under various flow conditions. This leads to the suggestion that small properly placed jets of air may drive the drift out of the boundary layer and back into the main stream. Another point worth investigating would be whether proper proportioning of velocity and radius of curvature could improve the drifting characteristics of large-angle bends. It should be noted that Table 1 shows that the position of the drift following the 184-deg bend is intermediate to the positions following the 90 and 135-deg bends. The author notes also that drifting is reduced by using smaller values of R/d. On the other hand, it is obvious that drifting is also reduced at infinite values of R/d and it may be the case that the value of $R/d = 5$ used in this investigation is close to the worst possible ratio.

RICHARD B. ENGDAHL[4]

This paper is most welcome because of the inordinate time which has been consumed in many large installations in the past in attempts to compensate for maldistribution of fuel and air flow and for drifting of coal in multiple burner systems. The

[4] Division Chief, Battelle Memorial Institute, Columbus, Ohio. Mem. ASME.

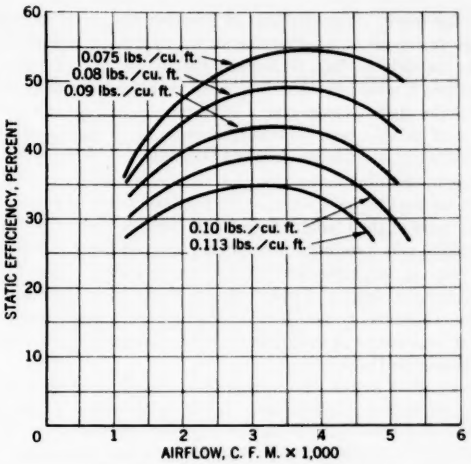

Fig. 24 Exhauster-efficiency curves

author is further to be commended for making available in this paper so much of what he and his associates have learned in this long period of research.

The results are particularly illuminating in helping in part to explain why some attempts to meter the flow of coal-air mixture in large systems have been unsuccessful. Where the metering depends on the acceleration of the air and coal particles, if disturbances ahead of the metering elements produce drifting or if, as the authors point out, segregation of flow in the lower half of a pipe occurs, metering is likely to show large and erratic errors.

On the other hand, in small pipes where drifting is less likely and uniform flow can be promoted by long runs rather than by special mixing devices, metering has been successful.

In various laboratory projects on pulverized coal the problem of plugging of pressure taps by drifted coal in the tap tube has been easily solved by use of porous stainless steel plugs inserted in the pressure-tap openings.

The unique and ingenious air-velocity probe and drift depth meter should prove of great value to all who have the problem of balancing multiple burner systems.

It is to be hoped that the author's excellent work can be carried on to develop devices for effective control of the uniformity and rate of flow of coal-air mixtures.

J. B. GRAHAM[5]

The author is to be congratulated on a very fine paper and very excellent handling of a difficult subject. As anyone in the field of pneumatic conveying knows, the information in this field is meager and worth-while contributions such as this are welcome.

We have been interested for some time in similar problems of conveying particulate matter in an air stream. Our experience along this line prompts us to call attention to several items in this paper. Under the heading Test Results and the subheading Exhauster Performance there is an explanation of the reason for the diverging line of static pressure with increased rate of coal feed. This particular section of the paper treats the energy or inertia of the coal leaving the fan blades, and explains how the inertia of the particle affects the static pressure developed in the fan. We would like to call attention to the fact that one important parameter of this action has been omitted and that is the effect of particle size on the development of

[5] Research Department, Buffalo Forge Company, Buffalo, N. Y.

static pressure. The problem of whether the particle imparts energy to the air or whether the air is required to impart energy to the particle is due, to a great extent, on the particle size. Therefore, it would be most helpful to those of us working in this field if the author could give a little more detail on the particle size used in this test, especially during those tests where this particular phase of the program was studied.

Also, in handling material within the fan wheel, it is of considerable interest to know whether the material tends to concentrate in any part of the blade passages. If there is separation or concentration this produces nonuniform flow within the fan wheel and may in some instances cause recirculation. The present test is not involved in detail studies of flow within the fan wheel, but we would like to ask the author whether he found any indication of concentrated coal flow by observing erosion patterns on the wheels used in this test.

The author states that various fan wheels were used in this test, and that evaluations were made on the effect of wheel diameter and blade protection on fan performance. The author states that improvement in blade protection was noted. It would be interesting to know what shape blades afforded the best protection during these tests. It has been our observation that fan wheels having the highest static efficiency were in general the blades that had an inherently high blade-protection value. In Fig. 1 the author shows the sketch of the exhauster used on these tests. He indicates one type of fan wheel, namely, a flat bladed wheel. We are especially interested to know whether he tried any curved bladed wheels, since in our experience this has afforded definite improvement in a number of cases.

There is a minor point we would like to bring out in connection with Fig. 2 and some of the subsequent figures. The substitution of the straight inlet duct for fan tests for the elbow used on the recirculating portion of the test is not completely valid. The straight section affords a good inlet condition for the fan, while the elbow used in the test will affect fan performance and, therefore, appears as an unaccounted for variable in the fan-performance figures. We simply want to call attention to this minor discrepancy in case some unaccounted for errors appeared. We do not feel that under the test conditions the error due to this elbow would be an important factor.

AUTHOR'S CLOSURE

The points which the discussers raise all are interesting and illustrative of the broad nature of the whole problem of pneumatic transport.

Mr. Graham's question regarding the effect of particle size on the static pressure developed by a fan cannot be answered in any more detail than already given in the paper. The coal fineness in all tests can be considered to be of the order of 99 per cent through 200 mesh, 90 per cent through 325 mesh. I would expect a natural particle-size distribution, but we did not refine the work to the degree of determining complete particle-size distribution. It can be said, however, that the fan-test results have proved useful over the years in predicting our fan performance with commercial pulverized coal.

No wear or erosion patterns ever were observed on the test fans. Despite voluminous testing, the operating hours were not significant compared to those logged by a commercial fan in continuous operation. We just did not run the fans long enough to get significant wear. We have tested curved blade fan wheels in our general fan performance evaluation work, but we have no wear information on curved blades and have never to my knowledge used anything but a flat-bladed radial-type wheel in our commercial work. We have found that use of "protected" or whizzer-type fan inlets consisting of an annular pick-off at the fan inlet and short, radial-angle iron blades bolted to the inlet shroud of the wheel results in good main blade protection. Some loss in fan performance results, but short-circuiting of a large portion of the coal away from the main fan blades and through the stub blades is quite effective in reducing wear.

Mr. Graham is quite correct in pointing out that substitution of straight inlet duct fan tests for tests with an inlet elbow in a recirculating system is not completely valid. We conducted the straight inlet duct tests to give us a basis for comparison of loop tests (including inlet elbow) with our usual standard free-blow fan tests. The only clean air fan test reported in the paper is that of Fig. 10 with the exhauster operating in a loop. We did not feel justified in reporting the free-blow tests in this paper, although only slight differences were found.

The author is familiar with some of the work done at Battelle by Mr. Engdahl and his associates and hopes that they will find much that is useful to them in this work. Our chief regret is for the unavoidable delay in making our information available.

Mr. Weintraub's comments and supplementary calculations and plots are quite pertinent and extremely useful as a more generalized approach to fan performance than was attempted in the paper. We do not consider the "crossover" of efficiency curves to be as disturbing as does Mr. Weintraub since we are able to apply the results more directly to pulverizer and exhauster performance than would be the case if we had to evaluate the results in terms of transport of other materials of substantially different physical properties. Similarly, the variations in static head which Mr. Weintraub cites for Fig. 11 are principally of academic interest to us since the dust loadings in the range for which he works out an explanation are far outside the usual commercial range. Mr. Weintraub's analyses will have considerable interest to those attempting generalized correlations with other work.

We have not attempted calculations of hydrostatic head in vertical pipe, but such heads could well be 0.5 in. H_2O in 25 ft depending on air-coal ratio and uniformity of mixture. Mr. Weintraub's comments on separation and drifting are quite interesting, and generally agree with our impressions of the mechanisms of drifting. Use of air jets to re-entrain drifts would have to be investigated experimentally to determine usefulness. Source of such air would be one problem in a commercial system, and some of our results indicate that the jets might create drifting elsewhere. Selection of elbow R/d must be done on the basis of several factors other than drifting alone, system pressure loss being the major item. Since line length proportioning can be used in most cases to minimize drifting in our work, we utilize that approach wherever possible. Small R/d ratios are used where necessary and feasible.

Mr. Weintraub's question as to accuracy of a metering orifice in a dust laden stream was answered in the original uncondensed version of this paper. Briefly, an orifice differential is not significantly affected by presence of dust in the air stream, even at high mixture densities (low air/coal ratios). In addition, cyclone collector efficiencies are quite high, perhaps 99 per cent, in the heaviest mixture density range in which the tests were conducted.

The probable cause of early cessation of drifting following the 184-deg bend was lack of sufficient length of horizontal pipe to accommodate the natural amount of drifting which would have occurred if the straight horizontal run had not ended.

E. DAMAN[1]
H. PHILLIPS[2]
J. VAIL[3]
S. LING[4]

Operating Results of an Experimental Supercritical Steam Generator

This paper presents some of the results achieved with a 2000 lb/hr supercritical pilot plant after 5000 hours of operation. Data on water side conditioning and the effect of final steam temperature on corrosion rate are presented. The paper also describes a successful automatic control system which was developed. Tests and test results from control runs are presented and it is shown how these results can be applied to the design of central station once-through steam generator control systems.

Description of Plant

In order to obtain information needed to design once-through central station steam generators, operating at subcritical and supercritical steam conditions, a pilot plant was erected and operated at the Carteret Laboratory of the Foster Wheeler Corporation. This plant has been in operation since 1956, and, as of January, 1958, has operated about 5000 hours.

The main objectives set for investigation were as follows:

1 Water treatment
2 Control
3 Circuit stability

This paper will discuss some of the experimental results obtained under the first two items.

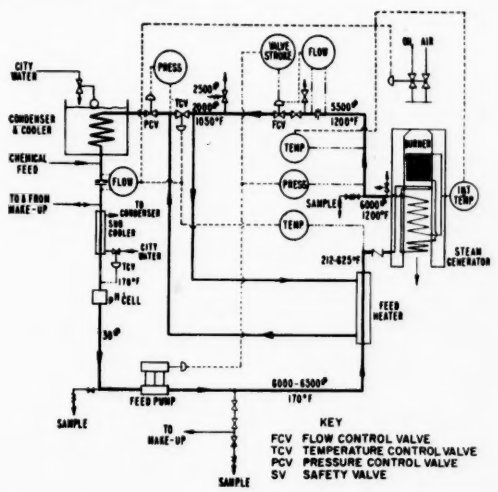

Fig. 1

The test loop is shown in Fig. 1. The plant is designed to generate 2000 pounds of steam an hour at pressures and temperatures up to 5500 psi and 1200 F. Water from the reciprocating, variable stroke, feed pump passes through a pipe-within-a-pipe feedwater heater, a nonreturn valve, and through the generator in two parallel circuits. Leaving the generator, the steam is metered by an orifice and reduced in pressure by a flow control valve (FCV), which simulates the action of a turbine throttle valve. After being used for feedwater heating, the steam is reduced in pressure through a pressure control valve (PCV), and the heat is rejected by condensing the steam in a spiral tube immersed in a tank of water boiling at atmospheric pressure. The condensate is metered, subcooled, and returned to the feed pump suction. The feedwater temperature is controlled by varying the opening of the temperature control valve (TCV).

The make-up feedwater is obtained by condensing steam from the plant heating boilers. It is demineralized in a mixed bed ion exchanger and sprayed into a deaerator and feed storage tank. Heating steam for the deaerator is provided by the evaporation of deaerated water by the means of an external heat exchanger.

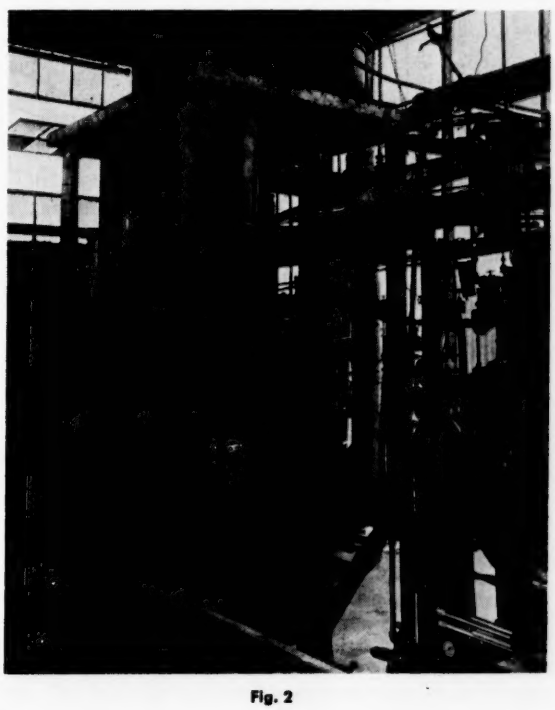

Fig. 2

---

[1] Deputy Director of Research, Foster Wheeler Corporation, New York, N. Y. Mem. ASME.

[2] Project Engineer, Research Department, Foster Wheeler Corporation. Assoc. Mem. ASME.

[3] Project Engineer, Research Department, Foster Wheeler Corporation.

[4] Proposal Engineer, Steam Department, Foster Wheeler Corporation. Assoc. Mem. ASME.

Contributed by the Power Division and presented at a joint session of the Power and Fuels Divisions at the Semi-Annual Meeting, Detroit, Mich., June 15–19, 1958, of The American Society of Mechanical Engineers.

Note: Statements and opinions advanced in papers are to be understood as individual expressions of their authors and not those of the Society. Manuscript received at ASME Headquarters, February 25, 1958. Paper No. 58—SA-17.

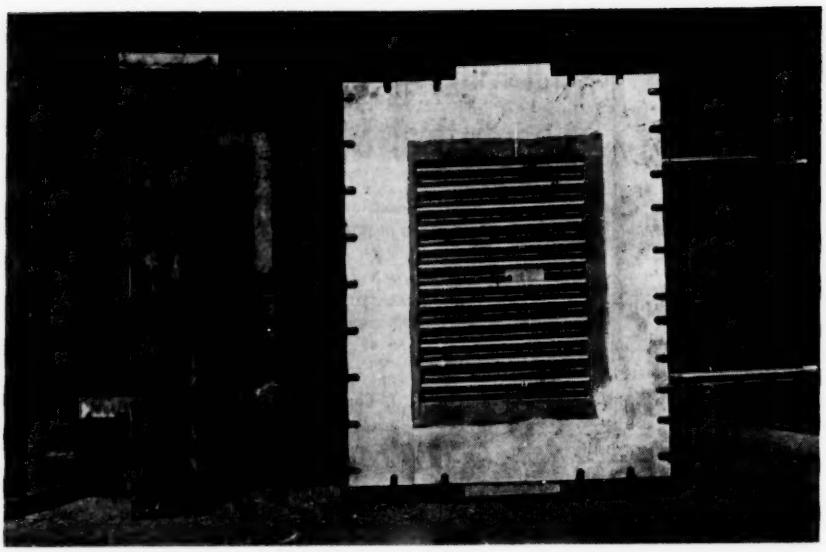

Fig. 3

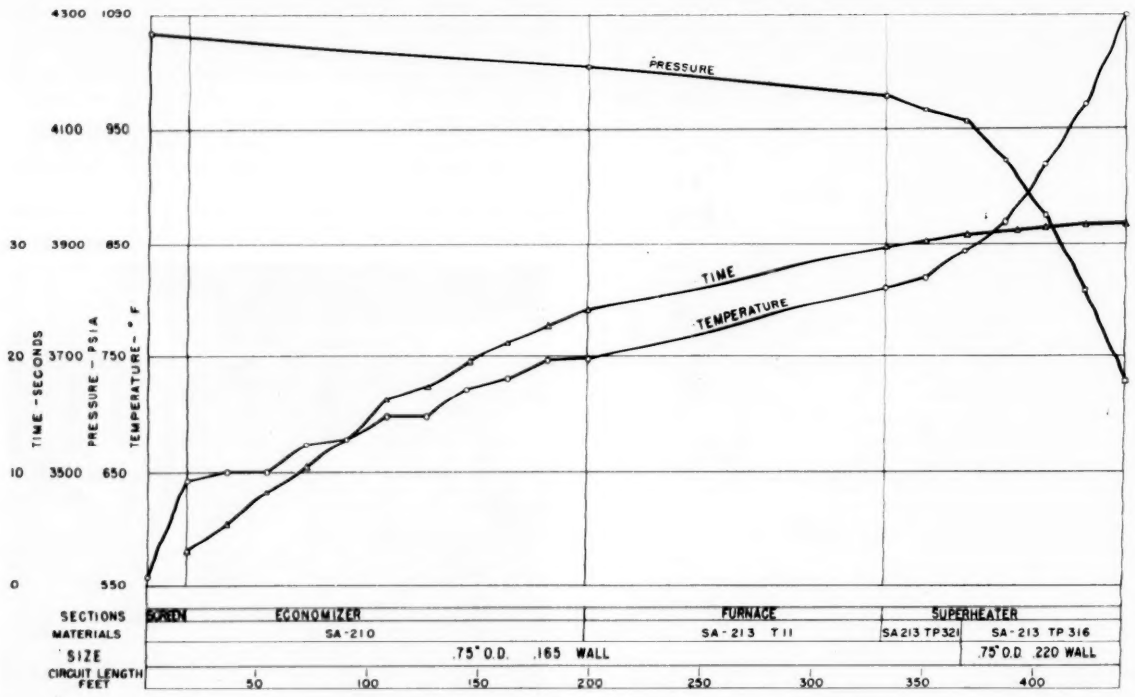

Fig. 4 Pressure, temperature, and residence time in test unit at 2000 lb-hr steam flow

The external heat exchanger is necessary to avoid contamination of the make-up water.

The steam generator with side panels, furnace insulation, and with two platens removed for inspection is shown in Fig. 2. The unit is fired with distillate oil from the top and the gases pass downward through a tangent tube furnace two feet square and thirty inches long, and then over tubes arranged in seventeen platens, two of which are shown in Fig. 3, with one platen partially dismantled. Each platen consists of two horizontal layers of tubes. Connections between platens are made through external headers.

There are two independent water circuits in the generator, each about 500 ft long, which are connected only at the inlet and at the outlet of the generator. Feedwater entering the unit passes through a platen located below the furnace, forming the exit screen. It then goes to the bottom of the unit and passes upward through ten convection platens in series. Carbon steel tubes are used throughout these platens. After leaving the last convection

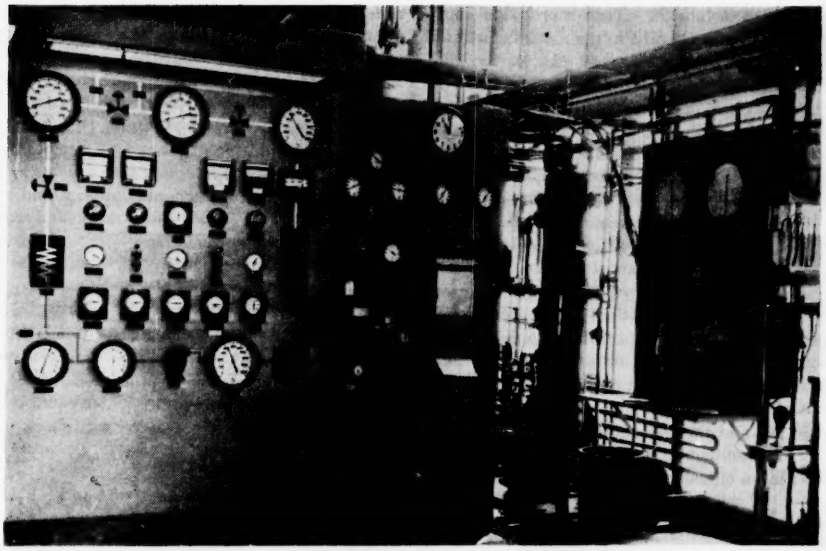

Fig. 5

platen, the steam passes through the chrome moly tangent furnace tubes. The steam leaving the furnace then passes through two type 321 stainless steel superheater platens, and then through four type 316 stainless steel superheater outlet platens. All tubing has a 0.75-in. outside diameter with a 0.165-in. wall, except for the four type 316 stainless steel platens which have a wall thickness of 0.22 in.

Fig. 4 shows the pressure and temperature of the fluid as it passes through the unit during a typical full load run at 3750 psi, with a temperature of 1050 F at the outlet. This figure also gives circuit length and residence time, as well as the tube material of each section. Particular emphasis was placed in the design to insure a unit in which the rate of heat absorption and the pressure gradient in the tubes are similar to those in large once-through boilers. Headers are located in such a way that by a simple rearrangement of external piping the flow path of the water may be altered.

The main control panel is shown in Fig. 5 with the boiler operating at a pressure of 3750 psi and 1100 F for a water treatment run, and shows the automatic control equipment, simplified schematic plan diagram, and supervisory instruments. The plant is completely automatic in operation.

The plant is started up by pressurizing the generator above 3500 psi with feedwater control valve (FCV). The feedwater flow is held constant and the firing rate is increased until the desired temperature is obtained. The generator is normally put on the line from a cold condition to 900 F steam outlet temperature in one hour. Quick start tests have been conducted, with the start-up time reduced to eighteen minutes. Shut-down time is limited by the ability of the control valves to undergo rapid temperature changes without flange leakage. The generator has operated about 5000 hr, most of this time above the critical pressure. For the remainder it was operated at outlet conditions of 2400 psi and 1050 F.

Besides the usual instruments, temperatures and pressures can be measured at 18 points in each loop. Provision for fluid sampling has been made at six points. An aspirated, water-cooled thermocouple probe measured gas temperatures at the furnace outlet and at the generator outlet. Fluid pressures were measured at each platen with a precision pressure indicator. Fluid flow, pressure, temperature, conductivity, dissolved oxygen, and hydrogen recorders are provided for steady state and transient tests.

Water Treatment Investigation

Successful operation of a supercritical steam generator depends to a large extent on the quality of the water supplied. This water must be practically free from total solids and exhibit minimum corrosive tendencies. In order to meet these conditions, the water in the test unit was maintained within the following typical limits for the first 3600 hr of operation:

pH at 25 C	9.0–9.5
Dissolved oxygen	0.007 ppm
Iron as Fe	0.005–0.010 ppm
Silica as SiO_2	0.010–0.020 ppm
Ammonia as NH_3	1.5 ppm
Total dissolved solids	0.25 ppm
Copper as Cu	Trace

Little difficulty was experienced in maintaining these limits with the exception that, initially, final steam temperature was limited until the silica concentration was reduced. It was necessary to operate the unit for a few weeks before the silica was reduced to the required concentration.

At the end of 3600 hr of operation at 3750 psi and 1050 F final steam temperature, tube sections were removed for visual and metallurgical examination. This inspection revealed the following:

1 There was no evidence of localized corrosion (pitting).

2 The internal tube surface, irrespective of the material, was covered with a fairly uniform, extremely thin coating of black iron oxide. The maximum thickness of the scale measured as follows:

a	Carbon steel tubing	0.0009 in.
b	Chrome moly	0.0007 in.
c	Stainless steel (316)	0.0015 in.

Considerable effort was expended in trying to determine a corrosion rate of component parts of the steam generator and the system as a whole. This effort was largely unsuccessful. The lack of success was due to the inability to repeat iron analyses taken at 5 and 10-min intervals during steady-state conditions. The failure to reproduce these iron analyses was not considered to

be primarily due to analysis technique. There was no significant difference between the iron concentration in the water before and after components of the unit (screen, furnace, etc.) or the unit considered as a whole; therefore, a corrosion rate could not be determined. For the most part, the iron values varied between 5 and 10 ppb when operating with the boiler water conditions as noted previously, at an output of 1300 lb of steam an hour. The average blowdown rate during this period was approximately 130 lb/hr.

An attempt was made also to determine corrosion rate of the test unit by determining the dissolved hydrogen concentration in the water. This was done by passing a part of the blowdown from the system through a Cambridge Oxygen-Hydrogen Analyzer. Fig. 6 is a plot which shows the relation between hydrogen concentrations and the final steam temperature at various constant blowdown rates. The following conditions were maintained when obtaining these results. The steam generator was operated at a constant output of 1700 lb of steam an hour with the outlet pressure held at 3750 psi, and the feedwater temperature to the unit held at 550 F. No ammonia was added for pH control. The unit operated within a closed cycle as described previously.

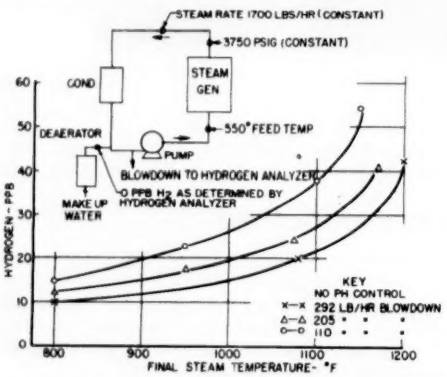

Fig. 6 Observed hydrogen evolution versus final steam temperature

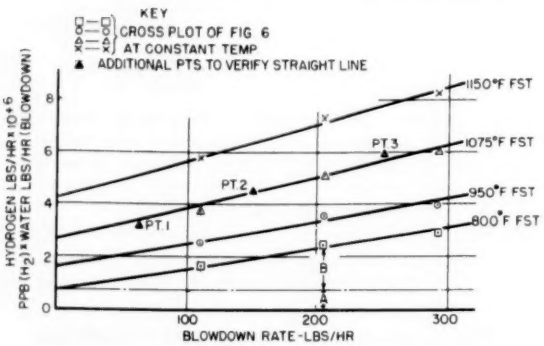

Fig. 7 Observed hydrogen evolution versus blowdown rate

The make-up water rate was equal to the blowdown rate and was obtained from the deaerator; its hydrogen concentration as determined by the hydrogen analyzer was zero. The operation just described is shown schematically on Fig. 6.

Fig. 7 is a cross plot of the data of Fig. 6. This plot shows how the total observed pounds of hydrogen an hour varied with the blowdown rate at constant final steam temperature. The total pounds of hydrogen an hour at a given temperature was obtained by multiplying the hydrogen concentration by its respective blowdown rate. Points 1 to 3 inclusively were additional runs to verify the straight line relationship between the observed pounds of hydrogen an hour and the sampling rate (lb/hr). It is apparent from this plot that the pounds of hydrogen an hour increased with increased blowdown at steady operating conditions. Assuming that the dissolved hydrogen is caused by the chemical reaction of the water with the tubes, then under steady state conditions, one would expect a constant rate of production of hydrogen, regardless of the sampling rate. Thus as the sampling rate increased, the hydrogen concentration would be expected to decrease, the product of the concentration and sampling rate always remaining constant. This may be explained by supposing that the total rate of production of hydrogen was caused partly by corrosion and partly from the decomposition of a contaminant entering with the make-up water. With this thought in mind, consider the production of hydrogen at an infinitesimally small blowdown rate. At a very small blowdown rate, the pounds of hydrogen observed would then be caused only by corrosion.

The slopes of the lines on Fig. 7 are equal to the concentration of the hydrogen due to the decomposition of the contaminant at the temperature considered. It will be noticed that as the final steam temperature increased, the amount of decomposition of the contaminant also increased. At a final steam temperature of 800 F, with 205 lb/hr blowdown, the pounds of hydrogen an hour due to corrosion is shown as "A," the pounds of hydrogen an hour due to decomposition of the contaminant is shown as "B."

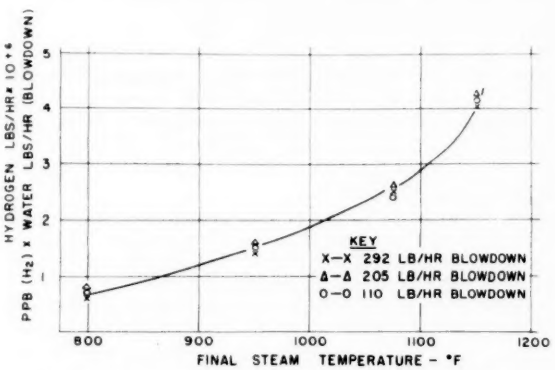
HYDROGEN LBS/HR * 10**6
PPB (H2) * WATER LBS/HR (BLOWDOWN)
KEY
X—X 292 LB/HR BLOWDOWN
Δ—Δ 205 LB/HR BLOWDOWN
O—O 110 LB/HR BLOWDOWN
FINAL STEAM TEMPERATURE - °F

Fig. 8 Observed hydrogen evolution versus blowdown rate

Similar values can be obtained for any combination of final steam temperatures and blowdown rates.

Fig. 8 is a plot showing the relation between the adjusted rate of production of hydrogen and the final steam temperature. The adjusted rate of production of hydrogen was obtained by subtracting the pounds of hydrogen an hour due to the decomposition of the contaminant from the total hydrogen observed at the respective temperature and sampling rate. It is apparent from this plot that this adjusted rate of production of hydrogen is now constant at steady operating conditions, regardless of the sampling rate. This is in agreement with what could be expected for the type of test conducted.

Fig. 9, curves A and B, shows the relation between the observed hydrogen concentration and the final steam temperature, with the system operated as noted. Curve A was obtained with the pH of the boiler water controlled at an approximate value of 9.5 at 25 C, by the addition of ammonia. Curve B was obtained with no ammonia added. The water supplied was demineralized and deaerated, its conductivity was less than 0.1 micromho per cm at 25 C, with a pH of approximately 6 to 7 at 25 C. Curves A′ and B′ were obtained by subtracting the hydrogen concentration due to the decomposition of the contaminant introduced with the make-up water from the observed hydrogen concentration. In

effect, this is equivalent to the subtraction of the slopes of the lines in Fig. 7 at the desired temperature from the observed hydrogen value, at the respective temperature considered. The slopes of the lines on Fig. 7 are 8, 9, 11½, and 14 at the respective temperatures of 800, 950, 1075, and 1150 F. The subtraction of these values was used whether or not ammonia was present.

The following comments can be made in reference to operation of the supercritical pressure unit as described within this paper.

1 The visual inspection of the tubing removed from the test unit after 3600 hr of operation revealed satisfactory water side treatment. There has been no inspection after the 5000 hr of operation; however, there has been no indication of any difficulty.

2 The corrosion rate corresponding to the determination of iron in the water differed significantly from that corresponding to the determination of the hydrogen concentration in the blowdown water. A typical set of steady-state operating conditions is as follows:

Final steam temperature	1075 F
Steam output	1300 lb/hr
Pressure	3750 psig
Blowdown rate	110 lb/hr
Average iron concentration	6 ppb
Average adjusted hydrogen concentration	20 ppb

Using the chemical reaction

$$3Fe + 4H_2O \rightarrow Fe_3O_4 + 4H_2$$

and assuming no corrosion products are deposited within the system, the corrosion rate obtained from the chemical analysis of iron in the blowdown water would be 0.007 mg Fe/dm² day. The corrosion rate based on the adjusted hydrogen value would be 0.48 mg Fe/dm² day. The ratio of the corrosion rate, determined from the hydrogen concentration, is approximately seventy times that determined from the chemical analyses. A simple explanation might be that the products of corrosion are for the most part remaining in place. Periodic flaking of the iron oxide may account for the typical scattering of iron values obtained.

3 An indication of the corrosion rate, as determined from the adjusted dissolved hydrogen values at various temperatures with and without ammonia addition as compared to the corrosion rate at 800 F with ammonia, is shown on Fig. 9, curves A″ and B″. We believe this curve to be of significant interest in showing the relative corrosion rate within the system at various temperatures. It is felt that the corrosion rate in a large supercritical unit would not be excessive. While there seems to be good evidence that the method of interpreting the data presented is correct, it must be remembered that there are many variables which could influence this analysis, which have not been taken into consideration. Such variables include flow rate, heat-transfer rate, stress, tube material and surface finish, the amount of hydrogen absorbed by the metal, and the effect of the hydrogen concentration on the corrosion rate.

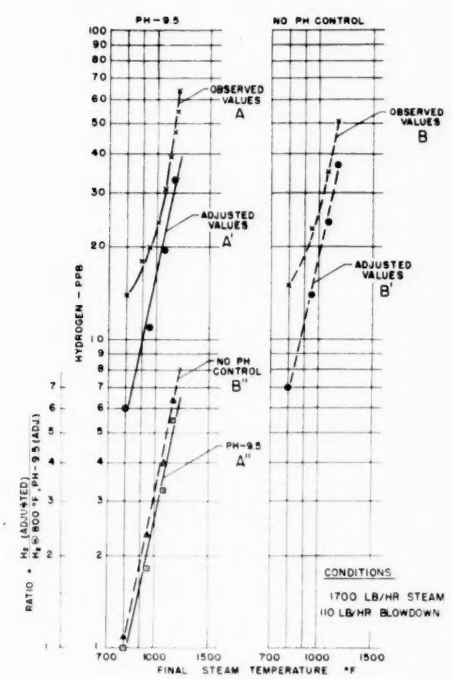

Fig. 9

Controls

One of the primary objectives of this test unit was to obtain control information. Tests at both supercritical and subcritical conditions have been conducted. Some results of the latter are included for reasons of comparison and general interest.

The study has resulted in the development of an automatic control scheme which has proved adequate for constant load and widely fluctuating load operation. To appreciate fully the difficulty of the control problem for a small tube unit such as the test generator described, Table 1 has been prepared, comparing the ratio of the internal volume of the primary circuit pressure parts to the primary steam flow, as well as the ratio of primary circuit pressure parts weight to primary circuit steam flow. The primary circuit consists of all steam generating sections excluding any reheating circuits.

Table 1 A comparison of steam generator stability factors

	VOL/CAP	WT/CAP
CARTERET SUPERCRITICAL UNIT	0.000516	0.65
SUPERCRITICAL UNIT	0.001630	1.18
SUBCRITICAL UNIT	0.007810	2.72

NOTE

WT/CAP = WEIGHT OF PRIMARY CIRCUIT PRESSURE PARTS / PRIMARY STEAM FLOW

VOL/CAP = INTERNAL VOLUME OF PRIMARY CIRCUIT PRESSURE PARTS / PRIMARY STEAM FLOW

These comparisons are made for three boilers:

1 The test unit under discussion.

2 A supercritical generator design for a 300 mw plant, 3500 psi, 1050 F, 1000 F, 1000 F.

3 A natural circulation steam generator design for a 300 mw plant, 2400 psi, 1050 F, 1000 F.

From the tabulation it becomes apparent that the heat storage in the fluid and tube metal for the test unit is considerably smaller per unit of flow than in either a large central station subcritical or supercritical steam generator, and consequently the test unit is much more sensitive and difficult to control. The difference in the tabulated ratios for the three units is almost entirely due to the difference in the tube size used in these units.

A simplified diagram of the pneumatic control system used with the test unit is shown in Fig. 10. The pressure ahead of the simulated turbine throttle valve is controlled by adjusting the feedwater flow. The steam temperature is controlled by adjusting the firing rate. Modifying signals for the two primary con-

trols are provided by steam flow and intermediate temperature points. Anticipatory signals are provided by interconnection between the two primary control systems. Using this control scheme a typical load increase and decrease with the resulting response of generator outlet pressure and temperature is plotted in Figs. 11 and 12. These swings represent a load change rate of approximately 13.5 per cent per minute, with a maximum final steam temperature variation of 15 F, and a maximum steam outlet pressure variation of 50 psi.

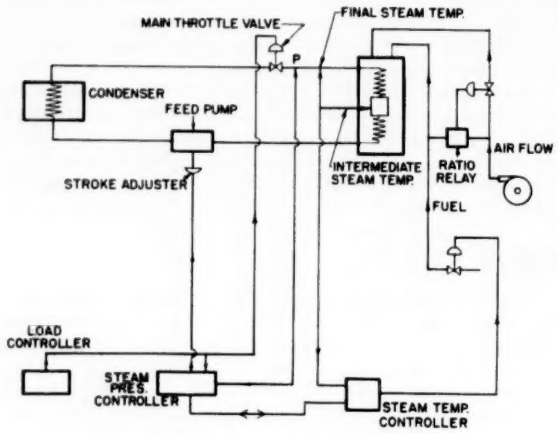

Fig. 10 Simplified control diagram

To study the effect of transient behavior of the fluid in the generator for given input and output disturbances, tests were conducted with the generator on manual control and with one of the following three values upset instantaneously one at a time:

1 D = output demand, obtained by changing the simulated governor valve position.
2 F = feed flow, obtained by changing feed pump stroke.
3 C = heat input, obtained by changing firing rate.

Fig. 13 shows a series of tests in which heat input was increased and decreased, while the effect of these changes was measured in terms of pressure and temperature changes at the generator outlet. In this test feed flow and output demand were held constant.

The data are represented for four rates of upset, that is, an increase of 10 per cent and then 20 per cent in firing rate and a decrease of 10 per cent and then 20 per cent in firing rate. The effect of these changes on pressure and temperature is plotted against time. The symbol $(\Delta C)_{D,F}$ indicates a change in heat input but no change in feed flow or demand.

Fig. 14 represents a composite picture of the results for the three sets of upset functions, i.e., $(\Delta C)_{D,F}$ as just explained, $(\Delta F)_{C,D}$ indicating upset in feed flow, and $(\Delta D)_{F,C}$ indicating upset in demand with the two other variables unchanged.

This type of test facilitates the derivation of mathematical expressions from which it is possible to predict how the pressure

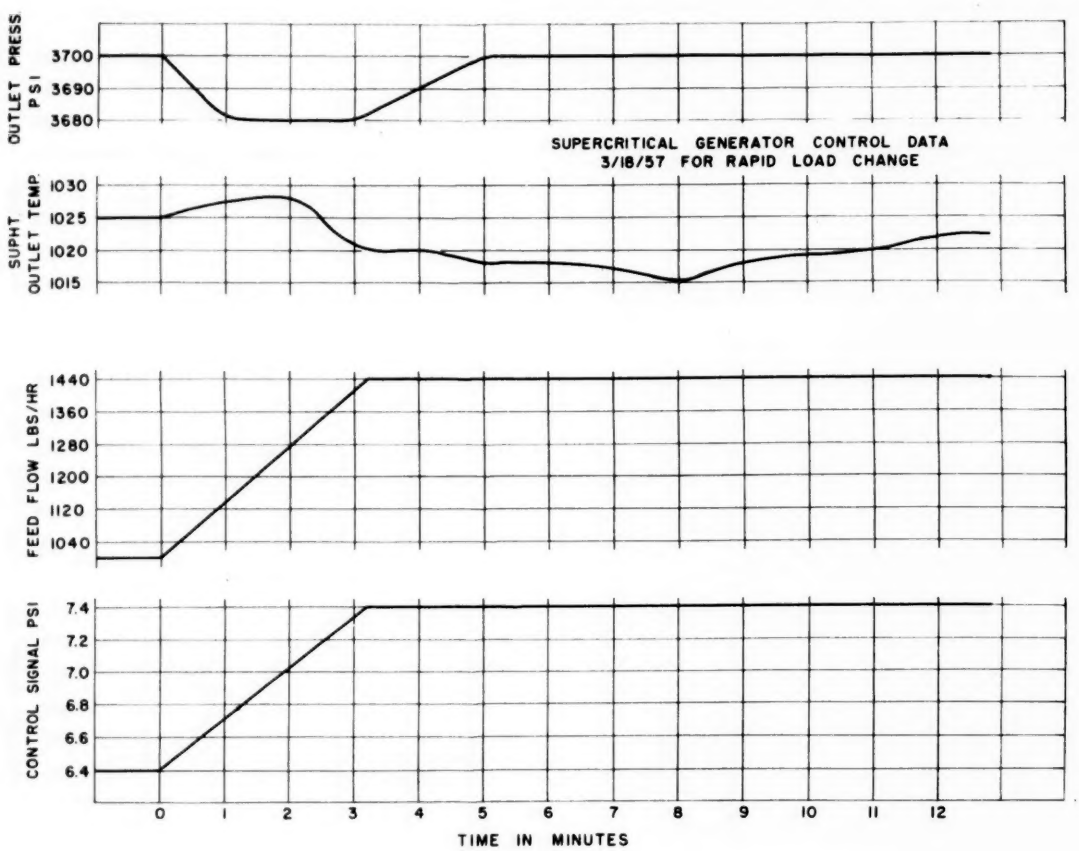

Fig. 11

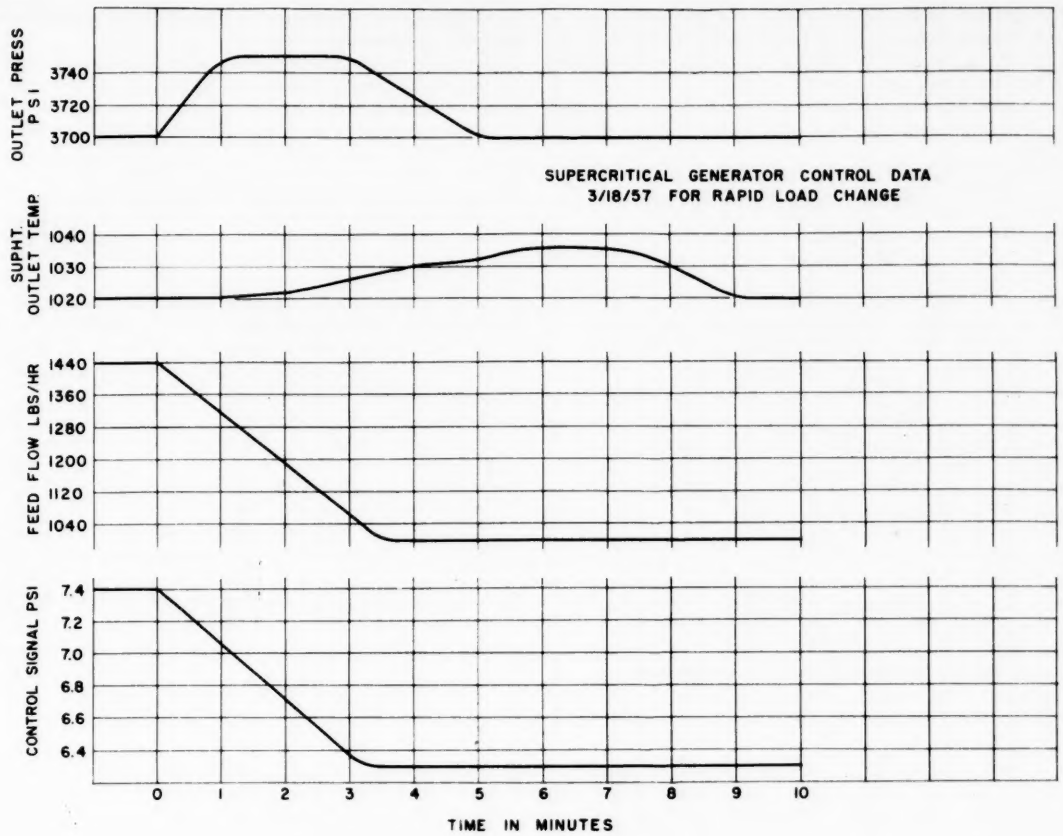

Fig. 12

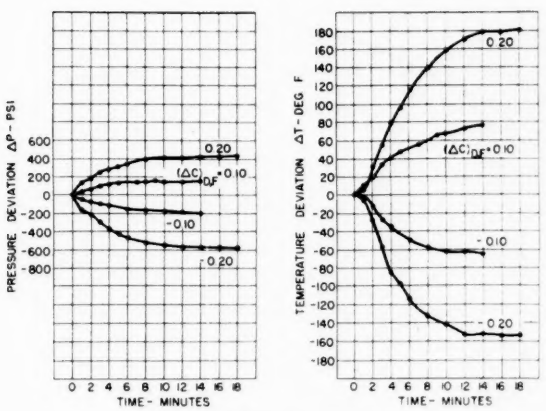

Fig. 13 Transient response test

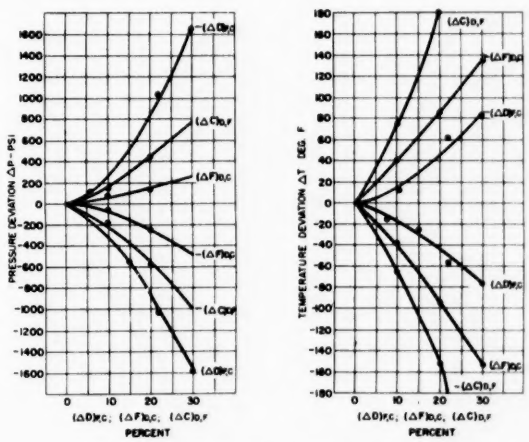

Fig. 14 Transient response test results

and temperature of the steam change as the heat input or steam output demand changes. Derivation of such expressions is considered outside the scope of this paper; however, solutions have been obtained which approximately correlate these data. In addition, analog simulation of the test unit response has been carried out. With these data and the analog, control response of large supercritical steam generators can be studied to obtain the best over-all control system.

The single upset function tests furthermore allow one to select the optimum control points, as well as to study the transient behavior of the fluid in the circuits during a load change.

The result of such a test is best illustrated in Fig. 15. Here the

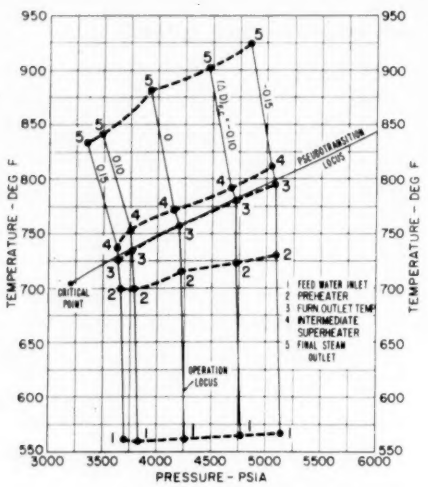

Fig. 15 Temperature control point selection tests

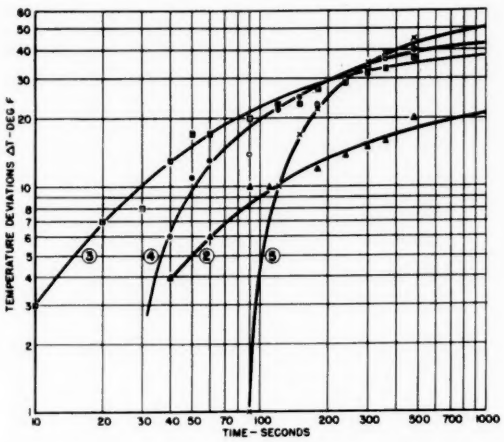

Fig. 16 Temperature control point selection tests, $(\Delta D)F,C = -0.15$

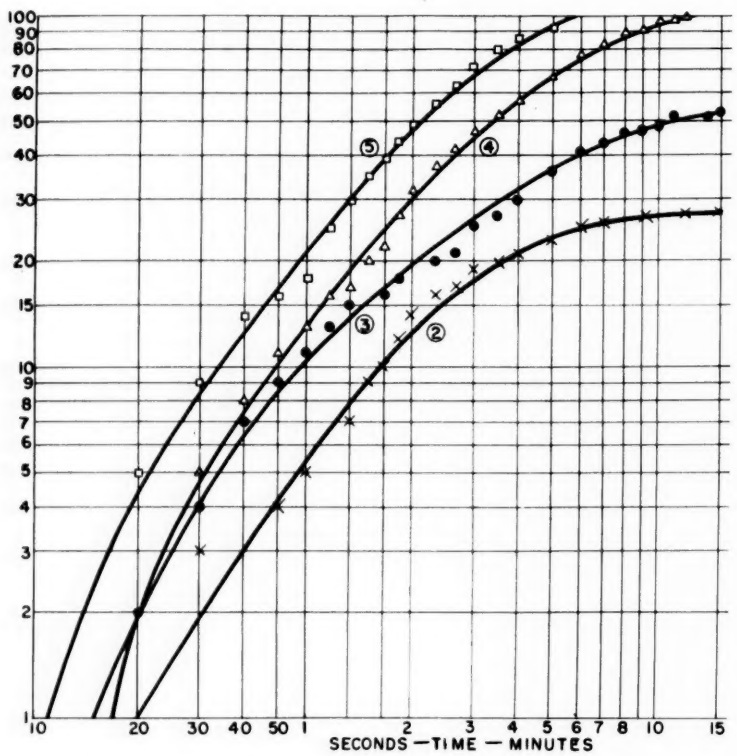

Fig. 17 Temperature control point selection tests, $(\Delta C)F,D = +0.20$

changes in pressure and temperature of the fluid in the circuit are represented as a load demand change is made. The data represent steady-state conditions after the per cent change indicated has been made. The temperature measuring points indicated are located in the following regions of the steam generator circuit:

Point 1 Feedwater inlet
2 Preheater intermediate
3 Furnace outlet
4 Intermediate superheater
5 Final superheater outlet

Information obtained from tests presented in this manner facilitates the understanding of the fluid behavior in terms of pressure and temperature levels in the circuit. It should be noticed that a line marked pseudotransition locus is drawn on Fig. 15 which coincides closely with temperature point number 3 at the furnace outlet. The concept of "pseudotransition region" was presented in a previous paper by one of the authors.[5]

Test conditions for the experiments to be outlined were set up in such a manner that the "pseudotransition temperature" in the circuit occurred close to the location of temperature point number 3.

Fig. 16 presents data from single upset function response tests which are particularly useful in determining optimum control signal location. This figure shows the results obtained during a 15 per cent load demand change tracing the temperature response at the locations described in the previous figure.

The temperature change is plotted against time. Similar plots for changes in heat input and feed flow are presented in Figs. 17 and 18.

[5] S. Ling, "A Note on Pseudotransition Locus for Water in the Supercritical Region," ASME Paper No. 57—A-200.

From these tests it appears that, for load demand changes, temperature at point 3 offers the quickest response to the demand change. For firing rate change as shown on Fig. 17, point number 5 (final steam temperature) appears to give the quickest indication that a change has occurred. The same holds true for feedwater flow changes as shown on Fig. 18.

The behavior of the temperature at point number 3, as shown on Fig. 18, is interesting and can be used to advantage in the control scheme as a modifying or anticipating device.

Figs. 19, 20, and 21 show results of tests similar to those described in Figs. 15 through 18 for supercritical operation, except that these tests were conducted at a base steam condition of 2400 psi and 1050 F leaving the generator. The behavior of the various temperature points during changes differs only slightly from those experienced at supercritical conditions.

The most interesting temperature behavior in all these tests is that exhibited by point number 3. No attempt will be made here to explain this behavior except to point out the following: Referring to Figs. 16 and 19, both representing a decrease in demand, the first at supercritical, the second at subcritical condition, it can be seen that the response rate of point number 3 is the most sensitive in both instances. Temperature point number 3 in Fig. 19 is located at the end of the boiling region and in Fig. 16 this point, as mentioned, was located in the so-called pseudotransition region. The similarity in behavior of this temperature point in the supercritical and subcritical tests is most interesting.

Similarity in behavior of temperature point 3 was also evident for the combustion rate and feedwater rate upsets at subcritical and supercritical conditions. The temperature reversal of this point during feedwater flow changes can be partially explained by the rapidly changing properties of the fluid in this region.

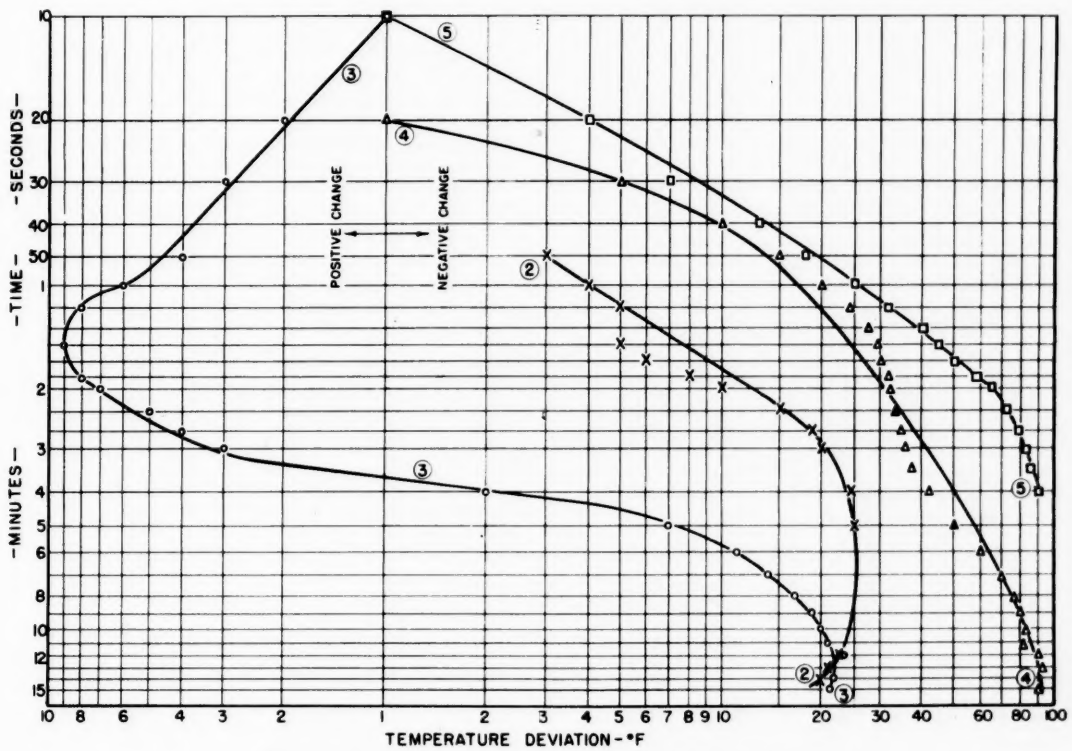

Fig. 18 Temperature control point selection tests, $(\Delta F)C,D = +0.20$

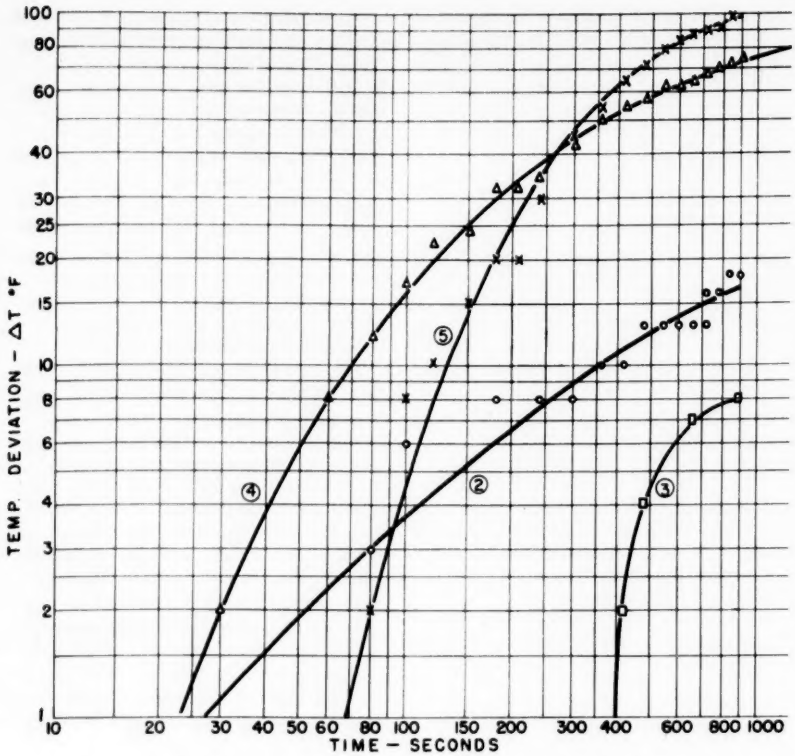

Fig. 20 Temperature control point selection tests (subcritical operation), $(\Delta C)D$, $F = +0.2$

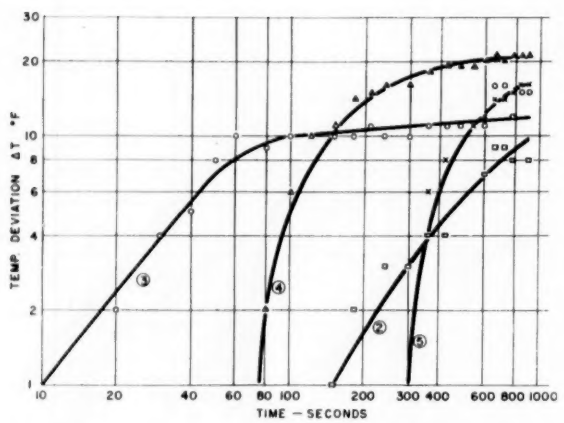

Fig. 19 Temperature control point selection tests (subcritical operation), $(\Delta D)F, C = -0.20$

It is apparent from these experiments that, depending on the basic control system selected, the intermediate temperature or anticipatory control signal location is of considerable importance in achieving satisfactory results.

The type of investigation described is invaluable in deriving basic information required for designing a proper control system for once-through steam generators. The success of the automatic control scheme used on this test unit is a direct result of such step-by-step investigation. With the successful simulation of the test generator on an analog computer, optimizing of the control arrangement for a central station supercritical or subcritical once-through steam generator can be carried out with confidence, avoiding costly field adjustments.

Acknowledgments

The writers wish to acknowledge the assistance given by Dr. Everett P. Partridge and his associates of Hall Laboratories for their active participation throughout the water-side investigation.

Acknowledgment is due Mr. John Blizard, under whose direction this work is being conducted.

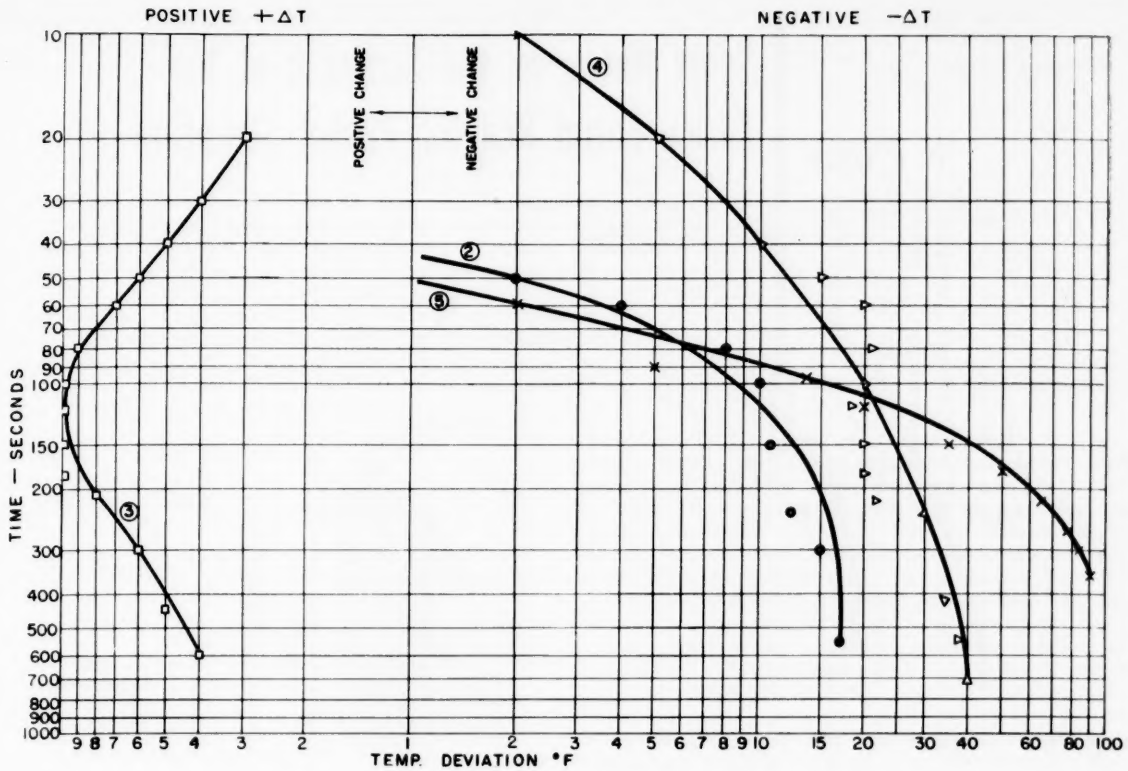

Fig. 21 Temperature control point selection tests (subcritical operation), $(\Delta F)D,C = +0.20$

Some Notes on the Strength of the Enrico Fermi Reactor Vessel Structure

F. R. BEYER

Atomic Power Development Associates, Inc., Detroit, Mich.

The place and function of the reactor vessel in the Enrico Fermi Atomic Power Plant—the most complex nuclear structure built to date—is described. The design basis must lead to a conservative structure. Evaluation of the design of any new and radically different structure must be based upon tests. Strain gaging during hydrostatic testing gave limited results. High-temperature strain gages will be used during simulated-service tests prior to start-up. A successful high temperature strain-gaging technique for long-time static applications up to at least 900 F is developed and described.

THE REACTOR VESSEL for the Enrico Fermi Atomic Power Plant is the most complex nuclear structure built to date. Once the reactor has been started it will be inaccessible. The design basis must lead to a conservative functional structure. A proper perspective of stress and strength must be maintained. The effect of the various loading conditions on these factors must be carefully considered. Even with an adequate and established guide, and assuming good engineering and shop techniques, final evaluation of a new design must be based upon simulated-service tests. Other additional tests should be used to evaluate various phases of the design prior to the time simulated-service tests can be commenced. Techniques which measure surface strain are valuable for structural-strength evaluation. The use of bonded-resistance-wire strain gages as transducers produced limited data during the hydrostatic tests. There is no standard technique for making static-strain measurements under simulated-service test conditions where temperatures of at least 900 F will be encountered for long periods of time. Such a strain gage and the technique adapting it to our situation will be described in this paper. Excellent stability over long periods of time at temperatures of at least 900 F has been achieved. Results of evaluation tests of these gages are given. Field-installed gages are expected to yield valuable structural and operational information from simulated-service tests.

The Plant

The Enrico Fermi Atomic Power Plant located near Monroe, Mich., includes a 300-mw thermal-output fast-breeder reactor and its associated heat-removal and utilization equipment. Its major components include the reactor, the intermediate heat exchanger, the steam generator, and the turbine-generator. Heat generated in the reactor is transferred to the liquid-sodium coolant which in passing through the intermediate heat exchanger transfers heat to the isolated secondary liquid-sodium loop. The final heat transfer takes place in the once-through steam generator from which steam at 740 F and 600 psia is taken and used to drive the 100-mw electrical-output turbine-generator.

Fig. 1 is a schematic representation of the liquid-metal and steam-generating system. There are three independent primary-sodium-coolant loops and three secondary-sodium loops. Each primary loop includes an intermediate heat exchanger and circulating pump. Each secondary loop includes a steam generator and circulating pump. The purpose of the secondary-coolant loops is to isolate the radioactive primary coolant from the steam-water system and thereby prevent the release of radioactivity in the event of a sodium-water reaction. The steam is used to drive a conventional turbine-generator. Both liquid-metal loops operate at virtually no pressure.

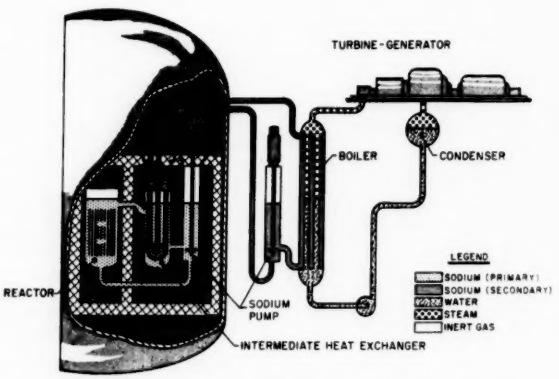

Fig. 1 Schematic of liquid-metal and steam-generating systems

All radioactive materials are housed in a gastight containment building. This building rises about 70 ft above ground level and is 72 ft in diam with a hemispherical dome. The purpose of the building is to contain any fission products or radioactive sodium. The building is fabricated from $1^1/_8$-in-thick ASTM A-201-B carbon-steel plate and designed for a pressure range of -5 to $+32$ psig. It has a total height of 120 ft of which 50 ft are underground. The foundation extends to bedrock.

The reactor vessel is located in the center of this building inside a second gastight containment vessel, the primary shield tank. This vessel, shown in Fig. 2, is fabricated from $^5/_8$-in-thick ASTM A-285-C carbon-steel plate. It extends 38 ft below the operating floor and is capped by the machinery dome over the various operating mechanisms. The primary shield tank has a 24-ft max diam. The design pressure is 20 psig.

The Reactor Vessel

This paper is concerned with the reactor vessel which is shown inside the primary shield tank in Fig. 2. This vessel is fabricated from Type 304 stainless-steel plate varying in thickness from $1^1/_2$ to 2 in. It is about 36 ft high and has a $14^1/_2$-ft max diam. It consists of four main components, namely, the lower reactor vessel, the upper reactor vessel, the transfer rotor container, and the

Contributed by the Nuclear Engineering Division and presented at the Semi-Annual Meeting, Detroit, Mich., June 15–19, 1958, of THE AMERICAN SOCIETY OF MECHANICAL ENGINEERS.

NOTE: Statements and opinions advanced in papers are to be understood as individual expressions of their authors and not those of the Society. Manuscript received at ASME Headquarters, June 2, 1958. This paper was not preprinted.

plug container. The fabricator has described it as the largest and most complex nuclear component built to date.

The vessel presents a variety of structural configurations and intersections. The center line of the 9-ft 3-in. ID lower reactor vessel is offset 24.237 in. from that of the 14-ft 2½-in. ID upper reactor vessel to facilitate manipulation of the fuel subassemblies. The transition between these two vessel components is an unsymmetrical toroidal structure of rectangular cross section, 26 in. deep, stiffened with 17 radial ribs. The transfer rotor container is a 6-ft-diam 11-ft-high cylindrical chamber through which the fuel subassemblies enter and leave the reactor vessel. It intersects the upper reactor vessel just above the rectangular transition and results in an unconventional penetration which is generously reinforced.

The plug container is a two-stepped cylindrical shell with a mean ID of 9 ft 4 in. and is concentric with the upper reactor vessel. A symmetrical conical transition connects the plug container with the upper reactor vessel. A heavy flange at the open upper end of the plug container provides support for the rotating shield plug. This plug closes the reactor vessel.

Penetrations for three 6-in. and three 14-in-diam inlet nozzles and three 30-in-diam outlet nozzles are made in the lower reactor vessel and upper reactor vessel, respectively. A number of other minor penetrations for overflow, drain, vent, gas-circulation nozzles, and surveillance, thermocouple, and liquid-level indicator tubes are made in the main body of the reactor vessel. The transfer rotor container has a 14-in-diam exit-tube nozzle and a 6-in-diam transfer-rotor drive-shaft nozzle in its upper head.

An integral support structure for the fuel and blanket-subassemblies support plates is built into the lower reactor vessel. This structure is 17 in. deep and has a 34-in. centrally located square hole. It consists of upper and lower deck plates 1½ in. thick, reinforced with 12 radial ribs.

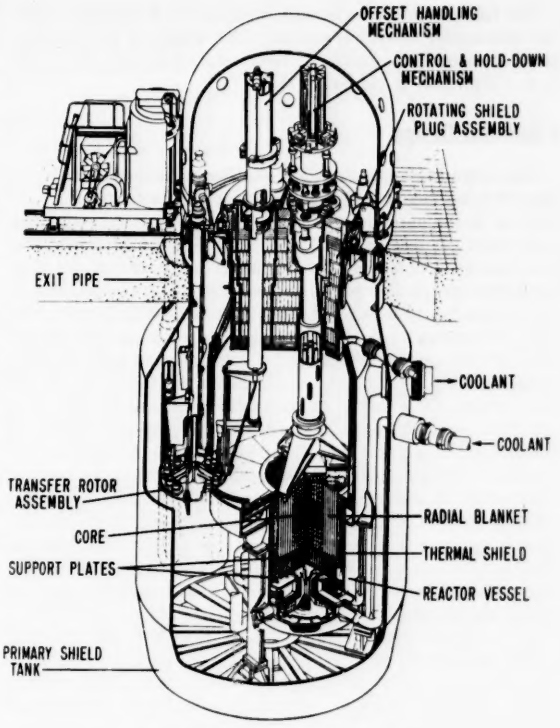

Fig. 2 Perspective view of reactor

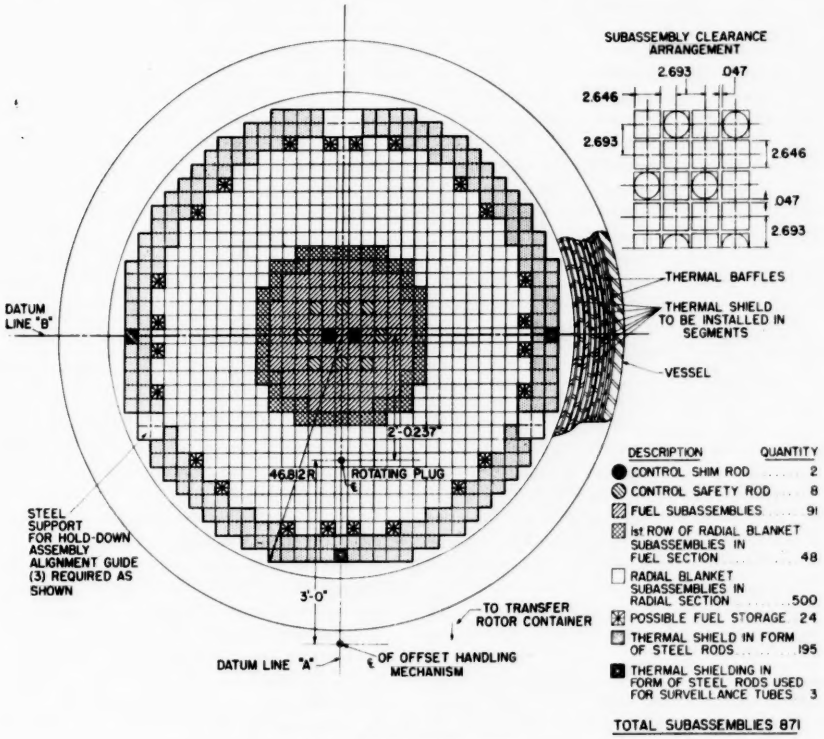

Fig. 3 Reactor cross section

The reactor vessel is externally supported on 8 flex-plates from the rectangular transition section. The weight of the transfer-rotor container is supported by constant-load hangers suspended from the primary shield tank.

Functional Design

The core and blanket fuel subassemblies are housed in the lower reactor vessel as shown in Fig. 2. Sodium coolant flows from the bottom of the lower reactor vessel through these subassemblies into the upper reactor vessel which serves as a mixing pool and provides space for remote fuel handling. A cross-sectional view giving the orientation of the fuel subassemblies, the control-rod guide tubes, and the thermal-shield rods is shown in Fig. 3. The fuel section consists of two operating control rods, eight safety rods, 91 fuel subassemblies, and the 48 first-row radial-blanket subassemblies. Ninety per cent of the coolant flows through the core section, entering the primary-inlet plenum at a pressure of about 75 psig through the 14-in. nozzles. It passes through these subassemblies at a rate of nearly 12 million lb per hr resulting in a heat-transfer rate of 665,000 Btu per hr per sq ft in the heart of the reactor, the fuel core. The coolant for the plutonium breeder blanket enters the radial-blanket plenum through the 6-in. inlet nozzles at a pressure of about 10 psig. It is distributed through the thermal baffling as well as the 524 blanket rods by appropriately sized orifices. Each subassembly is located and supported in the support plate by a nozzle 18 in. long. The support plates, which rest upon the support structure, consist of two 2-in-thick plates separated by several $^3/_8$ and $^1/_2$-in-thick ribs 14 in. high. The center section supports the fuel-section subassemblies and is independently removable. It rests on a seal rail which isolates the main coolant flow. A hold-down device holds the core subassemblies down against the hydraulic forces resulting from upward coolant flow and also maintains radial alignment.

The upper reactor vessel in addition to being a mixing pool also provides space for hold-down and mechanical-handling devices which are suspended from the rotating shield plug. The offset handling mechanism, shown in Fig. 2, is used, in conjunction with the rotating plug, to remove spent-fuel and blanket subassemblies from the reactor vessel and to deposit them in finned pots in the transfer-rotor container. These subassemblies are subsequently raised through the 14-in. transfer-rotor-container exit port into a self-propelled cask car. New subassemblies are loaded into the reactor by reversing this process. Stainless-steel thermal baffle plates varying in thickness from $^1/_8$ in. to 1 in. are fitted inside the vessel wall to a minimum thickness of 5 in. This thickness of steel added to the 5-in. thickness of shield rods and 2-in-thick reactor-vessel shell also acts as a radiation shield and neutron reflector. Coolant circulated between the baffle plates reduces the effect of thermal gradients and transients.

Design Basis

Good design is a balance between stress and strength. Caution must be the watchword when a new design is being evolved. This is especially true here, where a complex unconventional vessel is inaccessible after the plant is in operation. Conservative procedures and assumptions must be augmented by evaluation and testing wherever and whenever feasible. A design must be realistic if it is to be conservative. Under certain conditions overconservatism does not result in a conservative design, for example, thinner sections are much more resistant to thermal shock.

By strength is meant the capacity of a material to withstand stress. This is commonly called the allowable stress. The proper value of allowable stress for a given situation depends upon a variety of factors. The variation of any one of these factors may dictate a change in allowable stress. The material properties, the geometry of the part, the surface finish, the processing of the material, the type of load application, and the ambient exposure are some of the more important factors.

Stress, on the other hand, is used to refer to the force intensity which is calculated, and indeed in a few simple cases may actually exist, at a point in a structure from its geometry and a knowledge of the applied loads and of the constraints. A structure need not be at all complicated to defy exact analysis.

When code rules, such as ASME Boiler and Pressure Vessel Code, are used for design there is assurance of an adequate design based principally upon experience. These code rules are welcomed because it is possible to come up with properly, or at any rate, adequately, proportioned structures. The stresses are not known and in general are not of much concern. But what is done when a situation is not covered by code? Generally, assumptions are made which will give not the exact stress but rather something higher than the exact value. How much higher depends on ability to cope with the situation and experience and judgment.

Strength then involves knowledge of the material and how it reacts to different conditions. An accurate knowledge of stress depends on ability to calculate reliable values of force intensity for a given situation. There is more to be known about both of these factors. Material properties are not completely known. Stress analysis involves approximations. Prescribing low strength values (allowable stresses) is not justified by reason of a poor stress analysis.

A third factor to be considered is the loading conditions. These are generally prescribed for a new design and will influence both strength and stress. Material strength depends on the mode of the applied loading, whether static, fatigue, shock, or thermal. The validity of calculated stress depends in part on how nearly the load distribution used in the stress analysis approaches that actually felt by the structure.

The Enrico Fermi reactor-vessel design is conservative. ASME Boiler and Pressure Vessel Code as modified by the special ruling of Code Case Number 1234 is used wherever applicable. Continuous thorough inspection was maintained during the construction of the vessel. Ultrasonic testing was employed to determine internal material defects. Liquid-penetrant tests and radiographs were made of the welds. The structural integrity of the completed reactor vessel was tested by pneumatic and hydrostatic-pressure tests. Gastightness was verified by a vacuum test. Extensive testing is scheduled after erection at the site. The mechanical and hydraulic operation of the reactor will be evaluated during tests with hot gas and sodium prior to start-up.

Design Strength Limits

The specifications for the reactor vessel consider the following load conditions:

1 Primary coolant pressures including pressure surges.

2 Weight of vessel and internal structures, static heads, superimposed weights or forces, support reactions.

3 Pipe reactions.

4 Steady-state thermal conditions: (*a*) Internal heat generation; (*b*) thermal gradients.

5 Transient thermal conditions: (*a*) Normal power changes; (*b*) rapid power changes; (*c*) start-up; (*d*) shutdown; (*e*) scrams other than emergency cooling; (*f*) emergency cooling.

6 Combinations of 1 and 2.

7 Combinations of 1, 2, and 3.

8 Combinations of 1, 2, 3, and 4.

9 Combinations of 1, 2, 3, 4, and 5.

10 Mechanical shock.

11 Mechanical vibration.

This list attempts to recognize every possible load condition but it leaves the interpretation and specific application to the designer. Design pressures and temperatures are specified for each major component and are shown in Table 1. Several transient conditions are specified and are listed in Tables 2*a* and 2*b*. From here the designer must come up with the figures. This is not an easy task since, at the start of the project, the detailed design configuration is not well established. The approach, in order to be conservative, is to assume conditions which are known to be worse than any that can reasonably be expected. However, if these values are not realistic the design will suffer. Extensive thermal analyses have resulted in realistic values for thermal transients and for temperature gradients through the vessel wall.

It is not the intent of this paper to propose a new design basis for design-strength limits, but rather to briefly state the basic criteria of the design-strength limits used for the Enrico Fermi reactor vessel. In arriving at an acceptable design basis the work of Langer [1],[1] Cooper [2], and others [3], in addition to the ASME Code have been heavily drawn upon. It should be restated that a workable, conservative design basis must be realistic and that ignorance of loading resulting from any normal or abnormal operating, or emergency condition, or that inability to stress analyze a component cannot justifiably be accounted for by applying an additional "safety" factor to the strength limits.

The static-strength properties of the material throughout the required temperature range are well known. The ultimate and yield strengths, the Young's modulus, and the coefficient of thermal expansion for Type 304 stainless steel are published in standard references.

Thermal-stress fatigue data are relatively scarce. Those obtained by Coffin were used by Langer to obtain Fig. 4. The basis of this curve is pointed out by Langer [4] as follows. It was constructed by drawing a "lower-limit" curve through the lowest test points and then constructing the curve of Fig. 4 to have a safety factor of at least ten based on cycles, and of at least 1.5 based on strain range. The data include various types of steel and such variables as temperature, surface finish, and direction of rolling. However, temperatures higher than 662 F were not used.

Discretion must be used in applying these data because of their limited scope both in quantity and in the number of variables treated. Coffin [5] points out that constrained thermal cycling appears to be four times as severe as constant-temperature strain cycling. With the foregoing in mind, an outline is presented of the design-strength limits for the Enrico Fermi reactor vessel.

[1] Numbers in brackets designate References at end of paper.

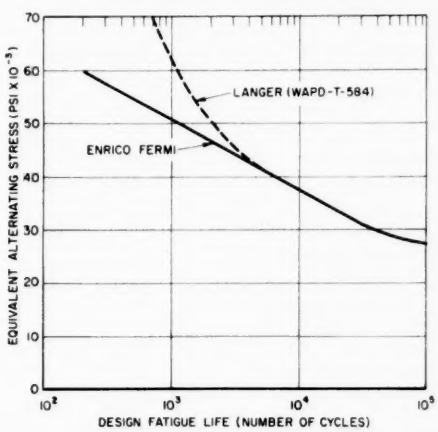

Fig. 4 Thermal-stress fatigue curve

A *General*

1 ASME Boiler and Pressure Vessel Code Section VIII together with Code Case No. 1234 are used whenever they apply.

2 The maximum shear-stress criterion is used, being conservative and simple.

B *Steady-State Condition*

1 Membrane stresses arising from steady-state pressure and mechanical forces or their combinations shall be limited to code allowables.

2 Each part of the vessel shall be proportioned according to code rules where applicable.

3 Stresses arising from combinations of steady-state pressure and mechanical forces with thermal stresses due to temperature distribution at any level of steady-power operation including internal heat generation shall not exceed 1.5 times code allowables.

Table 1 Steady-state pressures and temperatures

Component	Design temperature, deg F	Operating temperature, deg F	Design pressure, psig
14-in. inlet nozzle	750	600	110
Core-section inlet plenum	750	600	110
6-in. inlet nozzle	750	600	50
Radial-section inlet plenum	750	600	50
30-in. outlet nozzle	1000	900	50
Upper-reactor-vessel wall	900	750	50
Transfer-rotor container	800	650	50
Support plates	750	600	...
Hold-down	1100	1000	...

NOTE: The entire vessel is to be designed for isothermal operation at 1000 F. For this condition the 14-in. inlet nozzle and the core-section-inlet-plenum pressure will be limited to 93.5 psig.

Table 2a Transient design temperatures, normal operation

Condition	Average temperatures, Inlet, Initial, deg F	Inlet, Final, deg F	Outlet, Initial, deg F	Outlet, Final, deg F	Frequency
Plant start-up	400	600	400	900	100
Plant shutdown	600	400	900	400	100
0 to 100% power	750	600	750	900	1000
100% to 0 power	600	750	900	750	1000
Shutdown prior to refueling	600	550	900	600	1000
Start-up after refueling	550	600	600	900	1000

Table 2b Transient design temperatures, abnormal operation

Component	Condition	From, deg F	To, deg F	Duration, sec	Frequency
Hold-down plate	Scram	900	600	1	25
Outlet nozzles	Scram	900	600	19	25
Internal surface upper-reactor-vessel shield	Scram	900	600	25	25
Radial-section inlet nozzles and plenum	Loss of one pump	600	700	30	5
Radial-section inlet nozzles and plenum	Cold sodium accident	600	550	5	25
Fuel-section inlet nozzles	Loss of one pump	600	900	30	5
Fuel-section inlet nozzles	Cold sodium accident	600	450	7	25
Fuel-section inlet plenum	Loss of one pump	600	750	30	5
Fuel-section inlet plenum	Cold sodium accident	600	550	5	25

4 Peak stresses due to steady-state pressure and mechanical loads or their combinations including the effects of gross structural discontinuities shall not exceed 1.5 times code allowables.

C *Combinations of Steady-State and Transient Conditions*

1 Steady-state and transient conditions shall be combined by applying the Soderberg straight-line rule. Accordingly, the stress due to combinations of steady-state and transient conditions can be resolved into an average or mean component and an alternating component.

2 The value of the mean stress component at any point including gross structural discontinuities shall not exceed the yield strength at temperature.

3 The alternating stress component for structural members including the effect of any structural discontinuity shall not exceed two times the yield strength at temperature or 34,000 psi, whichever is less.

4 The alternating stress component for nonstructural members shall not exceed the values given by Fig. 4.

D *Deformation*

Deformations shall be consistent with operation and safety requirements.

Design Evaluation

Application of the foregoing as a guide together with good design and fabrication practice, a careful and conservative stress analysis and load evaluation, and thorough material and workmanship control, should result in an adequate structure. Final proof of this is a proper and successful simulated-service test.

Several unconventional features of the design configuration warrant special tests to obtain information from which the strength of these features may be further evaluated. The rectangular transition section from the lower to the upper reactor vessel and the intersection of the transfer-rotor container with the upper reactor vessel defy good stress analysis using theoretical techniques. These regions, and the support-plate support structure and the 30-in. nozzles appear to be critically stressed areas.

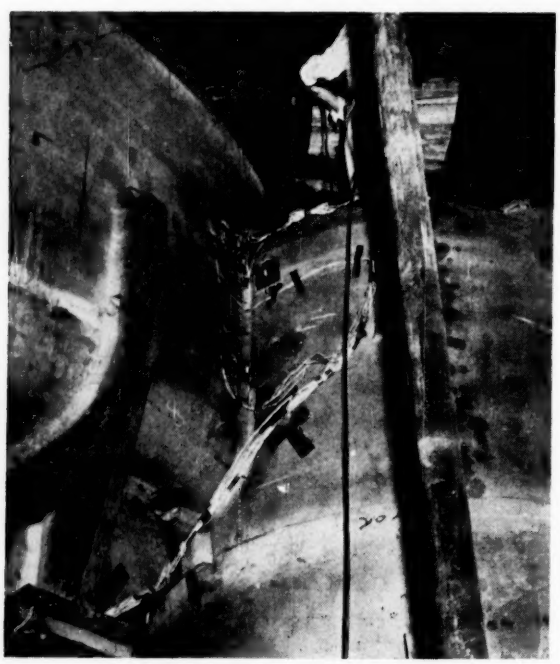

Fig. 5 Typical strain-gage installation

The hydrostatic-pressure tests presented a good opportunity to experimentally measure the stresses in these regions arising from an internal pressure. Accordingly, a number of bonded-resistance-wire strain gages were mounted on the reactor vessel at carefully chosen points. Fig. 5 shows a typical installation at the transfer-rotor-container and upper-reactor-vessel intersection. During these tests, shop conditions had to be tolerated. These involved large ambient-temperature variations and other more or less tolerable shop conditions. To minimize the effect of temperature variation, a number of temperature-compensating gages were used. By comparing the compensating gages with the active gages for a period of several hours before pressure was applied the effect of the temperature variation was noted. By continuing to compare each compensating gage with a control gage the effect of the temperature changes was observed throughout the test. Control gages are gages mounted on an isolated piece of Type 304 stainless steel subjected to no mechanical or thermal strain. They are also used to note instrument stability by reading one control gage against another. The strain-gage installation was made using standard techniques. SR-4 Type A gages were cemented in place with epoxy cement. Petrosene wax was used for moisture proofing. Lead wires were of No. 18 solid copper with waterproof insulation and of a length such that capacitive effects and change in gage factor could be ignored. Lessels-type strain-gage connectors were used to prevent damage to the gage lead wires. All lead wires were connected into Lessels multiple-point switching units. A Baldwin-Lima-Hamilton Type NA Strain Indicator was used to read the gages. Temperature stability throughout the test was good in view of the severe shop conditions. In most cases the maximum observed apparent strain due to temperature change was no greater than 30 μin. per in.

Three separate pressure tests were made. The radial-blanket inlet plenum was pneumatically tested to 94 psig; the core-section inlet plenum was hydrostatically tested to 210 psig; the rest of the reactor vessel was hydrostatically tested to 112.5 psig. These were the pressures required to satisfy ASME Code. Table 3 gives the magnitudes of the maximum stresses in various parts of the vessel due to these applied pressures as obtained from the strain gages. As far as pressure loading is concerned it appears that the vessel is satisfactorily proportioned, the maximum stress magnitude being of about the same order throughout. The structural discontinuities producing the greatest stress rise are the junctions of the 30-in. nozzle with the upper reactor vessel and of the plug container with the conical transition. In each case the maximum stresses are about twice the nominal shell stresses.

Table 3 Stresses measured during hydrostatic tests

	Hydrostatic test		Design condition	
Location	Pressure, psig	Stress, psi	Pressure, psig	Stress, psi
30-in. outlet nozzle	112.5	12,000	50	5400
Lower-reactor-vessel shell at support-plate structure	210	7500	110	3900
Transfer-rotor-container junction with upper reactor vessel	112.5	6000	50	2700
Lower-reactor-vessel junction with rectangular transition	112.5	9000	50	4000
Upper-reactor-vessel junction with conical transition	112.5	9000	50	4000
Plug-container junction with conical transition	112.5	9000	50	4000

Tests using a partial $^1/_4$-size model were made to evaluate the effects of pipe reactions and plug weight on the 30-in. outlet nozzle. Another $^1/_4$-size model of the upper reactor vessel was used to determine coolant mixing in the upper pool and pressure losses through the hold-down region. Thermal-transient studies of the system for various emergency-cooling and scram conditions were made. Space does not permit comments on these studies.

High-Temperature Strain Gages

Strain gaging the vessel to measure strains during simulated-service testing involving temperatures up to about 1000 F is quite different from strain gaging at room temperature. We know of no successful long-time strain-gage installation at temperatures much higher than 600 F. No off-the-shelf gage suitable for long-time operation at 1000 F has proved successful. This is strictly a development problem. Some of the difficulties encountered are basic material problems. The gage-element alloy must be stable throughout the required temperature range and should produce a low temperature coefficient, that is, the curve of apparent strain versus temperature should be flat. A large resistance and a high, stable gage factor are also desirable. A second and equally important factor is the cement used to attach the strain gage. Its desired qualities are a low curing temperature, and good bond and high electrical resistance at high temperatures.

Our best laboratory-test results to date have been obtained using series-600 Metalfilm gages manufactured by the Tatnall Measuring Systems Company. These are foil gages about 0.1 mil thick which are supplied on a temporary backing and are shaped as shown in Fig. 6(*A*). Long-time stability has been achieved with the use of compensating gages.

The ceramic cements used with high-temperature gages must be cured at temperatures of about 600 F. When considering attaching a goodly number of gages to a vessel the size of the Enrico Fermi reactor vessel this is quite an obstacle. Furthermore, in order to achieve repeatability up to at least 900 F it is necessary to temperature cycle the gages in a manner prescribed on the basis of experience. Repeatability simply means that the curve of apparent strain versus temperature is repeated for successive temperature cycles. In order to achieve stability with respect to time, even when the gages are connected compensated, a period of operation at temperature for about 15 to 20 hr is required.

Direct attachment to the reactor vessel is obviously out of the question. Curing, cycling, and stabilizing must be done before the gages are attached to the vessel. This can be done by cementing them to a carrier or coupon which in turn can be attached to the vessel. Various configurations and sizes of 0.010-in-thick stainless-steel coupons were evaluated using SR-4 gages at room temperature. These coupons, with strain gages attached, were spotwelded back to back in pairs on a beam. The beam was loaded and the resulting strain-gage readings were compared with the known strains. Results varied with the cross section of the coupon and the locations of the spotwelds. Nearly 100 per cent strain transfer was obtained using single-thickness, flat pieces about $^3/_4 \times 1^1/_2$ in. in size with the spotwelds closely spaced all around. The details of the completed strain-gage coupon are given in Fig. 6(*B*). These coupons are furnished by the gage manufacturer in a precycled and stabilized condition ready for attachment by spotwelding with a capacitor-discharge-type spot-welder.

A pair of Type 630 Metalfilm high-temperature strain gages were mounted back-to-back on a stainless-steel beam for evaluation tests and stabilized by cycling in a prescribed manner. The cement was cured at 600 F for 1 hr, after thorough air drying. Subsequent cycles of 1 hr at 700 F, 1 hr at 850 F, and 1 hr at 900 F were applied. Then the gages were connected, compensated into a recorder, and were brought up to 900 F and held there. The subsequent change in apparent strain with respect to time is shown in Fig. 7. After about 17 hr, stability was achieved. After 22 hr the temperature was dropped to room temperature so that a different furnace and indicating system could be employed.

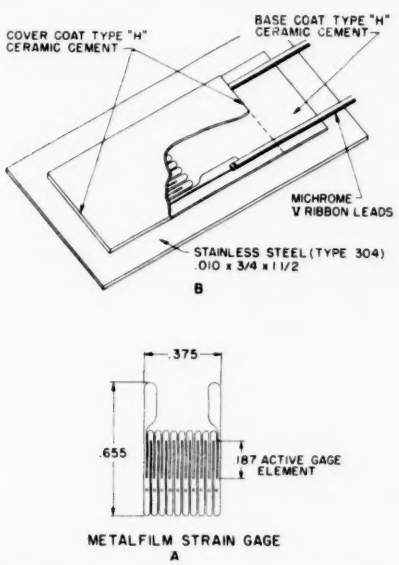

Fig. 6 High-temperature strain gage mounted on coupon ready for attachment to vessel

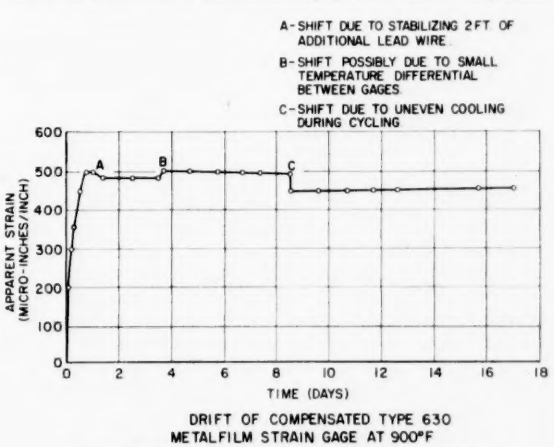
A - SHIFT DUE TO STABILIZING 2 FT OF ADDITIONAL LEAD WIRE
B - SHIFT POSSIBLY DUE TO SMALL TEMPERATURE DIFFERENTIAL BETWEEN GAGES
C - SHIFT DUE TO UNEVEN COOLING DURING CYCLING
APPARENT STRAIN (MICRO-INCHES/INCH)
TIME (DAYS)
DRIFT OF COMPENSATED TYPE 630 METALFILM STRAIN GAGE AT 900°F

Fig. 7 Stability of compensated strain gages at 900 F

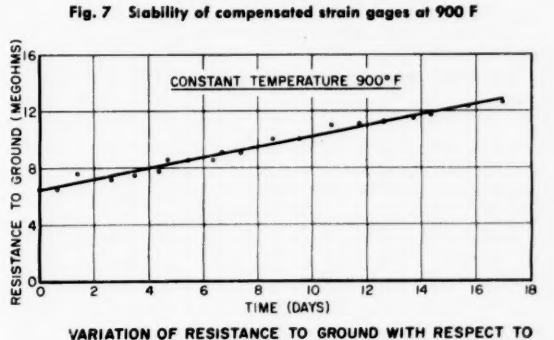
CONSTANT TEMPERATURE 900° F
RESISTANCE TO GROUND (MEGOHMS)
TIME (DAYS)
VARIATION OF RESISTANCE TO GROUND WITH RESPECT TO TIME OF TYPE 630 METALFILM STRAIN GAGE AT 900° F

Fig. 8 Leakage resistance of strain gages at 900 F

After reheating to 900 F a drop of 21 μin. per in. apparent strain was noted over a 16-hr period. This is due to the 2 ft of additional lead wire being heated in the new furnace. High-temperature lead wire requires stabilizing. The cause for the increase in apparent strain of about 15 μin. per in. at 86 hr is not known but may be due to the two gages being at slightly different temperatures at this time. It is noted that this shift is accompanied by an increase in leakage resistance of 1 megohm. At $8^1/_2$ days cycling of the gages between room temperature and 900 F was started. Cooling was accomplished by taking the gaged beam out of the furnace, placing it on a cold copper slab, and blowing air over the cooling beam with a fan. The resulting unequal cooling caused a shift of 60 μin. per in. in apparent strain. When more care was taken to provide uniform cooling no such shift occurred. During the 4-week testing period the gages were held at 900 F for a total of 17 days. The remaining time was used for cycling and holding at room temperature. The change in apparent strain at 900 F during this entire period was a total of 50 μin. per in., most of it due to specific events in the gage history. Drift, as such, amounted to less than 20 μin. per in. during the 17 days at 900 F. This is phenomenal at the present stage of development.

It must be emphasized that the stability achieved depends on the compensation. Resistance measurements made on the individual gages show that the apparent strain increases about 400 μin. per in. per day at 900 F. This indicates that it is important that both the active and compensating gage have identical histories in order that they follow one another closely.

Two other items merit comment. A change of 800 F produces a shift of about 80 μin. per in. for the compensated gages. Secondly, the leakage resistance to ground at 900 F shown in Fig. 8 was about 6.5 megohm at the start of the test period and showed considerable improvement as the test progressed.

The coupon shown in Fig. 6(B) will be attached to the vessel in groups, to make two or three-gage rosettes as required. One compensating gage will be used with each rosette. All gages will be externally attached.

Conclusion

A complex structure subjected to severe operating conditions has been designed and built. The guiding philosophy has been a realistic conservatism. Evaluation of the structure and of the design principles is continuing. The high-temperature strain-gaging technique described is expected to provide a sound basis for further evaluation of the structure.

Acknowledgments

This paper would not be complete without acknowledging and giving full credit to Combustion Engineering Inc., for the detail design and fabrication of the Enrico Fermi reactor vessel from the basic designs submitted by Atomic Power Development Associates, Inc. When a new design is evolved for an entirely new application many problems with which there is very little, if any, experience will be encountered. Time and time again, no effort was spared by Combustion Engineering Inc., to satisfactorily and effectively solve these problems.

The Franklin Institute contributed much to the basic design of the reactor vessel.

References

1 B. F. Langer, "Design Values for Thermal Stress in Ductile Materials," Westinghouse Atomic Power Division Report T-584, 1957.

2 W. E. Cooper, "Proposed Structural Design Basis for Nuclear Reactor Pressure Vessels," in "Problems in Nuclear Engineering, Selected Papers From the First Nuclear Engineering and Science Congress," vol. 2, Pergamon Press, New York, N. Y., 1957, vol. 1, pp. 26–33.

3 "Structural Design Basis for Reactor Pressure Vessel," U. S. Department of the Navy, Bureau of Ships, SSN/S51(551B) Ser. 551B-2860, 1957.

4 Op. cit. p. 14.

5 L. F. Coffin, Jr., "Thermal Stress and Thermal-Stress Fatigue," *Society for Experimental Stress Analysis Proceedings*, vol. XV, no. 2, 1958, pp. 117–130.

A. T. BOWDEN

Director and Chief Research Engineer, C. A. Parsons & Company Limited

W. HRYNISZAK

Research Engineer, C. A. Parsons & Company Limited, Newcastle-on-Tyne, England

Some Thoughts About the Development of Automotive Gas-Turbine Units

Possible configurations for an automotive gas-turbine unit are considered. Comparisons are made of designs taking the drive from the high-pressure and low-pressure portions of a split turbine, as well as the advantages to be gained with a divided-compressor and differential-gear arrangement.

Introduction

In his address before the engineering section of the British Association for the Advancement of Science in 1951 [1],[1] Sir Claude Gibb, Chairman of C. A. Parsons & Company Limited, stated that the gas turbine will supplant the diesel engine to a great extent: "There is no difficulty in making gas turbines of 100 hp which can easily be fitted to motor cars within the space now occupied by petrol or diesel engines. . . Once the pure rotating prime mover has been found suitable for a given application it always becomes possible to supplant an alternative reciprocating type and there is little doubt but that within the next 50 years the gas-turbine-driven motor will be used to the exclusion of all others."

The developments made since then in Great Britain [2], Germany [3], France [4], Italy [5], and the U. S. [6] give promise that the prediction made in 1951 will be fully met. There has been progress not only in design of automotive gas turbines but also in the development of special materials [7] and manufacturing methods [8] suitable for their mass production.

At the end of the last war gas-turbine propulsion of military vehicles such as heavy tanks was studied intensively in Europe, and as a result C. A. Parsons & Company Limited were entrusted by the Ministry of Supply with the task of developing a suitable gas turbine for propulsion of military vehicles such as heavy trucks. A team under Dr. A. T. Bowden designed such a gas turbine, two units were made by the Company, and in 1954 the first gas-turbine-propelled tank in the world was publicly shown [9]. Since then extensive tests have given proof of the suitability of this type of prime mover for such a duty.

The development of a gas-turbine unit as the main power plant of a tank, Fig. 1, gave rise to a large number of problems common to road-vehicle application. The simplest kind of gas turbine (consisting of one compressor driven by one turbine and employing, apart from the combustion chamber, an air preheater) has certain disadvantages which can successfully be overcome.

Improvement is closely connected with the number and arrangement of the turbomachines, the increase in their efficiency, as well as the efficiencies of the other components. The incorporation of an air preheater is imperative especially where a good performance is required at a low average load. The employment of such a heat exchanger in the gas-turbine unit, especially if the utmost compactness is to be met, is difficult as low parasitic-pressure losses are essential. The important step toward the standardization of the heat exchanger for universal use in gas-turbine units of any design—which should be the ultimate aim—is therefore very hard to achieve especially if the regenerative instead of the recuperative process is chosen for the exchange of heat.

General Characteristics of a Simple Gas-Turbine Unit Having Regard to Its Suitability for Vehicle Propulsion

The simplest type of gas-turbine unit produces a positive (pulling) torque which decreases when the speed of the vehicle is reduced because of its mechanical connection with the turbine through a reduction gear of fixed ratio. A gas-turbine unit of this kind is inferior in positive-torque behavior to a conventional petrol or diesel engine. On the other hand, its negative (braking) torque is sufficient in most cases.

Thermodynamically speaking, there is a whole field of possible working conditions limited only by the surge line of the compressor, the line of maximum permissible stresses (mainly in the rotors of the turbomachines) and the line of maximum permissible air-to-fuel ratio of the combustion chamber. The gas-turbine unit can be well adapted to the requirements of the vehicle, which reduces the working field to a single line.

It has been realized for some time that splitting the turbine into a compressor-driving and a power-providing part gives a considerable improvement, in so far as the positive torque behavior of the gas-turbine unit is concerned. Split turbines are, therefore, used in all known designs concerning automotive applications. When the power-turbine part is completely stalled a maximum theoretical positive-torque ratio of 2.83 is obtained, when the torques at zero and optimum (maximum efficiency) speed are compared. Apart from the effect of losses, say, in the blades or vanes of the turbine, any change in mass flow and consequently in gas temperature and pressure before and after the turbine, which are closely connected with these losses, will affect the maximum obtainable positive torque.

The mechanical disconnection of the compressor-driving turbine and the power turbine means that no appreciable negative torque can be provided by the gas-turbine unit and additional means have to be introduced if motor braking is required. One system consists of a gear and an overspeed clutch automatically linking the two turbine parts when such braking is required [10].

The splitting of the turbine reduces the number of possible working lines to one which is fixed by the relation governing mass flow, temperature, and pressure of the gas passing through the two separate turbine parts. This working line will be different from the one dictated by the vehicle. As a result the power turbine will, under most conditions, run at a speed different from that leading to maximum turbine efficiency. As this efficiency directly affects the specific fuel consumption and hence the miles per gallon obtained, a further consequence will be a deterioration in performance of both the gas-turbine unit and the vehicle driven by it.

One of the great difficulties encountered when developing a gas-turbine unit for vehicle propulsion is the very low average load usually required. If the power turbine is designed for maxi-

[1] Numbers in brackets designate References at end of paper.

Contributed by the Gas Turbine Power Division and presented at the Semi-Annual Meeting, Detroit, Mich., June 15–19, 1958, of The American Society of Mechanical Engineers.

Note: Statements and opinions advanced in papers are to be understood as individual expressions of their authors and not those of the Society. Manuscript received at ASME Headquarters, March 24, 1958. Paper No. 58—SA-26.

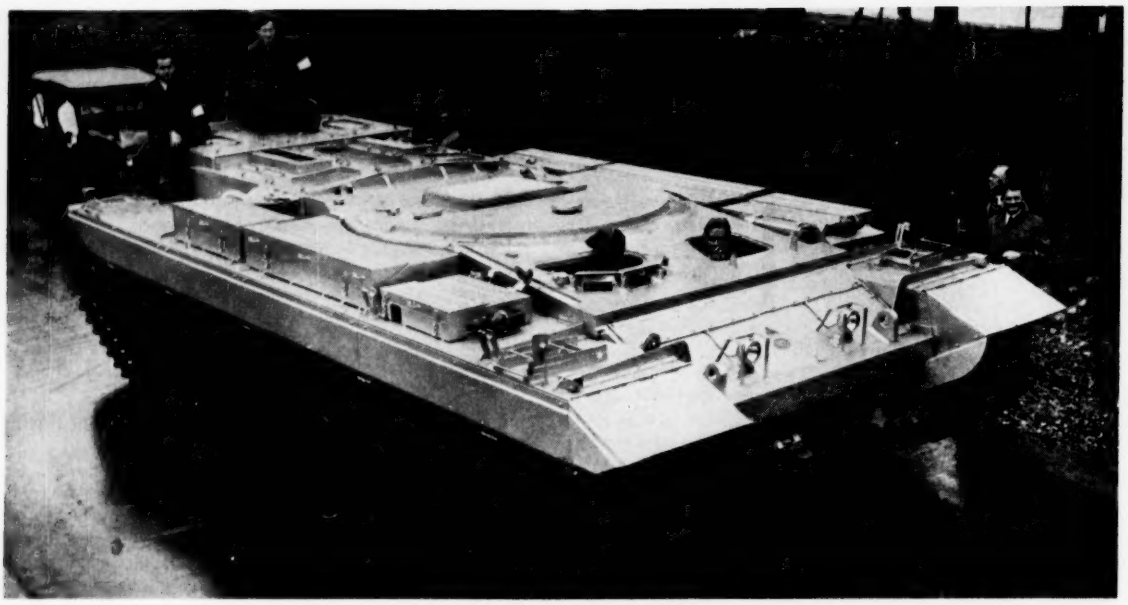

Fig. 1 Gas-turbine propelled tank

mum efficiency at this average load, the turbine will be overspeeded at larger loads and underspeeded at lower loads, with an adverse effect on the specific fuel consumption.

Splitting the turbine makes both the mechanical and the gas-dynamical design of the turbine more difficult. As far as mechanical design is concerned, two bearings have to be provided instead of one; overhung rotors usually lead to larger clearance losses and hence to a lower turbine efficiency; cooling of the bearings when placed between the two turbine parts is more difficult and again affects turbine efficiency indirectly in an unfavorable way. In addition it may have some gas-dynamical disadvantages from the increased resistance in the transition part between the two turbines housing the bearings. As far as this gas-dynamical design is concerned the power balance between compressor and its driving turbine requires a certain subdivision of the total available turbine power and consequently restricts the layout of the blading (or the choice of the speed) in such a way that the best turbine efficiency is difficult to achieve at the lowest possible weight. Such a low weight is, however, highly important from an acceleration or deceleration point of view.

Another important consequence of dividing the turbine in two parts concerns governing and the time lag experienced when changing load. The power requirements of the vehicle are met by changing the amount of fuel burnt in the combustion chamber. This means that the h-p turbine part immediately following this component will be the one directly controlled by the governing system. The other turbine part will get "what is left" and is therefore indirectly controlled. From this point of view it is obviously important which turbine part drives the compressor and which provides the power for the vehicle. Apart from this influence of turbine arrangement, the dynamic inertia of all the masses to be accelerated or decelerated and the thermal inertia of all the masses to be heated or cooled play an important role when it comes to the response of the gas-turbine unit to load changes. The design of the turbomachines (dynamic inertia) and that of the air preheater (thermal inertia) are important in this connection.

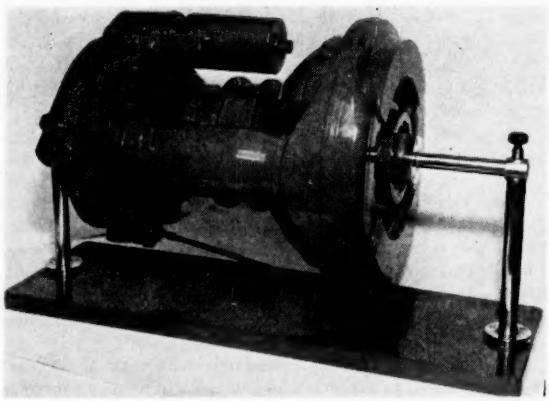

Fig. 2 Model of a gas turbine in which the l-p section is the power-providing section

Gas-Turbine Unit With the L-P Turbine Part Propelling a Long-Distance Coach

The decision which turbine part is to provide the power affects, to a large extent, the working conditions of the gas-turbine unit and the performance of the vehicle it propels. In all known designs of such a unit the l-p part is the power-providing section of turbine. Table 1 gives a short specification of such a gas turbine unit, Fig. 2, for a long distance coach with few stops to make and a full pay load assured throughout the journey. Table 2 gives the assumptions made regarding the weight of the coach fitted, respectively, with a diesel engine and gas-turbine unit of similar power. With a gas-turbine unit a reduction in speed of the compressor and compressor-driving h-p turbine results in a reduction of mass flow, temperature, and pressure of the gas, and therefore a decrease in available power. However, due to a relative rise in waste heat, fuel consumption is not decreased to the same extent, and as a result the specific fuel consumption is increased.

Table 1 General data

Type:	Simple open-cycle gas turbine with air preheater.
Turbine Arrangement:	Separate compressor-driving and power-providing turbine part (split turbine). *Compressor-Driving Turbine Part:* Single-stage axial-flow h-p turbine Gas temperature before turbine: 850 C (1560 F) at 30,000 rpm. *Power-Providing Turbine Part:* Two-stage axial-flow-lip turbine. Gas temperature after turbine: 650 C (1200 F) at 15,000 rpm.
Compressor:	Single-stage centrifugal compressor. Air mass flow at intake, 3 lb per sec at 30,000 rpm. Pressure ratio at this speed, 3:1.
Combustion Chambers:	Two can-type combustion chambers with upstream injection and counterflow cooling with air flowing from the compressor to the air preheater.
Air Preheater:	Regenerative heat exchanger with annular-disk rotor. Two gas sides and two air sides. The ratio of areas is 2:1 (gas/air). Matrix of wire gauze. Total area of matrix: 2 sq ft. (Normal) rotor speed: 30 rpm.
Fuel System:	Gear-type pump.
Lubrication System:	Two oil-suction pumps and one oil-pressure pump (gear-type).
Starting System:	Generator used at the same time as starter motor.
Reduction Gear:	Epicyclic. Ratio 10:1 giving a (normal) speed at the power shaft of 3000 rpm.
Exhaust Nozzle:	Two exhaust ducts symmetrical to the output shaft.

Apart from raising the component efficiencies, there are two methods of improving specific fuel consumption [11]. One is by increasing the pressure ratio, the other by waste-heat recovery. A substantial increase in pressure ratio would either reduce the size of the turbomachines in most applications beyond the limit where a sufficiently high efficiency could be maintained or would result in a large amount of surplus power which is only needed under certain driving conditions. This means that only the second method can be adopted by introducing an effective air preheater. One with a high degree of waste-heat recovery at a low power expenditure is desired because of the additional pressure losses and—in the case of the regenerator—additional mass-flow losses and power output needed for actuation. The introduction of a heat exchanger means, however, a considerable increase in weight of the gas-turbine unit, although the effect is partly offset by the reduction in weight of the fuel and fuel tanks for a certain range of the vehicle. These weight changes may also affect the weight of its carrying structure [12].

When comparing the regenerative with the recuperative process of heat exchange for the air preheater of a gas-turbine unit, it is important to keep in mind that, with a decrease in load, the effect on performance of the additional mass-flow losses of the former becomes less and less important because of the decreasing difference in pressure between the two heat-exchanging gases [13]. On the other hand, the pressure loss becomes more important. Considering the large cross-sectional areas of the rotor and stator available for the inflow and outflow of gases, even when these areas are necessarily reduced to decrease the mass-flow loss, this pressure loss should be smallest with the rotary type of regenerative air preheater [14]. A continuous gas flow is possible, an important property indeed, when this heat exchanger is connected to the other components of the gas-turbine unit.

Table 2 Assumptions made with regard to weights when comparing a long-distance coach powered by a diesel engine (conventional transmission) with one powered by a gas-turbine unit (split turbine), l-p turbine power-providing

Weight of coach (empty, without engine, transmissions, fuel and fuel tanks, lub oil and oil tanks)		16,820 lb
Weight of pay load (37 people + luggage)		6250 lb
	Total:	23,070 lb
Engine + transmission		
(*a*) Diesel engine		
Weight of engine (including transmission, battery, etc.)		3770 lb
Weight of fuel (40 gal of diesel oil)		350 lb
Weight of fuel tank		86 lb
	Total:	4206 lb
(*b*) Gas-turbine unit (including transmission, battery, etc., but without air preheater)		724 lb

Air preheater, fuel, and fuel tank

	Preheater, lb	Fuel, lb	Gal, lb	Fuel tank, lb	Gas-turbine, unit total, lb
Size "27 D" (Thermal ratio 76 per cent)	465	595	68	122	1906
Size "29 D" (Thermal ratio 83 per cent)	525	525	60	113	1887
Size "32 D" (Thermal ratio 90 per cent)	635	464	53	104	1927

Hence the regenerative air preheater chosen for the gas-turbine unit just mentioned has a rotor which is shaped as an annular disk. The matrix is housed in 24 separate but similar compartments, Fig. 3, fitted with their circular inlet and outlets into appropriate openings of the two frontal plates, Fig. 4, including the rotating parts of the seals (sliding type on the l-t and nonsliding type on the h-t side). These two plates are connected by an inner and outer ring, the former with the races for the rotor support and the latter with the gear ring for the rotor drive. This drive is actuated by the compressor-driving turbine through two gears and a connecting shaft. The stator, Fig. 5, includes the two frontal sealing plates with the stationary parts of the seals. Mass-flow losses of less than 4 per cent can be achieved at full-load conditions with this sealing arrangement. Two air and two gas sides are arranged symmetrically so as to reduce distortion, the area of the latter being twice the area of the former in accordance with full-load optimization.

The all important dimensions of such an air preheater are governed by the temperature changes required and the total pressure drop—effective and ineffective with regard to heat transfer—permitted. With the small equivalent diameters of the matrix necessary because of the restrictions mainly in weight, the most important dimensional property is the frontal area of the matrix. With certain shapes such as the annular disk, an increase in frontal area does not affect the size of the whole gas-turbine unit as much as with other shapes. Three gas-turbine units are shown in Fig. 6 differing mainly in the size of frontal area and hence the performance of the preheater. It can be seen that an increase in the area of the regenerator only slightly changes the space taken up by the whole gas-turbine unit. The change in its weight which depends on the OD of the matrix (27, 29, and 32 in. have been chosen as examples) is given in Fig. 7. Two types of matrix

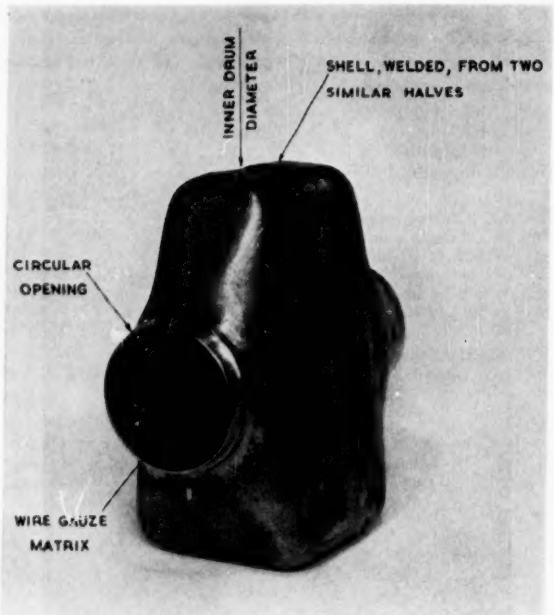

Fig. 3 Regenerative air preheater for the gas-turbine unit

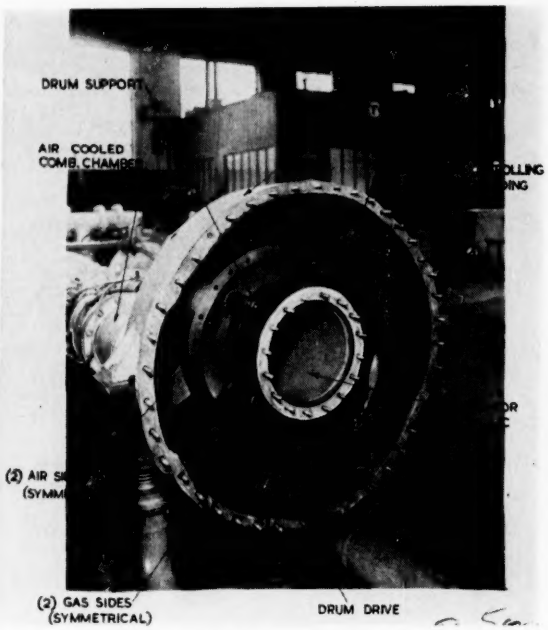

Fig. 5 The stator

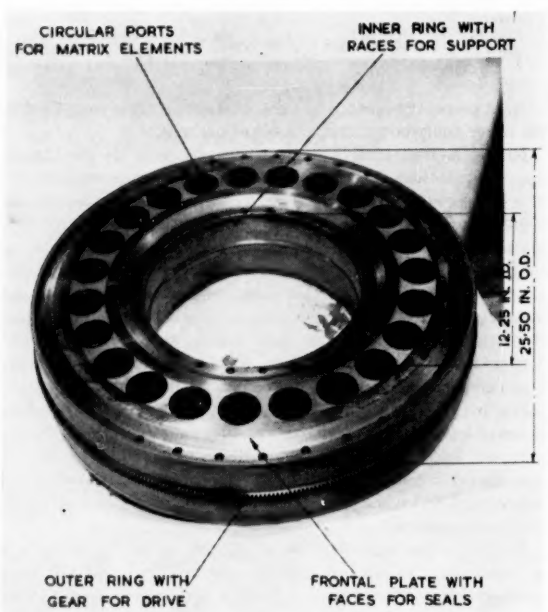
CIRCULAR PORTS FOR MATRIX ELEMENTS
INNER RING WITH RACES FOR SUPPORT
25·50 IN. O.D.
OUTER RING WITH GEAR FOR DRIVE
FRONTAL PLATE WITH FACES FOR SEALS

Fig. 4 Frontal plate for regenerative air preheater

have been studied, the plate (or flame-trap) type and the wire (gauze) type. From these investigations it can be concluded that the type of matrix has little effect on the weight. It is, however, interesting to note how large the parasitic-weight ratio of such a regenerative air preheater can be. By this ratio is meant a quotient of effective (matrix) weight to total weight of the air preheater.

The total weight of the gas-turbine unit has been correlated in Fig. 8 with the size of the air preheater and hence the specific fuel

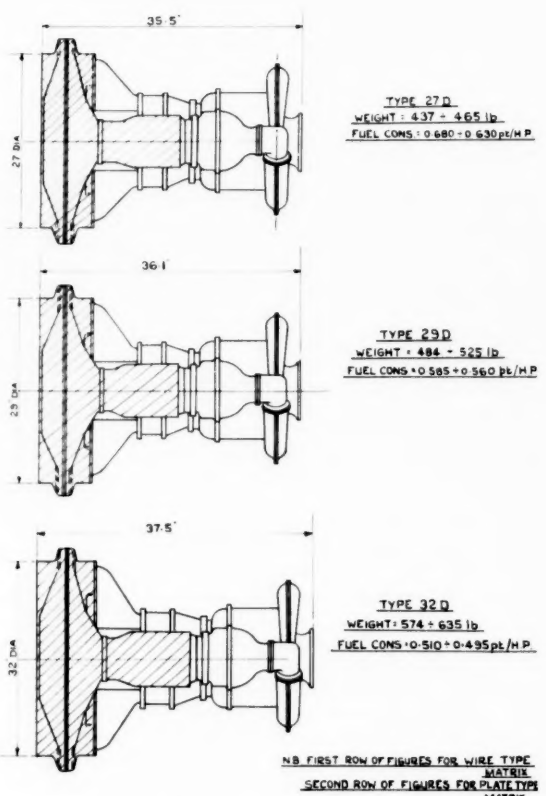
35·5"
27 DIA
TYPE 27D
WEIGHT : 437 ÷ 465 lb
FUEL CONS. : 0·680 ÷ 0·630 pt/H.P.
36·1
29 DIA
TYPE 29D
WEIGHT : 484 ÷ 525 lb
FUEL CONS. 0·585 ÷ 0·560 pt/H.P.
37·5
32 DIA
TYPE 32D
WEIGHT : 574 ÷ 635 lb
FUEL CONS. 0·510 ÷ 0·495 pt/H.P.
N.B. FIRST ROW OF FIGURES FOR WIRE TYPE MATRIX
SECOND ROW OF FIGURES FOR PLATE TYPE MATRIX

Fig. 6 Effect of air preheater size

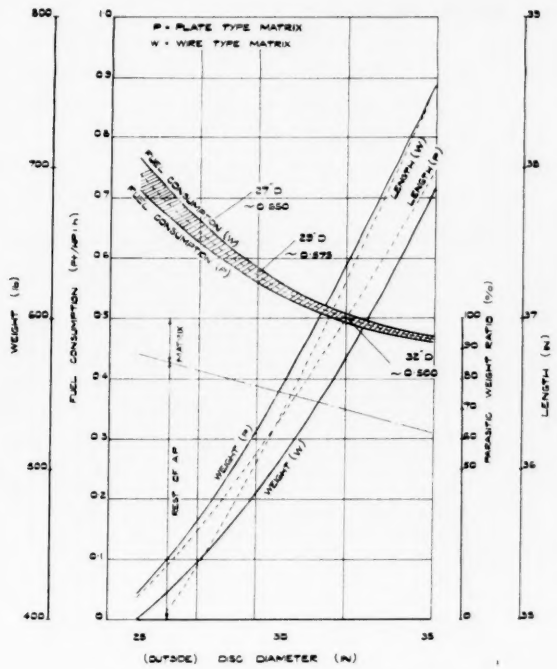

Fig. 7 Dimensions and weight of gas-turbine unit

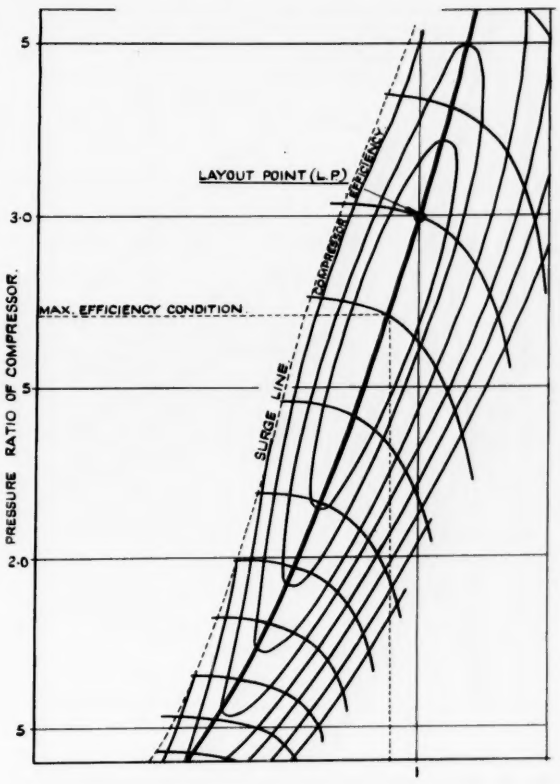

Fig. 9 Working line of gas-turbine unit with lp-vd turbine

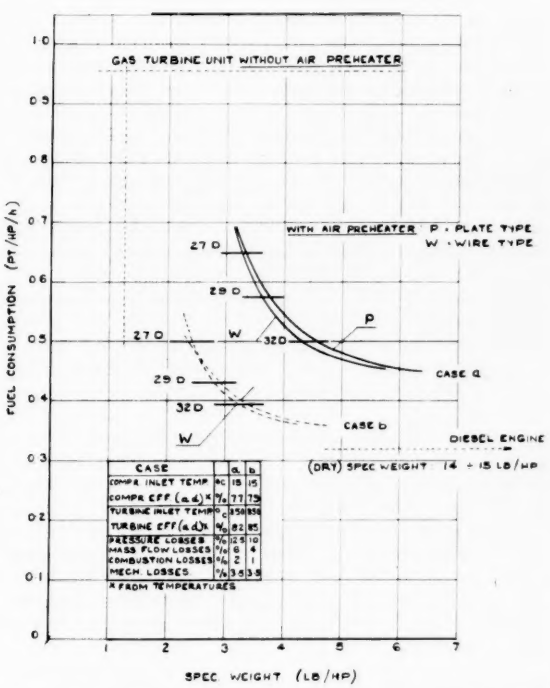
GAS TURBINE UNIT WITHOUT AIR PREHEATER
WITH AIR PREHEATER P = PLATE TYPE
W = WIRE TYPE
27 D
29 D
32 D
CASE a
CASE b
DIESEL ENGINE
(DRY) SPEC WEIGHT 14 ÷ 15 LB/HP
FUEL CONSUMPTION (PT/HP/h)
SPEC WEIGHT (LB/HP)
CASE | a | b
COMPR. INLET TEMP. °C | 15 | 15
COMPR. EFF (a.d)* % | 77 | 75
TURBINE INLET TEMP° C | 850 | 850
TURBINE EFF (a.d)* % | 82 | 85
PRESSURE LOSSES % | 12.5 | 10
MASS FLOW LOSSES % | 6 | 4
COMBUSTION LOSSES % | 2 | 1
MECH. LOSSES % | 3.5 | 3.5
* FROM TEMPERATURES

Fig. 8 Fuel consumption in terms of specific weight of gas-turbine unit

consumption as affected by this component. In this way the weight of the gas-turbine unit can be compared with the weight of a diesel engine having the same output. It is interesting to note how a slight improvement in the efficiency of the turbomachines coupled with a reduction in parasitic-pressure losses can greatly improve the specific weight of the gas-turbine unit.

Where the l-p turbine is the power-providing section, the working line will closely follow the line of maximum compressor efficiency (assuming for instance, a single-stage radial compressor, Fig. 9).

These working conditions do not quite coincide with those where maximum efficiency of the synchronous running power turbine is achieved, and they differ even more from those actually obtained because of the mechanical link of the power turbine with the vehicle. Optimum working conditions, that is, the best matching of gas-turbine performance and vehicle requirements can—at a certain gradient—be achieved only at one vehicle speed. If the gear ratio between the power providing and absorbing shafts is fixed accordingly, the power turbine will run either over or under-synchronous at any other speed, resulting in a decrease of turbine efficiency. With an l-p power turbine the difference between optimum and actual turbine speed, say at full load, is therefore large, with the result that an appreciable increase in specific fuel consumption is experienced, Fig. 10, due to a decrease in power available at the wheels of the vehicle and hence in its speed. This reduction in power does not affect the maximum positive torque

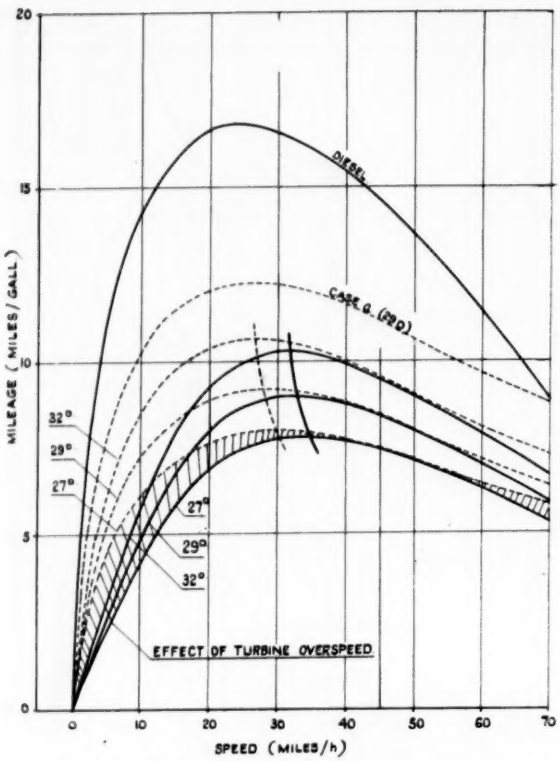

Fig. 10 Mileage comparison between diesel engine and gas-turbine unit

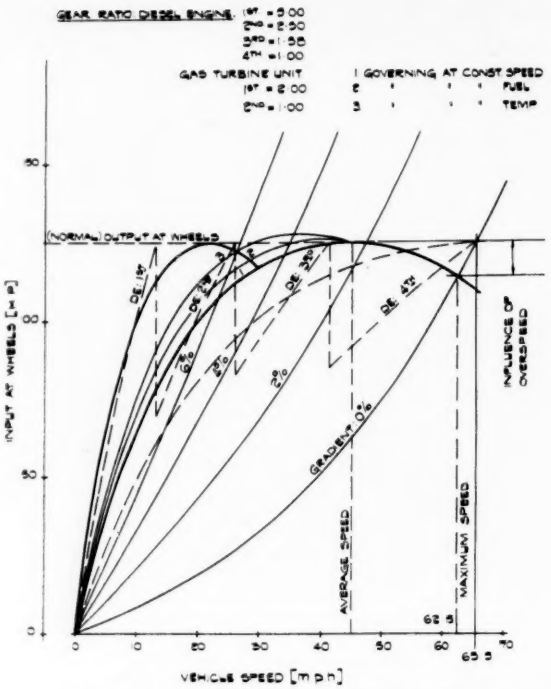

Fig. 11 Choice of gear ratio and influence of governing on gas-turbine performance

available. Due to the overspeed of the turbine, a larger maximum torque ratio is obtained making up for the reduction in available power due to the inefficiency of the turbine.

This torque is, however, not sufficient to exclude the need for gear change. When comparing the diesel with the gas-turbine-powered coach, a reduction in forward-gear stages from 4 to 2 seems possible, Fig. 11. When choosing the best gear ratio it should be kept in mind that the maximum torque can be slightly raised if the mass flow and consequently the temperature and pressure before the h-p turbine is increased during the time of stalling the power turbine. To what extent this is possible depends, for instance, on the characteristics of the turbine blading especially under part-load conditions. Wide-pitched, bull-nosed profiles (usually giving a lower maximum but a higher average efficiency) require an increase in mass flow, and hence, temperature and pressure to an appreciable degree, coupled with an overspeed of the carefully matched compressor and its driving turbine.

In the case of overspeeding, the mode of governing during the times the power turbine is stalled is of considerable importance. Governing at constant fuel supply is better than at constant speed and governing at constant turbine-inlet temperature is again better than at constant fuel supply, Fig. 11. However, the method of governing during this period of stalling the power turbine has to be properly adjusted to those at normal working conditions. As far as governing in general is concerned, it is to be noted that where the l-p turbine drives the vehicle, only the compressor and the compressor-driving h-p turbine part are directly controlled, provided that no special means are installed for an additional direct control of the power turbine.

For applications, such as the propulsion of fast intercity coaches where the average load is high, the use of a gas-turbine unit with its l-p turbine driving such a vehicle seems to have certain advantages. If the weight of the air preheater, fuel, and fuel tank (as affected by the heat exchanger) is added to the weight of the gas turbine unit—without air preheater—including transmission, battery, and so forth, the minimum total weight can be obtained at a certain size ("29 D") of the air preheater, this weight being considerably lower than the weight of the diesel engine, Table 2. Hence, payload and earnings are increased with this weight saving [15]. Beyond a certain distance, the coach with a gas-turbine unit could be more economical than that with a diesel engine. There are also differences in costs for maintenance (including lubrication). From a comparison made with high-average-load gas-turbine units and diesel engines of about 2.5 to 5.0-mw power output it seems that these costs are very much in favor of the gas-turbine units. A similar picture should be obtained in the course of development of smaller power outputs for vehicle propulsion, Fig. 12.

The regenerative air preheater is an expensive component of the gas-turbine unit as it consists of fixed and moving parts requiring tolerances so as to secure small clearance losses, despite considerable thermal distortions. In addition a device is needed for actuating the moving part. The matrix, too, can be expensive if it is made from plates or wires because of: (*a*) Small dimensions (large gages) required, which have been optimized from a cost point of view; (*b*) either expensive materials or expensive protective methods for cheaper materials, so as to counteract the effect of scaling.

Regenerator Sealing Problems and One Solution

The power losses due to a regenerative air preheater, additional to those experienced when a recuperative preheater is used, are mainly due to mass-flow losses caused by the gap between the

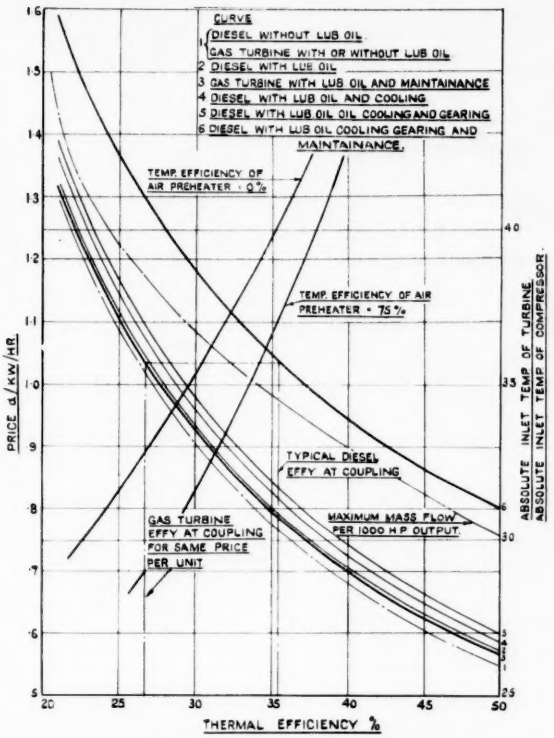
CURVE
1 DIESEL WITHOUT LUB OIL
GAS TURBINE WITH OR WITHOUT LUB OIL
2 DIESEL WITH LUB OIL
3 GAS TURBINE WITH LUB OIL AND MAINTAINANCE
4 DIESEL WITH LUB OIL AND COOLING
5 DIESEL WITH LUB OIL OIL COOLING AND GEARING
6 DIESEL WITH LUB OIL COOLING GEARING AND MAINTAINANCE.
TEMP. EFFICIENCY OF AIR PREHEATER - 0 %
TEMP. EFFICIENCY OF AIR PREHEATER - 75 %
TYPICAL DIESEL EFFY AT COUPLING
GAS TURBINE EFFY AT COUPLING FOR SAME PRICE PER UNIT
MAXIMUM MASS FLOW PER 1000 H.P OUTPUT
PRICE d/KW/HR
ABSOLUTE INLET TEMP OF TURBINE
ABSOLUTE INLET TEMP OF COMPRESSOR
THERMAL EFFICIENCY %

Fig. 12 Comparison of diesel and gas-turbine electrical unit prices

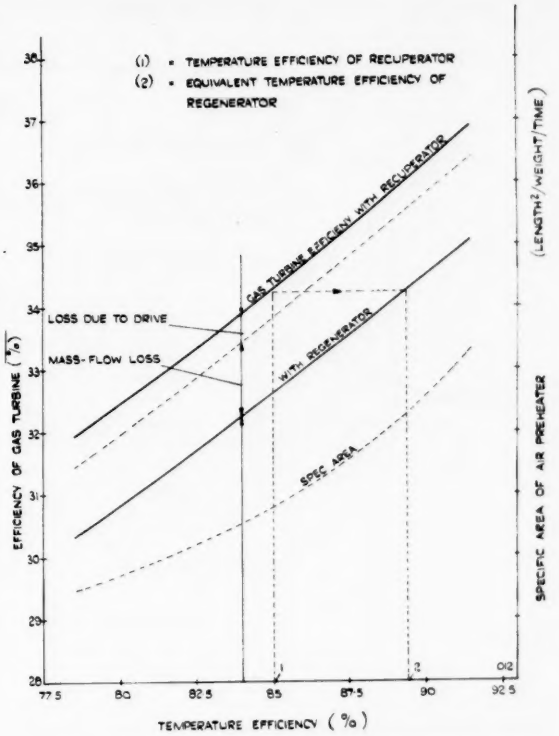
(1) = TEMPERATURE EFFICIENCY OF RECUPERATOR
(2) = EQUIVALENT TEMPERATURE EFFICIENCY OF REGENERATOR
GAS TURBINE EFFICIENCY WITH RECUPERATOR
LOSS DUE TO DRIVE
MASS-FLOW LOSS
WITH REGENERATOR
SPEC. AREA
EFFICIENCY OF GAS TURBINE (%)
SPECIFIC AREA OF AIR PREHEATER (LENGTH²/WEIGHT/TIME)
TEMPERATURE EFFICIENCY (%)

Fig. 13 Comparison of regenerator and recuperator

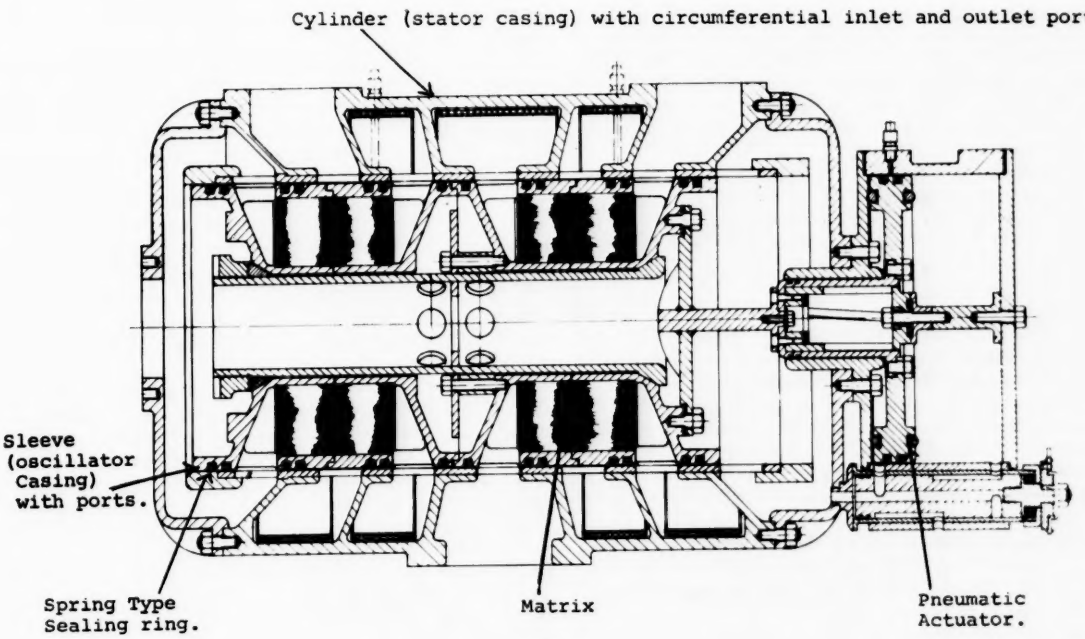
Cylinder (stator casing) with circumferential inlet and outlet ports.
Sleeve (oscillator Casing) with ports.
Spring Type Sealing ring.
Matrix
Pneumatic Actuator.

Fig. 14

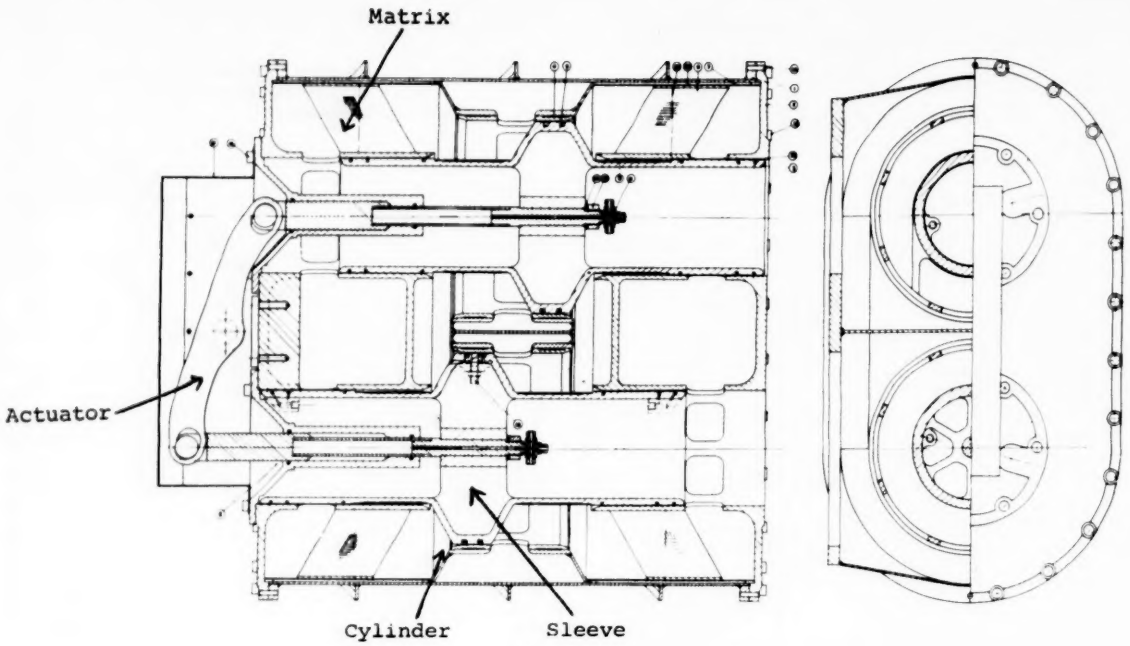

Fig. 15

fixed and movable parts of the regenerator, and the development of an effective seal is a major problem. These additional losses can be balanced, Fig. 13, by an increase in matrix area and hence weight of the regenerator so as to reduce the pressure losses in its matrix. This area increase can be considerable, especially where a large temperature rise is required.

Generally speaking, both noncontact [16] and contact seals can be employed, but in view of the penalty to be paid for any leakage at high loads, it will be advisable to use the latter type of seals whenever possible. Unfortunately, temperature conditions encountered are very severe when it comes to, say, a sliding seal. Cooling can be provided for, but a more complicated design results.

A large number of tests have been undertaken under relatively high temperatures to determine wear of different materials forming a sliding seal. The effect of suspending dry lubricants [17] such as graphite in at least one of the two contacting materials or protecting their sliding faces with molybdenum disulfide and other dry lubricants has been studied.

The effective clearance area between the mating faces depends on: (*a*) The shape, (*b*) the length, and (*c*) the gap of the seal [18]. Any measures leading to a reduction in sealing length will cause an increase in pressure loss. Optimization leads to a sealing length where the combined effect on gas-turbine performance of mass-flow and pressure losses is at a minimum. Circular shaped seals will always be easier to handle than other shapes. In the case of the regenerator with a disk-type rotor, for instance, two circular seals plus four interspersed straight seals are necessary, the latter number depending on the number of sides chosen. Straight seals are awkward when it comes to providing for a small effective gap. Surface roughness and waviness have to be taken into account. Temperature gradients also have an influence.

Straight seals can be eliminated in a design [19] where annular sleeves slide in a cylinder actuating its inlet and outlet ports in very much the same way as in a two-stroke piston engine. In this case, a well-tried sealing element, the piston ring, can be successfully employed. Provided that the weight is not too large the matrix can be embedded in the sleeves, Fig. 14. Small amplitudes and a low average velocity, together with a relatively small pressure difference to be sealed off, ease the working conditions of the piston rings. On the other hand, conditions are very severe on the high-temperature side of the heat exchanger. Lubrication with oil or graphite suspended in a volatile liquid is necessary, and precautions should be taken so that no fouling of the matrix takes place.

The matrix can be kept stationary and hence only the sleeves actuated, where the larger weights are encountered (which would make acceleration and deceleration more difficult), Fig. 15. This design has the additional advantage that the matrix shape need not be circular to better accommodate the matrix in a given space.

Whatever design is being used two regenerators, or a "twin unit," are necessary to allow for a more or less continuous gas flow as provided by the turbomachines of the gas-turbine unit. Tests have shown that the short interval during which flow is cut off from the combustion chambers has no major effect on the proper working of these components. These tests also gave proof that specific mass-flow losses less than 1 per cent can be achieved with a spring-type seal, such as the piston ring.

Despite the introduction of such an expensive component as the air preheater, the part-load performance of the gas-turbine unit still needs to be improved mainly because of the reduction in maximum cycle temperature with load. As a result, thermal load of the different components of the gas-turbine unit is reduced with speed, an advantage where this load at maximum-power output is high and required for short periods only. The wisdom of doing so especially where relatively small maximum-power outputs are involved can, however, be disputed. In this case a moderate thermal load at maximum-power conditions might allow an increase in this load when speed is reduced with consequent improvement in specific fuel consumption if such part-load conditions could be realized.

The greatly improved positive-torque behavior is in most cases still inadequate for dispensing with forward-gear changes whereas

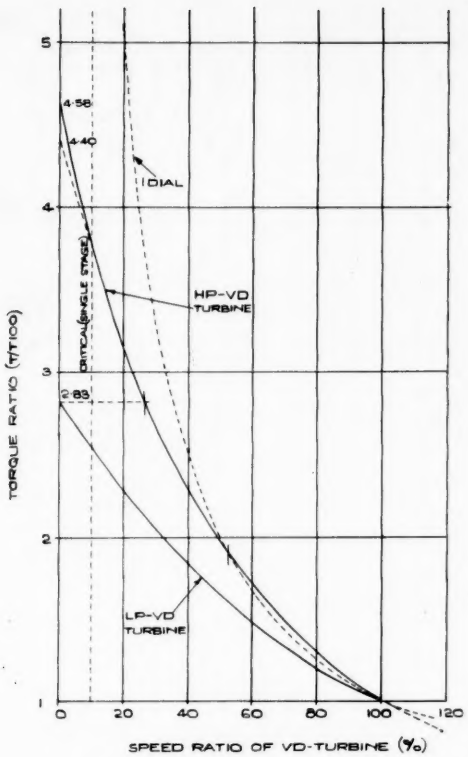

Fig. 16 Torque ratio versus speed ratio

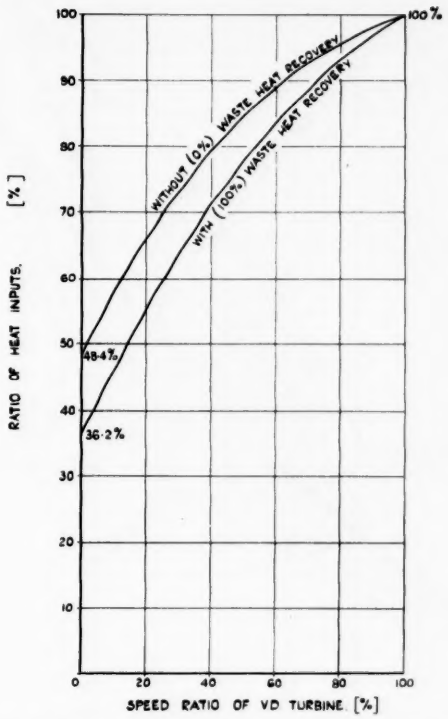

Fig. 17 Reduction in fuel consumption when hp-vd turbine is stalled

the good negative-torque behavior can only be maintained by introducing a device adding to cost, weight, and unreliability.

An alternative solution has therefore been sought and the following section considers in some detail a propulsion unit wherein power is taken from the h-p in place of the usual l-p part of the turbine.

Design Study of a Gas-Turbine Unit, the H-P Part of Its Turbine Driving a Passenger Car

Stalling the l-p turbine part results in a power loss affecting the velocity and the temperature of its exhaust gases and therefore the working conditions of the air preheater, as well as the control of the whole gas-turbine unit. A rise in the available power of the h-p turbine part by an increase in the swallowing capacity of the l-p part due to such stalling slightly improves the positive torque obtained. The aim should be to increase such "surplus power" during the time when a large positive torque is needed, if possible, without any increase in fuel expenditure because of a recovery of the power wasted by the stalled turbine part. Such an improvement in the behavior of the gas-turbine unit is actually possible if its h-p turbine part is coupled to the vehicle.

In such a unit, which allows for direct control of the power turbine, any stalling will affect the power available for the compressor driving turbine and hence the compressor, but will have little effect on the air preheater. Power lost by the h-p turbine part will be recovered to a certain extent by the following l-p turbine part with consequent increase in mass flow, pressure, and temperature, resulting in an increase in positive torque. Due to such power recovery, the positive-torque ratio is considerably improved, Fig. 16, even if the compressor and its driving turbine cannot be overspeeded. At the same time, fuel consumption is reduced, Fig. 17, thus favorably affecting the average miles per gallon of the vehicle.

For other reasons, too, the gas-turbine unit with the h-p power turbine is a typical "low-average-load" prime mover. Over the whole range of loads, the maximum cycle temperature will change very little. The extent and kind of change depends greatly on the compressor characteristics. This means that better use is made of the material strength, the difference between maximum-permissible and actual material temperature being reduced. Mass flow is reduced faster than with the l-p power turbine and the air preheater effectiveness will also increase more quickly especially in the case of a laminar-flow matrix. A better specific fuel consumption is therefore obtained in the part-load region. This consumption is affected very little if the gas-turbine unit is installed in a vehicle.

In view of the low average load required for passenger cars a compressor should be chosen with maximum efficiency at a relatively low pressure ratio. The working line will follow a line of constant temperature rather than a line of maximum compressor efficiency, Fig. 18. Maximum-power efficiency drop has little effect on average specific fuel consumption since maximum-load conditions obtain only for short periods. On the other hand, the working conditions dictated by the mechanical link of the driven wheels with the power turbine differ little from those conditions where this turbine runs at its best efficiency, Fig. 19. As a result the specific fuel consumption is little affected by the difference in actual and optimal working conditions.

Apart from the effect of dividing the turbine on negative-torque behavior and on the mechanical and gas-dynamical design as mentioned before, the performance of the gas-turbine unit can be improved as far as requirements for vehicle propulsion are concerned by choosing the h-p instead of the l-p turbine for power.

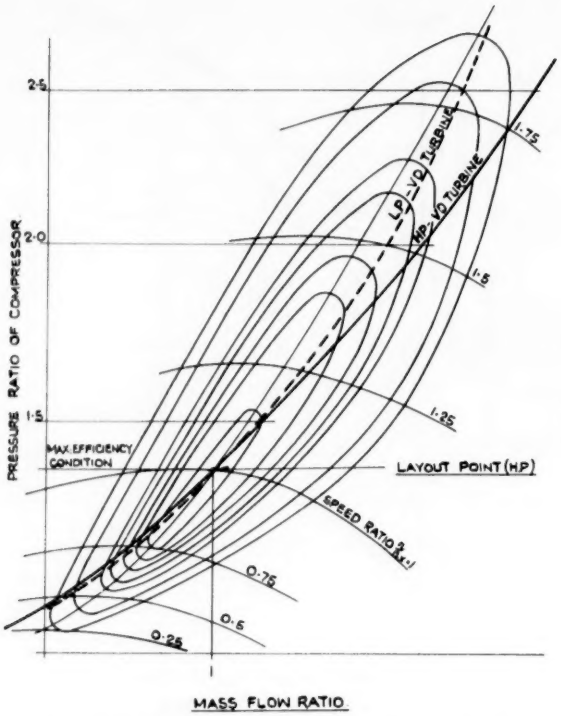

Fig. 18 Working line of gas-turbine unit with hp-vd turbine

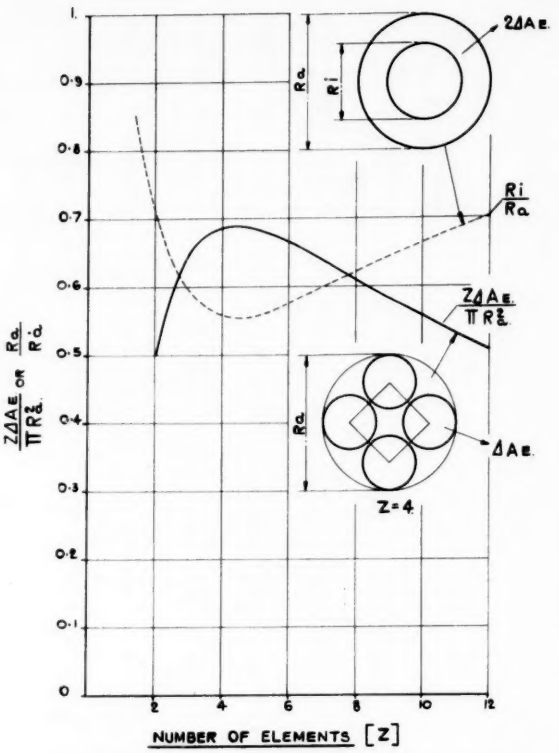

Fig. 20 Matrix area for frontal arrangement of elements

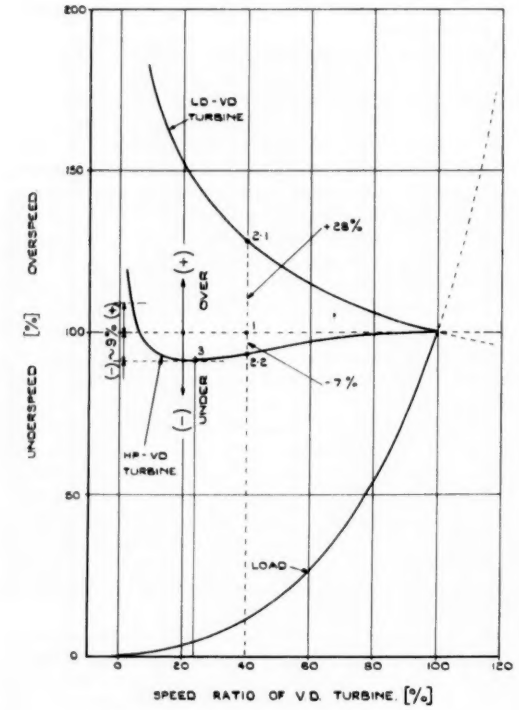

Fig. 19 Over or under speed of vd turbine

The maximum working temperature of the air preheater is increased with this design when the load is reduced allowing an attractive alternative design of the heat exchanger, particularly if a regenerative type is chosen.

Three aims should be uppermost:

1 Reduction in weight without a deterioration in temperature gain and pressure loss.

2 Indifference to sudden temperature peaks due, for example, to after-burning between the turbine outlet and the preheater inlet, the location and extent of such peaks being largely uncontrollable.

3 Reduction in parasitic-pressure losses caused by the ducts needed to join the preheater with the other components of the gas-turbine unit.

As far as the last point is concerned, the fact is significant that interleaving of these ducts cannot be prevented, when a single annular-disk drum is used as the rotor of the regenerator, in spite of a well-executed design, Fig. 2.

Where high thermal load is coupled with low stresses mainly due to thermal distortion, an excellent opportunity is offered to introduce light-weight, nonmetallic materials such as ceramics. Materials of this kind have been developed [20] to give a very small coefficient of thermal expansion even at high temperatures. In addition, methods have been devised to spray such materials in very thin layers [21], which facilitate the production of a matrix having a small equivalent diameter and at the same time a high ratio of transflux and initial area (permeability). Further progress in the realization of such matrices will undoubtedly be achieved by the use of ceramic papers [22].

The rotary regenerative heat exchanger is basically simple as it consists of only three different parts, namely the stator

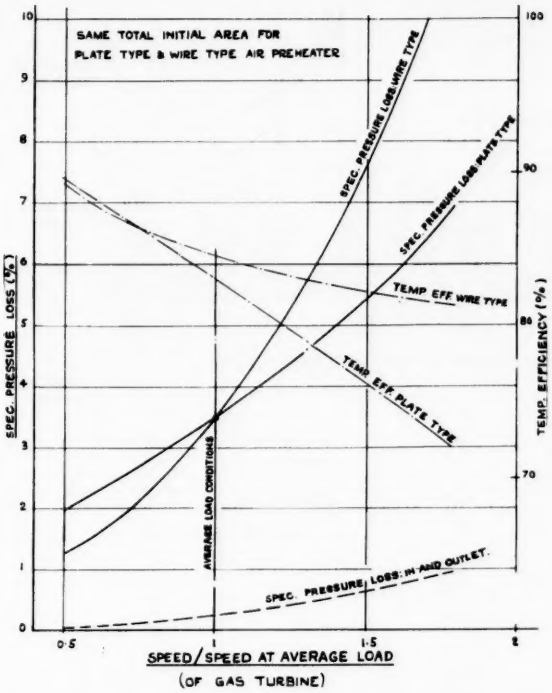
SAME TOTAL INITIAL AREA FOR
PLATE TYPE & WIRE TYPE AIR PREHEATER
SPEC. PRESSURE LOSS WIRE TYPE
SPEC. PRESSURE LOSS PLATE TYPE
TEMP. EFF. WIRE TYPE
TEMP. EFF. PLATE TYPE
SPEC. PRESSURE LOSS IN AND OUTLET
AVERAGE LOAD CONDITIONS
SPEC. PRESSURE LOSS (%)
TEMP. EFFICIENCY (%)
SPEED/SPEED AT AVERAGE LOAD
(OF GAS TURBINE)

Fig. 21 Change of specific pressure loss and temperature efficiency of air preheater in terms of speed

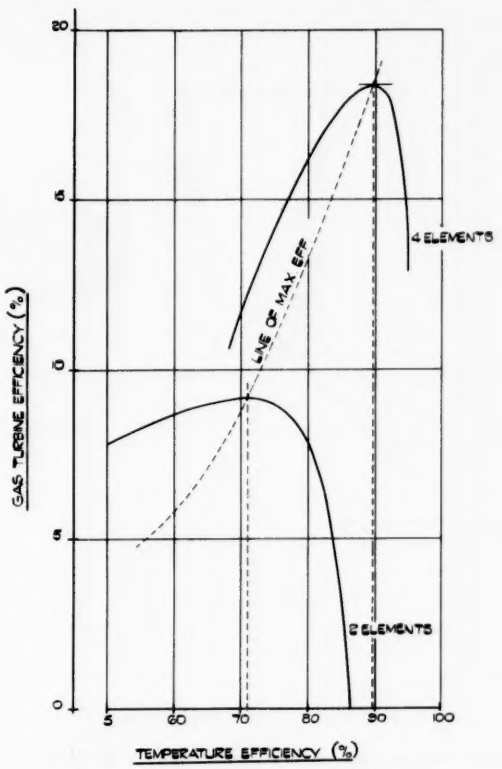

Fig. 22 Maximum efficiency for two and four elements

plate, the rotor plate, both with the mating faces for the radial and circumferential seals, and the center part of the rotor casing with the matrix. The whole rotor has to be subdivided by ribs into compartments whereby their optimum number depends on the thickness as well as the number of ribs continuously covered by one of the circumferential seals, and the number of sides.

The use of ceramic materials will restrict the size and shape of these parts of the heat exchanger and consequently leads to what may be called a composite regenerative heat exchanger, consisting of a number of similar elements as described, suitably arranged either frontally or polygonally in a common stator casing. If, for instance, the frontal arrangement of the elements is chosen, good use is made of the available space as can be seen from Fig. 20.

The extent of frontal matrix area accommodated in this space is, of course, one criterion of a successful design. How far the kind of matrix affects the possibilities in this respect is shown in Fig. 21, where the effect of matrix choice on part-load behavior of the air preheater is also illustrated. It must, however, be kept in mind that at layout conditions, which usually mean average-load conditions, a correlation is possible between temperature gain and pressure loss to give maximum efficiency of the gas-turbine unit as a function of the number of elements, Fig. 22. A large number of alternative sealing designs can be considered with the overriding consideration that where ceramic materials are being employed the utmost simplicity is an important design requirement. Apart from plain, sliding seals, spring-type rings can be employed for either axial or radial sealing, and suitable flexible ceramic materials have been devised lately for such rings. The mass-flow loss due to clearance between the mating faces of the seals depends on the effective gap which in turn is governed not only by the finish of these faces but also the surface configuration as influenced by the dimensions, the temperature gradients, and last but not least by the coefficient of thermal expansion. With the pressure differences encountered in gas-turbine units the flow in these gaps will be supersonic in the region of larger loads, and subsonic in the region of lower loads, with a transition zone in between, Fig. 23.

Weight is governed by the number of elements used as is the weight of the fuel and fuel tank necessary for a certain distance to be covered by the car. Adding these together leads to an optimum number of elements giving a minimum over-all weight governed, as will be seen from Fig. 24, by the type of matrix as well as its characteristic properties.

Taking all these thermodynamic considerations into account, a certain amount of standardization may be possible with a composite air preheater as previously described. The number of elements employed (as the actual standardized portion of the heat exchanger) allows adaptation to different mass flows and temperature changes whereas a small number of rotor parts of the elements, differing in the depth of the matrix only, can cater for any reasonable pressure-drop requirements. The simplicity of the different parts of the element facilitates mass production. Full freedom can be given to the design of the actual stator casing, which if required can be split up, enabling each element to be contained in its own housing and thereby reducing weight and thermal distortion. In this case pressed sheets can be used for the stator casing of the air preheater.

In a design study of a 120-h-p gas-turbine unit, Fig. 25, suitable for installation in the rear (because of the large volume of exhaust gases and the sensitivity to l-p pressure losses in the exhaust duct) of a low-average-load car, such a regenerative air preheater composed of four frontally arranged ceramic elements with an annular-disk rotor has been chosen in connection with an h-p power turbine. The four rotors having an outside gear ring are driven

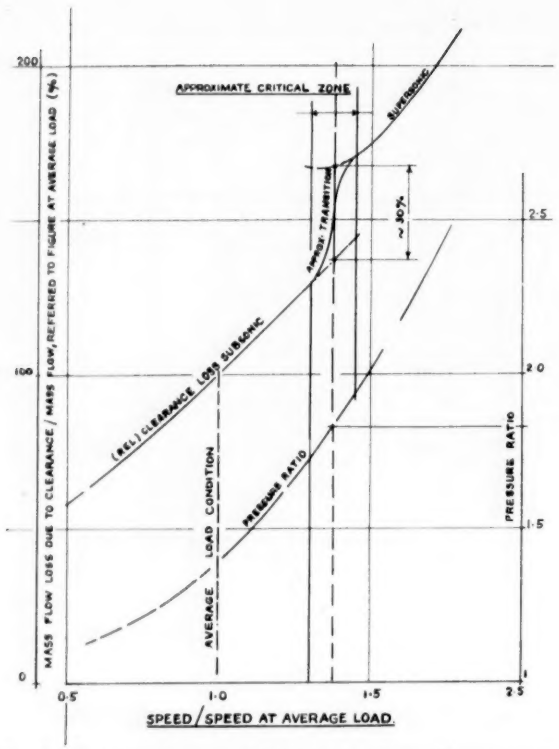
APPROXIMATE CRITICAL ZONE
SUPERSONIC
APPROX TRANSITION
30%
(REL) CLEARANCE LOSS SUBSONIC
PRESSURE RATIO
AVERAGE LOAD CONDITION
MASS FLOW LOSS DUE TO CLEARANCE / MASS FLOW, REFERRED TO FIGURE AT AVERAGE LOAD (%)
PRESSURE RATIO
SPEED / SPEED AT AVERAGE LOAD

Fig. 23 Part load performance of plate type air preheater (clearance loss)

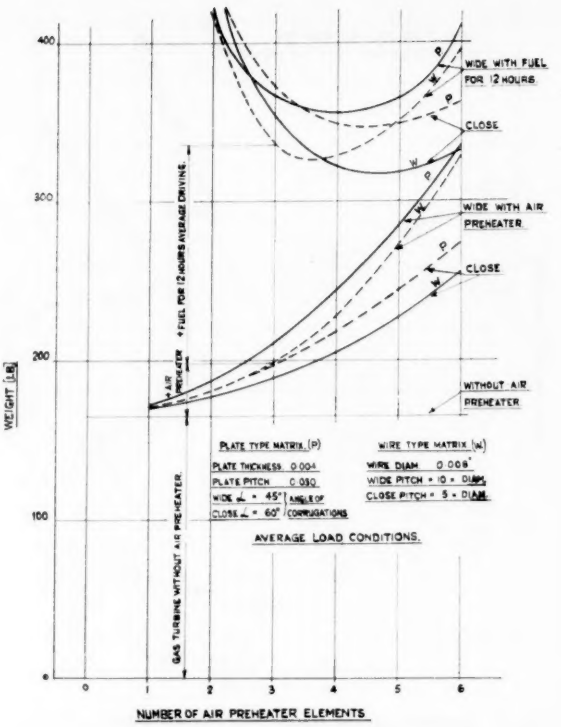
WIDE WITH FUEL FOR 12 HOURS
CLOSE
WIDE WITH AIR PREHEATER
CLOSE
WITHOUT AIR PREHEATER
WEIGHT (LB)
+ FUEL FOR 12 HOURS AVERAGE DRIVING
+ AIR PREHEATER
GAS TURBINE WITHOUT AIR PREHEATER
PLATE TYPE MATRIX (P)
PLATE THICKNESS 0.004
PLATE PITCH 0.050
WIDE ∠ = 45° ANGLE OF CORRUGATIONS
CLOSE ∠ = 60°
WIRE TYPE MATRIX (W)
WIRE DIAM 0.008"
WIDE PITCH = 10 × DIAM.
CLOSE PITCH = 5 × DIAM.
AVERAGE LOAD CONDITIONS.
NUMBER OF AIR PREHEATER ELEMENTS

Fig. 24 Influence of air preheater

by a common central-gear arrangement and actuated by means of a hydraulic motor coupled to a hydraulic generator which in turn is driven by the l-p turbine. The turbine-exhaust gases are led to the gas sides of the elements through an inner, annular duct of the common stator casing. In a similar way the air sides are connected by an outer duct in such a way that a single annular combustion chamber can be fitted with very low transition losses. Vaporization of fuel by means of the exhaust gases and distribution over a flame trap of the fuel vapor mixed with a small amount of preheated air, permits highly efficient combustion at all loads with a nonluminous flame, and allows low mixing-pressure loss, despite the small space available.

A two-stage tangential-flow turbine has been chosen for the h-p turbine. Because of a small mean circumferential velocity and a large-mean-diameter-to-height ratio of the blades, these parts of the turbine can be integrally cast with the blade-carrier ring which is supported in a disk common to both stages. This layout leads to a relatively low speed and therefore allows the use of a simple conventional reduction gear. Only one forward and one reverse-gear step is used because of the good positive-torque behavior of such a gas-turbine unit.

The single-stage centrifugal compressor is driven together with the auxiliaries near the inlet of this compressor by the single-stage centripetal turbine. The air is filtered, before entering the compressor, in a battery of straight-through vortex tubes housed in two compartments on each side of the gas-turbine unit. The dust thus collected is continuously removed by a suction blower.

A practical optimization of the design requires a compromise between practical considerations and theoretical requirements such as the different thermodynamical optimum conditions [23]:

1 The pressure change in the compressor and turbine and the temperature change in the air and gas sides of the preheater.

2 The sizes of these two sides as governed mainly by the pressure change in the compressor.

3 The temperature and pressure change in the preheater for a given over-all size of preheater.

4 The weight of the whole gas-turbine unit including fuel and fuel tank as governed by factors 1 to 3 and the miles per gallon of the car propelled by it.

These factors indicate that the performance [24] of such a car, Fig. 26, compares favorably with that obtainable when it is propelled by a conventional petrol engine even if allowance is made for the further improvements in specific fuel consumption which may accrue from even larger compression ratios than are now in common use. Due to the inclusion of an air preheater the optimum car speed at which the best fuel consumption can be achieved—say at zero gradient—is considerably reduced. A very good performance can be obtained as practically no detrimental effect of turbine efficiency is experienced due to over or underspeeding and favorable thermodynamic conditions prevail especially in the range of low loads.

Summarizing the analysis up to this point it would appear that a number of important problems pertinent to the successful design of a gas turbine for vehicle propulsion can be solved (especially where a good performance at low average loads is demanded) if the h-p instead of the l-p part of the turbine is used for power. The use of ceramic materials in the construction of regenerative air preheaters will not only eliminate any difficulties arising from unduly high temperatures but will also reduce weight.

There are still, however, a number of outstanding problems. Apart from the fact that, for different vehicle requirements, different turbine arrangements have to be chosen—a disadvantage from a manufacturing point of view—there remain the design drawbacks resulting from splitting the turbine, the lack of a nega-

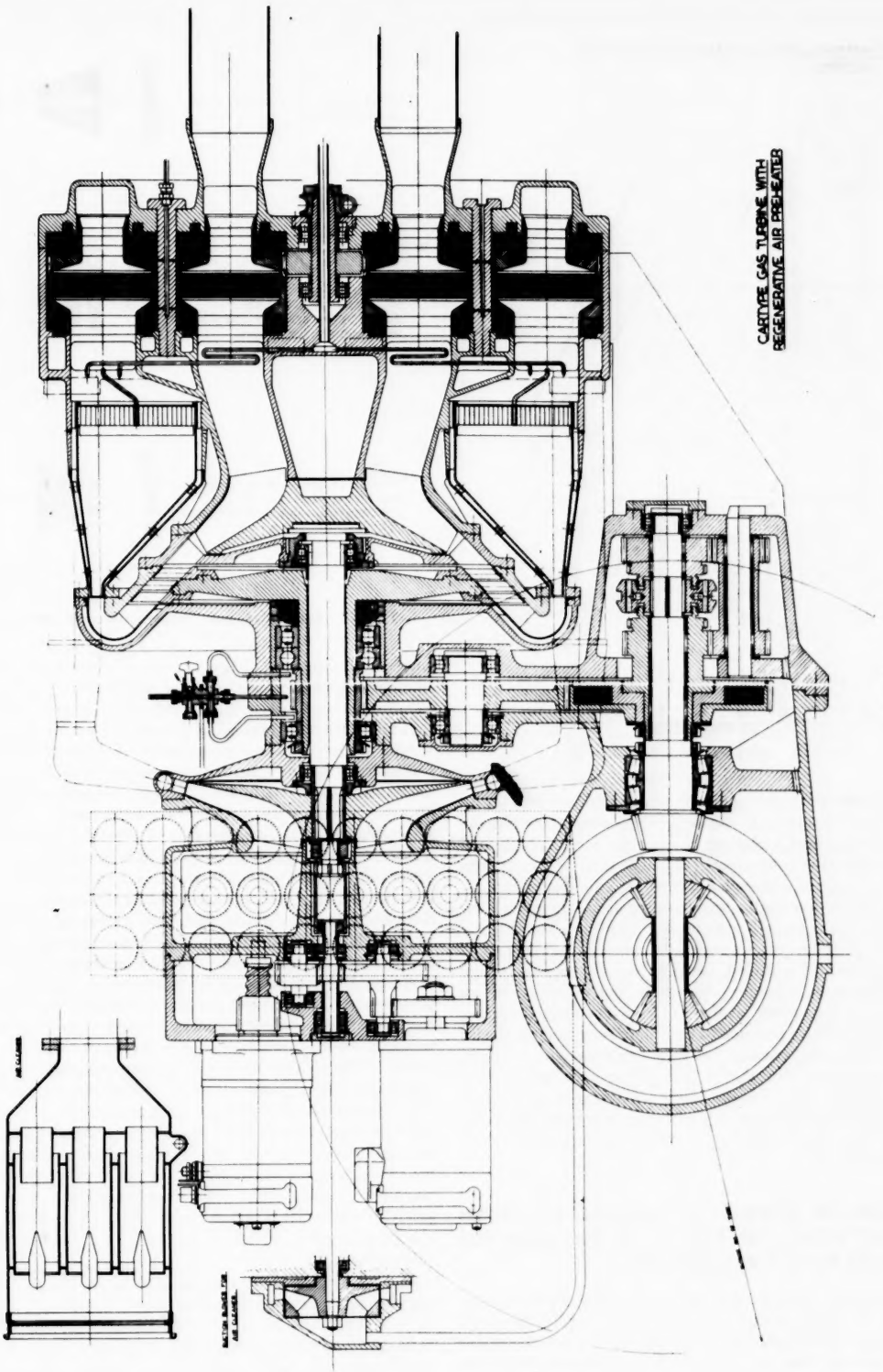

Fig. 25

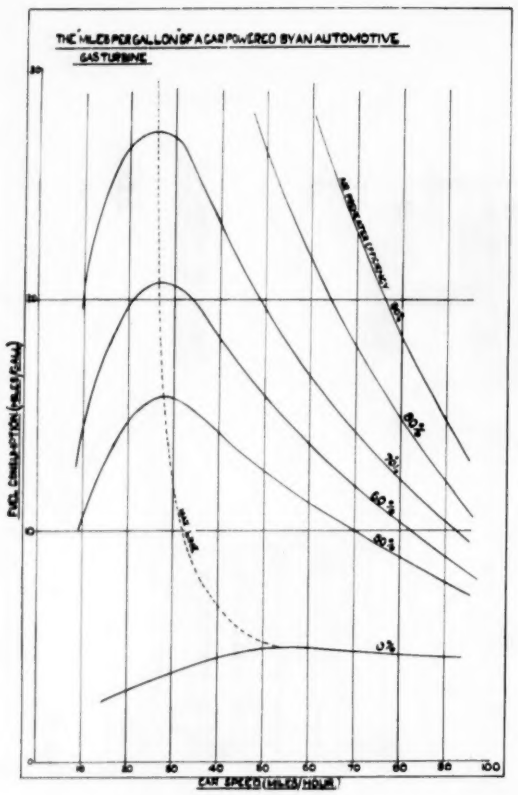

Fig. 26

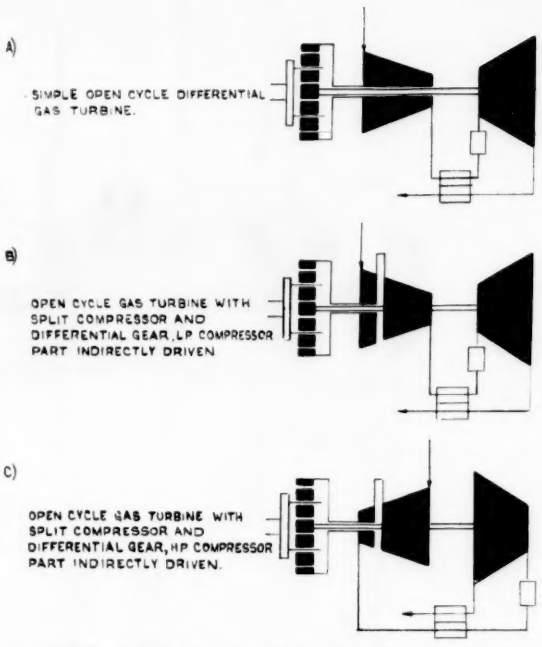
A)
SIMPLE OPEN CYCLE DIFFERENTIAL GAS TURBINE.
B)
OPEN CYCLE GAS TURBINE WITH SPLIT COMPRESSOR AND DIFFERENTIAL GEAR, LP COMPRESSOR PART INDIRECTLY DRIVEN
C)
OPEN CYCLE GAS TURBINE WITH SPLIT COMPRESSOR AND DIFFERENTIAL GEAR, HP COMPRESSOR PART INDIRECTLY DRIVEN.

Fig. 27 Automotive gas turbine with split compressor

tive torque, and the partly indirect control with its effect on response to load changes [11]. Again, in spite of its attractiveness, the regenerative heat exchanger is certainly more complicated than its recuperative counterpart [12]. The positive-torque ratio which can be realized, although sufficient for a number of applications may still be too small where heavy vehicles are involved or where such vehicles have to work under difficult conditions [12].

Recovery of power, otherwise wasted when the power shaft of the gas-turbine unit is stalled, seems to show a way for further improvement in its behavior when propelling vehicles. Where the h-p part of the turbine is affected by such stalling, the power recovered is indirectly supplied to the compressor through the l-p turbine. The question arises: "Is there any possibility of affecting the compressor directly by this power recovery so that splitting of the turbine is unnecessary?" The answer to this question leads to the gas-turbine unit with a split compressor, and a differential gear between the two compressor parts and the power-transmitting shaft.

Gas-Turbine Unit With a Divided Compressor and a Differential Gear Between the Shafts of the Two Compressor Parts and the Power-Transmitting Shaft

The problem is to design a simple open-cycle gas-turbine unit, Fig. 27(*a*), consisting of one compressor and one turbine with a device which allows preservation of its power when the power shaft is stalled so that the positive torque applied to this shaft can be increased. This can actually be achieved by supercharging such a gas-turbine unit to an extent depending on its working conditions, and hence making full use of its adaptability to large surplus power. What is needed then, is to divide the compressor into two parts (or to put it differently to add a second compressor) and to introduce a differential gear in such a way that under normal working conditions far more compressor work is done by the compressor part directly linked with the undivided turbine than by the other compressor part. Two arrangements are possible as either the l-p or the h-p compressor part can be directly driven by the turbine, Figs. 27(*b* and *c*). If in such a gas-turbine unit, the power shaft is stalled (the best way of visualizing the effect is by assuming standstill) some of the power which under normal working conditions is transmitted by the shaft to the wheels of the vehicle is diverted to the compressor part indirectly connected to the turbine, thus increasing its compression work. The extent to which power is transferred in such a way depends on the stalling condition of the power-transmitting shaft; at standstill the whole power is transmitted to the additional compressor part. Due to the increase in compression work of both compressor parts, aerodynamically coupled in series, pressure and temperature of the working gas at the inlet of the turbine will be raised. Thus the torque on the power-transmitting shaft will increase continuously until either the vehicle requirements are fulfilled or the limits of such supercharging are reached. The working conditions of the turbine as far as the difference in its actual and optimal speed are concerned will be altered during this process of stalling and will have an additional effect on the torque produced by the turbine. In this way a positive torque can be achieved which will be sufficient for all vehicle requirements, and this torque can be adjusted in a simple way to such needs by the ratio of the differential gear.

Fig. 28 illustrates how the gear ratio affects the maximum positive torque (complete stalling) at a constant over-all pressure ratio of the two compressor parts together. The higher the gear ratio the larger this torque, with a ceiling value of 4.60 at an infinite gear ratio. In this illustration a comparison has also been made between the differential gas turbine having only one compressor and one turbine [25], and the gas turbine with a split compressor. Although the former is, mathematically speaking, a

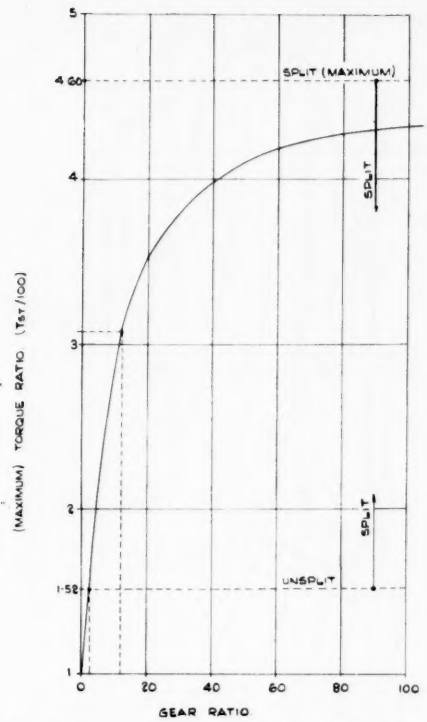

Fig. 28 Maximum torque ratio (stalling at layout condition)

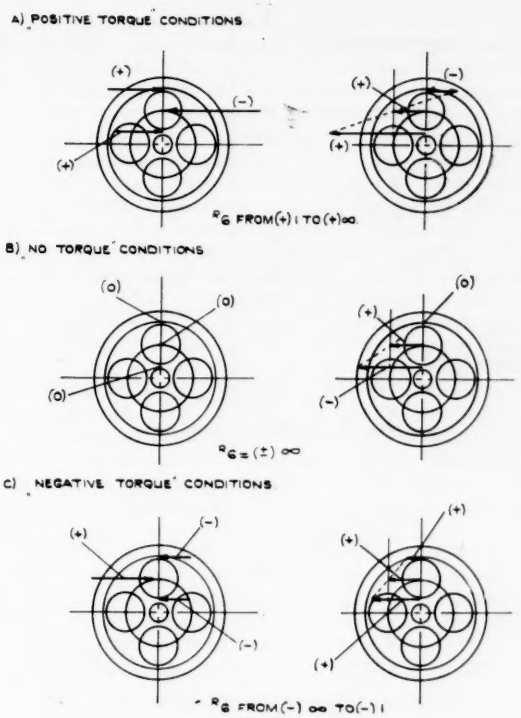

Fig. 29 The different torque conditions

border case of the latter, there is no resemblance whatsoever in the basic principle of how these two gas-turbine units work with the exception of the use of a differential gear. A much larger positive torque can be obtained if the capacity of the two compressors is fully exploited. Very large positive-torque ratios can indeed be obtained with an increase in this temperature under such conditions.

A further advantage of this design is that existing gas-turbine units without a split compressor can be adapted to the requirements of vehicle propulsion in a relatively simple way without the need of splitting the turbine. This is especially important where, for instance, a centripetal turbine [26] has been chosen not only for its simplicity and favorable stressing under high-temperature conditions but also because of the conditions as far as matching is concerned, due to the similarity of its characteristics with those of the centrifugal compressor [27].

All turbomachines are mechanically linked with the power-transmitting shaft which means that they can be directly controlled without additional means. A quick response to load changes is therefore secured.

A further advantage of such gas-turbine units is the fact that they can produce a sufficiently large negative torque without the introduction of another additional device.

The maximum negative torque which again depends on the gear ratio will be about two thirds of the maximum positive torque. If means are introduced for blocking either the movement of the outer or the inner gear train, this negative-torque ratio can be increased considerably.

The behavior of the gas-turbine unit from a thermodynamic point of view is closely connected with:

(a) The requirements of the gear (that is, the law linking forces and velocities applied to the different gear trains). Three distinct conditions are of interest: The "positive-torque" conditions, Fig. 29(a); the "no-torque" condition, Fig. 29(b); and the "negative-torque" condition, Fig. 29(c).

(b) The requirements of the turbine (that is, the law linking mass flow, pressure, and temperature).

If the change in maximum cycle temperature, say, at constant maximum pressure, and therefore the change of power output and heat input with load are studied, it is useful to introduce the ratio of the speeds of the outer and inner gear train as the variable. This speed ratio is linked with the speed of the output shaft in a rather complicated way, Fig. 30. How much the gear ratio affects, for instance, the maximum cycle temperature can be seen from Fig. 31. The turbine-inlet temperature of the differential gas turbine with an unsplit compressor decreases with the speed ratio, whereas the temperature of the gas turbine with a split compressor is increased first, to reach a maximum value, and is then decreased below its initial value. Location and value of the maximum turbine-inlet temperature again is a function of the gear ratio. The mass flow is slightly decreased until it reaches a minimum value and then increases toward the maximum torque conditions. The power output, arising mainly from the turbine-inlet temperature, is increased to reach a maximum value occurring at a certain speed ratio and is then reduced if this ratio is further decreased. Fig. 32 gives an idea of this favorable change of output with speed ratio achieved by splitting the compressor. With an unsplit compressor, the output is reduced continuously with the speed ratio. The heat input changes in a similar way to the power output. Again a maximum value is obtained, Fig. 33.

The quotient of power output and heat input is the efficiency. This important property is favorable too, showing, for instance, with high waste-heat recovery, a minimum value at a certain speed ratio. Over a large part of the load range, the change in specific fuel consumption is relatively small.

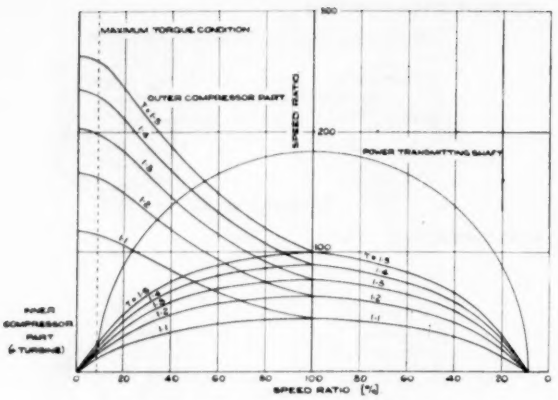

Fig. 30 The different speed ratios

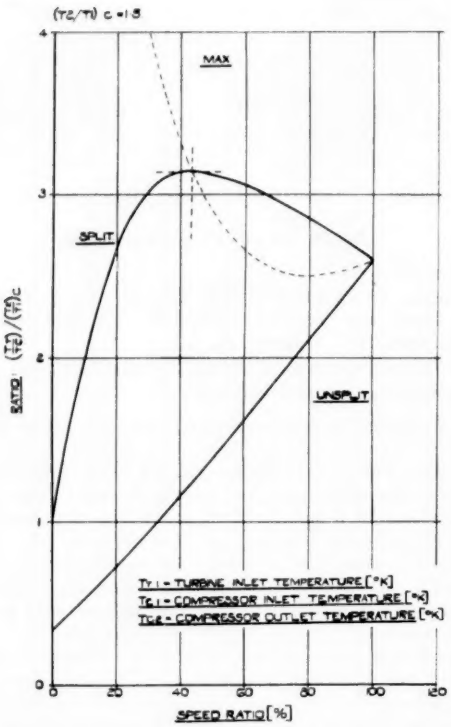

Fig. 31 Initial temperature ratio. Gear ratio, split: 11.93; unsplit: 2.60.

One of the main difficulties when designing a gas-turbine unit with a split compressor concerns the two compressor parts. Apart from its effect on the mechanical design of the gas-turbine unit, the decision, which of the two-part compressors should be indirectly and which directly linked with the turbine, affects the working conditions of the compressors. These conditions govern those compressor characteristics, the realization of which should be aimed at so as to achieve a good over-all performance of the gas-turbine unit concerned. The use of centrifugal compressors with a vaneless diffuser and a centripetal turbine with a vaneless nozzle is interesting in this respect.

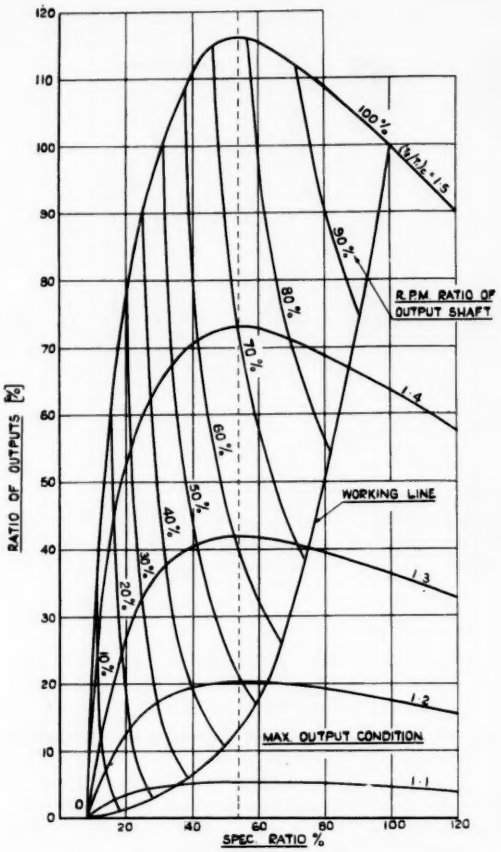

Fig. 32 Power output

There are many existing gas-turbine units where splitting the turbine is considered an undesirable way of adjustment to vehicle-propulsion requirements. This applies, for instance, to all those units especially suitable for small mass flows where a one or two-stage centrifugal compressor is driven by a single-stage centripetal turbine. This type of turbine cannot be split easily; on the other hand it is advantageous in many ways when connected to a centrifugal compressor [28].

By realizing a gas-turbine unit with a split compressor, all the important problems connected with the requirements of vehicle propulsion would appear to be solved satisfactorily. This gas-turbine unit, truly suitable for this purpose, can be designed in such a way that different requirements can be met mainly by the choice of its gear ratio and the adaptation of its turbomachines to give the best possible performance.

Recuperator Composed of Standardized, Mass-Produced Elements

Whatever mode of heat transfer and design of heat exchanger is chosen, the air preheater will be an expensive component of the gas-turbine unit, mainly because of material costs. The only way of keeping down the price of such a heat exchanger is by a design which allows mass production. It should be adaptable to different component arrangements of the gas-turbine unit as well as to different working conditions with regard to mass flow, temperature, and pressure changes.

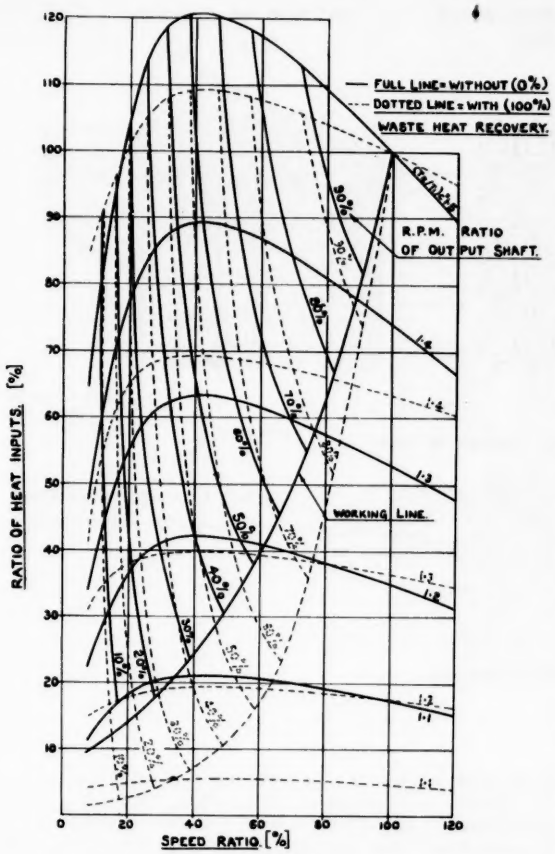
FULL LINE = WITHOUT (0%)
DOTTED LINE = WITH (100%)
WASTE HEAT RECOVERY.
R.P.M. RATIO OF OUTPUT SHAFT.
WORKING LINE.
RATIO OF HEAT INPUTS. [%]
SPEED RATIO [%]

Fig. 33 Heat Input

An appropriate solution to this problem of adaptability seems to be a recuperative air preheater composed of a certain number of similar, mass-produced elements. Again, different working conditions lead to different element numbers. Greater freedom with regard to arrangement than with the regenerative elements (mainly because of their drive) is, however, obtained when recuperative elements are fitted into the general design of a gas-turbine unit in such a way that parasitic-pressure losses are kept small despite compactness.

Two basic types of matrix have to be considered in this respect when a recuperative heat exchanger is designed; one built up by tubes, the other by plates. A two-pass air preheater, following the annular outlet of the turbine, with an annular arrangement of its tube nests, fits nicely into most designs of gas-turbine units. The well-diffused turbine-exhaust gas enters the tube nests centrally and circumflows the tubes without change of direction. On the other hand the air inside the tubes changes direction (180-deg angle) in such a way that it enters and leaves on the same side of the tube nests. An annular combustion chamber, cooled by the air before entering the tubes, can therefore be fitted between air-preheater outlet and turbine inlet.

The diameters of plain, thin-walled tubes necessary to keep the bulk of the preheater within limits are so small that not only the cost of the tubes themselves, but also the cost of fixing them reliably in the tube plate, would be prohibitive. However, the situation as far as the diameter is concerned, can be considerably improved if a convoluted tube is used instead of a plain one, Fig. 34. Larger diameters can then be employed, thus facilitating fixing, Fig. 34(*a*). Again it is useful to have the gas outside and the air inside the tubes. The use of spacers which can be made from any suitable light-weight materials, Fig. 34(*b*), not only improves the gas flow but also prevents mixing of the gas and hence increases heat transfer considerably. If such spacers (which can have different shapes) are used, a certain amount of self-cleaning of the gas can be achieved because of the centrifugal forces acting on the bends around the tubes on the contaminating particles. For the same reason, heat transfer is improved as the cold gas is continuously removed from the tube surface and replaced by the hot, Fig. 34(*c*). Heat transfer and flow resistance on the tube inside depend very much on both the shape and size of the convolutes as well as the air velocity. Conditions in this respect can be improved in some cases by using an insert for the tubes, thus forcing the air toward the convolutes. In addition a helical movement of the air inside the tubes can improve the relation between heat transfer and flow resistance. A matrix built up by such convoluted tubes has the advantage of a good adjustability to the effect of thermal expansion, a property especially important in the case of a cross-flow heat exchanger. On the other hand, the costs of such tubes, especially where large gages are asked for, are again too high for most practical applications.

The matrix consisting of convoluted tubes leads to the plate-type matrix. Elements based on this kind of matrix seem to have the greatest chance of providing a good solution to the air-preheater problem in connection with automotive gas-turbine units.

Only four different parts, simple in their design, are needed, Fig. 35, to make up a plate-type matrix:

1 The backing plates arranged parallel to each other,
2 The spacer bars, following the outer contour of the backing plates thus forming flat channels with two openings,
3 The rectangular center (main) corrugation,
4 The triangular inlet and outlet (additional) corrugations, which subdivide the channel into a large number of open ducts.

Heat transfer as well as flow resistance can be increased if the corrugations are interrupted by slits and if, in addition, sections between consecutive slits are deformed in such a way that staggered fins are formed.

All these parts can be made from sheet material, the wall thickness of which can be optimized from a cost point of view. The kind of material to be used as well as other factors such as fuel costs, maintenance costs, and serviceable life (effect of scaling) affect such optimum considerations.

One backing plate, two spacer bars, one inlet, one center, and one outlet corrugation form what may be called a cell as the basic assembly of the matrix. A matrix block consists of about 100 to 200 cells their number being limited mainly by production considerations as well as considerations concerning the effect of thermal expansion. All the parts forming such a block are joined together by brazing; the brazing material is applied by different methods to the two surfaces of the backing plate only.

When choosing the dimensions of the matrix block, which govern the equivalent diameter, it has to be remembered that the gap between the backing plates and the length of the corrugations (together with their wall thickness) affect the flow area of the ducts formed by these parts. Hence small equivalent diameters lead to small areas. A periodically and automatically working cleaning device is therefore essential to prevent clogging of these areas of flow. Means for its actuation can be included in the design of the matrix block, Fig. 36. The spacer bars on the gas side have slots penetrating about half their width which join similar slots in the center corrugation. The spacer bars on the air side have no such slots. Hence, after the matrix block has been brazed, approximately half-circular recesses on each side of this block can be milled out in such a way that the slots in the spacer bars and hence those in the center corrugations are con-

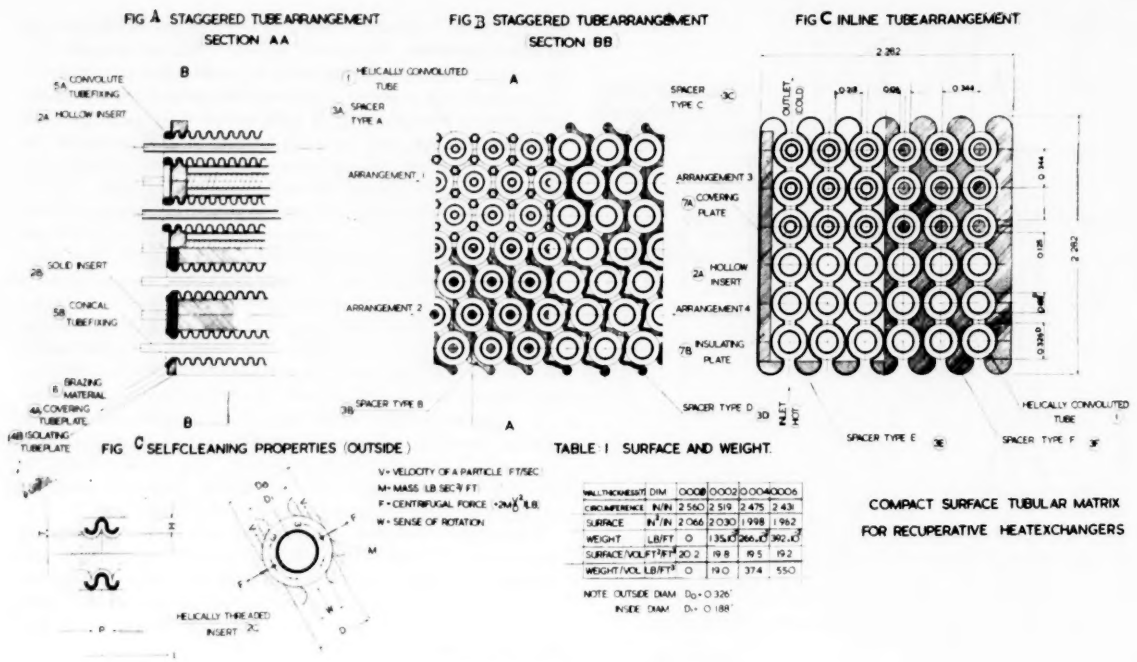

WALLTHICKNESS	DIM	0008	0002	0.0040006	
CIRCUMFERENCE	IN/IN	2 560	2 519	2 475	2 431
SURFACE	IN²/IN	2 066	2 030	1 998	1 962
WEIGHT	LB/FT	0	135.10⁻³	266.10⁻³	392.10⁻³
SURFACE/VOLFT²/FT³		20 2	19 8	19 5	19 2
WEIGHT/VOL	LB/FT³	0	19 0	37 4	55 0

NOTE OUTSIDE DIAM $D_0 = 0.326''$
INSIDE DIAM $D_i = 0.188''$

Fig. 34 Convoluted tubular matrix

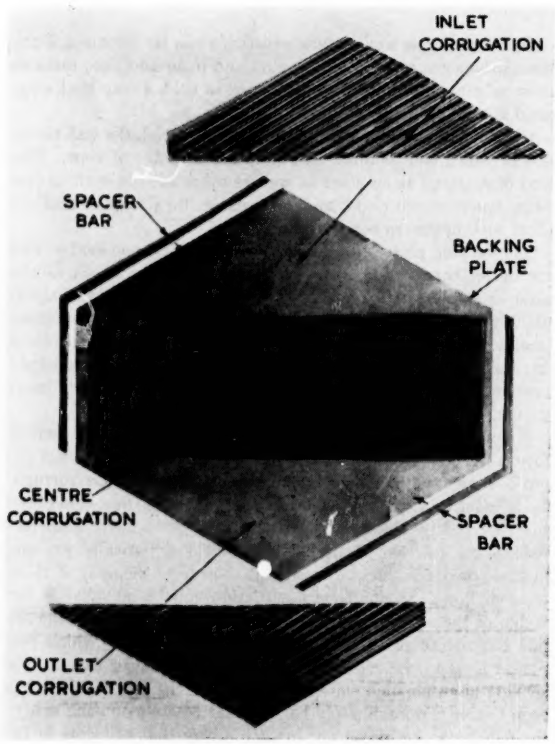

Fig. 35 Parts of a plate type matrix

nected with the outside. By welding a slit tube of proper OD into these recesses, a cleaning fluid such as, for instance, compressed air with or without a suitable detergent, can be led from these tubes into the center corrugation of the gas side. This fluid will expand in both directions through the ducts of the corrugations and finally escape together with the contamination removed, through their inlet and outlet openings in very much the same way as in a regenerator.

The backing plate and hence the spacer bars can, of course, have different shapes. A circular shape was chosen for a matrix block, Fig. 37, used for testing the effect of thermal shocks on the tightness of the matrix.

Two or more matrix blocks are joined together to form an element by a common inlet and outlet header for the air, Fig. 38. The inlet and outlet ducts for the nonpressurized gas can be simply formed by the casings of the composite heat exchanger, made from sheet material. Simple light-weight headers, as distributing ducts for the high-pressure air, designed to suit the requirements of different gas-turbine units, are as important as the matrix, because of their effect on exchangeability and interchangeability. Simplicity, flexibility, and gas-tightness of the joints have to be matched with the need for a low parasitic-pressure loss. For this reason simple tubular shapes are preferred because of strength-to-weight as well as manufacturing considerations. Several designs of such headers are possible; one is shown in Fig. 39.

The choice of shape of the backing plates can be affected by optimum considerations [29], which in turn depend on the average load of the gas-turbine unit concerned. A "symmetrical" design has been obtained with a hexagonally-shaped backing plate which is especially suitable for low average loads. Spacer bars and corrugations are the same on the air and the gas sides, that is, one and the same cell can be used for both sides, thus greatly facilitating mass production.

If, however, the average load is high the cells on the air and gas

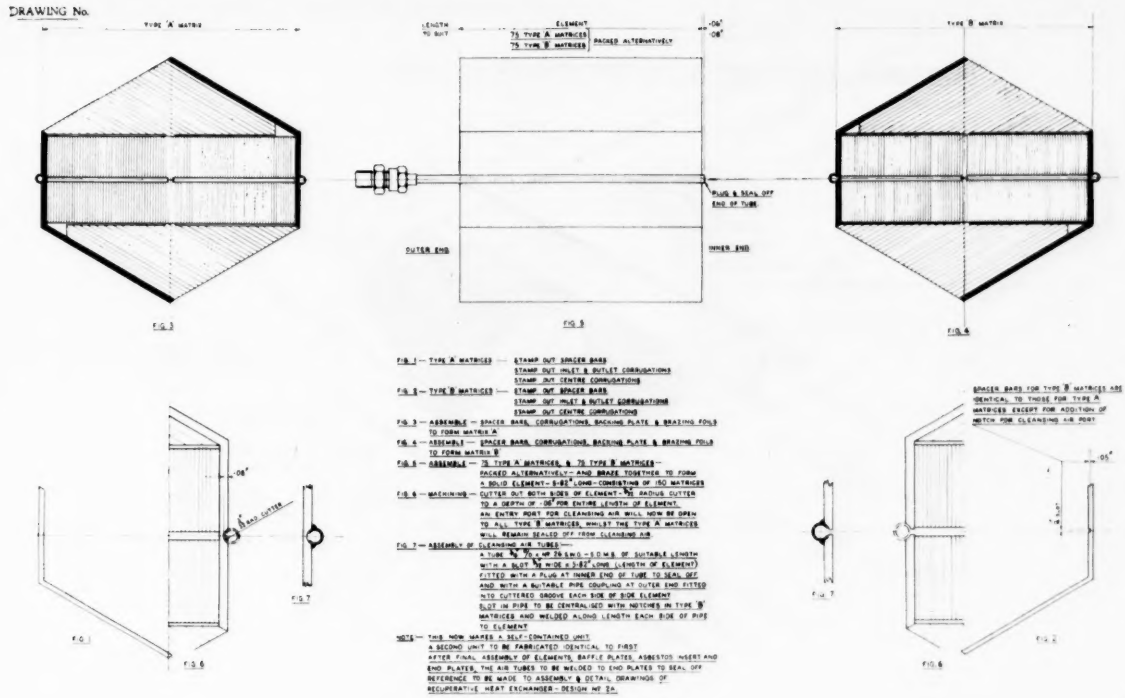
DRAWING No.
TYPE 'A' MATRIX
TYPE 'B' MATRIX
ELEMENT
75 TYPE A MATRICES
75 TYPE B MATRICES
PACKED ALTERNATIVELY
PLUG & SEAL OFF END OF TUBE
OUTER END
INNER END
FIG. 3
FIG. 5
FIG. 4
FIG. 1 — TYPE A MATRICES — STAMP OUT SPACER BARS
STAMP OUT INLET & OUTLET CORRUGATIONS
STAMP OUT CENTRE CORRUGATIONS
FIG. 2 — TYPE B MATRICES — STAMP OUT SPACER BARS
STAMP OUT INLET & OUTLET CORRUGATIONS
STAMP OUT CENTRE CORRUGATIONS
FIG. 3 — ASSEMBLE — SPACER BARS, CORRUGATIONS, BACKING PLATE & BRAZING FOILS TO FORM MATRIX A
FIG. 4 — ASSEMBLE — SPACER BARS, CORRUGATIONS, BACKING PLATE & BRAZING FOILS TO FORM MATRIX B
FIG. 5 — ASSEMBLE — 75 TYPE A MATRICES & 75 TYPE B MATRICES — PACKED ALTERNATIVELY — AND BRAZE TOGETHER TO FORM A SOLID ELEMENT — 5·82" LONG — CONSISTING OF 150 MATRICES
FIG. 6 — MACHINING — CUTTER OUT BOTH SIDES OF ELEMENT — 1/4" RADIUS CUTTER TO A DEPTH OF .08" FOR ENTIRE LENGTH OF ELEMENT. AN ENTRY PORT FOR CLEANSING AIR WILL NOW BE OPEN TO ALL TYPE 'B' MATRICES, WHILST THE TYPE A MATRICES WILL REMAIN SEALED OFF FROM CLEANSING AIR
FIG. 7 — ASSEMBLY OF CLEANSING AIR TUBES — A TUBE 3/8" x 20 s.w.g. x 26 s.w.g. — S.S.W.G. OF SUITABLE LENGTH WITH A SLOT 1/8" WIDE x 3·82" LONG (LENGTH OF ELEMENT) FITTED WITH A PLUG AT INNER END OF TUBE TO SEAL OFF AND WITH A SUITABLE PIPE COUPLING AT OUTER END FITTED INTO CUTTERED GROOVE EACH SIDE OF SIDE ELEMENT SLOT IN PIPE TO BE CENTRAL (IE) WITH NOTCHES IN TYPE 'B' MATRICES AND WELDED ALONG LENGTH EACH SIDE OF PIPE TO ELEMENT
NOTE — THIS NOW MAKES A SELF-CONTAINED UNIT A SECOND UNIT TO BE FABRICATED IDENTICAL TO FIRST AFTER FINAL ASSEMBLY OF ELEMENTS, BAFFLE PLATES, ASBESTOS INSERT AND END PLATES, THE AIR TUBES TO BE WELDED TO END PLATES TO SEAL OFF REFERENCE TO BE MADE TO ASSEMBLY & DETAIL DRAWINGS OF RECUPERATIVE HEAT EXCHANGER — DESIGN NO 24
SPACER BARS FOR TYPE 'B' MATRICES ARE IDENTICAL TO THOSE FOR TYPE A MATRICES EXCEPT FOR ADDITION OF NOTCH FOR CLEANSING AIR PORT
FIG. 1
FIG. 2
FIG. 6
FIG. 7

Fig. 36

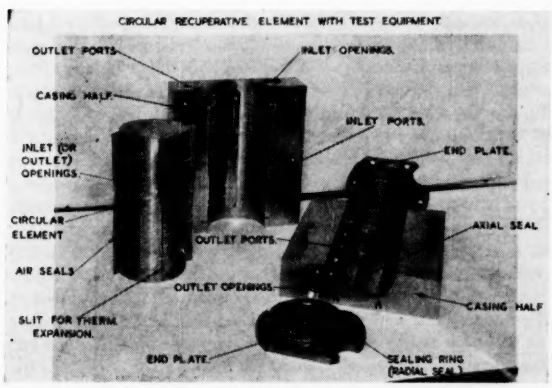

Fig. 37

sides may be different because of optimum considerations concerning the minimum specific fuel consumption of the gas-turbine unit at average-load conditions. The higher the average load the greater difference in dimensions on the two sides for optimum working conditions.

An unsymmetrical rectangular-backing-plate design, Fig. 40, may best serve where large average loads are experienced. All parts on air and gas sides with the exception of the backing plates are different in shape and size.

The parasitic weight of such recuperative elements is greatly reduced, Fig. 41, when compared with regenerative elements. A further reduction can be achieved if the straight spacer bars on the gas side are made hollow instead of solid say by using U-shaped strips, which also add to flexibility. Not only the parasitic weight but also the total weight of the element is affected by the choice of the width, with effect on thermal expansion and contraction and consequent stresses. This weight should be kept within such limits that the element can be readily fitted without unduly increasing the number of ducts to be joined when so doing.

New protective methods for parts of the elements directly exposed to the hot gases will result in a reduction in material costs, improve reliability, will lengthen serviceable life of the air preheater, and therefore remove the last drawback when comparing the recuperative with the future regenerative-type of heat exchanger.

It can be assumed that standardization of the elements will be possible so that they can be used for different designs and different sizes of gas-turbine units. The dimension upon which such standardization should be based is the height of the center corrugation. A study of the requirements with regard to these dimensional changes shows that very few element sizes are necessary to cater for all such requirements.

Conclusions, With a Look Into the Future

Because of the conditions encountered, a road vehicle requires a gas-turbine unit differing from the designs employed, for example, in connection with aircraft propulsion. The disadvantages introduced when splitting the turbine are overcome and the advantages gained are even enhanced, if the compressor is divided instead of the turbine and a differential gear introduced. Without any basic changes in this design such a gas-turbine unit can be adapted to different average-load requirements simply by a change in the ratio of this gear.

Compared with the present-day multicylinder piston engine coupled to the driving wheels through a complicated transmission

HEXAGONAL RECUPERATIVE HEATEXCHANGER ELEMENT

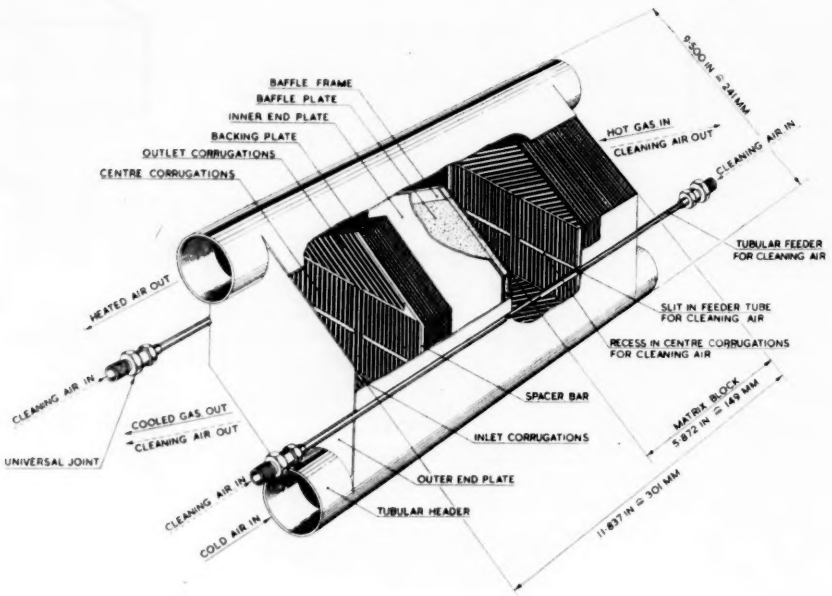

Fig. 38

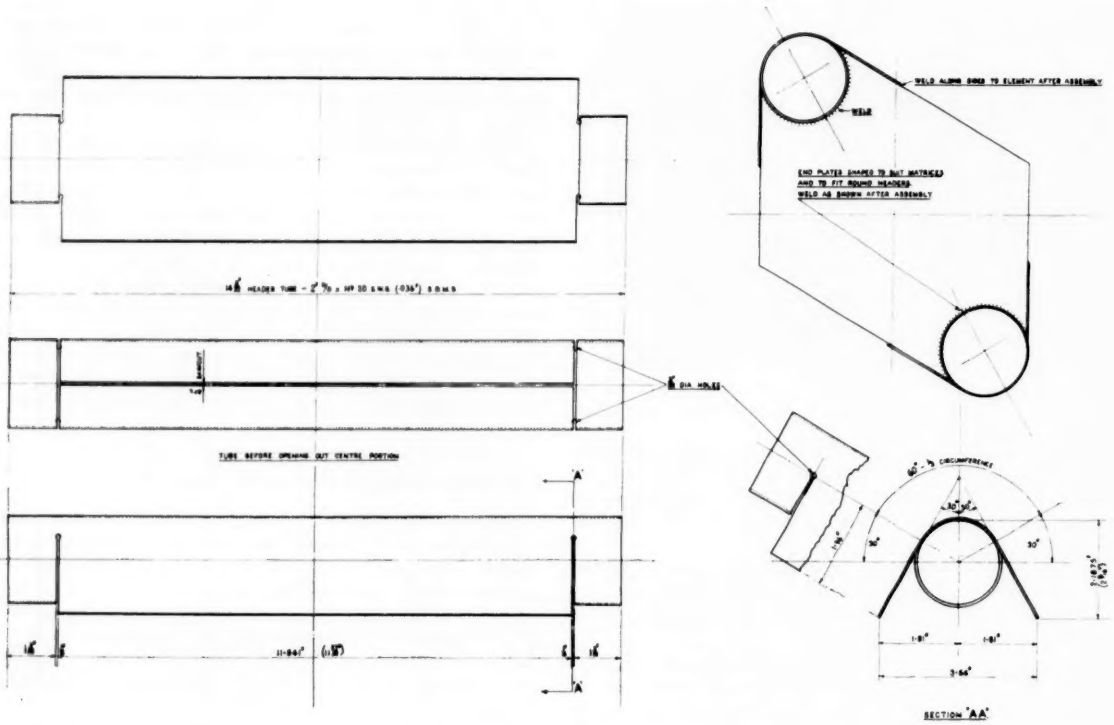
WELD ALONG EDGE TO ELEMENT AFTER ASSEMBLY
WELD
END PLATES SHAPED TO SUIT MATRICES AND TO FIT ROUND HEADERS WELD AS SHOWN AFTER ASSEMBLY
TUBE BEFORE OPENING OUT CENTRE PORTION
SECTION 'AA'

Fig. 39

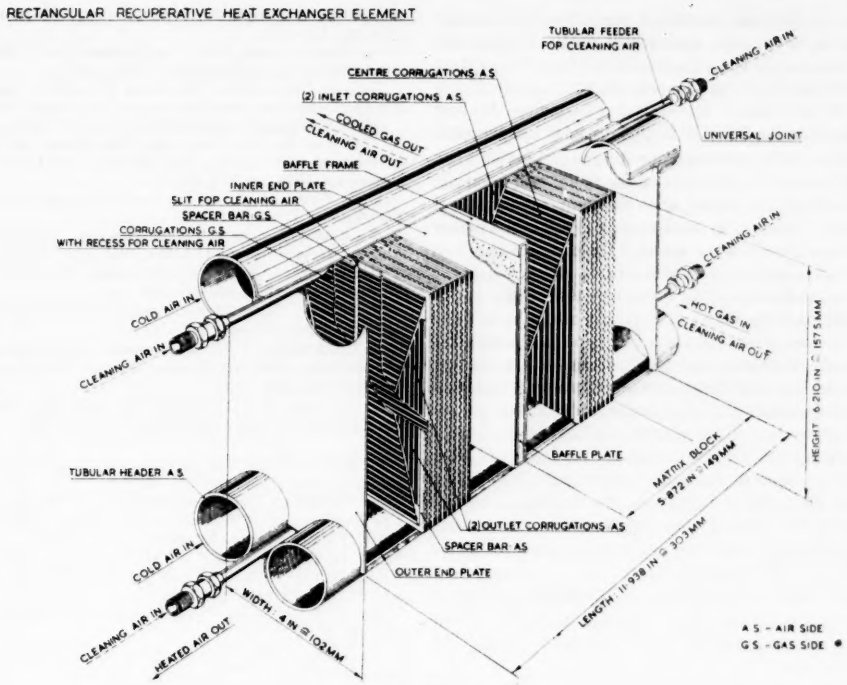
RECTANGULAR RECUPERATIVE HEAT EXCHANGER ELEMENT
TUBULAR FEEDER FOR CLEANING AIR
CLEANING AIR IN
CENTRE CORRUGATIONS A S
(2) INLET CORRUGATIONS A S
COOLED GAS OUT
CLEANING AIR OUT
UNIVERSAL JOINT
BAFFLE FRAME
INNER END PLATE
SLIT FOR CLEANING AIR
SPACER BAR G S
CORRUGATIONS G S WITH RECESS FOR CLEANING AIR
CLEANING AIR IN
COLD AIR IN
HOT GAS IN
CLEANING AIR IN
CLEANING AIR OUT
HEIGHT 6.210 IN = 157.5 MM
BAFFLE PLATE
MATRIX BLOCK 5.872 IN = 149 MM
TUBULAR HEADER A S
(2) OUTLET CORRUGATIONS A S
COLD AIR IN
SPACER BAR A S
OUTER END PLATE
CLEANING AIR IN
WIDTH 4 IN = 102 MM
HEATED AIR OUT
LENGTH 11.938 IN = 303 MM
A S - AIR SIDE
G S - GAS SIDE

Fig. 40

consisting of a fluid drive working in conjunction with a mechanical gear and the final drive, the simplicity of the gas-turbine unit is striking. As a high speed turbomachine such a unit is far more suitable for large "surplus-power" driving conditions than a piston engine where such power can only be obtained by a larger displacement due to either larger or more cylinders and a higher speed. In addition, a gas-turbine unit can show all the advantages gained by introducing a fluid drive for transmitting the power of the piston engine to the wheels of the vehicle without the complications involved. The fact that temperature is added as another variable to pressure and mass flow permits a larger flexibility of the gas-turbine unit to meet vehicle requirements, provided its components are properly chosen, arranged, and designed. The additional advantage of a greatly improved positive and negative-torque behavior at a reduced outlay in fuel under accelerating, idling, and decelerating conditions is obtained without additional means, such as a clutch and/or free wheel to cut out the effect of the lack of mechanical connection between pump and turbine in cases where motor braking is required.

These advantages of a gas-turbine unit should be assessed in the light of increases both in density and speed of traffic which lead to automatic fluid drive as a means of relieving the driver who has to cope with such conditions.

Apart from the effect of splitting the compressor, on fuel consumption during times of acceleration, idling, and deceleration, the realization of a simple and reliable recuperative air preheater makes such a gas turbine unit also competitive with the piston engine as far as average miles per gallon are concerned. The importance of a close study of optimum dimensions of such a heat exchanger because of their effect on the efficiency of the gas-turbine unit and its weight, should be emphasized at this point, together with the need for extreme care in designing ducts between the air preheater and other adjacent components of the gas-turbine unit so as to minimize parasitic-pressure losses. A high effectiveness when converting dynamic into static pressure and

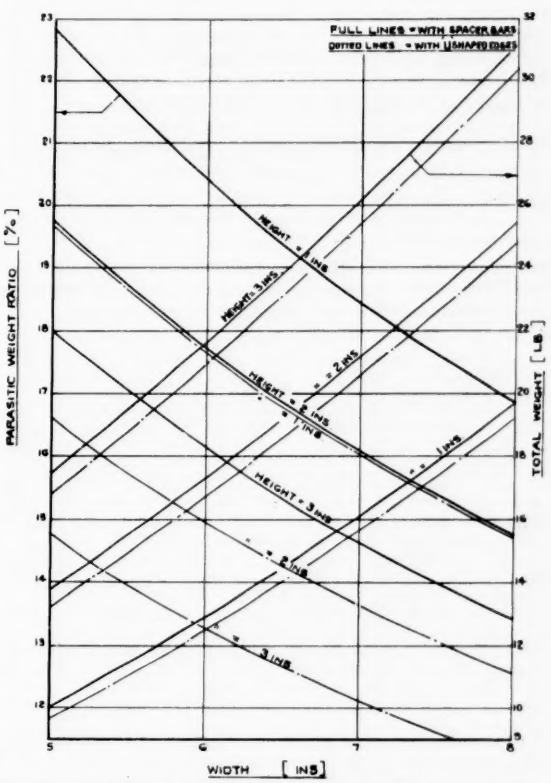

Fig. 41 Correlation of parasitic and actual weight for different widths and heights

vice versa is one of the most important properties to be sought when designing an automotive gas-turbine unit. Further improvements in fuel and air consumption should be attempted by increasing the efficiencies of its components such as the turbomachines, and the last step in the endeavor to realize the best performance should be an increase in turbine-inlet temperature.

The future of any heat engine such as the gas turbine unit can only be properly assessed in the light of the fuel it will be using. Higher octane numbers are needed when the compression ratio of the petrol engine is increased to its economical limit and a higher cetane number is necessary if the speed of the diesel engine is to be raised. Both development trends might be affected if direct cooling instead of indirect cooling is used in the future, and if turbosuperchargers are employed. No requirements have to be met in the gas turbine unit with regard to ignition temperature and ignition speed. Within reason, this heat engine can use any kind of fuel, provided it is free from subtances attacking materials wetted by the combustion gases, especially under high temperatures. In this connection, it should be emphasized that apart from the temperature this attack is governed by a number of other factors and that a proper design can greatly diminish the effect of such an attack [30]. The robustness of the centripetal turbine is one example in this respect. Attempts now being made to "construct" a fuel for the gas turbine, suitable for all working conditions, will no doubt continue.

The place which will eventually be taken by the gas turbine as a prime mover for vehicles can only be guessed in the light of the probable further development of atomic energy to replace our dwindling oil resources.

New types of reactors will be necessary requiring new materials as well as new coolants for the realization of improvements on the thermodynamic side with particular emphasis on the maximum permissible cycle temperature and pressure. The direct use of atomic energy [31] for road vehicle propulsion is hardly feasible for obvious reasons. The storage of atomic energy in an agent releasing this energy in the form of heat under certain conditions without any danger of irradiation in a heat engine especially designed for this purpose is required. The development of such an agent may be one of the greatest challenges to the chemical industry. The ever-increasing requirements for constructed fuels, say for rockets or the like, will undoubtedly speed up such developments.

In connection with the creation of new fuels by use of fission and later fusion, the gas-turbine unit—properly developed for these new kinds of fuel—will play an ever-increasing role.

References

1 *Reyrolle Review*, October–December, 1951, pp. 2–16.

2 Austin Motor Company, Ltd., "Austin 30 B.H.P. Unit for M. O. S.," *The Oil Engine and Gas Turbine*, vol. 21, January, 1954, p. 351.

L. J. Spinks, "More About Rover's T3 Car Engine," *The Oil Engine and Gas Turbine*, vol. 24, November, 1956, pp. 273–274.

J. H. Weaving, "The Austin Vehicle Gas Turbine," *Mechanical Engineering*, vol. 79, 1957, pp. 643–645.

3 R. H. Bright, "The Development of Gas Turbine Power Plants for Traction Purposes in Germany," *Proceedings of The Institution of Mechanical Engineers*, vol. 157, 1947, pp. 375–386.

K. Leist and K. Graf, "Small Gas Turbines Especially for Transport Vehicles," V.D.I., Ber. 7, June, 1956, p. 104.

4 C. Faroux, "The French Gas Turbine for Automobiles," *La View Automobile*, vol. 45, March 10–25, 1950, pp. 49–52. (Abstract in *Engineers Digest*, vol. 11, May, 1950, p. 189.

R. S. Parks, "Gas Turbines for Automotive Use," SAE Paper, March 12, 1951.

5 "Italy's First Gas Turbine Car" (Fiat S. A.), *The Oil Engine and Gas Turbine*, vol. 22, May, 1954, p. 35.

A. Carelli, "Development of Gas Turbines for Road Vehicles," *Mechanical Engineering*, vol. 79, 1957, pp. 645–647.

6 "Gas Turbine Surprise From General Motors," 370-bhp unit-propelling plastic-bodied experimental car, *The Autocar*, January 22, 1954, pp. 121–122.

"An Experimental U. S. Gas Turbine Car," *The Oil Engine and Gas Turbine*, vol. 21, February, 1954, p. 392.

Chrysler Corporation, "Chrylser 120 B.H.P. Gas Turbine Car," *The Oil Engine and Gas Turbine*, vol. 21, April, 1954, p. 474.

"Heat Exchanger Car Turbine," *Autocar*, April, 1954, p. 457.

"U. S. Gas Turbine Coach and High Power Car," General Motors 370-bhp research vehicle, *The Oil Engine and Gas Turbine*, vol. 22, November, 1954, pp. 277–281.

A. H. Beaufrere, "Gas Turbines: Progress Report From Fords," *The Autocar*, December, 1955.

7 E. R. Morgan and V. F. Zackay, "Ductile Iron-Aluminum Alloys," *Metal Progress*, October, 1955, pp. 126–128.

"Economical Alloys for Automobile Turbines," *Materials and Methods*, May, 1956, pp. 207–210.

D. N. Frey, "New Alloys for Automotive Turbines," *Materials and Methods*, June, 1956, pp. 108–111.

8 N. J. Grant, L. W. Kates, and N. E. Hamilton, "Development and Evaluation of Cast Turbine Rotors," *Foundry*, December, 1950, pp. 86–93. pp. 234–239.

C. D. Creme, F. J. Filippi, and R. S. Mueller, "High Temperature Brazing Applications," September-October, 1953. SAE Preprint No. 148.

H. Brown, "How Casting Can Fill Automotive Turbine Needs," *Foundry*, June, 1956, pp. 104–107.

9 "Military Tank Demonstration (C. A. Parsons Tank Unit)," *The Engineer*, vol. 198, October 8, 1954, pp. 486–487.

10 Patent on Braking Device, B.P. 641377, Coupling.

11 D. B. Harper and W. M. Rohsenow, "Effect of Rotary Regenerator Performance on Gas Turbine Plant Performance," TRANS. ASME, vol. 75, 1953, pp. 759–765.

12 F. L. Schwartz, "Gas Turbines for Vehicles," ASME Paper No. 49—F-12.

F. L. Schwartz, "Gas Turbine Progress Report—Automotive," TRANS. ASME, vol. 75, 1953, pp. 153–160.

13 A. T. Bowden and W. Hryniszak, "Rotary Regenerative Air Preheater for Gas Turbines," TRANS. ASME, vol. 75, 1953, pp. 767–777.

14 W. Hryniszak, "Design Problems Associated With Regenerative Preheaters of Gas Turbines" (Entwurfsprobleme von regenerativen Luftvorwärmern für Gasturbinen), *Maschinenbau und Wärmewirtschaft*, Heft 8 and 9, 1953, pp. 213–219, 254.

15 W. M. Brown, "Gas Turbine Propulsion for Ground Vehicles," *SAE Quarterly Transactions*, vol. 5, January, 1951.

16 J. E. Johnson, "Regenerator Heat Exchangers for Gas Turbines," ARC R & M 2630.

P. S. Lamb, "Regenerative Heat Exchanger for Gas Turbine Power Plant," NGTE Report, 1952.

17 C. Malmstron, R. Keen, and L. Green, "Some Mechanical Properties of Graphite at Elevated Temperatures," *Journal of Applied Physics*, vol. 22, May, 1951, pp. 593–600.

A. H. Stuart, "Lubrication at Extreme Temperatures," *Petroleum*, June, 1949, pp. 139–141, p. 158.

G. L. Sumner, "Two Heat Resisting Lubricants," *Westinghouse Engineer*, November, 1947, pp. 188–189.

18 D. B. Harper, "Seal Leakage in the Rotary Regenerator and Its Effect on Rotary Regenerator Design for Gas Turbines," TRANS. ASME, vol. 79, 1957, pp. 233–245.

19 "Improvements in and Relating to Regenerative Heat Exchangers," British Patent No. 760913.

20 R. E. Starke and B. H. Dilks, "New Lithium Ceramics Have High Thermal Shock Resistance, Controlled Thermal Expansion and Chemical Resistance at High Temperatures," *Materials and Methods*, vol. 35, January, 1952, pp. 98–99.

S. G. Kelley, "Technical Ceramics of Wear Resistant and Dimensionally Stable Parts," *Materials and Methods*, vol. 35, March, 1952, pp. 88–91.

W. L. Hawekotte, "Super Refractories for Use in Jet Engines." *Metal Progress*, vol. 64, December, 1953, pp. 67–70.

A. Peckman, "Ceramics for High Temperature Applications," *Aircraft Engineering*, May, 1954, pp. 157–160.

21 W. N. Harrison, D. G. Moor, and J. C. Richmond, "Ceramic Coatings for Steel Under High Temperature Service," ASTM Bulletin No. 145, 1947, pp. 56–62.

"Test on Ceramic Coated Air Heater," *Combustion*, vol. 25, June, 1954, pp. 61–62.

"New Flame Sprayed Ceramics," *Materials and Methods*, September, 1955, p. 98.

Solar Aircraft Company, "The Solaramic Process."

22 "New Ceramic Fiber," *Materials and Methods*, September, 1952, pp. 94–95.

T. D. Callinan, "Four Inorganic Papers," *Materials and Methods*, December, 1955, pp. 98–101.

23 W. Hryniszak, "Development Tendencies in Gas Turbine Design" (Entwicklungstendenzen in Gasturbinenbau), *Maschinenbau und Wärmewirtschaft*, 1955.

W. Hryniszak, "The Present Position of Gas Turbine Development" (Derzeitiger Stand der Gasturbinenentwicklung), *Motor Technische Zeitschrift*, no. 1, January, 1956, pp. 16–23; no. 2, February, 1956, pp. 53–58; no. 3, March, 1956, pp. 82–90.

24 W. A. Turunen, "Gas Turbine Possibilities for Cars Analyzed," *SAE Journal*, vol. 57, July, 1949, pp. 18–23.

P. Kyropoulos, "Review of Research and Development in Automotive Engines," *Applied Mechanics Review*, vol. 7, May, 1954, pp. 185–188.

J. H. Bohin and R. A. Harmon, "Factors Associated With the Use of Gas Turbines for Automotive Applications," Proceedings, 16th American Power Conference, 1954, pp. 323–330.

25 D. W. Hutchinson, "Differential Gas Turbines," SAE Golden Anniversary Transportation Meeting, October 31–November 2, 1955.

26 W. T. Von Der Nuell, "Single-Stage Radial Turbines for Gaseous Substances With High Rotative and Low Specific Speed," TRANS. ASME, vol. 74, 1952, pp. 499–515.

"Prospects of the Inward Flow Radial Gas Turbine," *The Oil Engine and Gas Turbine*, vol. 20, October, 1952, pp. 222–225.

E. N. Petrick and R. D. Smith, "Experimental Cooling of a Radial-Flow Turbine," ASME Paper No. 54—A-245.

R. L. Robinson, "Some Theoretical Aspects of Centripetal Turbines," ASME Paper No. 53—S-245.

27 O. E. Baljé, "A Contribution to the Problem of Designing Radial Turbo-Machines, TRANS. ASME, vol. 74, 1952, pp. 451–472.

L. R. Wosika, "Radial Flow Compressors and Turbines for the Simple Small Gas Turbine, *Aeronautics*, June, 1952, pp. 114–186; also *Mechanical Engineering*, vol. 74, 1952, pp. 408–409.

28 W. Hryniszak, "The Optimized Layout of a Simple Gas Turbine Consisting of a Single Stage Centrifugal Compressor and a Single Stage Centripetal Turbine" (Die optimale Auslegung einfacher Gasturbinen bestehend aus einem einstufigen Zentrifugalverdichter und einer einstufigen Zentripetalturbine), *Motor Technische Zeitschrift*, vol. 17, December, 1956, pp. 429–437.

A. T. Bowden and W. Hryniszak, "Symposium on High Temperature Steels and Alloys for Gas Turbines," in "Materials and Performance," Iron and Steel Special Report Series no. 43, pp. 11–17.

29 W. Hryniszak, "Optimization of Plate-Type Air Preheaters for Automotive Gas Turbines," TRANS. ASME, vol. 80, 1958, pp. 1791–1801.

30 T. P. Sulzer, "Effect of Fuel Additives on Oil-Ash Deposition," *Schweizer Archiv für angewandte Wissenschaft und Technik*, November, 1952, pp. 379–380.

A. T. Bowden, P. Draper, and H. Rowling, "The Problem of Fuel-Oil Ash Deposition in Open Cycle Gas Turbines," *Proceedings of The Institution of Mechanical Engineers*, series A, vol. 167, 1953, pp. 291–312.

31 F. L. Schwartz and H. A. Ohlgren, "Automotive Nuclear Heat Engines and Associated High-Temperature Materials," presented at the SAE Summer Meeting, Atlantic City, N. J., June 3–8, 1956.

DISCUSSION

D. W. HUTCHINSON[2]

The authors are to be congratulated on a most comprehensive and stimulating presentation including much information of value. The results of the work in the field of automotive heat exchangers will have particular influence on the design of future automotive gas turbines.

The suggested means for increasing the torque multiplication of vehicular turbine also has merit, but is not restricted to the split-compressor differential power plants described in detail. The ability of the simplest form of differential gas turbine to provide torque multiplication by similar means, and the disadvantages of such an approach, are noted in the literature.[3] The maximum torque multiplication of a simple differential-gas-turbine is about 4.0:1.

However, torque multiplication is not the most serious problem facing the gas turbine today as witnessed by the fact that our standard of reference, the piston engine, has marked inferiority in this respect. Increasing torque is beneficial but does not in itself provide a solution to the problems of present automotive gas turbine—the excessive time required to change from idle to full power—to mention one.[4]

The value of torque multiplication for vehicle acceleration (the only practical application for maximum power in an automobile) cannot be evaluated separately from the power-response and output-inertia characteristics of a power plant. For example, a simple differential gas turbine, having no steady-state torque multiplication, can accelerate an automobile from standstill to cruising speed quicker than a conventional free-turbine power plant having a steady-state torque multiplication of over 2:1. This apparently implausible result is explainable by the differential gas turbine's much shorter time requirement to accelerate the compressor from idle speed to maximum, and by the fact that by the time the "free turbine" achieves maximum compressor speed its output speed is sufficiently high to reduce its torque multiplication. These results also are influenced by the inertial characteristics which cause the transient output torque of the differential gas turbine to exceed steady-state values, and the transient output torque of a free-turbine to be less than steady-state values.

The authors might wish to provide additional information on the following factors in comparing the relative merits of the various forms of differential gas turbines for automotive use:

1 The cost of the torque-multiplication improvement resulting from the addition of a compressor to the simplest form of differential gas turbine—in terms of the reduction in the simpler power plant's advantages of faster power response, better part-load fuel economy, and lower output inertia, compared to the conventional free turbine. The cost of adding a turbine instead of a compressor has been established.[4]

2 The limitations imposed on the torque multiplication (gear ratio) of a split-compressor differential gas turbine by the allowable speed variation of the shafts resulting from the requirement for matching the compressor air flows and maintaining the turbine at or near its optimum velocity ratio.

J. C. MILES[5]

The authors are to be commended for the very broad scope of this paper. It provides challenging thoughts on many aspects of the earth-bound version of the gas turbine. Of particular interest are the comments on possible differential combinations, divided compressors, and turbines; also of interest are the behavior characteristics when the gas flow enters the high-pressure or power turbine first. Over-all behavior of such combinations, while appearing favorable at first inspection, requires very careful analysis to predict fully the actual performance.

Simplicity, small bulk, and small mass per horsepower constitute the primary merits of the gas turbine, and have won for it undisputed supremacy in the air. Compound systems, heat exchangers, and reduction gearing enter in strongly to neutralize these merits for ground application. Only those modifications are warranted which provide improved performance in proportion to cost, bulk, weight, and complexity of design. In other words, simplicity is still the keynote of good design.

The battle toward high efficiency is being waged on one hand by the proponents of high pressure ratios and high component efficiencies and, on the other hand, by the advocates of heat exchangers. Although this struggle is currently undecided, the majority of opinion seems to favor the heat exchanger. The

[2] President, The Turbex Corporation, Mamaroneck, N. Y. Assoc. Mem. ASME.

[3] D. W. Hutchinson, "The Differential Gas Turbine," *Trans. SAE*, vol. 64, 1956, pp. 510–521, and discussion pp. 521–523.

[4] W. A. Turunen and J. S. Collman, "The Regenerative Whirlfire Engine for Firebird II," SAE Summer Meeting, June 5, 1956.

[5] Professor, Mechanical Engineering Department, University of Illinois, Urbana, Ill. Assoc. Mem. ASME.

writer shares this viewpoint with the authors, since it is known that only 30 lb of heat exchanger can provide 82 per cent effectiveness per pound-second of air flow in a turbine of optimum design. Present practice assumes 300 lb of heat exchanger are necessary for 82 per cent effectiveness, and some large industrial turbines are currently using 1200 lb of heat exchanger per pound-second of air flow at only 70 per cent effectiveness.

The potential for further reduction of heat-exchanger mass and volume is as great as that for improving turbine-component efficiencies. The regenerated cycle will profit from all component improvements plus heat-exchanger improvements, but, of course, the nonregenerated cycle cannot profit from any heat-exchanger improvement.

Industrial and marine turbines, particularly those operating on the regenerated cycle, seemingly have suffered from an overinfluence of aircraft practice. To design an aircraft-type turbine for industrial use and then add a heat exchanger is as illogical as doing the reverse. A fully integrated design of heat exchanger and turbine would yield a much improved machine. The design should provide maximum simplicity, shortest possible flow path, single combustor, full annular flow, optimum pressure ratio, optimum torque characteristic, and a fuel consumption closely approaching that of a diesel.

J. M. GRUBER

Engineer, Medium Steam Turbine Generator and Gear Department, General Electric Company, West Lynn, Mass. Mem. ASME

E. F. HANSEN

Engineer, Medium A. C. Motor and Generator Department, General Electric Company, Schenectady, N. Y.

Electrostatic Shaft Voltage on Steam-Turbine Rotors[1]

Several different types of shaft voltages can be present on steam-turbine rotors. The one type that has gained increased significance in the past five years is the direct-current or electrostatic voltage. Prior to this period, electrostatic shaft voltage had not been a problem. This voltage has been causing damage to different turbine parts and, without warning to turbine operators, has been responsible for a number of serious turbine outages. The investigation which was undertaken by the authors was the result of a number of unexplainable bearing failures. The investigation showed that the cause of these failures was due to a static voltage generated in the steam turbine. The solution to the problem is to ground the turbine shaft. This has eliminated the turbine shutdowns caused by bearing failures resulting from electrostatic voltage.

Introduction

SHAFT CURRENTS in electric machinery, resulting from an a-c electromagnetic voltage, have been described by many authors during the past 50 years [1].[2] Published information on d-c electrostatic voltages on steam turbines is practically nonexistent. In 1948, one author [2] wrote that "as far as the author is aware, nothing has been published on the subject of electrostatic charges being caused by the brushing effects of steam on the turbine blading." This is not only true today, but owing to the absence of investigation in this field, the turbine industry has advanced in ever-increasing power output without gaining a working knowledge of the phenomenon of electrostatic voltage in steam turbines. At present, many turbine operators are aware of the presence and effects of static shaft voltage, but there exists a lack of understanding of the different types of voltage, their effects, and the need for removal.

The results of bearing damage from d-c voltage were first recognized by the authors in 1951, following a thrust-bearing failure on a 6250-kw turbine which was in service less than 1 year. The magnitude of the problem was established following 12 thrust-bearing failures on a group of 14 duplicate units late in 1953.

The investigation that followed resulted in a better understanding of all the types of voltages on turbine rotors. The field tests corroborated the concept that the static charges were generated by the water in the steam. With the aid of a laboratory bearing test stand the damage to bearings was duplicated and a contacting shoe that removed the voltage from the shaft was developed.

General Considerations

When an electrostatic potential is generated on a steam-turbine rotor, the voltage level is dependent upon many design variables which determine the resistance in the circuit to ground. Modern turbines are manufactured with either centrifugal or gear-driven main lubricating-oil pumps. These two types of pumps employ many different parts, each of which has an effect on the shaft voltage as the design is varied. As an example, on a turbine with a centrifugal pump the voltage is dependent upon thrust and journal-bearing design, while on the geared-type pump the voltage in all probability will be dependent on the worm-and-gear drive and any antifriction bearings in the pump.

The nature of the damage in all cases is similar. Steel or babbitt surfaces, originally shiny, assume a satin or gray finish to the naked eye. The surface otherwise appears normal and may be very easily overlooked by servicemen except those familiar with shaft-voltage effects.

The nature of the damage becomes more apparent when a gray surface is viewed with a magnification of ×25.

A representative sample of babbitt damage is the thrust bearing shown in Fig. 1. This is a tapered-land main thrust plate from a turbine with a centrifugal pump front standard. The light-gray areas are in the region of the minimum oil-film thickness and extend into the tapered, or approach side of the land. Fig. 2 is one location on the plate at ×25. This type of damage alters the shape of the bearing surface to the extent that the plate loses its capacity to carry the load. After this condition is reached, the babbitt wipes away, taking with it any evidence that the source of trouble was shaft voltage.

Steel surfaces become damaged by pitting in a manner similar to babbitt; however, at a slower wear rate. An example of shaft-voltage effects on steel is shown in Figs. 3 and 4. These are ×1 and ×25 photographs of a case-hardened mild-carbon-steel thrust runner with 3-in. OD which operated against a babbitt plate in the main oil pump of a geared-type pump. The pitting on steel is normally smaller in diameter and in depth.

Field Investigations

A program of field tests was undertaken to determine what types of turbines have d-c voltage and to study the nature of d-c voltage to determine what controls its presence and magnitude.

To obtain the desired information, turbines were selected to cover a range of condensing and noncondensing steam conditions. Generator and mechanical drive units covering a range of ratings from 4600 to 25,000 kw were included. Table 1 is a summary of the turbines tested. The voltage recorded in the last column of this table is the maximum d-c voltage taken with a 20,000-ohm per volt voltmeter, covering a 10 to 30-min period of time on the specific day of the test. Subsequent to the initial tests on these turbines a few were singled out for daily checks over a period of

[1] When this paper was written the authors included information and expressed opinions believed to be correct and reliable. Because of the constant advance of technical knowledge, the widely differing conditions of possible specific applications, and the possibility of misapplication, any application of the contents of this paper must be at the sole discretion and responsibility of the user.

[2] Numbers in brackets designate References at end of Paper.

Contributed by the Power Division and presented at the Semi-Annual Meeting, Detroit, Mich., June 15–19, 1958, of THE AMERICAN SOCIETY OF MECHANICAL ENGINEERS.

NOTE: Statements and opinions advanced in papers are to be understood as individual expressions of their authors and not those of the Society. Manuscript received at ASME Headquarters, January 3, 1958. Paper No. 58—SA-5.

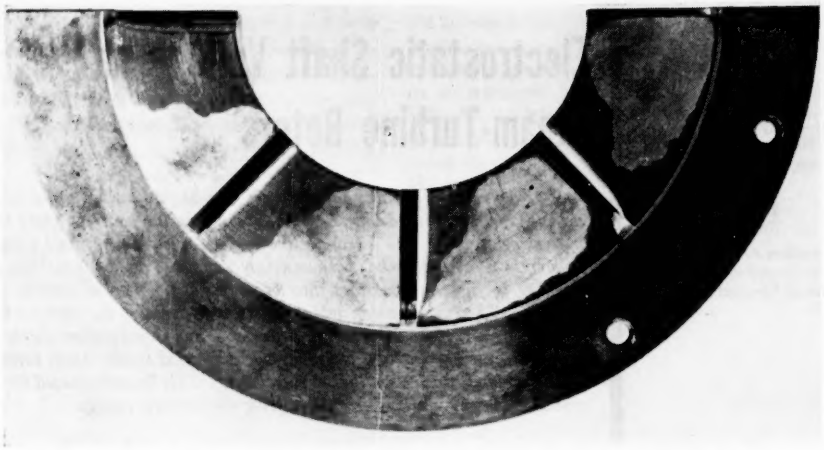

Fig. 1 Lower half tapered-land main turbine thrust bearing damaged by electrostatic voltage

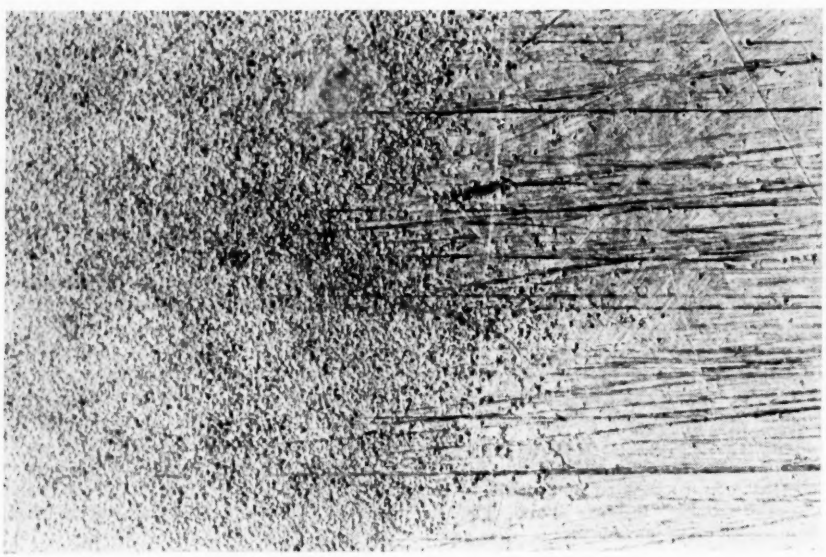

Fig. 2 Babbitt damage of bearing in Fig. 1; ×25

many months. A large variety of information was gathered as a result of the initial field tests. These can best be presented by discussing a few test details on 11 of the 20 units tested.

Turbine No. 1. This unit is a straight condensing turbine with a centrifugal pump front standard. The thrust bearing for the main oil pump was damaged from d-c voltage after the first 6 months of operation. It was redesigned to a larger capacity. Six months later the main-turbine thrust was removed for inspection. Fig. 1 shows the lower half active thrust plate after 12 months' total operation. It is a 61-sq-in. tapered-land bearing with $6^1/_2$ in. ID and $15^1/_4$ in. OD. In Fig. 1 the areas light in color are damaged due to pitting from shaft voltage. Fig. 2 is a photograph at ×25, of the bearing in Fig. 1 showing the surface midway between the damaged and undamaged areas. From an optical focus it was estimated that the depth of pits averaged 0.0002 in.

Turbine No. 4. Two oscillograms of the voltage found on this unit are shown in Fig. 5. The exposure time for both photographs was $^1/_{25}$ sec. The top photo was taken at 10,000-kw turbine load. It has a peak voltage of approximately +29 volts. The meter voltage was +25 volts d-c. The lower photo was taken at 5000 kw load. Peak voltage was +26, meter voltage was +18. This turbine is a straight condensing unit with a gear pump front standard. An inspection of the front end parts showed that the journal, journal bearing, and active thrust bearing were gray as a result of pitting. Also, the bronze worm gear of the pump and governor drive was pitted at both ends of each tooth.

Turbine No. 5. This 12,500-kw unit is a single automatic extraction, condensing turbine, with a special geared front end that drives a speed governor only. Shaft voltages were measured for a 5-hr period of operation covering the complete range of kilowatt load and extraction flow. A summary of the test conditions is given in Table 2. The oscillograms for this test are shown in Fig. 6. The exposure time for each photograph was $^1/_{25}$ sec. A subsequent inspection of the front-end parts showed the thrust plate

and journal bearing were pitted and gray in color.

Turbine No. 6. This unit is a duplicate of turbine No. 5. A continuous record of the d-c shaft voltage was made on a recording voltmeter for a 3-year period from 1954 to 1957. The d-c voltage was found to be very erratic in its magnitude and occurrence. When present, the voltage measured on different days, varied from −20 to +65 volts. The length of absence of voltage varied anywhere from 1 day to 6 months. The presence of voltage on this turbine was affected by such factors as load change, extraction flow changes, centrifuging the main oil supply or adding oil to the main tank. Voltage measurements for a 3-hr period at different kilowatt loads and extractions flows are given in Table 3 and Fig. 7. The duplicate turbines bear a similarity in the nature of the voltage but are different in magnitude and polarity at corresponding load and flow conditions.

Turbine No. 7. This is a straight condensing turbine with a gear-pump front end. The voltage measured on the day of the test was not large enough to cause damage. However, 6 months after the author's tests, the main thrust bearing failed, with complete removal of the babbitt from the thrust plate. Inspection of the parts in the front end revealed that shaft voltage was the cause of the failure. Surfaces, gray from pitting, included the turbine-rotor journal at the No. 1 bearing, the active side of the thrust runner, and the contact surfaces of the gear teeth on the quill drive for the geared oil pump. In addition, the bronze worm gear of the pump drive was found to have pin holes on the trailing end of each tooth. This case was one of many that revealed the erratic nature of electrostatic voltage, and that a single test for voltage is no assurance that a unit will be free of bearing failure.

Turbine No. 12. The tests on this condensing mechanical-drive turbine were first made following four thrust-bearing failures which occurred in a period of 6 months. Because of the complete

Fig. 3 Thrust runner from main oil pump damaged by electrostatic voltage

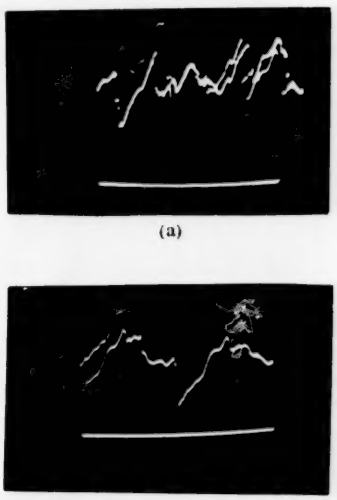

(a)

(b)

Fig. 5 Oscillograms of d-c electrostatic shaft voltage on a 12,500-kw steam turbine. (a) 10,000-kw load; (b) 5000-kw load.

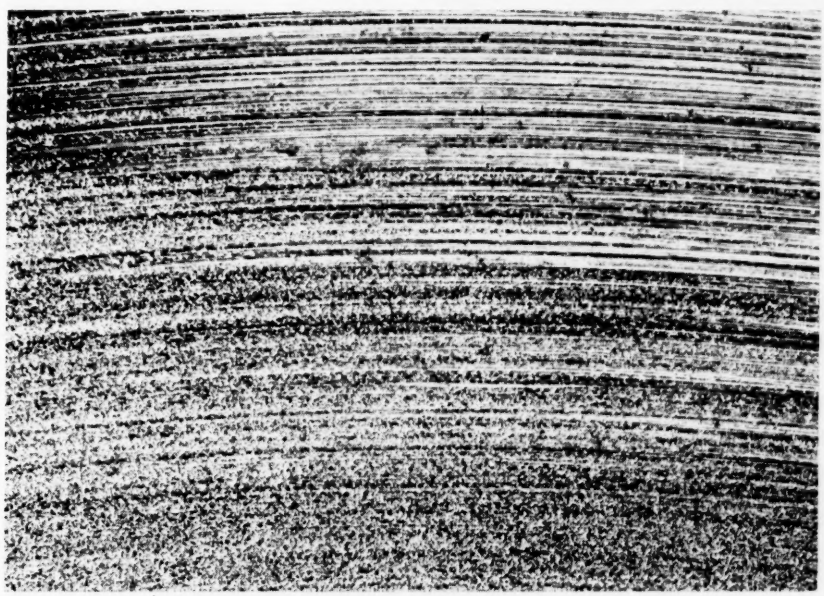

Fig. 4 Steel damage of runner in Fig. 3; X25

Table 1 Summary of field tests for electrostatic shaft voltage

Turbine no.	Kilowatt rating	Drive	Steam inlet—Press, psig	Steam inlet—Temp, deg F	Back pressure, in. Hg	Average d-c shaft, volts
			Condensing Turbines			
1	25000	Generator	850	900	1½	−25
2	25000	Generator	850	900	1½	+10
3	12500	Generator	200	600	1½	−0.4
4	12500	Generator	600	825	2	+25
5	12500	Generator	625	825	2	+30
6	12500	Generator	625	825	2	+37
7	9375	Generator	850	825	1½	+1.1
8	9375	Generator	425	629	1	+0.5
9	9375	Generator	400	750	1½	+1.5
10	9375	Generator	200	500	1½	+1.3
11	6250	Generator	600	825	1½	+130
12	4600	Mechanical	410	725	2½	+0.4
13	4600	Mechanical	410	725	2½	0
14	4600	Mechanical	410	725	2½	0
15	4600	Mechanical	410	725	2½	+0.2
16	4600	Mechanical	410	725	2½	+65
17	4600	Mechanical	410	725	2½	+10
			Noncondensing Turbines			
					Psig	
18	12500	Generator	600	825	175	0
19	7500	Generator	600	825	200	0
20	6250	Generator	1400	900	210	0

absence of voltage, it was concluded originally that the bearing failures were due to mechanical reasons. Twelve months later an inspection of the replacement thrust bearing showed it was extensively pitted and worn. Tests at this time showed there was a d-c voltage of 76 volts on the turbine shaft.

Turbine No. 13. Subsequent tests 12 months later showed there was 44 volts d-c on the turbine shaft.

Turbine No. 14. Twenty-eight volts d-c was found on the turbine shaft 12 months later.

Turbine No. 15. Seven volts d-c was found 12 months later.

Turbine No. 16. On the first occasion to test this unit with load, 65 volts meter voltage was found on the turbine shaft. This unit was equipped with an electrically insulated main coupling. At the time that the 65 volts was measured on the turbine side of the insulated coupling, 0.02 volt was measured on the driven side. An oscillogram of the voltage found is shown in Fig. 8. Peak voltages reached a maximum of 120 volts. The pattern in this oscillogram is representative of the voltage found on the other mechanical-drive units tested.

Turbine No. 17. The maximum meter voltage on this unit, as reported by the operator, is +100 volts d-c.

Turbines No. 12 to 17 have special front standards that have a worm and gear which drives a speed governor only.

In addition to the author's field tests, voltage measurements have been made by service engineers and turbine operators on other turbines which now number well in the hundreds. Test data have been obtained on units ranging from a 1500-kw condensing unit which was found to have 22 volts d-c to a 100,000-kw low-pressure unit of a cross-compound turbine set which had 40 volts d-c.

Laboratory Investigations

The flow of electric current through journal bearings was studied using a laboratory journal-bearing test stand. The equipment was modified in order to apply a test voltage and current. The bearing was insulated from ground with a 1/16-in. layer of mica. Current was introduced to the shaft with a copper collector ring and silver-graphite brushes. The variables which were studied were in two categories; namely, the bearing or hydrodynamic variables, and the electrical variables. The first category included speed effects from 200 to 3600 rpm and load effects from 10 to 1000 psi. The electrical variables used included voltage from 0.1 volt to 200 volts d-c, current from 1 to 60 milliamp, and introduced circuit capacitance from 0.04 to 0.40 microfarad.

Table 2 D-C electrostatic voltage on a 12,500-kw steam turbine—voltage versus load and extraction flow

Fig. no.	Extraction steam flow, lb per hr	Generator load, megawatts	Meter voltage, d-c volts
6(*a*) Calibration voltage, 10 volts line to peak, 60 cycles per sec			
6(*b*)	0	7.5	0
6(*c*)	0	10	−3.0
6(*d*)	55000	5	+0.5 to +1.5
6(*e*)	55000	7.5	+1.0
6(*f*)	55000	10	−0.5 to −3.0
...	105000	2.5	0
6(*g*)	105000	5	+15
6(*h*)	105000	7.5	+25
6(*i*)	105000	10	+2.0
6(*j*)	145000	5	+0.5
6(*k*)	145000	7.5	+6.5
6(*l*)	145000	10	−3.0 to −7.0

Light turbine oil at 120 F inlet temperature was used for all the tests. Table 4 is a summary of one of the 8-hr life tests on a 6 × 6 × 0.012-in. cylindrical bearing. Fig. 9 is a photograph at ×25 of the damaged area resulting from run No. 5.

In the laboratory tests no correlation could be found between voltage and oil-film thickness at which breakdown occurs. Under identical hydrodynamic conditions, voltage breakdowns would vary from 1 volt to 200 volts impressed across the bearing. The summary of tests at one speed is given in Table 5. This same lack of correlation between voltage and oil film thickness was borne out in a stationary oil voltage cell test where two parallel circular plates submerged in oil were set at known distances apart with a micrometer adjustment. Five oil samples from three different brands were used for this test. Table 6 is a summary of the test data. Mr. Allen [3] in his experimental studies of the dielectric strength of oil films found there were disparities between the oil-film thickness computed from hydrodynamic theory and the oil-film thickness computed from the dielectric strength.

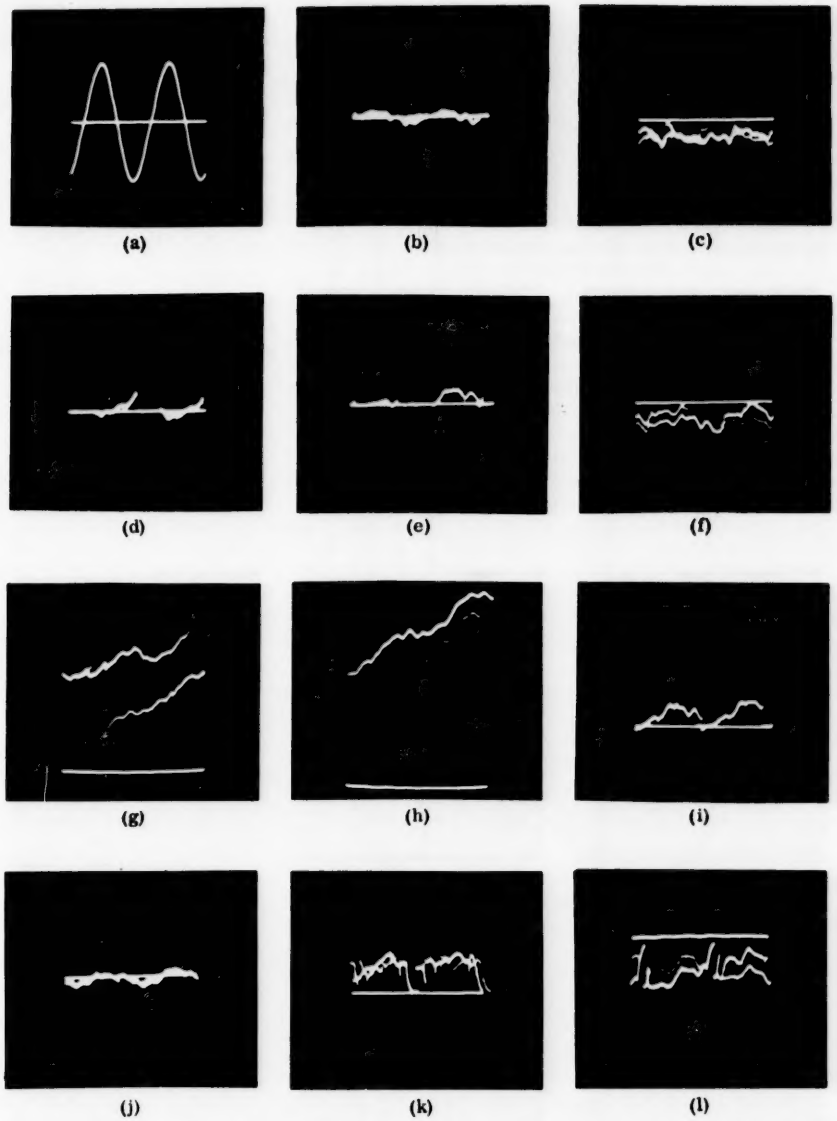

Fig. 6 Oscillograms of d-c electrostatic shaft voltage representing changes due to turbine load and extraction steam flow as shown in Table 2

Discussion

There are five recognized types of shaft voltage which can be found on a steam-turbine rotor. These are the electromagnetic or 60-cycle a-c voltage, a ground-detector 120-cycle a-c voltage, the ignitron excitation voltage, the high-frequency-exciter ripple voltage, and the electrostatic d-c voltage. To better understand the nature of the d-c electrostatic voltage, each of the five types is covered in order in this discussion.

The electromagnetic type of shaft voltage is induced in a conducting loop circuit which interlinks a synchronously alternating magnetic field. This type of shaft voltage originates in the generator rotor. It can be detected as a potential difference between the generator-shaft extremities. Its magnitude is approximately zero to 3 volts rms alternating current with no d-c component. The magnitude varies from one machine to another owing to small differences in manufacturing tolerances. The magnitude varies with the field ampere-turns on the rotor. The frequency of the electromagnetic shaft voltage is fundamentally shaft frequency or synchronous frequency. The wave shape is often not a pure sine wave but includes harmonics of multiples of the fundamental frequency. In rotors of two-pole turbine generators, the rotating field flux out of the North Pole crosses the air gap and then splits into two paths, to the right and to the left, in the stator and returns to the South Pole. If the magnetic reluctance of the left-hand path in the stator is slightly smaller than the right-hand path, then, when the rotating field turns 180 deg the right-hand path (viewed from the rotor) will change from the larger reluctance path to the smaller reluctance path. The resulting once-per-revolution alternate pulsations of magnetic flux interlink

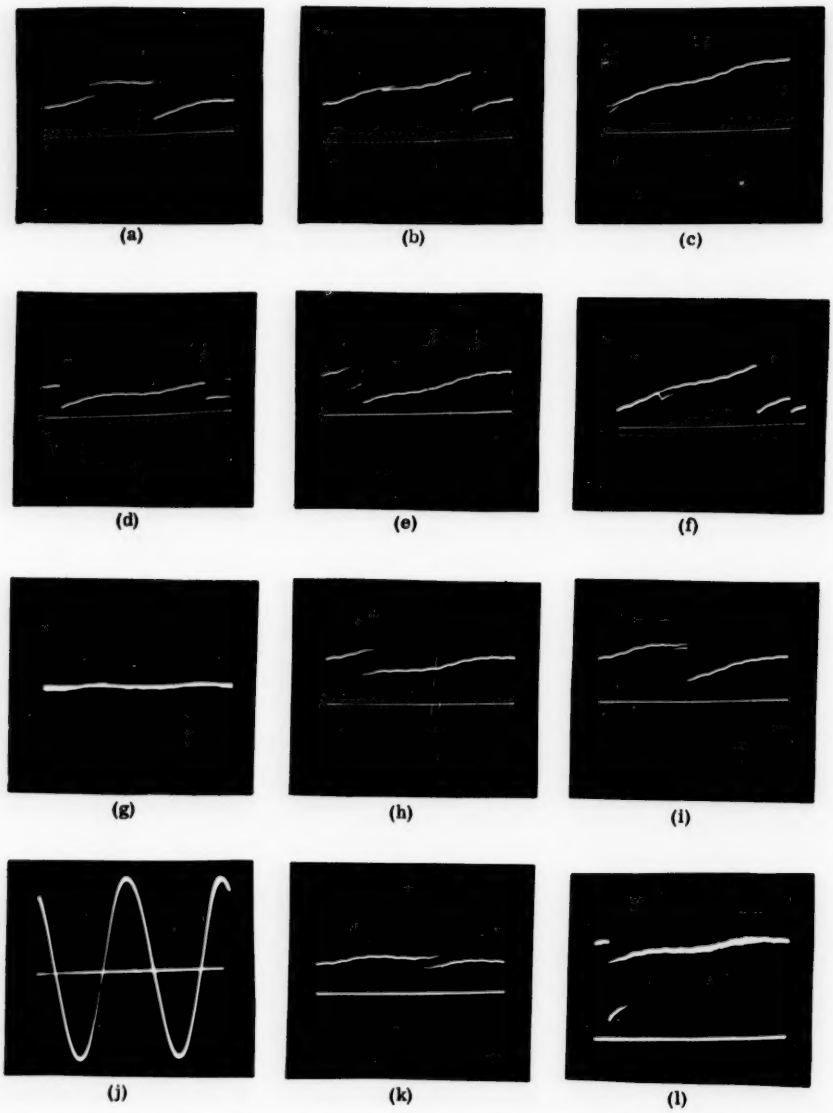

Fig. 7 Oscillograms from a steam turbine, duplicate of turbine in Fig. 6, representing load and flow changes as shown in Table 3

with the generator shaft acting as one leg of a single-turn conducting loop. The bearings and bearing pedestals complete the loop circuit with the generator stator and bedplate acting as the remaining leg. The most efficient design methods are utilized to keep the reluctance of the stator magnetic paths uniform. Nevertheless, relatively small variations are present in most generators, and this is enough to generate a small a-c voltage in the shaft-loop circuit.

Observations and tests show that bearing oil films sometimes conduct electricity and sometimes act as insulators. During conduction, the impedance of the loop path is so low that a few volts may cause pulses of several hundred amperes to flow momentarily. When such magnitudes of current are suddenly interrupted by a nonconducting oil film in a bearing, and the interruption takes place in a microsecond or less, the self-inductance of the single-turn loop causes a relatively high induced voltage across the oil film. When this induced voltage exceeds the minimum arcing voltage of the electrodes and system (never less than 10 or 15 volts for any electrode), an electric spark (transient arc) pierces the oil film between the shaft and babbitt bearing of the generator bearing. It is these destructive sparks which melt out numerous minute pits, mostly from the babbitt metal, and eventually cause enough loss of metal to result in a bearing failure. Since the electromagnetic type of shaft voltage is induced in a loop circuit, it is only necessary to open the loop circuit at one point to eliminate the current whose transient interruptions cause sparks. It has been standard practice for many years to insulate the generator outboard bearing or bearing pedestal from the stator. Any hydrogen shaft seals at the outboard end of the generator are also insulated from the stator. Insulated shaft couplings are used on direct-coupled exciter generators to prevent spark damage to the exciter bearings. Such insulation has successfully prevented

Table 3 D-C electrostatic voltage on a 12,500-kw steam turbine—voltage versus load and extraction flow

Fig. no.	Extraction steam flow, lb per hr	Generator load, megawatts	Meter voltage, d-c volts
...	0	2.5	+0.2
7(*a*)	0	5.0	+35
7(*b*)	30000	7.5	+45
7(*c*)	35000	10.0	+50
...	65000	2.5	+0.1
7(*d*)	50000	5.0	+30
7(*e*)	50000	7.5	+32
7(*f*)	50000	10.0	+35
...	100000	2.5	0
7(*g*)	100000	5.0	+0.1
7(*h*)	100000	7.5	+32
7(*i*)	100000	10.5	+40
7(*j*)	Calibration voltage, 100 volts line to peak, 60 cycles per sec		
...	140000	2.5	0
...	150000	5.0	−0.2
7(*k*)	150000	7.5	+35
7(*l*)	150000	10.0	+65

damage and eliminated failure of generator and exciter bearings from the electromagnetic type of shaft voltage.

The 120-cycle ground-detector voltage originates from a ground-detector control circuit. This detector is an alarm system which energizes a signal relay in case the generator-field-winding ground insulation fails. The alarm system uses a circuit energized by a 60-cycle a-c voltage which is rectified and then connected between one of the field-winding terminals and ground.

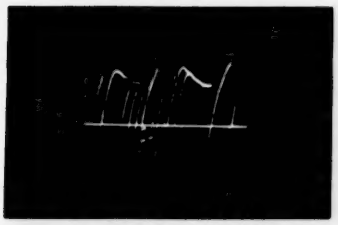

Fig. 8 Oscillogram of d-c electrostatic shaft voltage from steam-turbine rotor of a mechanical-drive unit

The full-wave-rectified 60-cycle voltage has a relatively large 120-cycle ripple-voltage component if not filtered. When the field-winding insulation is in good condition, it serves as an electrical capacitive impedance between the field conductor and the rotor steel. The 120-cycle a-c component of voltage may be as high as 90 volts and is capable of generating 20 milliamp of 120-cycle a-c current when any oil film in the bearings is in a conducting state. When this voltage is about 10 volts or over on a turbine shaft, it will damage turbine bearings to a point where the bearing fails. The 120-cycle a-c type of shaft voltage is capacitively induced or coupled to the shaft. A potential difference exists between shaft and stator (stator is grounded). The potential is the same at any point along the generator shaft or turbine shaft directly coupled to it. There is no potential difference between the extremities of the generator shaft. This voltage has no d-c component.

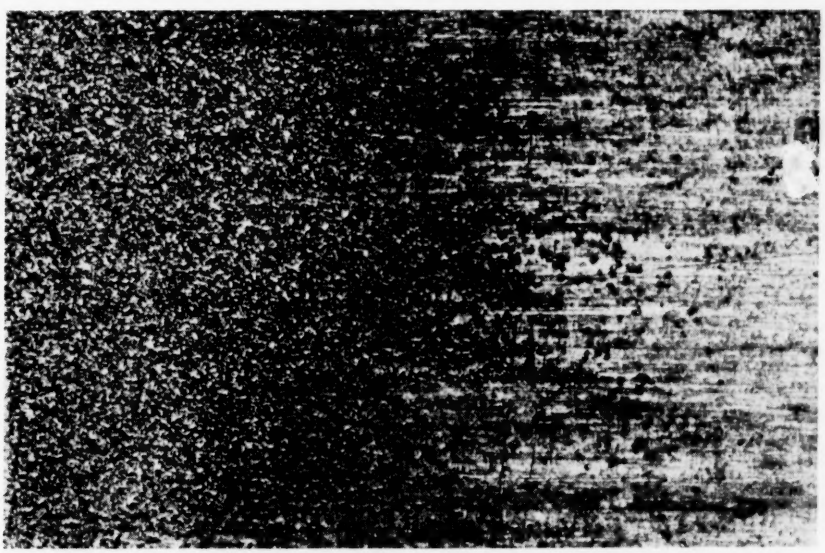

Fig. 9 Bearing damage of a 6-in-diam bearing after an 8-hr laboratory life test; ×25

Table 4 Bearing-wear tests

(6 × 6 × 0.012-in. cylindrical bearing, 200 rpm, 10 psi oil-inlet pressure)

Run no.	Time, hr	D-C, volts	External resistance, ohms	External capacitance, microfarad	Average current, milliamp	Nature of current, flow[a]	Calc. min oil-film thickness, in.	Damaged area, sq in.
1	8	76–70	1100	0.40	37	I	0.00078	13.5
2	8	77–79	2600	0.40	22	I	0.00072	21.9
3	8	82	7600	0.40	8	I	0.00072	9.0
4	8	80	7600	0.40	10	S	0.00072	0
5	8	82–84	100	0.04	1	I	0.00063	4.0

[a] I—Intermittent pulsating current flow (indicates sparking).
S—Steady, constant magnitude, d-c current (indicates no sparking).

Table 5 Bearing current versus voltage and bearing load

(6 × 6 × 0.012-in. bearing at 3600 rpm)

Bearing loading, psi	Calculated min oil-film thickness, in.	Applied voltage, volts d-c	Series resistance, kilohms	Current, milliamp		Oscilloscope	
				Max available	Meter value	Pattern code	Pulses per revolution
60	0.0046	200	100	2	0.1	d	0.2
10	0.0048	200	100	2	1.5	e	20
10	0.0048	200	100	2	1.0	d	10
60	0.0046	200	100	2	0.1	d	0.2
200	0.0022	200	100	2	0.1	d	0.2
350	0.0015	200	100	2	1.8	g	40
850	0.0008	200	100	2	1.8	g	40
850	0.0008	100	100	1	0.1	f	20
850	0.0008	50	100	0.5	0.2	a	3.5
850	0.0008	20	10	2	0.2	a	3
850	0.0008	10	10	1	0.0	a	3
850	0.0008	2	1	2	0.0	c	0.2
850	0.0008	1	1	1	0.0	b	0.2
850	0.0008	0.5	1	0.5	0.0	a	0.1
850	0.0008	0.1	1	0.1	0.0	a	0.1
850	0.0008	200	100	2	0.1	e	2
850	0.0008	200	100	2	2.0	h	35

Code: a—Occasional current pulses less than 0.5 milliamp.
b—Occasional current pulses less than 1.0 milliamp.
c—Occasional current pulses less than 2.0 milliamp.
d—Occasional current pulses of about 2.0 milliamp.
e—Repetitive pulses at least once per revolution of about 2 milliamp magnitude.
f—Repetitive pulses of 2 milliamp magnitude so frequent that minimum current values never go below 0.5 milliamp.
g—Minimum current value never below 1.5 milliamp.
h—Minimum current value never below 2.0 milliamp.

Table 6 Voltage breakdown between stationary flat-disk electrodes. Gap distance at breakdown, in. × 10^{-4}.

Applied voltage, volts d-c	Oil sample									
	A		B		C		D		E	
	Min	Max	Min	Max	Min	Max	Min	Max	Min	Max
1	6	7	3	15	8	17	5	7	17	19
2	2	5	3	15	10	14	4	5	14	16
5	5	8	6	13	7	8	5	6	11	18
10	3	6	12	14	10	11	10	10	11	19
15	2	7	7	18	3	7	6	6	11	14
25	2	6	7	9	2	8	4	6	10	14
50	3	7	4	5	2	8	4	7	11	17
100	4	7	4	5	3	8	4	8	13	17
200	4	7	2	5	6	11	6	10	17	25

Oil sample A—Brand 1 new oil.
B—Brand 1 used oil.
C—Brand 1 used oil.
D—Brand 2 used oil.
E—Brand 3 used oil.

A third source of turbine-shaft voltage is from the generator-excitation system. When generator field windings are supplied by rectifiers, the average magnitude of field voltage is direct current. However, the instantaneous magnitude of the voltage is not constant with respect to time, because of a large a-c component of ripple voltage. When the rectifiers are supplied from a three-phase 60-cycle voltage, there is a 360-cycle ripple voltage. The field-winding insulation serves as a distributed capacitive impedance which couples a component of the ripple voltage to the rotor steel. This component of ripple voltage, as it appears between the generator field winding and ground, turns out to be fundamentally a 180-cycle wave. With grid-controlled ignitron rectifiers, the field-to-ground potential difference is nearly a square wave. This voltage appears between shaft and ground and can cause electric currents to flow through bearings when the bearings are in a conducting state. The voltage from shaft to ground may be more than 100 volts peak value when bearings are not conducting. It will damage bearings to complete failure when present on a turbine shaft in magnitudes of about 10 volts or over. The complete circuit for current flow includes the capacitive impedance of the ground insulation of the three-phase 60-cycle voltage supply. The impedance is such as to limit the maximum average current flow to approximately 20 milliamp. This type of shaft potential is capacitively coupled from the field winding. The potential to ground is of essentially the same magnitude at every point along the length of the generator and turbine shafts. There is no potential difference between the extremities of the generator shaft.

The fourth type of turbine-shaft voltage, another type originating in the excitation system, is the exciter ripple voltage. Most turbine-generators obtain field excitation from a d-c generator. The voltage output of such a d-c generator is pure direct current, except for a component of commutator ripple voltage. The frequency of this ripple voltage is a function of the number of commutator segments and coils and speed of rotation on the exciter armature. The ripple frequency is 2400 cycles on some machines. The full magnitude of ripple voltage appears across the field-winding terminals. The commutator ripple type of shaft voltage is capacitively coupled from the field winding to the shaft. The potential between shaft and ground is the same magnitude at all points along the length of the generator and turbine shafts. No potential difference exists between the extremities of the generator

shaft. There is no known case to date of a bearing failure caused by this form of shaft voltage.

The fifth type of turbine shaft voltage is the electrostatic d-c voltage. This type of shaft voltage originates in the steam turbine. It has never been observed on noncondensing turbines where there is no wet steam. The electrostatic shaft voltage has been observed on many condensing turbines, but not on all. The voltage is direct current and exists between turbine rotor and ground. If the bearings, shaft seals, and worm gears on the turbine and direct-coupled generator or other coupled load are nonconducting, the voltage will tend to charge the electrical capacitance between shaft and ground higher and higher until limited by the leakage current, oil-film insulation resistance, and effective internal impedance of the voltage source; or until limited by voltage breakdown of a bearing oil film. When bearing films break down, the voltage to ground suddenly drops, in a microsecond or so, to zero or part way to zero, and then the voltage begins to climb again. The maximum magnitude of voltage is a function of steam flow in the turbine, but not a clear-cut linear function. The polarity of the shaft is generally positive with respect to ground. However, some turbines have been observed where shaft voltage was negative with respect to ground. On two turbines, the polarity was found to reverse temporarily and later revert back to its original polarity.

The electrostatic shaft voltage has been found to have several reasonably well-pronounced characteristics as follows:

1 The voltage between shaft and bed plate is direct current. This means that the polarity does not reverse periodically.

2 The magnitude is not usually constant and in some cases falls repeatedly to low values after which it climbs back up to higher values. This means that the voltage contains both a-c and d-c components even though the polarity does not reverse.

3 The maximum magnitude observed by oscilloscope was about 250 volts peak value.

4 The rate of rise of shaft voltage was often in the range of 200 volts per $^1/_{60}$ sec or 12,000 volts per sec.

5 The voltage decay when falling to zero is less than 0.1 millisec. The literature [4] indicates that decay times of 1 microsec or less are not unusual for sparks.

6 The minimum magnitude observed was a few tenths of a volt.

7 Typical magnitudes were between 30 and 100 volts peak value.

8 The shaft polarity was positive on many turbines and negative on fewer turbines.

9 The potential at any instant is essentially the same anywhere along the turbine or generator shaft. The shaft voltage appears between shaft and bedplate which is grounded.

10 The maximum current observed in a resistance circuit connected between shaft and ground, regardless of how small the magnitude of resistance, was approximately 1 milliamp.

What is the source of the type of shaft voltage we choose to call the "electrostatic" shaft voltage? Out of several types of electrification considered, a mechanism associated with steam flow in condensing turbines is dictated by the available data. Out of several mechanisms of electrification involving water in motion, the spray-impact mechanism is a likely candidate.

Electrification by contact of two unlike materials followed by separation of the two oppositely charged surfaces is as old as the word electricity. However, experimental work through the years has failed to clarify some of the confusing aspects of electrostatic generation where several types of mechanism are often superimposed on each other. Professor Loeb [5] has written as recently as 1945: "A review of these phenomena, in general, shows a most unsatisfactory array of discordant, often nonreproducible, and confusing results, whose theoretical interpretation in some cases is quite hopeless."

The generally accepted theory includes recognition of the existence of the Helmholtz double layer at the surface of a liquid. Dipole molecules and ions in the liquid react with surface or boundary-layer forces so that the surface is charged at one polarity whereas charges of opposite polarity reside just beneath the surface. When certain dielectric liquids flow through pipes, the outer charged layer tends to adhere to the walls of the pipe, allowing some of the inner charged layer to flow by. This mechanism is related to electro-osmosis (also electroendosmosis, cataphoresis, or electrocapillarity). In this way, liquids such as gasoline can build up dangerous voltages on ungrounded hoses, pipelines, and tanks. The presence of ionic impurities or water in some fluids is said to increase their tendency toward electrification. The flow of water is capable of considerable electrification, but we are protected from this danger by good conductivity of water which provides short-circuiting paths which prevent accumulation of charges. However, when water is in the form of drops, sprays, mists, fogs, and the like, considerable separation of charge can be achieved and the literature describes many cases where high voltages have been reported. Such cases include boiling, bubbling, steam leaks, spray mists of waterfalls, electrification of clouds associated with rainfall and lightning, water droplets in flowing gases, and electrification of airplanes in flight.

In the case of water, the double layer is said [5] to be about 2×10^{-6} cm thick, with perhaps one extra electronic charge per 10^4 to 10^5 molecules. When a drop of water breaks up into smaller drops, the total exposed surface area is increased. Cooper [6] suggests the assumption of equal density of charge packing. Then when a drop breaks up, extra charges are freed in proportion to the change in surface area. This indicates that particle size would be expected to influence the degree of electrification.

The effect of water-drop size is reported by Dorsey [7] when measurements were made in spray mists of waterfalls. He found particles of diameters less than 80×10^{-8} cm to be negatively charged. Particles 80×10^{-8} to 150×10^{-8} cm were positive. Larger drops were found to have no net charge.

Beach [8] reports that airplanes charge negatively and that electrification increases roughly as the third or fourth power of air speed. This indicates that relative speed of water drops and turbine-rotor blades would affect the rate of charge associated with impact charging.

As mentioned previously, the presence of ionic impurities could be expected to influence electrification of liquids. Also, as reported by Beach (9), surface contamination affects the quantity and polarity of charge and is often responsible for erratic and otherwise unexplainable changes in electrification phenomena. Beach mentions that attempts to eliminate charging on airplanes by coating the surfaces with noncharging waxes, lacquers, paints, and so on, have had only temporary success owing to the presence of surface contamination which almost invariably is present.

Some idea of the magnitude of voltage which can be built up by water drops is gained from an experiment by Lord Armstrong [6] in England back in 1840. A locomotive was insulated from ground. The droplets in the wet stream expelled from the stack resulted in electric sparks which jumped 22 in. to ground. The voltage must have been between 600 and 1800 kilovolts to jump that far.

In another case [10] a steam leak is reported to have generated voltage with a rate of rise of 20 kilovolts in 5 sec.

It is evident that polarity of the shaft voltage could be determined by several factors. The type of liquid, its impurities, the type of solid surface, and its contamination coating would affect the magnitude and polarity of charge on the liquid and the resulting opposite polarity on the solid. The size of water drops before and after impact is an additional factor. Also, we can visualize

droplets which become charged by impact with stationary nozzle parts and then carry the charge to the rotor. This might result in a positively charged rotor. On the other hand, uncharged particles striking rotor parts might result in a negatively charged rotor.

Conclusion

Direct-current static voltages are probably being generated on all condensing turbines by the action of the wet steam on the rotating elements. Some build up to a harmful magnitude, damaging turbine parts when they discharge to the ground. Others discharge at low-voltage levels leaving no trace of their existence.

The solution to the problem appears to be to ground the voltage without causing bearing damage rather than trying to eliminate the generation of the voltage at the source. Many possible means

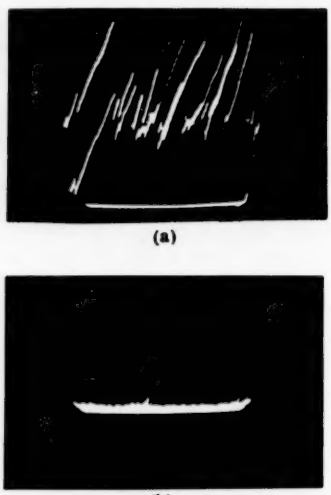

Fig. 10 Oscillograms of d-c electrostatic shaft voltage on a 12,500-kw steam turbine. (a) Represents normal shaft voltage; (b) voltage when shaft is grounded.

of grounding the voltage have been suggested; only a few have been tried. Grounding proposals include carbon brushes, metallic shoes, mercury baths, water seals, lubricating oil with high conductivity, or ionized air paths. The effects of the d-c voltage could be eliminated by applying an equal and opposite polarity voltage. The elimination of the voltage at the source might some day be accomplished by the control of droplet size, a change of bucket and nozzle material or surface finish, to mention a few.

Fig. 10 is an example of the results of a satisfactory grounding device. In this case a damaging voltage of 19 volts was reduced to a safe voltage of 1 volt.

The turbine-shaft-voltage phenomenon is a challenge to engineering. Further studies should and we are sure will be made.

Acknowledgment

The authors thank the many people who contributed in collecting data on this subject. The valuable assistance of Mr. Oscar Pinkus, General Electric Company, in planning and conducting the bearing voltage tests is recognized and deeply appreciated.

References

1 "Shaft Currents in Electric Machines," by P. L. Alger and H. W. Samson, *Trans. AIEE*, vol. 43, 1924, pp. 235–245.

"Shaft Currents in Engine Driven Generators," by A. H. Lauders, *Diesel Power and Diesel Transportation*, vol. 28, February, 1950, pp. 56–60.

"Effects of Electric Current Passing Through Roller Bearings," by O. Schenk, *The Engineers Digest*, vol. 15, March, 1954, pp. 108–110.

2 "Bearing Corrosion in Turbo-Generators," by J. A. Ten Broeke, *Corrosion*, vol. 4, 1948, pp. 590–598.

3 "The Dielectric Strength of Oil Film in Plain Bearings," by C. M. Allen, paper presented at the Wear Conference, Massachusetts Institute of Technology, June 16, 1948.

4 "Erosion of Electrical Contacts on Make," by L. H. Germer and F. E. Haworth, *Journal of Applied Physics*, vol. 20, 1949, pp. 1085–1108.

5 "The Basic Mechanism of Static Electrification," by L. B. Loeb, *Science*, vol. 102, 1945, pp. 573–576.

6 "The Electrification of Fluids in Motion," by W. F. Cooper, *British Journal of Applied Physics*, Supplement No. 2: "Static Electrification" (London, England), 1953, pp. S11–S12.

7 "Properties of Ordinary Water-Substance," by N. E. Dorsey, Reinhold Publishing Company, New York, N. Y., first edition, 1940, p. 610.

8 "What of Air Safety?" by R. Beach, *Electrical Engineering*, vol. 67, 1948, pp. 423–429.

9 "Electrostatic Ills and Cures of Aircraft, Part I," by R. Beach, *Electrical Engineering*, vol. 66, 1947, pp. 325–334.

10 "Grounding Principles and Practice V—Static Electricity in Industry," by R. Beach, *Electrical Engineering*, vol. 64, 1945, pp. 184–194.

DISCUSSION

ROBIN BEACH[3]

The authors are to be highly complimented for their excellent and thorough studies accounting for premature bearing failures from current discharges resulting from various types of potential generation, and particularly from electrostatic potential discharges caused by steam passing through the blades of steam-turbine rotors.

Near the turn of the century, Alfred Coehn in Germany related the magnitude of electrostatic charge developed by contact of solid substances to their dielectric constants, giving $q = k(K_1 - K_2)$. Here q, the electrostatic charge, is expressed in electrostatic units (esu) per sq cm; K_1 and K_2 represent the dielectric constants of the two contacting substances; and k, the proportionality factor, has been found closely equal to 4.4.

Electrons always are found to pass from an uncharged substance of higher K across the contact areas of the interface between the two contacting substances to an uncharged substance of lower K. If at least one of the contacting substances is an insulator then, on separating them, the one acquiring the electrons is charged to negative polarity and the one losing the electrons possesses an equal charge of positive polarity.

This improved and basic electrostatic concept revealed by Coehn, replacing the confusing and mystifying Helmholtz double-layer doctrine, has immeasurably simplified the study and practical application of engineering electrostatics.

While the Coehn relationship was developed for the contacting of solid substances, the writer has extended this principle by his own research to electrostatics of liquids and gases and solids in their variously paired contact combinations. During his consulting services on industrial electrostatic hazards, he has facilitated many fascinating resolutions of complex electrostatic problems through applying his extended Coehn relationship.

Assuming the metal of steam-turbine rotor blades possesses a dielectric constant of 3, dry steam like other gases possesses a dielectric constant slightly in excess of 1, and pure distilled water possesses a dielectric constant of 81, then the inlet superheated steam by contacting the short rotor blades creates on the rotor an electrostatic charge of positive polarity proportional to the low

[3] President, Robin Beach Engineers Associated, Brooklyn, N. Y.; Vice-President, Otis Auto Dynatester, Incorporated; Adjunct Professor of Electrical Engineering, Polytechnic Institute of Brooklyn.

value corresponding to $(K_1 - K_2) = (3 - 1) = 2$. This assumed dry steam, if it existed as such all the way to the exhaust end of the turbine throughout the rotor blades of increasing length and steam-contacting area under light load without becoming moist, would generate in principle sufficient electric charge of positive polarity on the rotor to create within the large electrostatic capacitance of the rotor system a moderate potential of positive polarity to ground by virtue of the relationship $V = Q/C$. In this equation Q is here defined as the electrostatic charge of the rotor system converted from esu to coulombs in the practical system, C is the electrostatic capacitance in farads of the rotor to ground, and V is the potential in volts of the rotor with respect to ground.

Now, on the other hand, assume the absurdly unrealistic condition of the steam becoming so wet that actual slugs of distilled water pass through the large low-pressure rotor blades, in which instance the electrostatic charge imparted to the rotor blades would be of negative polarity and proportional in this instance to the very high value corresponding to $(K_1 - K_2) = (81 - 3) = 78$. If this hypothetical situation actually existed, a very high negative electrification of the rotor could occur. The potential to ground could attain high values in the order of thousands of volts were it not for the fact that the thin films of the lubricating oil in the bearings would repeatedly permit capacitor spark discharges of the rapid transient growths of rotor electrification from the rotor shaft to ground through one or both of the grounded bearings. Also, even spark discharges could occur from the highly charged rotating blades to the grounded stationary blades within the rotor encasement.

Actually at full load on a condensing turbine, the smaller high-pressure rotor blades would be electrified in principle to positive polarity by the entering dry steam. But, as the steam approached the exhaust end of the turbine, becoming slightly moist en route, the larger areas of the low-pressure blades would acquire a relatively high negative electrification, as explained would occur for the hypothetical ultrawet steam mentioned in the previous paragraph. The actual electrification attained by the rotor at the assumed full load under the foregoing positive and negative electrifications would comprise their resulting difference of (1) the low-intensity positive electrification on the smaller high-pressure blading from the entering dry steam, and (2) the greater negative electrification on the large low-pressure blading from the moist steam. Hence the differential electrification of the rotor shaft would be predominantly of negative potential. However, for light load on the same turbine with dry exhaust steam prevailing throughout, the predominating positive electrification throughout the turbine blading would provide wholly positive potential of low order on the rotor shaft.

The writer, from his extensive research with high-velocity gases contacting metals, as in steel, stainless-steel, brass, and copper pipes, has found that during the first seconds of gas flow the Coehn relation holds and therefore the metal at higher K than for the gas develops positive charge polarity by passing electrons to the gas. Then an unexpected but impressive phenomenon occurs whereby the dry gas with its small molecules is readily adsorbed into the surface pores, fissures, and large crystals of surface metal and, if the adsorbed gas is sufficiently compacted, the flowing gas, as it continues to contact the gas-coated metal surface, inappreciably contacts the parent metal itself but rather the adhering gas. Hence, as the flowing gas now largely contacts the adsorbed gas, the dielectric constants of each at the contacting interface being closely unity, their difference $(K_1 - K_2) = (1 - 1) = 0$. Therefore the generated electrostatic charge reduces closely to zero.

From this abortive behavior of dry steam as a gas, we find that this adsorption of the dry steam by the blades of the rotor properly accounts by both principle and practice for the zero electrification of rotors in the three noncondensing turbines shown at the bottom of the authors' Table 1, as well as for lightly loaded condensing turbines with or without large steam extraction shown in the authors' Table 3 for the first case cited, as well as for 7(*c*) light load, 7(*f*) light load, and 7(*j*).

In electrostatic measurements, the choice of instrumentation is particularly important and significant. A D'Arsonval voltmeter, even with a sensitivity of 1,000,000 ohms per volt, would be quite unsatisfactory in measuring electrostatic potential, as it would discharge continuously 1 microamp while connected to the electrostatic system. One microampere in electrostatics may be considered under certain situations a large current. Also the foregoing situation applies similarly for oscilloscopes of the better types which commonly possess internal resistance in the order of 10 megohms and, therefore, they likewise would discharge appreciable current—0.1 microamp—continuously while connected to the electrostatic circuit.

Thus it appears from the paper that much of the electrostatic energy created and stored by the capacitor system within the turbine rotor which amounts to $E = 0.5CV^2$ joules becomes largely dissipated by the connected D'Arsonval an oscilloscopic potential-measuring instruments, in addition to whatever current discharges may occur by sparks or conduction through the oil films of the rotor bearings.

Electrostatic voltmeters are generally employed in measuring electrostatic potentials. In this type of voltmeter, the operating element consists of a small 2-plate capacitor, one plate being movable on a jewel bearing and the needle attached to it indicates on a scale the voltage, the capacitor taking negligible operating energy from the charged electrostatic system under measurement. A D'Arsonval microammeter with a 6-in. scale calibrated to 1 microamp may be used to read to 0.01 microamp; and, for lesser currents which are common in low-energy electrostatic measurements, electronic ammeters are available which measure currents in the order of and even lower than a micro-microampere.

During 1947–1948 the writer investigated many bearing failures in the engines of DC-6 airplanes at La Guardia Airport. New main bearings of engines would fail during a single round trip from New York City to Chicago during a snow storm or equivalent inclement weather. A pilot would report that the engines were rough and needed overhaul before he would fly the airplane again. This happened with seven airplanes of one company within 24 hr on the New York-Chicago nonstop flights.

The bearings were composed of silver-steel alloy and their dimensions were about $1^1/_2$ in. wide by 12 in. diam. The failed-bearing surfaces were found pitted with many fused craters a few mils in diameter and depth; and, the normally high-polished surfaces otherwise were impaired by wiped, excoriated, and disintegrated forms of erosion. The discharge current, in striking contrast to microampere-discharge currents in industrial electrostatics, was found to be of ampere magnitude resulting from the high totalized capacitance of the engine pistons, bearings, and gearing with potentials in the order of 100,000 volts or more.

The overhauled engines of 2800-hp capacity were operated in test cells with special propellers attached. In order to study the spark discharges, large carbon-dioxide cylinders were discharged against the propellers to simulate snow for generating static electricity. In these research tests, it is an interesting coincidence that here also the electrical resistance of oil films within bearings exhibited erratic behavior ranging between momentary states of conduction and excellent dielectric properties, as were reported by the authors for turbine bearings. The conduction currents were of much lesser intensity than the currents in spark discharges because, in the former instances, the potential and electric-charge intensities were considerably reduced by their lower time rates of discharge.

Ionizing bristles were placed at the propeller shaft to dispel by ionization the electrostatic charge before it could enter the reduction gearing and the engine. This method of discharge for the high potential served the same end result as the grounding brushes placed against the rotor shafts of the steam turbines by the authors.

E. R. BOOSER[4]

Among the many significant observations provided in this paper are those on current flow through bearings. The relative independence of the breakdown voltage from the thickness of the oil film in a bearing is of interest. Surprisingly, from the data given in Table 6 for flat-plate electrodes, changes in applied voltage appear to have very little effect. The "breakdown thickness" of the oil film is relatively constant and may be the important factor. The over-all average breakdown thickness from Table 6 might be summarized as follows:

	Oil sample	Average breakdown thickness, in. $\times 10^{-4}$
A	Brand 1 new oil	5.1
B	Brand 1 used oil	8.2
C	Brand 1 used oil	7.9
D	Brand 2 used oil	6.2
E	Brand 3 used oil	15.2

Perhaps significantly these average breakdown thicknesses correspond closely to the minimum oil-film thicknesses calculated for many of the bearing tests in Table 5. Might it be concluded that dirt or metallic particles are inducing breakdown? Did the authors observe any significant difference in the nature or amount of lint, water, dirt, acidity, or any other such factors with the oils for which the results are reported in Table 6?

A striking similarity exists between many of the observations for oil films in this paper and those made by C. M. Allen in reference [3]. Allen, among other things, found that a breakdown potential of 0.4 to 1.0 volt existed over a wide range of moderate to heavy bearing loads. Did the authors conclude from their results whether or not a minimum breakdown potential existed in the bearing systems they examined?

It is hoped that this thought-provoking study will lead to an explanation of the fundamental nature of current flow through oil-film bearings. With such an understanding, the still occasional cases of current damage should rapidly become things of the past.

[4] General Electric Company, Schenectady, N. Y.

PAUL C. WARNER[5]

This paper presents a difficult but interesting subject, and provides many valuable data. As the authors point out, the deleterious effects of bearing currents have been known for many years, and, as a matter of course, generator bearings are designed to eliminate such currents. It is believed that the authors have rendered a valuable service in pointing out that at least one type of electrical current can exist on steam turbines which may cause serious bearing damage.

It is, however, rather disconcerting to find major differences between the experience cited by the authors, and that of the writer's company. While we have had occasional thrust-bearing failures, to the present time none has occurred which we feel can reasonably be ascribed to shaft currents. (A possible exception to this statement will be discussed subsequently.) In this connection it is important to realize, as noted by the authors, that after a bearing failure, most if not all of the useful evidence is gone, making diagnosis of the cause of failure difficult and subject to some degree of uncertainty. It is then somewhat risky to assume a causative effect because of the presence of some factor harmful to bearing performance, such as electrical pitting, foreign particles in the lubricant, more bearing load or less oil flow than the designer might desire, or other like effects. It is for this reason that the correction of conditions felt to be the cause of a bearing failure is usually regarded as somewhat tentative until

[5] Steam Division, Westinghouse Electric Corporation, Philadelphia, Pa. Assoc. Mem. ASME.

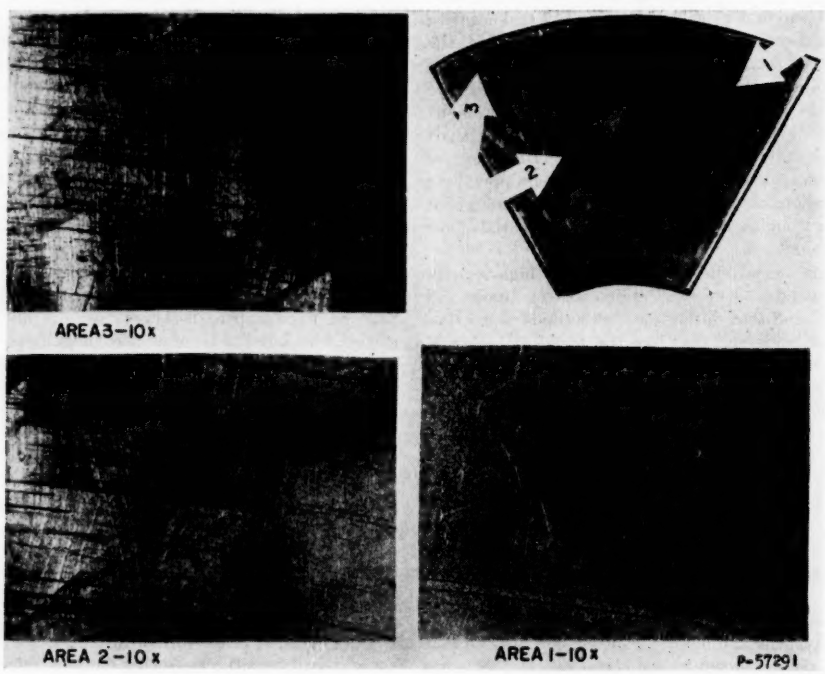

Fig. 11 Thrust bearing shoe showing effects of electrical damage

such time as it has been demonstrated by a reasonable period of operation that the bearing can indeed carry the required load without failure or signs of distress.

It is with these thoughts in mind that the foregoing statement relative to bearing failures from electrical causes is made; that is, the causes assigned to the various bearing failures are assumed, in general, to be correct since there have been few, if any, repeat failures. It is assumed that these facts were duly considered when the numerous thrust-bearing failures assigned by the authors to electrical effects were considered, and thus a very real variation in experience exists between the authors' company and that of the writer.

In conjecturing on the possible reasons for this variation, one is led naturally to consider differences in design which might lead to (*a*) more susceptibility to generation of electrostatic charge, (*b*) more tendency to damage when discharging static electricity, or (*c*) more sensitivity of parts, particularly bearings, to damage from electrical effects.

Nothing along the lines of (*a*) and perhaps (*b*) seems reasonable to the writer. There is a possible question relative to (*c*), since it would appear that the Kingsbury type of bearing would adjust to compensate somewhat for babbitt pitting whereas the tapered-land bearing, being fixed, cannot. Could the authors give a breakdown as to the number of Kingsbury versus the number of tapered-land bearings among those failed as a result of pitting?

As noted previously, we have had no bearing failure which we could ascribe to electrical effects. However, we do have one verified case of thrust-bearing damage from electrical currents. This bearing, of the Kingsbury type, was installed in an 18,750-kw-capacity, industrial, condensing, bleeder machine. This bearing had suffered two failures prior to the inspection which resulted in the finding of shoes pitted by electrical currents. In each case there is good reason to believe the trouble was caused at least in large part by high-thrust loading as a result of blade deposits, and operation at high overloads. Fig. 11 shows one of the shoes from this bearing. It is believed that pitting resulted from electrical effects since appreciable voltages had been measured on this particular machine, and detailed inspection of the pitting indicated it to be practically identical in nature to some bearings purposely pitted by the lubrication section of our Research Laboratories a few years ago. The shoes themselves were not appreciably out of flat, though had the pitting continued for a sufficient time, no doubt they would have been. Incidentally, it is not felt that any reasonably alert service engineer would miss noting a condition such as this.

As a result of this experience a test program was undertaken to ascertain how serious the pitting might be. One of the more enlightening tests involved the operation of two thrust bearings at 4000 rpm carrying 400 to 450 psi, and sustaining 100 milliamp for a 20-hr period. The pitting resulted in a change in shoe flatness on the order of 0.5 mil maximum, and an increase in temperature rise across the shoe averaging 8.5 deg F. While these figures are appreciable, they do not indicate total, or even large loss of load-carrying capacity, and it is concluded that considerably more pitting would be required to affect the load-carrying capability of the bearing seriously. It would seem then that pitting while definitely harmful, is not catastrophic, at least for this type of bearing. It is agreed that steps should be taken to prevent this type of pitting, and it is on this basis that new machines are being supplied with shaft-grounding brushes to leak off any electrical charge.

AUTHORS' CLOSURE

The authors thank the discussers for their contributions of data and their thought-provoking views.

Electrostatic discharge is a problem that must be reckoned with in many different industries. Of particular note is the fact that in each problem the solution has been to lead the voltage off harmlessly to ground. The authors feel that the elimination of the electrostatic voltage at the source remains a real challenge and should be given further study and research.

Professor Beach has suggested that positive shaft polarity is contributed by dry steam, whereas negative polarity is due to water droplets in the low pressure stages. The net shaft polarity would then be the differential effect of the two types of electrostatic generation. He later mentions that the absorption of dry gases into metal surfaces seems to reduce the generation of charges from dry gases "closely to zero" after the first few seconds of gas flow. The authors feel that the differential polarity theory may help to explain some of the transient polarity effects which they have observed. However, our paper demonstrates that no significant level of voltage has ever been measured on a noncondensing turbine shaft. Also, no electrostatic pitting damage of bearings has been observed on noncondensing turbines. This leads to the authors' assumption that dry steam in turbines does not generate appreciable steady state shaft voltage. Our data also indicate that steady state voltages of both polarities are generated by condensing turbines. If, as Professor Beach points out, dry steam would be expected to generate no steady state voltage, then we must look to the moisture in the steam as a source of both polarities. The references in the authors' paper cite cases where water droplet size is associated with polarity of electrostatic charges.

Professor Beach's remarks on instrumentation and the use of high resistance voltmeters for electrostatic measurements are very pertinent. The authors made a comprehensive study of the instrumentation problems involved and feel that our measurements and oscillograms are reliable. Our several years of experience in obtaining rather complete data on shaft voltages has demonstrated over and over again that the electrostatic generator in a turbine generates in the order of 500 to 1000 microamperes of current and not fractions of microamperes as do some other more familiar sources. We have taken many measurements while varying the value of a resistance connected from shaft to ground and have also taken measurements where the resistance in series with the voltmeter was varied. All of these studies demonstrated that the resistance of our oscilloscope and voltmeters was high enough so that no serious error was introduced due to the connection of the instruments to the circuit.

Our measurements demonstrate that the magnitude and rate of rise of shaft voltage were a function of the source voltage, source impedance, and shaft-to-ground impedance of the turbine-generator and were not altered by our instrumentation. On some turbines, the measured shaft voltage was still rising rapidly at 200 or 250 volts when an oil film broke down (electrically). If it were not for electrical breakdown of oil films, the voltage would no doubt rise much higher than the maximum values measured. On some other turbines, the shaft voltage leveled off at some voltage below 100 volts. In one such case, various values of resistance were connected from shaft to ground demonstrating that the internal resistance of oil films from shaft to ground was about 35,000 ohms. It was concluded that this level of resistance was the insulation resistance of the bearing oil films on this machine. The leakage current associated with insulation resistance of oil films causes no sparking damage.

Considerable research work was done on a 12,500-kw turbine to study the effects of the variables in oil such as water, dirt, age, and others. The results were inconsistent and the work was stopped after about six months of testing. It can be concluded, however, from these tests that there is no minimum breakdown voltage for oil in a steam turbine bearing. Voltage breakdowns were found to occur anywhere from about one volt to as high a value as 200 volts and over.

The authors wish to stress that turbine component design plays a very important part on the magnitude and effect of electrostatic shaft voltage. Inadvertently built-in grounding sources, such as loaded worm and worm gear drives, carbon packing, metallic labyrinth seals, water shaft seals, and even others have in the past prolonged the life of turbine bearings from the standpoint of current damage.

Bearing design, too, plays a part in the magnitude of current damage from electrostatic voltage. Basically this can be simplified into those factors which control the oil film thickness. These are principally the bearing load, speed, length to diameter (L/D) ratio, design clearance, and oil viscosity. Thrust bearing failures on steam turbines do not separate themselves by the general type of bearing design. The authors are aware of many failures of tilting pad thrust bearings that were catastrophic failures resulting from electrostatic voltage. These failures, too, occurred after very short periods of operation. The nature of the failure on a tilting pad bearing is not the simple process of eating away the babbitt, or a loss of flatness, but rather a combination of babbitt pitting and a deposit of carbon (result of breakdown of the oil film due to sparks) on the face of the pads. Where temperature recording devices were in use in the pads themselves, it was found that the carbon deposit would cause a small daily increase in temperature in the order of one or two degrees Fahrenheit. This increase would continue for a relatively short period of time after which the bearing would wipe out completely, taking with it any evidence of the shaft voltage effects.